Development of Copper Peptide Complexes as Anti-Inflammatory Drugs

A dissertation submitted to the

University of Cape Town

In fulfilment of the requirements for the degree of

DOCTOR OF PHILOSOPHY

By

Ahmed. N. H. Hammouda

Supervisor:

Prof. Graham E. Jackson

Department of Chemistry
University of Cape Town
Rondebosch 7701
South Africa

December 2014

DEDICATION

I dedicate this entire dissertation to my wife (Fatin), my children (Rana and Rwad) and our family for their love and support during my study at the University of Cape Town.

DECLARATION

I hereby sincerely and solemnly declare that **"Development of Copper Peptide Complexes as Anti-Inflammatory Drugs"** is my own unaided work both in concept and execution and that all sources that I have used and quoted have been indicated and acknowledged by means of complete and clear references. This thesis is submitted for the Doctor of Philosophy (PhD) degree to the Department of Chemistry at the Faculty of Science at the University of Cape Town. It has not been submitted before for any degree or any examination at the University of Cape Town or any other university.

…….

Ahmed Hammouda

December 2014

ACKNOWLEDGEMENTS

In the name of Allah, the Most Gracious and the Most Merciful Alhamdulillah. All praises to Allah for providing me the blessings to complete this study. I also would like to ask him that this project would be another tool to help in the treatment of rheumatoid arthritis.

During my pursuing my degree, I have received help, support, courage and much more from many people. I could not have done it without them.

Foremost and special appreciation goes to my supervisor Professor Graham Jackson, for his elaborated mentoring through four years. It is his patient guidance and encouraging advice that pulled me out of straying and lead me to every step toward success.

A big thanks is given to my colleagues in the research group for their contribution and discussion.

I thank all the administrative and technical staffs at chemistry department for the contributions, seminars and conferences, especially thanks to Mr. Peter Roberts for running the NMR experiments and Dr. Shirley Churms for spends time checking read this thesis and good advices.

Last but not least, I would like to thank all my respected friends and all members of my family for their enthusiasm and encouragements.

In conclusion, I recognize that this research would not have been possible without the financial assistance of the Libyan ministry of higher education.

CONFERENCES PROCEEDINGS

Parts of the results in this thesis have been presented in the following conferences;

- **41st** National Convention of the South African Chemical institute (**SACI2013**) (1-6th December 2013) in the East London. (***Potentiometric and Spectroscopic Studies on Cu(II), Ni(II) and Zn(II) Complexes with Tripeptide as Anti-inflammatory Drugs*).**

- International Conference on Pure and Applied Chemistry (**ICPAC2014**) (23rd to 27th June 2014) in Mauritius. (***Potentiometric, Partition coefficient and dermal absorption studies of Cu(II) Tripeptide Complexes as Potential Anti-Inflammatory Drugs*).**

- **41st** International Conference on Coordination Chemistry (**ICCC-41**) (21st -25th July 2014) in Singapore. (***Tripeptide Copper Complexes as Potential Anti-Inflammatory Drugs for Rheumatoid Arthritis*).**

ABSTRACT

Copper complexes have been reported to have anti-inflammatory activities for the alleviation of inflammation associated with rheumatoid arthritis (RA). The present study focuses on the design of new drugs that could be used to change the bioavailability of copper and hence alleviate inflammation. The ligands chosen were sarcosyl-L-histidyl-L-lysine, sarcosyl-L-lysyl-L-histidine, sarcosyl-L-histidyl-L-histidine, sarcosyl-L-lysyl-L-lysine and sarcosyl-L-glycyl-L-histidine. Equilibrium constants of H^+, Cu(II), Ni(II) and Zn(II) with the peptides were measured in aqueous solution at 25±0.01^oC and an ionic strength of 0.15M (NaCl) using glass electrode potentiometry. The tripeptides species showed significantly different coordination behaviour. The results that Cu(II) coordinates to one amino group, two deprotonated peptides and one imidazole nitrogen atoms to give a neutral complex.

The structures of the complex species were investigated using ultraviolet-visible (Uv-Vis), nuclear magnetic resonance (NMR), electrospray ionisation mass spectrometry (ESI-MS) spectroscopy as well as molecular mechanics (MM) calculations. The visible spectra obtained for the different species in solution were typical of Cu(II) and Ni(II) complexes. ^1H NMR identified the active binding sites to be the imidazole nitrogen, the amide nitrogen and the terminal amino group. The imidazole nitrogen was involved in coordination first, followed by the amide and then the terminal amine groups. The ε-amino group of lysine did not coordinate to the Cu(II). Molecular mechanics was used to support the Cu(II) structures postulated from potentiometric and spectroscopic data.

The prefered method of increasing the available pool of low molecular weight Cu(II) species *in vivo* is *via* dermal absorption. For this reason the drugs were designed so that they could be administered dermally and be selective for Cu(II) so that they do not affect the speciation of other metal ions in blood plasma. Speciation calculations of Cu(II) using a computer model of blood plasma indicated that Sar-Lys-His was the best at mobilising copper *in vivo*.

This study also considered percutaneous skin absorption. Octanol/water partition coefficients and Franz cell permeation studies showed that the Cu(II) complexes are hydrophilic but that Sar-Gly-His caused a 2 fold increase in membrane permeability of Cu(II).

LIST OF ABBREVIATIONS AND SYMBOLS

RA	-Rheumatoid arthritis
RF	- Rheumatoid factor
SLE	-Systematic lupus erythematosus
Anti-CCP	-Anticitrullinated cyclic protein
NSAIDs	-Non-steroidal anti-inflammatory drugs
COX	-Cyclooxygenase
DMARD	-Disease modifying anti-rheumatic drugs
SOD	-Superoxide dismutase
HSA	-Human serum albumin
Gly	-Glycine
Sar	-Sarcosine
SHK	-Sarcosyl-L-histidyl-L-lysine (Sar-His-Lys)
SKH	-Sarcosyl-L-lysyl-L-histidine (Sar-Lys-His)
SHH	-Sarcosyl-L-histidyl-L-histidine (Sar-His-His)
SKK	-Sarcosyl-L-lysyl-L-lysine (Sar-Lys-Lys)
SGH	-Sarcosyl-L-glycyl-L-histidine (Sar-Gly-His)
EDTA	-ethylenediaminetetraacetic acid
ESTA	-Equilibrium Simulations for Titration Analysis
Log β	-Logarithm (to base 10) of the cumulative equilibrium constants
Log K	-Logarithm (to base 10) of the equilibrium constants
Z_H-bar	-The protonation function
Z_M-bar	-The metal formation function
Q_M-bar	-The deprotonation function
n-bar	-The formation function
σ	-Standard deviation
R_f^H	-The Hamiltonian R- factor
R^H_{lim}	-R_{lim} is the Hamiltonian R-limit
n_T	-Number of titrations

n_P	-Number of titration points
T	-Temperature
N	-Number of binding sites on the ligand
K	-Equilibrium constant
Uv-Vis	-Ultraviolet-Visible
NMR	-Nuclear magnetic resonance
ECCLES	-Evaluation of Constituent Concentrations in Large Equilibrium Systems
E_{tot}	-Total strain energy
E_b	-The total bond deformation strain
E_s	-The total steric strain (van der Waals strain)
E_a	-The angle strain
E_t	-The torsional strain
Esff	-Extensible systematic force field
p.m.i	-Plasma mobilizing indices
Log $P_{oct/aq}$	-Octanol/water partition coefficient
J	-Flux in g/cm^{2}h
K_p	-Permeability coefficient in cm/h

LIST OF FIGURES

LIST OF TABLES

TABLE OF CONTENTS

CHAPTER ONE

RHEUMATOID ARTHRITIS

1.1 Introduction

Rheumatoid arthritis (RA) is an autoimmune disorder characterized by systemic, erosive synovitis, and extra-articular involvement. It may result in nearly complete functional defect, lead to chronic pain and also cause chronic inflammation of the joints [1,2]. The cause of RA is not yet known, but the symptoms include morning stiffness, non-specific joint pains, swelling and tenderness around inflamed joints, and loss of functioning and mobility of joints [3,4]. The joints usually in the hands, wrists, knees or feet, on both sides of the body swell and become painful, tender and stiff. A typical RA joint is shown in Figure 1.1.

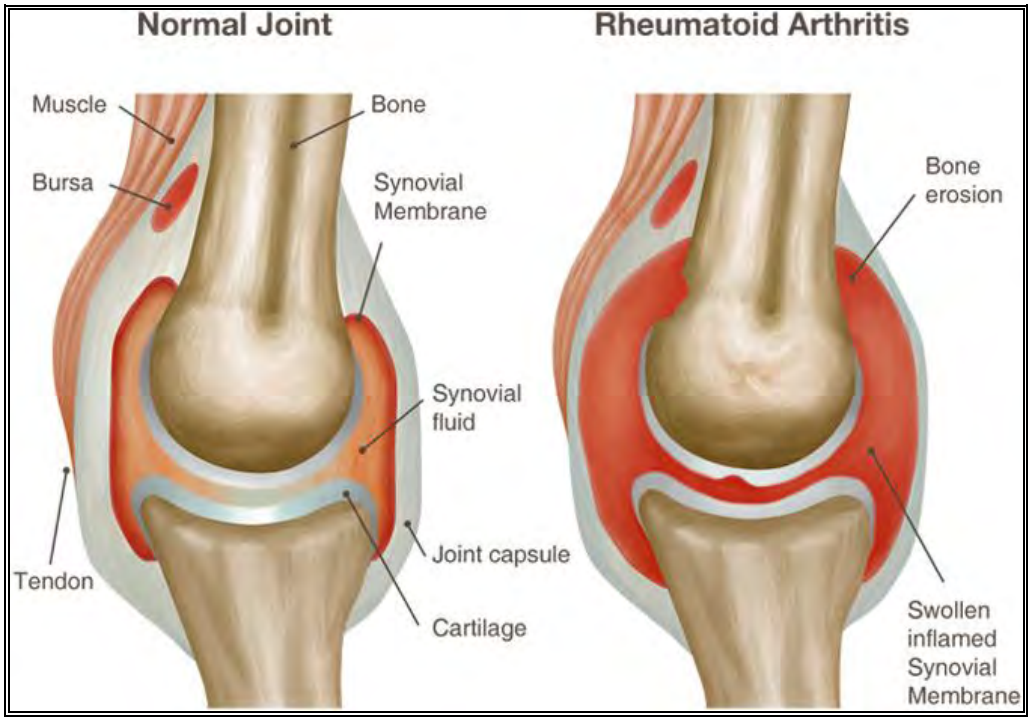

Figure 1.1: Normal, healthy joint and a joint affected by Rheumatoid Arthritis.

Furthermore, acute and chronic inflammation is characterized by changes in the metabolism of copper [5,6].

Previous studies have shown that RA patients have increased levels of copper in their blood plasma [7,8]. One view is that the rise in total serum copper measured in inflammation is held to represent the natural anti-inflammatory (AI) response of the organism itself. The responsiveness of inflammatory disorders to copper supplementation suggests that the control exerted by endogenous copper on inflammation be susceptible to enhance by exogenous sources. When copper complexes

were administered subcutaneously, the reduction in inflammation was proportional to the total amount of copper injected [9]. However, the precise mechanism by which this is achieved has not yet been established. Copper bracelets are reported to reduce the inflammation associated with rheumatoid arthritis. It is believed that sweat transports copper through the skin to its target site. Pharmacological evidence suggests that copper complexes can be beneficial in alleviation and treatment of RA and that these compounds have disease remitting qualities [10,11]. Unbound (free) copper is not found in large amounts in the human body. Instead, almost all copper is bound to either the storage proteins (metallothioneins), the transport proteins (ceruloplasmin and serum albumin), or copper-containing enzymes [12].

Copper complexes almost always have stronger activity than their parent compounds or ligands. It has been hypothesized that the active form of a number of general anti-inflammatory drugs are their copper complexes. The sum of this research has demonstrated that the copper complexes of most of the anti-inflammatory compounds, as well as of many other compounds, possess strong anti-inflammatory activity in various models of inflammation. In addition, these copper complexes have been found to exhibit lower toxicity as well as higher anti-inflammatory activity as compared to their parent compounds or ligands [13].

1.2 Copper Complexes as Anti-Inflammatory

Copper exists as a metal in the oxidation states (0), (I), (II) and unstable (III), but as Cu(II) ion in aqueous solution [14].

Copper is an essential trace element that acts as a cofactor for a variety of enzymes by virtue of its ability to accept and donate electrons under physiological conditions. The copper content and ceruloplasmin activity of serum are significantly elevated above normal values in inflammatory diseases in both human and animals. The copper in widely different chemical forms is used as a therapeutic agent in therapy for chronic and acute inflammation [15].

The most popular medications used in such situations are the non-steroidal anti-inflammatory drugs, generally known by the acronym NSAIDs, such as local anaesthetics, opioids, N-methyl D-aspartate (NMDA) receptor antagonists, aspirin, ibuprofen etc. These have been found to be effective in controlling pain. Opioids and

NSAIDs are the central analgesics in animal practice [16]. Copper chelation of the parent NSAID (such as indomethacin) produces a unique pharmacological substance with significantly increased anti-inflammatory potency, broader inhibition of inflammatory reactions, and virtual elimination of adverse side effects, especially gastrointestinal ulceration. The Cu-Algesic (it is copper indomethacin 40mg/g) is indicated for conditions requiring a potent anti-inflammatory action with excellent analgesia, and with reduction of side-effects usually associated with long-term use of other NSAIDs. It is also used in treatment of acute and sub-acute musculoskeletal/ locomotor inflammatory conditions in horses [17].
Most of the ingested copper is excreted via the bile, the major excretory route, thus preventing tissue toxicity. Trace amounts of copper are excreted via urine except in cases of copper overload. Excess copper in the tissue leads to the production of damaging free radicals and subsequent DNA cleavage [18].

In blood plasma, at least 90% of copper is irreversibly bound to ceruloplasmin in a non-exchangeable form, while about 10% is reversibly bound to serum albumin and less than 1% is distributed amongst low molecular weight (l.m.w) complexes, predominantly [Cu(histidinate)(cystinate)] as the exchangeable copper fraction in the blood [18,19]. Serum albumin (SA) has been considered to facilitate the transport of trace metals between tissues and blood and it is a major metal-binding protein in the body, with about 40 μg of copper able to bind to the albumin contained in 1ml of human plasma. Albumin appears to be the primary copper carrier protein in the body [20,21]. It has been observed that serum levels of copper are significantly increased during acute phases of RA inflammation, returning to normal with remission. This rise in serum copper is due to an increase in ceruloplasmin concentration and represents a physiological response to inflammation. It has, however, been shown that ceruloplasmin is a powerful antioxidant and could thus provide protection against cellular destruction [14].

The role of copper in rheumatoid arthritis (RA) appears to be firmly established [22-27]. Irrespective of this contradiction, copper complexes were successfully used from the 1940's to 1970's in the treatment of various conditions characterized by arthritic changes and inflammation [28,29]. However, the development of steroids and aspirin-like non-steroidal anti-inflammatory drugs (NSAIDs) quickly replaced copper compounds in the treatment of such conditions. Several researchers have examined the contradictory role of copper in the process of inflammation, and they have determined that the enhancement in serum copper is

a physiological response to inflammation, rather than a cause [30]. In conjunction , the main copper-containing enzyme, ceruloplasmin, is significantly increased in inflammatory conditions and has anti-inflammatory activity [31]. In addition, it has been found that copper deficiency enhances the severity of experimentally induced inflammation [32] and that the dietary copper must be enhanced to maintain adequate copper status of animals in an inflammatory state [33].

1.3 Literature Review

Franco and Velo [34] demonstrated that the copper complexes reduce gastric damage caused by acetylsalicylic acid (ASA) in animal studies. Chemical interaction of copper (II) with non-steroidal anti-inflammatory agents (NSAIDs) including acetylsalicylic acid (ASA) and related substances has been studied in detail by Brumas *et al* [35]. A relationship between copper deficiency and anti-inflammatory (AI) activity of ASA has been described [36].

Fiabane [37] investigated various metal complexes involved in rheumatoid arthritis. The drug-serum albumin copper(II) interactions have been investigated using visible spectrophotometry. In studies on the release of copper(II) from bovine serum albumin it was found that the release might occur by a direct complexing mechanism or through a remote mechanism involving the drug-copper binding, facilitating the copper release by allosteric effects. Indomethacin, naproxen, ketoprofen, and fenoprofen released copper ions remotely to a low molecular weight pharmacoactive form. Acetylsalicylic acid (ASA) and D-pencillamine had different modes of action. Copper supplementation is desirable during rheumatoid arthritis treatment with these drugs. Jackson [38] carried out computer simulation study of low-molecular-weight metal complexes involved in rheumatoid arthritis. Sorenson and Jackson *et al* [19,20] have shown that Cu(II) complexes are effective in reducing the inflammation associated with RA, enhancing bio-availability of copper and reducing toxicity [39].

The Ni(II) ion coordination of properties towards the blocked hexapeptide model -TESHHK- (Ac-ThrGluSerHisHisLys-am) which contains the C-terminal "tail" -ESHH- (-Glu-Ser-His-His-Lys-) of histone H2A was studied. At pH above 7.4, Ni(II) complexes with the hexapeptide formed a square-planar complex with the peptide fragment SHHK- (SerHisHisLys-am) [40,41].

Cu(II) and Ni(II) cations are well known for their ability to interact with histidyl residues in peptides, particularly with those containing the N-terminal sequence X–Y–His that is encountered in serum albumin [42-44]. The coordinating properties are affected by numerous factors, but if an imidazole is present in the side-chain of an amino acid or derivatives [45], in small peptides [46,47] or large protein molecules [43], very often this group is one of the most effective metal-binding sites of the molecule.

Investigation of the Cu(II)-cyclic (HGHK) system revealed that cyclic (HGHK) is capable of providing a variety of coordination environments for copper(II) ions depending on pH. It was shown that cyclic HGHK can form Cu(II) complexes of comparable stability to linear, N-terminally protected, AcHGHG [48]. The metal-binding features of oligopeptides, including the effect of the number and position of histidine residues within the peptide chain have been summarized in a couple of reviews within the last decade [49,50]. These have included equilibrium and solution structural investigation of the copper(II) and nickel(II) complexes of Gly-Gly-Gly-Histamine (GGGHa) and its N-terminally Boc-protected derivative Boc-Gly-Gly-Gly-Histamine (BGGGHa) [51].

Copper(II) complexes of the His-tripeptide (Cu(II) Xaa–Yaa–His, Xaa–His–Yaa and His–Xaa–Yaa) molecules are of significant biological importance. The copper(II) coordination of the tripeptides, mostly with Xaa = Yaa = Gly has been extensively investigated, and the coordination mode of copper(II) in the oligopeptide complexes with terminally protected groups or peptides containing more than one histidine has been established [52]. The investigations of the complex formation equilibria of Lys-containing oligopeptides with the Cu(II) ion [53,54], supported the view that the ε-NH_2 of Lys residue interacts with copper, but only at alkaline pH; no deprotonation of ε-NH_2 was found at neutral pH, and under physiological conditions protonated Lys residue of metal-peptides can act as an ‘anchor’ for biological receptors [55].

The sarcosine SAR (N-methyl of glycine) was a natural amino acid in muscles and other body tissues. It was metabolized to glycine by the enzyme sarcosine dehydrogenase while glycine-N-methyltransferase generates it. The sarcosine has no known toxicity and was identified as a biomarker as invasive prostate cancer. It was seen to be greatly improved during prostate cancer progression to metastasis also could be identified in urine [56]. It was found by Mohajane [57] that the Cu-GLY peptides were slightly more stable than the Cu-SAR. The explanation given was the possibility that the methyl group caused a steric effect as well as an inductive effect. However, since the two results were comparable, the

conclusion was that the N-methylated dipeptides would not affect the stability of the complex, but still improve the lipophilicity of the complex, since N-methylated groups are more lipophilic than non-N-methylated groups [58].

1.4 Aims of the Present Research

The present study concentrates on the design of new drugs that will alleviate the inflammation associated with rheumatoid arthritis. These drugs an required be administered dermally and be selective for Cu(II) so that they do not affect the speciation of other metal ions in blood plasma. The ligands are also expected to be soluble both in lipids and in water; however, they are believed to be more lipophilic than hydrophilic thus promoting dermal absorption of copper. In general, the ligands are expected to have comparable thermodynamic properties to those of glycyl-L-histidyl-L-lysine [58- 60]. The proposed ligands are expected to form stable and kinetically labile complexes with copper.

1.5 Objectives of the Present Research

- Measurement of formation constants for tripeptides (drugs) with Cu(II), Zn(II) and Ni(II) complexes by glass electrode potentiometry data. The protonation/deprotonation constants and the equilibrium of the ligand and metal-ligand complexes will be calculated. These constants will give information on how many dissociable protons each ligand has, how stable the metal-ligand complexes are and the distribution of species in solution at different pH.
- Determination of the structure of the formed complexes in solution using; Uv-Vis, ESI-MS and ^{1}H NMR spectroscopy and molecular mechanics (MM) to investigate the possible structures.
- Evaluation of plasma mobilization ability of Cu(II) tripeptide using a computer model of blood plasma (ECCLES) to assess the speciation *in vivo* of the copper complexes.
- Drug administration and distribution studies will be achieved using octanol/water and Franz cell at physiological pH of copper complexes at room temperature through a Cerasome 9005. This indicates the possibility of dermal absorption of the copper (II).

References

1. T. M. Madland, E. M. Apalset, A. E. Johannessen, B. Rossebö, and J. G. Brun, *J. Rheumatol.*, 2005, **32**, 1918–22.

2. E. D. Harris, *N. Engl. J. Med.*, 1990, **322**, 1277–89.

3. W. E. Clair, D. S. Pisetsky and B. F. Haynes, *Rheumatoid Arthritis. Wolters Kluwer Health.*, 2004.

4. B. R. Aeschlinmann, A., Munzinger, U., Simmen, *Rheumatoid Arthritis. Thieme Medical Publishers*, 1995.

5. J. J.Cush and K. Arthur, *Rheumatoid Arthritis: Early Diagnosis andTreatment. Wolters Kluwer Health.*, 2005.

6. J. R. Sorenson, *J. Med. Chem.*, 1976, **19**, 135–48.

7. N. A. ROBERTS and P. A. ROBINSON, *Rheumatology*, 1985, **24**, 128–136.

8. V. Honkanen, Y. T. Konttinen, T. Sorsa, M. Hukkanen, P. Kemppinen, S. Santavirta, H. Saari, and T. Westermarck, *J. Trace Elem. Electrolytes Health Dis.*, 1991, **5**, 261–3.

9. G. E. Jackson, L. Mkhonta-Gama, A. Voyé, and M. Kelly, *J. Inorg. Biochem.*, 2000, **79**, 147–152.

10. J. R. J. Sorenson, *Sigel H.,Mercel decker, Inc.*, 1982, **14**, 77–113.

11. K. M. Stuhlmeier, *J. Biol. Chem.*, 2007, **282**, 2250–8.

12. S. N. Gacheru, P. C. Trackman, M. a Shah, C. Y. O'Gara, P. Spacciapoli, F. T. Greenaway, and H. M. Kagan, *J. Biol. Chem.*, 1990, **265**, 19022–7.

13. D. H. Brown, W. E. Smith, J. W. Teape, and A. J. Lewis, *J. Med. Chem.*, 1980, **23**, 729–34.

14. Zvimba N. John, *PhD Thesis*. University of Cape Town, 2005.

15. M. L. Schilsky, *Pediatr. Transplant.*, 2002, **6**, 15–19.

16. Subhahar, Michael, *PhD Thesis*. University of Central Lancashire Preston, 2013.

17. J. E. Weder, T. W. Hambley, B. J. Kennedy, P. a. Lay, D. MacLachlan, R. Bramley, C. D. Delfs, K. S. Murray, B. Moubaraki, B. Warwick, J. R. Biffin, and H. L. Regtop, *Inorg. Chem.*, 1999, **38**, 1736–1744.

18. D. W. Cox, *Br. Med. Bull.*, 1999, **55**, 544–55.

19. M. C. Linder and M. Hazegh-Azam, *Am. J. Clin. Nutr.*, 1996, **63**, 797S–811S.

20. G. E. Jackson, P. M. May, and D. R. Williams, *J. Inorg. Nucl. Chem.*, 1978, **40**, 1227–1234.

21. J. N. Zvimba and G. E. Jackson, *J. Inorg. Biochem.*, 2007, **101**, 1120–8.

22. T. P. A. Kruck and B. Sarkar, *Inorg. Chem.*, 1975, **14**, 2383–2388.

23. M. S. Iqbal, S. J. Khurshid, and M. Z. Iqbal, *Can. J. Chem.*, 1993, **71**, 629–633.

24. J. R. Sorenson, *Inflammation*, 1976, **1**, 317–31.

25. K. D. Rainsford and M. W. Whitehouse, *Experientia*, 1976, **32**, 1172–3.

26. M. S. Iqbal, A. R. Ahmad, M. Sabir, and S. M. Asad, *J. Pharm. Pharmacol.*, 1999, **51**, 371–5.

27. M. W. Whitehouse, *Agents Actions*, 1976, **6**, 201–6.

28. A. J. Lewis, *Agents Actions*, 1984, **15**, 513–9.

29. J. R. Sorenson and W. Hangarter, *Inflammation*, 1977, **2**, 217–38.

30. B. S. J. and W. M. W. Walker. W.R., *Humana Press. Clifton, NJ. USA*, 1982, 453–467.

31. J. R. Sorenson, *J. Pharm. Pharmacol.*, 1977, **29**, 450–2.

32. E. Frieden, *Clin. Physiol. Biochem.*, 1986, **4**, 11–9.

33. Sorenson. J.R.J and Kishore. V., *Tr. Elem. Med.*, 1984, **1**, 93–102.

34. R. Milanino, A. Conforti, L. Franco, M. Marrella, and G. Velo, *Agents Actions*, 1985, **16**, 504–13.

35. V. Brumas, B. Brumas, and G. Berthon, *J. Inorg. Biochem.*, 1995, **57**, 191–207.

36. L. Franco and G. P. Velo, *Prostaglandins*, 1996, **51**, 331–8.

37. A. Lopez-Anaya, C. Dawson, C. Gonzales, M. Bacolod, and V. Kishore, *Biol. Trace Elem. Res.*, 1994, **40**, 161–76.

38. A. M. Fiabane and D. R. Williams, *J. Inorg. Nucl. Chem.*, 1978, **40**, 1195–1200.

39. W. R. Walker and R. R. Reeves, *Bioinorg. Chem.*, 1977, **7**, 271–6.

40. W. Bal, J. Lukszo, K. Bialkowski, and K. S. Kasprzak, Chem. Res. Toxicol., 1998, **11**, 1014–1023.

41. M. Mylonas, A. Krezel, J. C. Plakatouras, N. Hadjiliadis, and W. Bal, *Bioinorg. Chem. Appl.*, 2004, 125–40.

42. H. Kozłowski, W. Bal, M. Dyba, and T. Kowalik-Jankowska, *Coord. Chem. Rev.*, 1999, **184**, 319–346.

43. Y. Zhang, S. Akilesh, and D. E. Wilcox, *Inorg. Chem.*, 2000, **39**, 3057–64.

44. M. Orfei, M. C. Alcaro, G. Marcon, M. Chelli, M. Ginanneschi, H. Kozlowski, J. Brasuń, and L. Messori, *J. Inorg. Biochem.*, 2003, **97**, 299–307.

45. R. W. Hay, M. M. Hassan, and C. You-Quan, *J. Inorg. Biochem.*, 1993, **52**, 17–25.

46. B. Kurzak, H. Kozłowski and E. Farkas, *Coord. Chem. Rev.*, 1992, **114**, 169–200.

47. H. Sigel and R. B. Martin, *Chem. Rev.*, 1982, **82**, 385–426.

48. I. Török, T. Gajda, B. Gyurcsik, G. K. Tóth, and A. Péter, *J. Chem. Soc. Dalt. Trans.*, 1998, 1205–1212.

49. M. Casolaro, M. Chelli, M. Ginanneschi, F. Laschi, L. Messori, M. Muniz-Miranda, A. M. Papini, T. Kowalik-Jankowska, and H. Kozłowski, *J. Inorg. Biochem.*, 2002, **89**, 181–190.

50. H. Kozłowski, T. Kowalik-Jankowska, and M. Jeżowska-Bojczuk, *Coord. Chem. Rev.*, 2005, **249**, 2323–2334.

51. I. Sóvágó and K. Osz, *Dalton Trans.*, 2006, 3841–54.

52. A. Jancsó, K. Selmeczi, P. Gizzi, N. V Nagy, T. Gajda, and B. Henry, *J. Inorg. Biochem.*, 2011, **105**, 92–101.

53. N. I. Jakab, B. Gyurcsik, T. Körtvélyesi, I. Vosekalna, J. Jensen, and E. Larsen, *J. Inorg. Biochem.*, 2007, **101**, 1376–85.

54. B. Radomska, I. Sovago, and T. Kiss, *J. Chem. Soc. Dalt. Trans.*, 1990, 289.

55. C. Conato, R. Gavioli, R. Guerrini, H. Kozlowski, P. Mlynarz, C. Pasti, F. Pulidori, and M. Remelli, *Biochim. Biophys. Acta*, 2001, **1526**, 199–210.

56. A. Sreekumar, L. M. Poisson, T. M. Rajendiran, A. P. Khan, Q. Cao, J. Yu, B. Laxman, R. Mehra, R. J. Lonigro, Y. Li, M. K. Nyati, A. Ahsan, S. Kalyana-Sundaram, B. Han, X. Cao, J. Byun, G. S. Omenn, D. Ghosh, S. Pennathur, D. C. Alexander, A. Berger, J. R. Shuster, J. T. Wei, S. Varambally, C. Beecher, and A. M. Chinnaiyan, *Nature*, 2009, **457**, 910–4.

57. M. Mohajane, *PhD Thesis*. University of Cape Town, 2013.

58. L. Pickart, J. H. Freedman, W. J. Loker, J. Peisach, C. M. Perkins, R. E. Stenkamp, and B. Weinstein, *Nature*, 1980, **288**, 715–7.

59. J. H. Freedman, L. Pickart, B. Weinstein, W. B. Mims, and J. Peisach, *Biochemistry*, 1982, **21**, 4540–4.

60. E. J. Billo, *Inorg. Nucl. Chem. Lett.*, 1974, **10**, 613–617.

CHAPTER TWO

LIGAND PROPERTIES AND DESIGN

2.1 Introduction

Copper is transported *in vivo* as the human serum albumin complex. *In vivo*, copper exists in three different forms: irreversibly bound to metalloproteins like ceruloplasmin, reversibly bound to plasma proteins as serum albumin and as low molecular mass (l.m.m) complexes. The type of organic ligands in such copper complexes seems to affect and regulate their activity. They (i) neutralize the electric charge of the copper ion, (ii) increase the lipophilicity of the complex, facilitating transport through cell membrane, and (iii) intercalate to DNA or interact noncovalently with proteins [1]. Human serum albumin (HSA) is the most abundant protein found in plasma and shows a typical blood concentration of 5 g/100 ml. It is a major metal-binding protein in the body, with about 40μg of copper able to bind to the albumin contained in 1 ml of human plasma [2]. The methylated N-terminals of amines are more lipophilic than their non-methylated analogues [3,4]. N-methylated peptides are also less susceptible to metabolism [5]. Drugs that will be administered transdermally are preferred over drugs that will be administered orally; therefore, the ligands have to be slightly lipophilic. However, it has to be achieved without compromising the stability of the Cu(II) complexes. The proposed ligands combine these two ideas and the effect of N-methylation of tripeptides on copper(II) complexation and tissue permeability.

2.2 Principles of Drug (Ligand) Design

Peptides are complex biomolecules and depending on the amino acid composition each peptide is unique in its chemical and physical properties. Although some peptides are easy to dissolve in aqueous solutions, a common problem encountered is very low solubility or even insolubility of peptides, especially of peptides with hydrophobic amino acids. Coordination chemistry of peptides has been studied since the early 1960s [6-8]. An important key in metal coordination chemistry is the formation of stable 5- and/or 6-membered chelate rings through the N-terminal amino, C-terminal carboxylate, and side-chain donor groups if present [9]. The most important donor atoms of peptide side-chains in terms of coordinating metal ions are the imidazole nitrogen of histidine and the amino nitrogen of lysine and the amide nitrogen and carbonyl oxygen of peptide linkages can also coordinate metal ions, but are less active donor atoms than those in the terminal amino and terminal carboxylate groups [6,10]. However, metal ions such as copper promote the deprotonation of the amide nitrogen of the peptide bond to form a very stable metal −N− bond. The design of the ligands was based on the structure of human serum albumin (HSA).

Therefore, the copper(II) ion has the same peptidic binding site at the N-terminus of human serum albumin HSA, which is its transfer route in the human body [10-12].

2.3 Solubility of Peptides in Aqueous Solutions

Peptides shorter than five residues are usually soluble in water or aqueous buffer, except if the whole sequence consists of hydrophobic amino acids. Hydrophilic peptides containing >25% charged residues are usually soluble in water or aqueous buffer. Hydrophobic peptides containing 50% and more hydrophobic residues may be insoluble or only partly soluble in aqueous solutions. Peptides containing a very high (>75%) proportion of hydrophobic residues are capable of building intermolecular hydrogen bonds (cross-linking), thus forming gels in aqueous solutions [13].

2.4 Metal-Binding Properties of Amino Acids and Peptides

The binding modes of amino acids and tripeptides are polydentate ligands. Consequently, Cu(II) ions can be used to form complexes in order to block functional groups selectively. Some of the side-chains in peptides and proteins, especially those of Glu and His, are excellent ligands for transition metal ions. The ability of transition metal ions to complex with a variety of groups found in peptides and proteins probably accounts in large measure for the toxicity of these cations [14,15]. Peptides are very useful and often specific ligands for a variety of metal ions. They contain a range of potential donor atoms and the complexes formed exist in a variety of conformations [16,17]. Among metal ions, Cu(II) and Ni(II) have been widely studied and seem to have the most interesting chemistry. In particular, these two metal ions share the peptidic binding site at the N-terminus of human serum albumin, which is the transport form of both in the human body [18,19]. In the presence of equimolar concentrations of albumin and peptide, and approximately 20-fold excess of L-histidine, there is about 18% of Cu(II) present in the forms of Cu(II)-albumin and L-histidine-Cu(II)-albumin, 36% in the forms of Cu(II)-peptide and L-histidine-Cu(II)-peptide, and 46% as Cu(II)-L-histidine. The extension of the tripeptide chain with an additional residue results in an increase of stability of the final 4N complex at the expense of the 3N species [16,20-22]. This unusual effect has been interpreted as evidence for the presence of a particular conformation of the C-terminal part of the peptide in the 4N complex, stabilised indirectly by Cu(II) [23]. In particular, log K_{HL} (amine protonation) is high when Pro or Sar is in the first position of the peptide chain, as a result, of inductive

effects, and drops towards the value for tetraglycine as the substituent is moved along the chain [24,25].

Previous studies have shown how the pK_a values of tripeptides composed of glutamic (Glu), glycine (Gly) and histidine (His) residues are influenced by the kind and place of the residue in the peptide sequence [26].

Investigation of the influence of position of residues on the formation constants of copper(II) complex with tripeptides and report a systematic study of the effects of types and positions of amino acid amino acid residues of tripeptides. The length of tripeptides between the C-terminal and the N-terminal was the same for all these tripeptides in this present study because the length of the chain may also affect the solubility of organic compounds (Figure 2.1). The proposed ligands are expected to increase the lipophilicity and may also increase the stability of the metal complex by forcing the divalent metal into its favorable coordination geometry [27]. The ligands are also expected to promote dermal absorption of copper and have low toxicity [28].

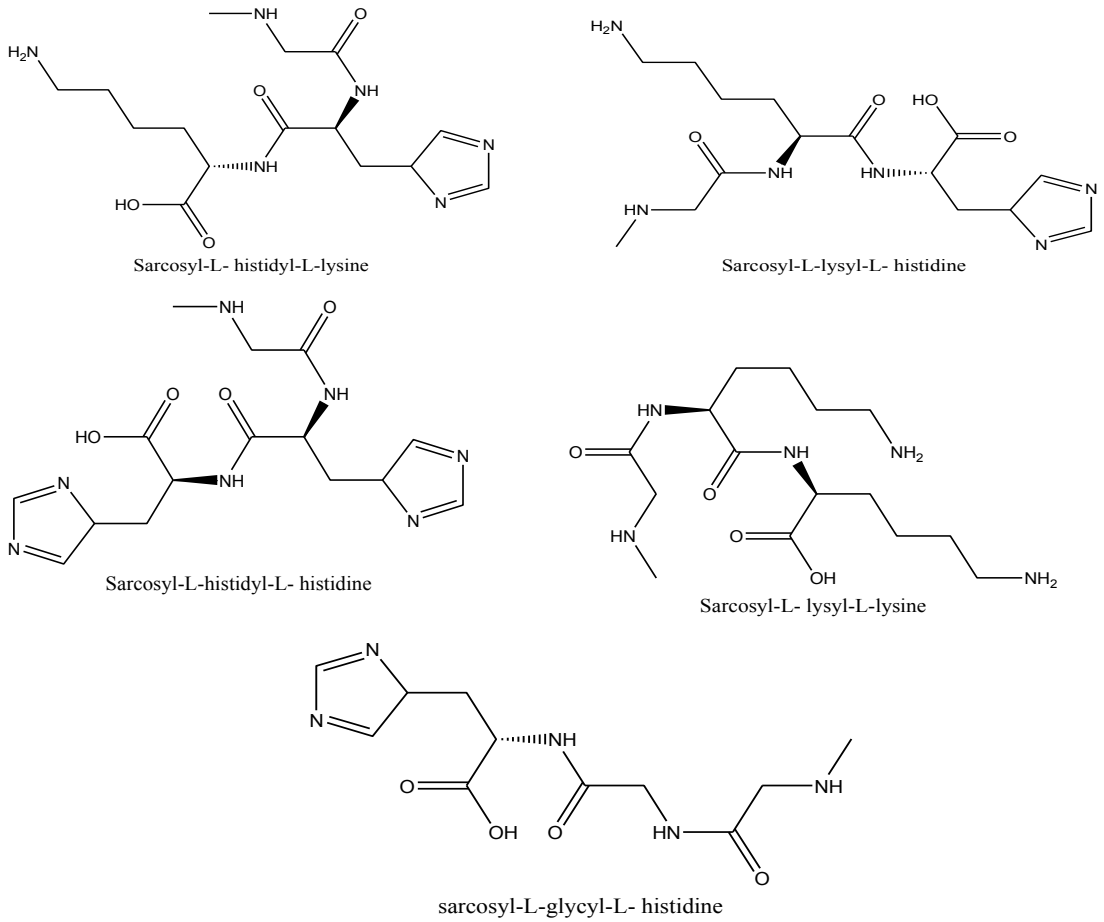

Figure 2.1: Structures of proposed ligands (drug design) used in this study.

References

1. I. Iakovidis, I. Delimaris, and S. M. Piperakis, *Mol. Biol. Int.*, 2011, **2011**, 594529.

2. K. J. Fehske, W. E. Müller, and U. Wollert, *Biochem. Pharmacol.*, 1981, **30**, 687–692.

3. T. Uhlmann, V. L. Geoghegan, B. Thomas, G. Ridlova, D. C. Trudgian, and O. Acuto, *Mol. Cell. Proteomics*, 2012, **11**, 1489–99.

4. D. Bekermann, D. Barreca, A. Gasparotto, and C. Maccato, *CrystEngComm*, 2012, **14**, 6347.

5. E. Biron, J. Chatterjee, O. Ovadia, D. Langenegger, J. Brueggen, D. Hoyer, H. a Schmid, R. Jelinek, C. Gilon, A. Hoffman, and H. Kessler, *Angew. Chem. Int. Ed. Engl.*, 2008, **47**, 2595–9.

6. D. E. Fenton and H. Okawa, *J. Chem. Soc. Dalt. Trans.*, 1993, 1349.

7. H. Kozłowski, W. Bal, M. Dyba, and T. Kowalik-Jankowska, *Coord. Chem. Rev.*, 1999, **184**, 319–346.

8. H. Sigel and R. B. Martin, *Chem. Rev.*, 1982, **82**, 385–426.

9. I. Sóvágó, C. Kállay, and K. Várnagy, *Coord. Chem. Rev.*, 2012, **256**, 2225–2233.

10. F. R. N. Gurd, *Pure Appl. Chem.*, 1963, **6**, 49–60.

11. L. Pickart, J. H. Freedman, W. J. Loker, J. Peisach, C. M. Perkins, R. E. Stenkamp, and B. Weinstein, *Nature*, 1980, **288**, 715–7.

12. W. T. Shearer, R. A. Bradshaw, F. R. Gurd, and T. Peters, *J. Biol. Chem.*, 1967, **242**, 5451–9.

13. M. Ryadnov, Ed., *Amino Acids, Peptides and Proteins*, Royal Society of Chemistry, Cambridge, 2012, vol. 37.

14. P. Y. Chou and G. D. Fasman, *Biochemistry*, 1974, **13**, 222–245.

15. G. E. Jackson, L. Mkhonta-Gama, A. Voyé, and M. Kelly, *J. Inorg. Biochem.*, 2000, **79**, 147–152.

16. P. M. M. Kevin B. Murray, *ESTA: Equilibrium Simulation for Titration Analysis*, University of Wales Institute of Science and Technology (UWIST) Department of Applied Chemistry, 1984.

17. L. D. Pettit, I. Steel, G. Formicka-Kozlowska, T. Tatarowski, and M. Bataille, *J. Chem. Soc. Dalt. Trans.*, 1985, 535.

18. W. Bal, M. Dyba, and H. Kozłowski, *Acta Biochim. Pol.*, 1997, **44**, 467–76.

19. R. A. Bradshaw, W. T. Shearer, and F. R. Gurd, *J. Biol. Chem.*, 1968, **243**, 3817–25.

20. P. J. Sadler and A. Tucker, *Eur. J. Biochem.*, 1993, **212**, 811–817.

21. Imre Sóvágó, E. Farkas and A. Gergly. *J. Chem. Soc. Dalt. Trans.*, 1982, 2159.

22. B. Decock-Le Reverend, L. Andrianarijaona, C. Livera, L. D. Pettit, I. Steel and H. Kozlowski, *J. Chem. Soc. Dalt. Trans.*, 1986, 2221.

23. C. R. Hartzell and F. R. Gurd, *J. Biol. Chem.*, 1969, **244**, 147–53.

24. S. J. Lau, T. P. Kruck, and B. Sarkar, *J. Biol. Chem.*, 1974, **249**, 5878–84.

25. J. J. Czarnecki and D. W. Margerum, *Inorg. Chem.*, 1977, **16**, 1997–2003.

26. R. R. Khoury, G. J. Sutton, D. B. Hibbert, and D. Ebrahimi, *Dalton Trans.*, 2013, **42**, 2940–7.

27. L. D. Pettit, I. Steel, G. Formicka-Kozlowska, T. Tatarowski, and M. Bataille, *J. Chem. Soc. Dalt. Trans.*, 1985, 535.

28. S. Odisitse, G. E. Jackson, T. Govender, H. G. Kruger, and A. Singh, *Dalton Trans.*, 2007, 1140–9.

CHAPTER THREE

GLASS ELECTRODE POTENTIOMETRY

3.1 Introduction

Glass electrode potentiometry (GEP) has been found to be one of the most reliable and accurate methods for measuring equilibrium constants in aqueous solution [1,2]. However, the measurement of metal complex stability constants is based on pH metric titrations of a ligand with and without metal ions and hence the ligand must be either an acid or a base. These coordination equilibria can then be used to approximate the metal ion speciation in complex biological systems [3]. In such situations, potentiometric titration, using a glass hydronium ion selective electrode, a suitable reference electrode and a sensitive potentiometer (a pH meter) may be advantageous.

3.1.1 Principles

The primary procedure of using chemicals of a known weight has been applied in standardising the acids/bases, which can then be used to standardise other solutions like the ligand solutions. Metal ion solutions should be standardized by described methods [4,5]. The titration vessel is filled with analyte solutions of known concentration and volume and the standard solutions of the titrant are injected into the titration vessel. The potential difference between the glass electrode and the reference electrode is measured, and these are direct measurements since indicators are not used. The output basically depends on the concentrations of the analyte solution and the titrant solution. The equilibrium constants of species have been calculated from the outputs with the potentiometric titrations being carried out at a fixed temperature and ionic strength [6,7].

A Gran plot is constructed to find the end point from the potentiometric data [8,9]. For this method, an acceptable plot should have two slopes meeting at one point (end point), and should there be any difference between the end points of the two slopes, this indicates CO_2 contamination which could affect the results since CO_2 forms carbonic acid in aqueous solutions [2-6,10].

The potentiometric data were here analysed using the computer program equilibrium simulation for titration analysis (ESTA) [3]. It was shown that the formation of metal/tripeptide complexes is strongly pH dependent as the metal competes with the protons bound to ligand. These data were also used to predict the possible metal/ligand models and to predict the distribution of species in solution.

3.2 Theory

The theory of metal complex stability constants and methods used to determine these constants has been widely covered in the literature [11,12]. Consider a general metal-ligand formation equilibrium involving metal ion (M) and ligand (L);

$M + L \rightleftharpoons ML$

The concentration equilibrium constant for ML can be expressed as

$$K_{ML} = \frac{[ML]}{[M][L]} \tag{3.1}$$

And for $MLn_{-1} + L \rightleftharpoons ML_n$

The concentration equilibrium constant can be expressed as;

$$K_{MLn} = \frac{[ML_n]}{[ML_{n-1}][L]} \tag{3.2}$$

Log K's for other species MLH_{-1}, MLH_{-2} do not have a fixed meaning but are defined by the equilibrium expression. For the reaction;

$ML \rightleftharpoons MLH_{-1} + H$

$$K_{MLH-1} = \frac{[MLH_{-1}][H]}{[ML]} \tag{3.3}$$

Log K for the more complicated species ML_2H_{-1}, ML_2H_{-2} depends on the pathway of the reaction. There are two (or more) possible routes for the formation of these species. ML_2H_{-1} can be formed by;

$ML_2 \rightleftharpoons ML_2H_{-1} + H$

$$K_{ML2H-1} = \frac{[ML_2H_{-1}][H]}{[ML_2]} \tag{3.4}$$

Or;

$MLH_{-1} + L \rightleftharpoons ML_2H_{-1}$

$$K_{ML2H-1} = \frac{[ML_2H_{-1}]}{[MLH_{-1}][L]} \tag{3.5}$$

Similarly, log K_{ML2H-2} from different routes;

$ML_2 \rightleftharpoons ML_2H_{-2} + 2H$

$MLH_{-2} + L \rightleftharpoons ML_2H_{-2}$

$ML_2H_{-1} \rightleftharpoons ML_2H_{-2} + H$

The stability of these species is therefore better described by the cumulative stability constants, log β's.

For the reaction; $pM + qL + rH \rightleftharpoons M_pL_qH_r$

Where p, q and r, are stoichiometric coefficients,

$$\beta_{MpLqHr} = \frac{[M_p\, L_q\, H_r\,]}{[M]^p[L]^q[H]^r} \tag{3.6}$$

Stepwise equilibrium constants can then be calculated from the β;

$M + L \rightleftharpoons ML$ $\qquad \beta_{ML} = K_{ML} = \frac{[ML]}{[M][L]}$ (3.7)

$ML + L \rightleftharpoons ML_2$ $\qquad \beta_{ML2} = K_{ML}\, K_{ML2} = \frac{[ML_2\,]}{[M][L]^2}$ (3.8)

$ML_2 + L \rightleftharpoons ML_3$ $\qquad \beta_{ML3} = K_{ML}\, K_{ML2}\, K_{ML3} = \frac{[ML_3\,]}{[M][L]^3}$ (3.9)

$ML_{n-1} + L \rightleftharpoons ML_n$ $\qquad \beta_{MLn} = K_{ML}\, K_{ML2}\, K_{ML3} \ldots K_{MLn} = \frac{[ML_n\,]}{[ML_{n-1}\,][L]^n}$ (3.10)

The electrode cell is the centre of any potentiometric investigation. An electrochemical cell consists of a test solution surrounding a glass electrode in electrical contact with a reference electrode through a salt bridge and can be represented as follows;

Reference electrode/ salt bridge/ analyte solution/glass electrode

$\mathbf{E_{ref}}$ $\qquad$ $\mathbf{E_j}$ $\qquad\qquad\qquad$ $\mathbf{E_g}$

where E_{ref}, the reference electrode potential, has a known constant value and it is not affected by the concentration of the analyte solution. E_g, the potential of the glass electrode varies with the concentration of the analyte solution [13,14]. E_j, the liquid junction potential, results from a difference in concentrations of the analyte solution and the internal reference solution. E_{cell}, the observed potential is the sum of all three;

$$E_{cell} = E_{ref} + E_j + E_g \tag{3.11}$$

E_g varies with the concentration of the analyte solution and the Nernst equation can be written as;

$$E_{cell} = E_{ref} + E_j + \left(E_g^0 + \frac{RTln\{H\}}{F}\right) \quad (3.12)$$

where the E_g^0 is the standard electrode potential and $\{H\}$ is the activity of the hydrogen ion. The activity of the proton is expressed as;

$$\{H\} = \Upsilon_H[H] \quad (3.13)$$

where Υ_H is the activity coefficient of the hydrogen ion and [H] is the concentration of the hydrogen ion. The ionic strength, I, can be expressed as:

$$I = \frac{1}{2}\sum(C_i Z_i)^2 \quad (3.14)$$

where C_i is the concentration of the ionic species, i and Z_i is the charge of the ion.

If the ionic strength is constant then equation 3.12 can be re-written as:

$$E_{cell} = E_{constant} + \frac{RTln[H]}{F} \quad (3.15)$$

However, the potential depends on temperature and the relationship between the two varies with the activity of the hydrogen ion. This can be expressed in terms of the slope factor, s.

$$s = \frac{2.30RT}{F} \quad (3.16)$$

Putting equation 3.16 into 3.15 yields;

$$E_{cell} = E_{constant} + s\log[H] \quad (3.17)$$

Calibration of the system requires the calibration of both s and E_{const}.

3.3 Experimental

3.3.1 Materials

All chemicals and reagents were of analytical grade and were used without any further purification. Sarcosyl-L-histidyl-L-lysine (SHK), sarcosyl-L-lysyl-L-histidine (SKH), sarcosyl-L-histidyl-L-histidine (SHH), sarcosyl-L-lysyl-L-lysine (SKK) and sarcosyl-L-glycyl-L-histidine (SGH) were purchased from GL Biochem (Shanghai) Ltd and the purity was checked by chromatographic methods and potentiometric titrations. The other chemicals were purchased from Sigma and used without further purification. The metal-ion stock solutions were prepared from analytical grade reagents and their concentration was checked using EDTA titration.

3.3.2 Preparation of solutions

The hydrochloric acid (HCl) solution was diluted and the exact concentration was determined by titration against standardised NaOH solution prepared from 0.1 mol dm^{-3} NaOH ampoules which were standardized against standard potassium hydrogen phthalate [15]. The ligand solution was prepared in standardised HCl (0.02 M) by direct weighing of tripeptides (0.01 M). The metal solutions were prepared by dissolving $NiCl_2.6H_2O$, $CuCl_2.2H_2O$ and $ZnCl_2$ (0.01 M) in boiled-out glass-distilled water. They were standardised by EDTA-murexide titration using a Metrohm 765 Dosimat automated burette dispensing 0.01 mol dm^{-3} EDTA solution. All of the stock solutions were prepared using NaCl as a background electrolyte to maintain a constant ionic strength of 0.15 mol dm^{-3}. All weighing was done to 5 decimal places on an A&D GH-202 analytical scale balance. Repeat titrations were done to check the reproducibility of the titrations.

3.3.3 Potentiometric measurements

All pH-metric measurements were carried out at 25 °C and at a constant ionic strength of 0.15 mol dm^{-3} (NaCl). The Metrohm glass electrode was calibrated with a set of Metrohm ion analysis pH buffers from which the pH and the Nernstian slopes were determined [9,13]. The slope varied from 58.71 to 59.19 over the pH range 2.0-11.0, using a Metrohm 6.0259.100 glass electrode. The standard electrode potential (E^0) and pK_w were calculated from NaOH/HCl titrations. E^0 ranged between 401.99 and 417.01 millivolts, pK_w ranged between 13.75 and 13.78. All the metal titrations were performed using 1:1 metal: ligand concentrations.

3.3.4 Data handling and calculations

Experimental data were analysed using the computer program, Equilibrium Simulations for Titration Analysis (ESTA). ESTA has a number of tasks. In this study ZBAR, QBAR and OBJE tasks were used.

3.3.4.1 Formation and deprotonation functions

ZBAR task is a simulation unit that uses mass balance equations to characterise the system on a point by point basis [3]. This task plots Z_H-bar curve for ligand protonation and Z_M-bar curve for complex formation titrations. The protonation/deprotonation formation function (Z_H-bar) is expressed as;

$$Z_{H-bar} = \frac{T_H - H + OH}{T_{lig}} \tag{3.18}$$

where T_H is the total concentration of hydronium ions, T_{lig} is the total concentration of the ligand and OH^-. It is possible to estimate pKa values from the half Z_H-bar values.

The complex formation function (Z_M-bar) depends on the cumulative protonation /deprotonation constants of the ligand to which the metal ion is binding. This can be expressed as;

$$Z_{M-bar} = \frac{T_L - A(1+\sum_n \beta_{LHn} H^n)}{T_M} \tag{3.19}$$

where T_M is the total metal concentration, and the free ligand concentration, A, is given by;

$$A = \frac{T_H - H + OH}{\sum_n (\beta_{LHn} H^n)} \tag{3.20}$$

This function assumes or is defined for simple, stepwise complex formation. If this assumption is not true, the curve will deviate and ultimately the free ligand concentration will become negative. Since $Z_{M\text{-}bar}$ is plotted against –logA (pA), at this point it is not possible to plot the curve as log of a negative number is not defined. ESTA calculates the residual;

$$Z_{-bar}\text{residual} = Z^o{}_{-bar} - Z^c{}_{-bar} \tag{3.21}$$

where Z^0-bar is the observed and Z^C-bar is the calculated Z-bar. A good agreement is observed if the observed and calculated Z-bar curves are superimposable. It is also important to know how many protons have been lost upon complexation with a metal ion. For this a deprotonation function (Q_M-bar) is calculated;

$$Q_{M-BAR} = \frac{T_H^* - T_H}{T_M} \tag{3.22}$$

where T^*_H is total concentration or H^+ ions in solution at the observed pH. The mass balance equations for T^*_H and T_L can be expressed as;

$$T_H^* = H - OH + \sum_{J=1}^{NJ} r\,[M_p\,L_q\,H_r\,]$$

$$T_L = L + H - OH + \sum_{J=1}^{NJ} q\,[M_p\,L_q\,H_r\,] \qquad (3.23)$$

Q_M-bar can be plotted as a function of pH. ESTA plots Q_M-bar on the same graph with n-bar which is. The total number of dissociable protons on the ligand in the absence of metal ion.

$$n_{-bar} = \frac{T_H^* - H + OH}{T_L^r} \qquad (3.24)$$

3.3.4.2 The objective function

The OBJE task of ESTA optimises titration parameters using a weighted or unweighted least squares method. The objective function, U_{obj} is given by the following equation;

$$U_{obj} = (N - n_p)^{-1} \sum_{n=1}^{N} n_e{}^{-1} \sum_{q=1}^{n_e} W_{nq} (Y_{nq}{}^{obs} - Y_{nq}{}^{calc})^2 \qquad (3.25)$$

where N is the total number of experimental titration points; n_p is the total number of points being optimised, n_e is the total number of electrodes; W_{nq} of the q^{th} residual at the n^{th} titration point, $Y_n{}^{calc}$ is the calculated variable of the q^{th} residual at the n^{th} titration point and $Y_{nq}{}^{obs}$ is the observed variable of the q^{th} residual at the n^{th} titration point. Using Gauss-Newton methods [16], Equation 3.25 can be expressed as a quadratic;

$$U_{obj} = a + p^t b + \frac{p^t H_p}{2} \qquad (3.26)$$

where a and b are Gauss-Newton quadratic parameter vectors, p is the optimization parameter vector and p^t is the rearranged form of Equation 3.26 (Hessian method);

$$H_{sr} = \frac{d^2 U_{obj}}{dp_s dp_r} \qquad (3.27)$$

3.3.4.3 Standard deviation and Hamilton R-factor

The standard deviations [17,18] (δ) are errors estimated for the parameters being optimized by OBJE and calculated as follows;

$$\delta = \left(\frac{U_{obj} G_{rr}}{N - n_p}\right)^{1/2} \tag{3.28}$$

OBJE also optimizes the Hamilton R-factor (R^H) to check if the model is accurate. R^H is expressed as;

$$R^H = \left(\frac{U_{obj}}{\sum n_e^{-1} \sum W_{nq} (Y_{nq}{}^{obs})^2}\right)^{1/2} \tag{3.29}$$

R^H depends on random errors and the number of variables optimised. Based on estimates of the random errors it is possible to calculate a theoretical limiting value for R^H and $R^H_{lim,}$ If R^H is less than R^H_{lim} then the model is precise as is statistically possible [19] or the error between the observed results and calculated results can be explained by random error. R^H_{lim} is expressed as;

$$R^H_{lim} = \left(\frac{N}{\sum n_e^{-1} \sum W_{nq} (Y_{nq}{}^{obs})^2}\right)^{1/2} \tag{3.30}$$

Once titration variables have been optimised and converged; the speciation graph can be plotted from the initial concentrations.

3.4 Results

3.41 Protonation titrations

The protonation constants for sarcosyl-L-histidyl-L-lysine (SHK), sarcosyl-L-lysyl-L-histidine (SKH), sarcosyl-L-histidyl-L-histidine (SHH), sarcosyl-L-lysyl-L-lysine (SKK) and sarcosyl-L-glycyl-L-histidine (SGH) are presented in Tables 3.1-3.5. The tripeptides contain four groups, respectively, which are capable of reversible proton binding. These groups are the carboxyl group of Lys and His, the N^3 imidazole nitrogens of His, the N-terminal of Sar and the ε-amino group of Lys. In general the standard deviations were small and the $R_f{}^H$ was less than $R_{lim}{}^H$ thus the model is within the maximum allowed experimental error. The log *K* values did not differ significantly from the literature values. The agreement between the theoretical and the experimental plot gives us confidence in the results.

3.4.1.1 Protonation of sarcosyl-L-histidyl-L-lysine

The Z_H-bar for protonation of sarcosyl-L-histidyl-L-lysine is given in Figure 3.1. The graph levels off between pH 11.4 ant pH 11.7 and then rises until it reaches Z_H-bar = 3 (between pH 5.5 and pH 3.6). The graph rises again from pH 3.5 to pH 2.0. Protonation constants of sarcosyl-L-histidyl-L-lysine were estimated from the half Z_H-bar values; log K_{LH} = 10.33, log K_{LH2} = 8.37, log K_{LH3} = 6.57 and log K_{LH4}= 2.83 and used as starting values in ESTA.

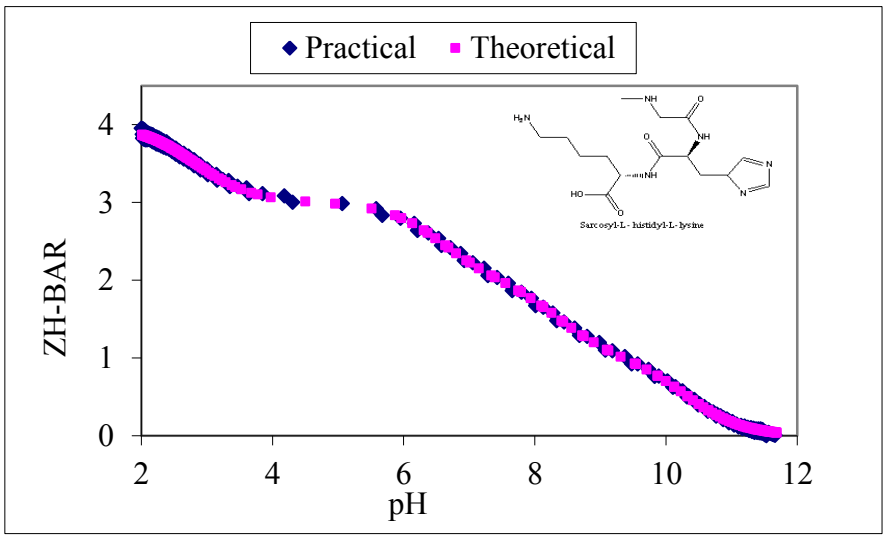

Figure 3.1: Z_H-bar for the protonation of sarcosyl-L-histidyl-L-lysine.

The final log *K*'s are given in Table 3.1. The results obtained are comparable with the results obtained for Gly-His-Lys protonation (pK_{a1}=10.44, pK_{a2}=7.93, pK_{a3}=6.53 and pK_{a4}=2.91) [20]. The standard deviations are small and the model is accurate since R^H is less than R^H_{lim}. This gives confidence in the results.

Table 3.1: Stability constants (log β_{pqr}) for sarcosyl-L-histidyl-L-lysine (SHK) β_{pqr} = [MpLqHr]/[M]p[L]q[H]r, I = 0.15 mol.dm^{-3} (NaCl), T = 25 ºC. S. dev denotes standard deviation in logβ_{pqr}; R_f^H is the Hamilton R-factor and R_{lim}^H its limit.

SHK	p	q	r	log β_{pqr}	S.dev	R_f^H	R_{lim}^H	$n_T(n_p)$
SHK-H	0	1	1	10.33	0.01			
SHK-H_2	0	1	2	18.70	0.01			
SHK-H_3	0	1	3	25.27	0.14	0.001	0.001	3(223)
SHK-H_4	0	1	4	28.1	0.02			

The speciation for sarcosyl-L-histidyl-L-lysine protonation titrations is given in Figure 3.2. From pH 7.20 to pH 10.85 the most predominate species is mono- protonated. The plots indicate that the ligand solution has a mixture of di-protonated, tri-protonated and tetra-protonated species. The di-protonated species were predominant at pH < 9.59 whereas the neutral form of the ligand predominates at pH > 8.9.

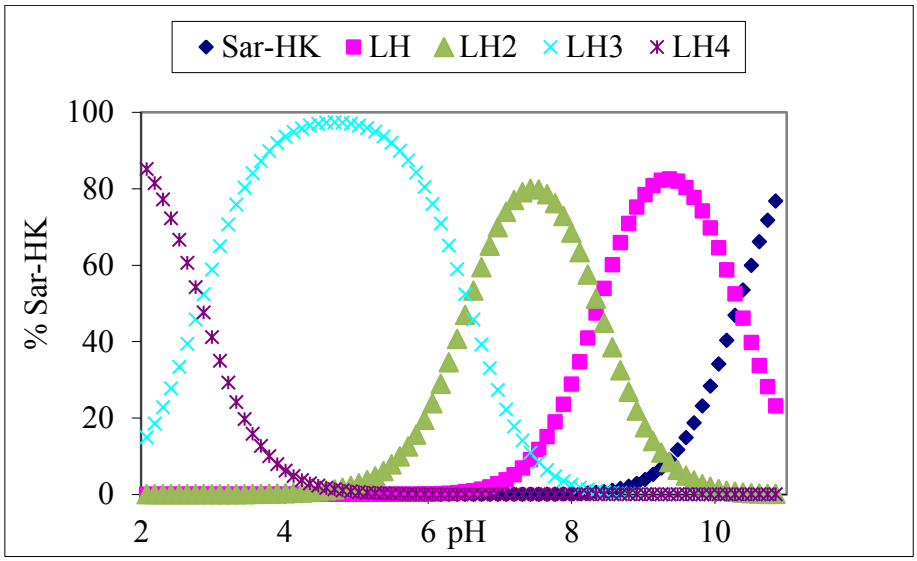

Figure 3.2: Distribution curve for the protonation of sarcosyl-L-histidyl-L-lysine

3.4.1.2 Protonation of sarcosyl-L-lysyl-L-histidine

The Z_H-bar function in Figure 3.3 indicates that there are four dissociable protons in the sarcosyl-L-lysyl-L-histidine. From pH 11.05 to pH 11.52, the Sar-Lys-His was completely deprotonated (Z_H-bar is zero).

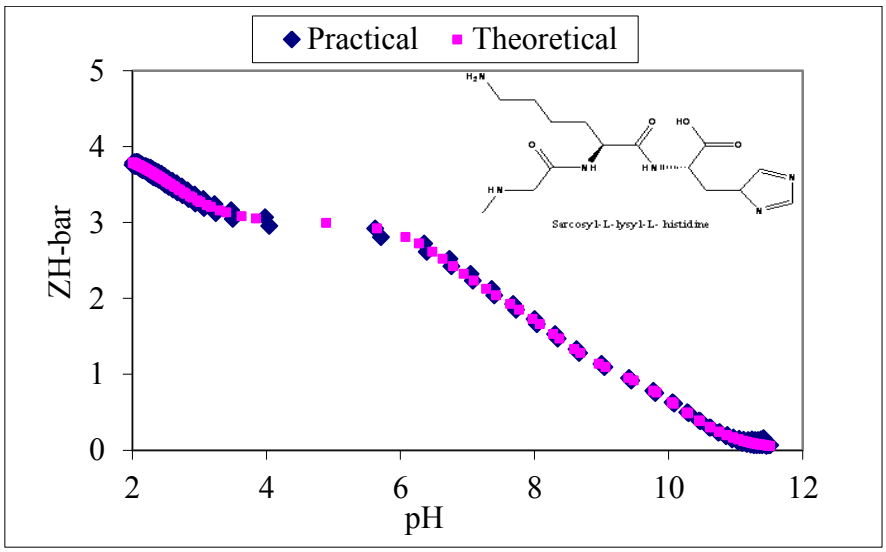

Figure 3.3: Z_H-bar for the protonation of sarcosyl-L-lysyl-L-histidine.

The graph rises from pH 10.87 to pH 6.28. From pH 6.08 to pH 3.85 the Z_H-bar = 3 was maintained. The graph rises from pH 3.63 to pH 2.08 where Z_H-bar ≈ 4 was reached. The excellent agreement between the experimental and theoretical curves as well as the low standard deviations and Hamilton R-factors lends confidence to this model. Table 3.2 shows calculated log β's for the sarcosyl-L-lysyl-L-histidine.

Table 3.2: Stability constants (log β_{pqr}) for sarcosyl-L-lysyl-L-histidine (SKH) β_{pqr} = [MpLqHr]/[M]p[L]q[H]r, I = 0.15 mol.dm^{-3} (NaCl), T = 25 ºC. S. dev denotes standard deviation in logβpqr; R_f^H is the Hamilton R-factor and R_{lim}^H its limit.

SKH	p	q	r	log β_{pqr}	S.dev	R_f^H	R_{lim}^H	$n_T(n_p)$
SKH-H	0	1	1	10.25	0.01			
SKH-H_2	0	1	2	18.55	0.02			
						0.001	0.002	2(130)
SKH-H_3	0	1	3	25.24	0.02			
SKH-H_4	0	1	4	27.81	0.02			

The calculated speciation graphs in Figure 3.4 show that the solution has a mixture of protonated species in the pH range of 2.19-10.85. This is because of the closeness of the pK_a values for the protonated sites of the ligand. At pH =8.80 only the neutral form of the ligand species is present in solution.

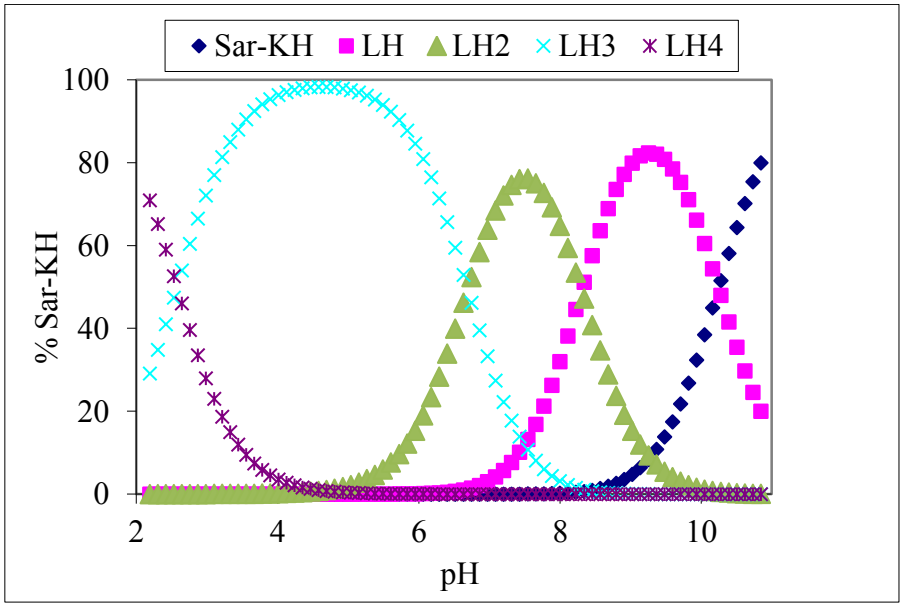

Figure 3.4: Distribution curve for the protonation of sarcosyl-L-lysyl-L-histidine.

3.4.1.3 Protonation of sarcosyl-L-histidyl-L-histidine

Figure 3.5 shows the formation function, Z_H-bar as a function of pH for the protonation of sarcosyl-L-histidyl-L-histidine. The Z_H-bar plot changed direction at pH 6.09-9.26, rose up and then levelled off at Z_H-bar ≈ 3 at pH 3.44 to 5.19, and increased slightly above pH 2.06. This implies that the ligand has four dissociable protons. The agreement between the theoretical and the experimental plot gives us confidence in the results.

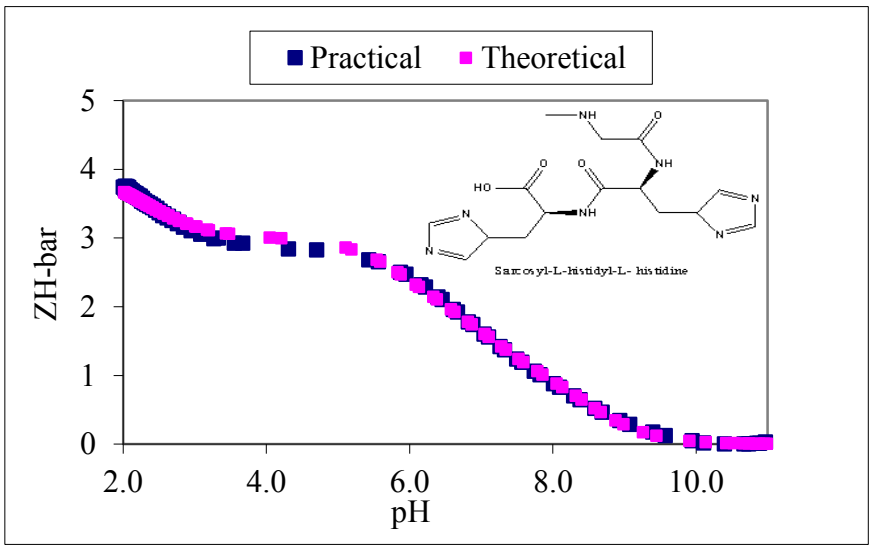

Figure 3.5: Z_H-bar for the protonation of sarcosyl-L-histidyl-L-histidine.

The experimental protonation constants of sarcosyl-L-histidyl-L-histidine are presented in Table 3.3. The standard deviations were small and the R^H was less than R^H_{lim} thus the model was within the maximum allowed experimental error.

Table 3.3: Stability constants (log β_{pqr}) for sarcosyl-L-histidyl-L-histidine (SHH) β_{pqr} = [MpLqHr]/[M]p[L]q[H]r, I = 0.15 mol.dm^{-3} (NaCl), T = 25 ºC. S. dev denotes standard deviation in logβ_{pqr}; R_f^H is the Hamilton R-factor and R_{lim}^H its limit.

SHH	p	q	r	log β_{pqr}	S.dev	R_f^H	R_{lim}^H	$n_T(n_p)$
SHH-H	0	1	1	08.57	0.02			
$SHH-H_2$	0	1	2	15.74	0.02	0.001	0.004	2(94)
$SHH-H_3$	0	1	3	21.64	0.03			
$SHH-H_4$	0	1	4	23.94	0.03			

The speciation diagrams in aqueous solution of sarcosyl-L-histidyl-L-histidine (Figure 3.6), confirms that the SHH-H_3 and SHH-H_4 species are predominant in the pH range 2.07 – 7.09 and the species SHH-H and SHH-H_2 dominates in the pH range 4.01 – 10.05, respectively.

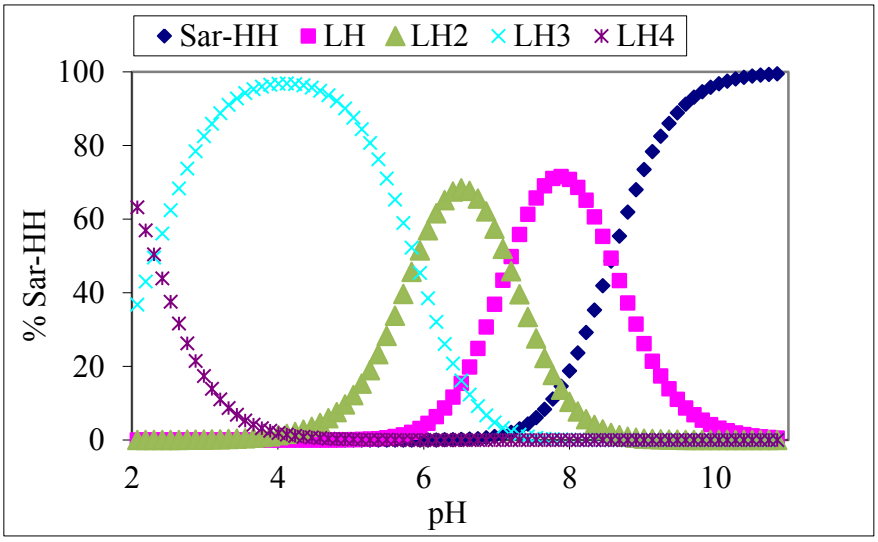

Figure 3.6: Distribution curve for the protonation of sarcosyl-L-histidyl-L-histidine.

3.4.1.4 Protonation of sarcosyl-L-lysyl-L-lysine

Figure 3.7 indicates that sarcosyl-L-lysyl-L-lysine contains four measurable protonation sites as revealed by the levelling off of the Z_H-bar = 4 at the pH 2.02, indicating that four protons were added to the ligand.

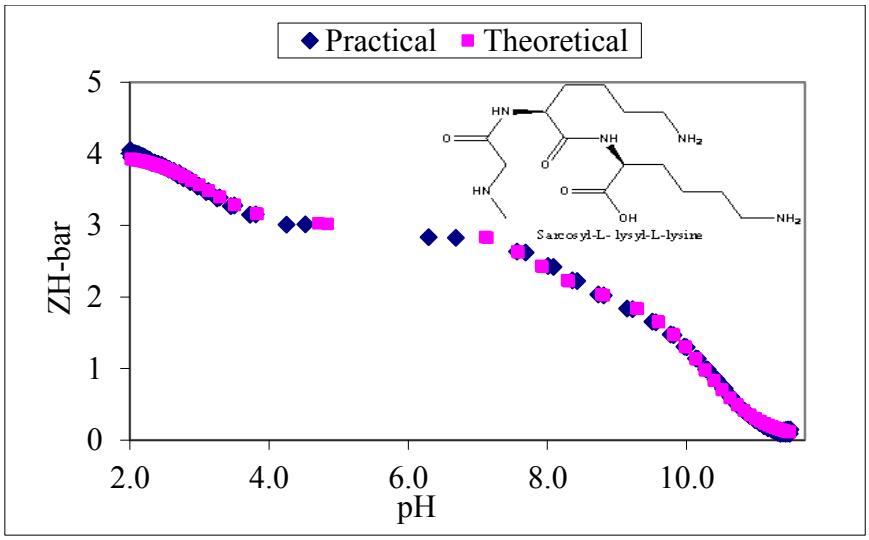

Figure 3.7: Z_H-bar for the protonation of sarcosyl-L-lysyl-L-lysine.

The function levels to zero at a high pH of 11.49, indicating that this completely deprotonated at this pH. The protonation of sarcosyl-L-lysyl-L-lysine has been reported in Table 3.4. However, the errors for log β's are small and R_f^H is less than R^H_{lim}. An excellent agreement between theoretical and experimental functions supports and gives confidence in the results.

Table 3.4: Stability constants (log β_{pqr}) for sarcosyl-L-lysyl-L-lysine (SKK) β_{pqr} = [MpLqHr]/[M]p[L]q[H]r, I = 0.15 mol.dm^{-3} (NaCl), T = 25 ºC. S. dev denotes standard deviation in logβ_{pqr}; R_f^H is the Hamilton R-factor and $R_{lim}{}^H$ its limit.

SKK	p	q	r	log β_{pqr}	S.dev	R_f^H	$R_{lim}{}^H$	$n_T(n_p)$
SKK-H	0	1	1	10.54	0.02	0.001	0.002	2(132)
$SKK-H_2$	0	1	2	20.49	0.01			
$SKK-H_3$	0	1	3	28.29	0.03			
$SKK-H_4$	0	1	4	31.40	0.03			

These four species are also confirmed by the distribution species diagram in Figure 3.8. The mono-protonated and the di-protonated species are predominant in the pH range 6.63 -10.58 respectively in aqueous solution.

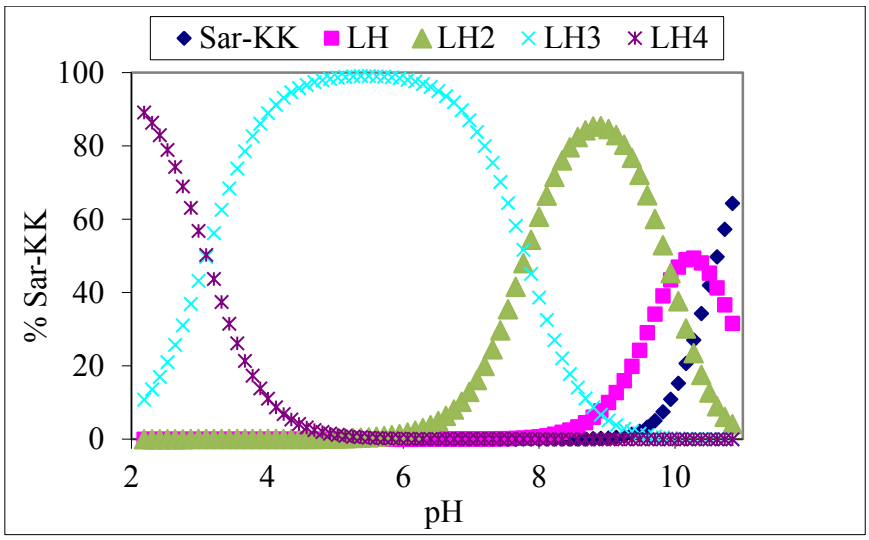

Figure 3.8: Distribution curve for the protonation of sarcosyl-L-lysyl-L-lysine.

3.4.1.5 Protonation of sarcosyl-L-glycyl-L-histidine

Figure 3.9 shows average number of protons bound to sarcosyl-L-glycyl-L-histidine as a function of pH. The protonation function curve indicates that there are three dissociable protons in SGH. The levelling off at Z_H-bar = 2 reflects two similar protons added to the

terminal amino groups and the rising of the curve at pH =2.05 is indicative of a proton adding to the imidazole nitrogen group. At high pH (pH = 9.74) the curve levels off at zero indicating that the last proton is lost at this pH.

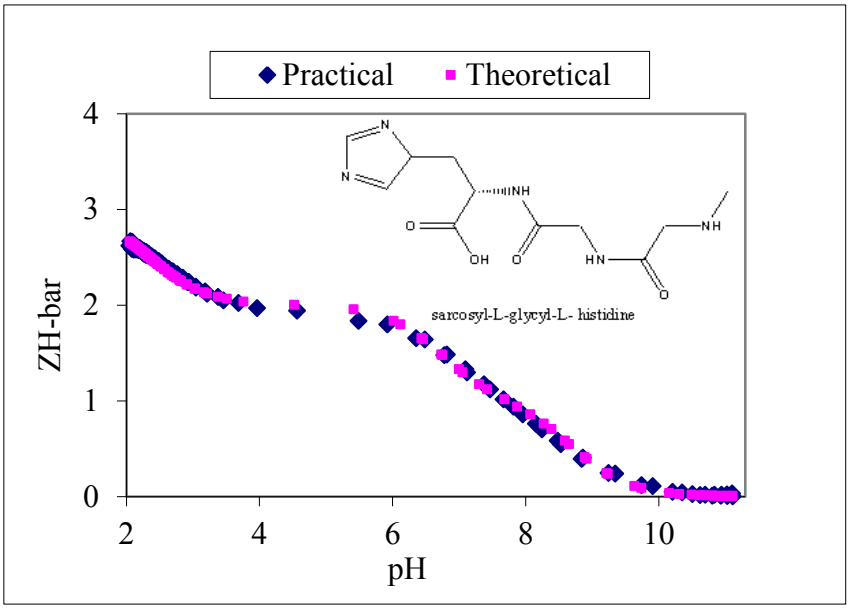

Figure 3.9: Z_H-bar for the protonation of sarcosyl-L-glycyl-L-histidine.

The superimposability of the theoretical and experimental Z_H-bar curves of Sar-Gly-His concentrations and this, as well as the low standard deviations and Hamilton R-factors confirm the validity of this model. Log β's values are given in Table 3.5.

Table 3.5: Stability constants (log β_{pqr}) for sarcosyl-L-glycyl-L-histidine (SGH) β_{pqr} = [MpLqHr]/[M]p[L]q[H]r, I = 0.15 mol.dm^{-3} (NaCl), T = 25 ºC. S. dev denotes standard deviation in logβ_{pqr}; R_f^H is the Hamilton R-factor and R_{lim}^H its limit.

SGH	p	q	r	log β_{pqr}	S.dev	R_f^H	R_{lim}^H	$n_T(n_p)$
SGH-H	0	1	1	08.72	0.02			
$SGH-H_2$	0	1	2	15.44	0.02	0.004	0.005	2(87)
$SGH-H_3$	0	1	3	17.79	0.03			

The calculated and species distribution curves shown in Figure 3.10 indicate that the solution has a mixture of mono-protonated; di-protonated and tri-protonated species in the pH range 2.19 – 10.16.

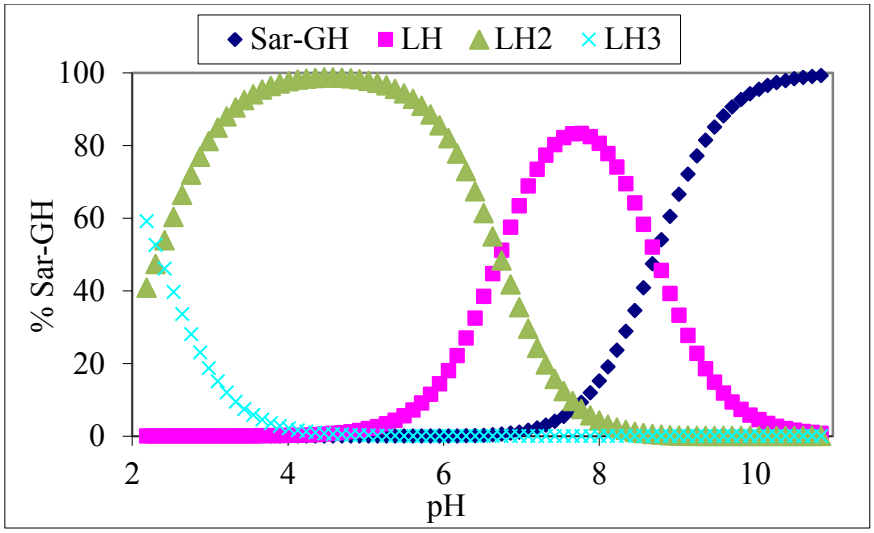

Figure 3.10: Distribution curve for the protonation of sarcosyl-L-glycyl-L-histidine.

3.4.2 Complex formation titrations

Two functions, the formation (Z_M-bar) and the deprotonation functions (Q-bar) were used to investigate the reproducibility of the experimental data and the reliability of evaluated log β_{pqr} values. The complex formation function, Z_M-bar, measures the average number of ligands bound per metal ion due to complexation. This function is plotted against the negative logarithm of the free ligand concentration (logA). The deprotonation function, Q-bar, indicates the average number of protons released due to complexation and is plotted against the pH of the solution. Q-bar is evaluated in conjunction with the *n*-bar function, which measures the average number of protons that would be bound to the ligand in the absence of complexation. These two functions serve two purposes. Firstly, they give a visual check on the experimental data and secondly, their shape gives an idea of the speciation model applicable to the system. However, if the curves at different metal: ligand ratios are not superimposable, protonated or polynuclear species formation is indicated, while if the Z_M-bar curves fan back hydroxyl species formation is indicated.

3.4.2.1 Sarcosyl-L-histidyl-L-lysine complexes

3.4.2.1.1 Cu(II)/Sarcosyl-L-histidyl-L-lysine

Figure 3.11 shows the complex formation function (Z_M-bar) levels off at value of ≈1.0 for mononuclear species formation indicating the presence of CuSHK as a major species. It is independent of component ratios and concentrations, suggesting a complex stoichiometry of 1: 1. As the titration continues, the curves rise steeply and fan back indicating the formation

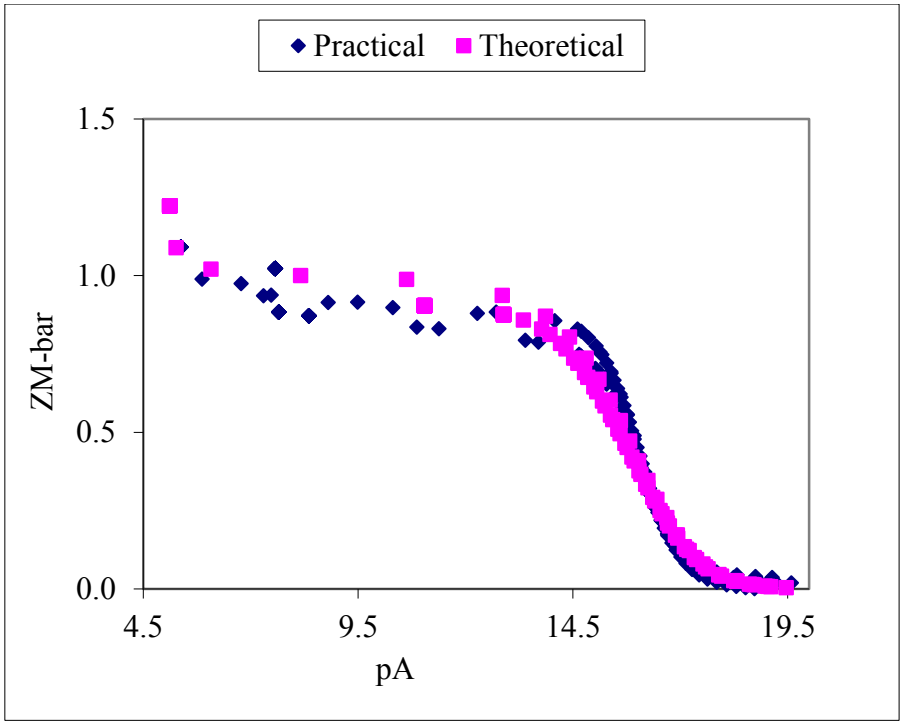

Figure 3.11: Z_M-bar as a function of pA for Cu(II) sarcosyl-L-histidyl-L-lysine complex.

of mixed-hydroxo complex species [21]. The stability constants (log β_{pqr}) are given in Table 3.6. The standard deviations are small and R_f^H is less than R_{lim}^H. This lends confidence to the model.

Table 3.6: Stability constants (log β_{pqr}) for Cu(II) sarcosyl-L-histidyl-L-lysine complex $\beta_{pqr} = [M_pL_qH_r]/[M]p[L]q[H]r$, I = 0.15 mol.dm^{-3} (NaCl), T = 25 ºC. S. dev denotes standard deviation in logβ_{pqr}; R_f^H is the Hamilton R-factor and R_{lim}^H its limit, n_T is the number of titrations, (n_P) is the number of titration points.

Complexes	p	q	r	log β_{pqr}	S.dev	R_f^H	R_{lim}^H	$n_T(n_p)$
CuSHK-H	1	1	1	20.05	0.03	0.002	0.003	4(202)
CuSHK	1	1	0	15.54	0.03			
CuSHK-H$_{-1}$	1	1	-1	6.09	0.05			
CuSHK-H$_{-2}$	1	1	-2	-4.55	0.05			

The total number of dissociable protons on the ligand (n-bar) and the total number protons lost upon complexation of Cu(II) with SHK (Q_M-bar) are shown in Figure 3.12. At a pH of 2.50, Q_M-bar is greater than zero indicating that complexation has already commenced. The function then increases rapidly in the pH range 2.50-5.50 to a maximum value of 2.56

indicating the release of approximately three protons due to complex formation. Form pH 5.50 to pH 8.84 Q_M-bar is parallel to n-bar indicating that no more protons are displaced by the metal in this pH range. Above pH 8.7 the curve rises again moving above the n-bar curve, which indicates that hydroxo species have begun to form. The theoretical plot and the practical plot are superimposable; this gives confidence in the results.

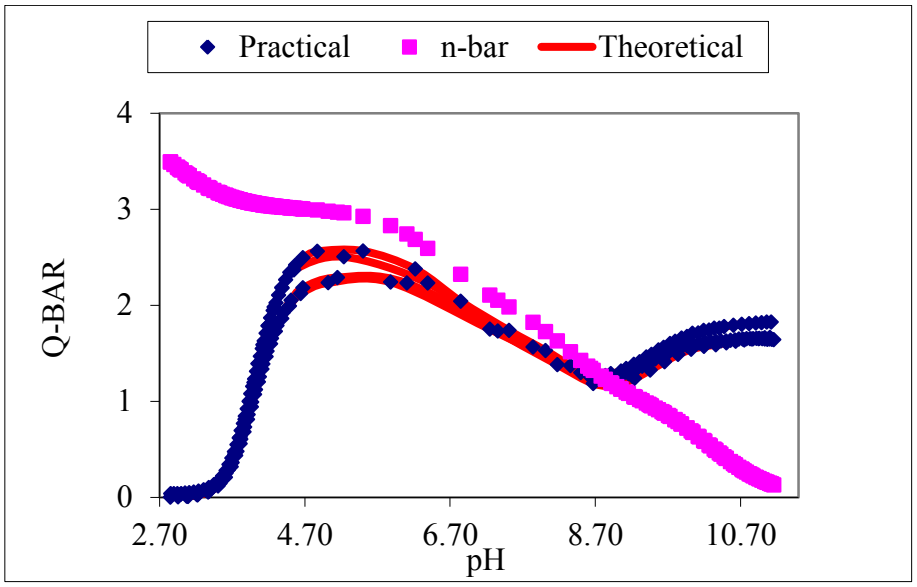

Figure 3.12: Q_M-bar as a function of pH for Cu(II) sarcosyl-L-histidyl-L-lysine complex.

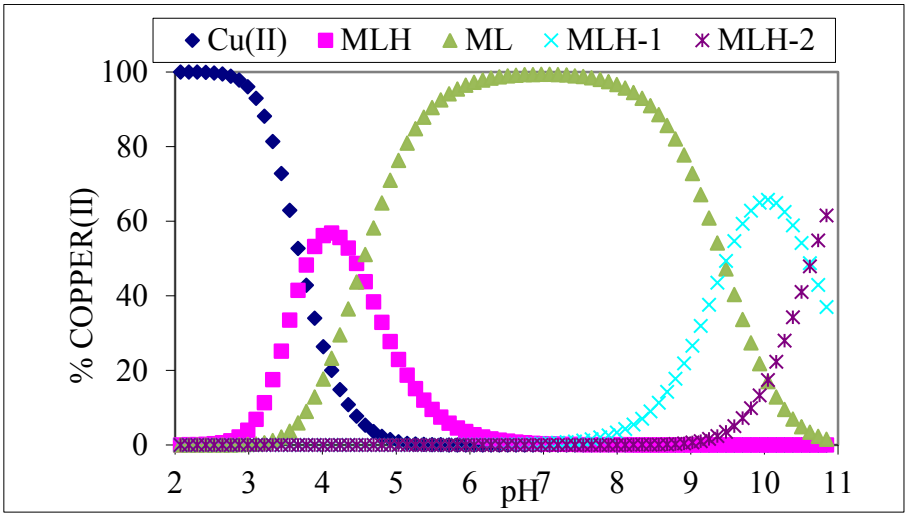

Figure 3.13: The distribution curve for the Cu(II) sarcosyl-L-histidyl-L-lysine complex.

The species distribution curves in above Figure 3.13 shows that different species predominate at different regions of the pH range. At pH 7.05 a high % Cu(II) peak is observed for CuSHK species and the lowest % Cu(II) peak is observed for CuSHK-H species at pH 4.13.

The Z_M-bar and Q-bar plots concur with the species distribution curves as shows in Figure 3.13.

3.4.2.1.2 Ni(II)/Sarcosyl-L-histidyl-L-lysine

Z_M-bar for Ni(II) sarcosyl-L-histidyl-L-lysine is given in Figure 3.14. At pA 11.02 the graph rises and fans back at pA 6.09 indicating the formation of hydroxo species. The optimised stability constants are given in Table 3.7.

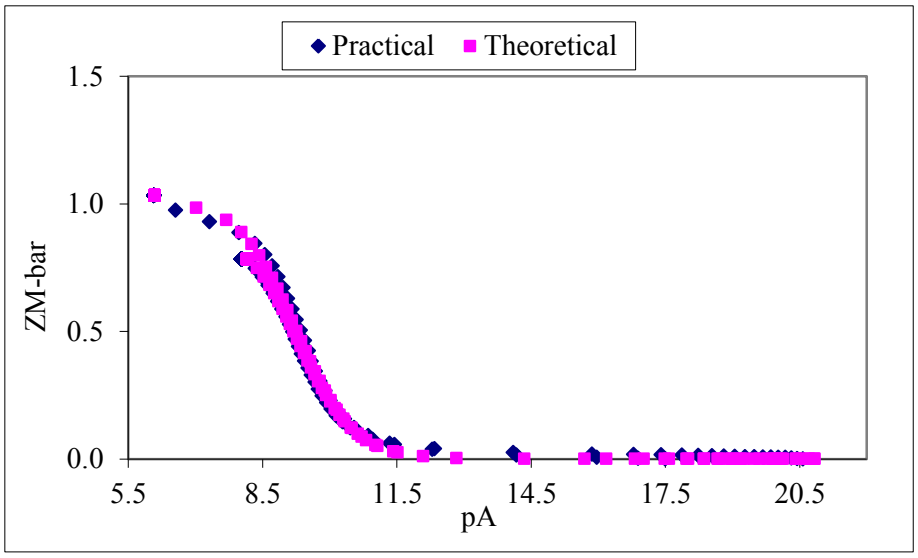

Figure 3.14: Z_M-bar as a function of pA for Ni(II) sarcosyl-L-histidyl-L-lysine complex.

Table 3.7: Stability constants (log β_{pqr}) for Ni(II) sarcosyl-L-histidyl-L-lysine complex $\beta_{pqr} = [M_pL_qH_r]/[M]p[L]q[H]r$, I = 0.15 mol.dm^{-3} (NaCl), T = 25 ºC. S. dev denotes standard deviation in logβ_{pqr}; R_f^H is the Hamilton R-factor and R_{lim}^H its limit, n_T is the number of titrations, (n_P) is the number of titration points.

Complexes	p	q	r	log β_{pqr}	S.dev	R_f^H	R_{lim}^H	$n_T(n_p)$
NiSHK-H	1	1	1	15.47	0.03	0.01	0.003	2(147)
NiSHK	1	1	0	09.27	0.01			
NiSHK-H$_{-1}$	1	1	-1	-0.33	0.02			
NiSHK-H$_{-2}$	1	1	-2	-10.40	0.02			

The Q_M-bar for Ni(II) sarcosyl-L-histidyl-L-lysine titrations is given in Figure 3.15. Sar-His-Lys has four dissociable protons and it loses three protons upon complexation with Ni(II). From pH 8.0 to pH 10.85, the system consists mostly of hydroxo species NiSHK-H$_{-1}$

and NiSHK-H_{-2}. The distribution graph for Ni(II) Sar-His-Lys titrations is shown in Figure 3.16, where the complexation occurs from pH 5.26 to pH 10.86.

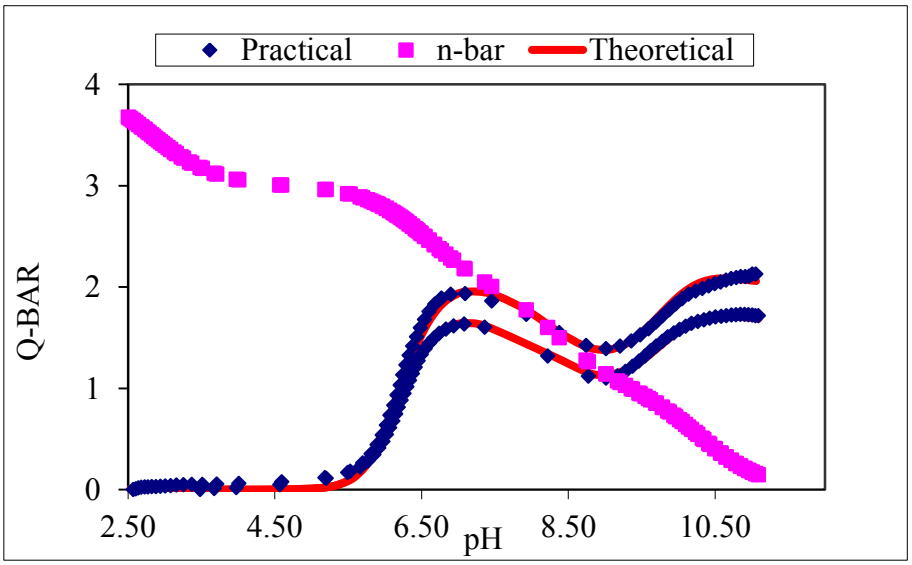

Figure 3.15: Q_M-bar as a function of pH for Ni(II) sarcosyl-L-histidyl-L-lysine complex.

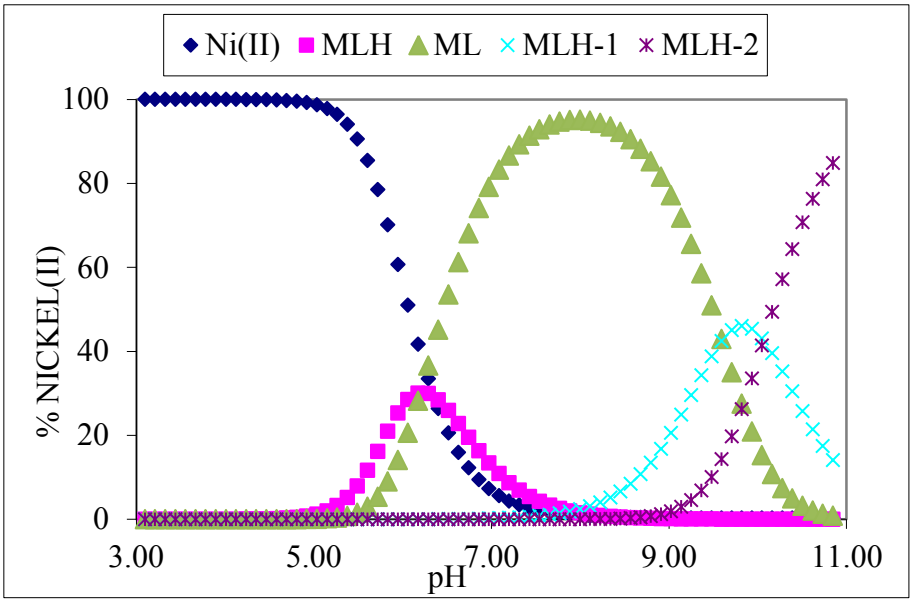

Figure 3.16: The distribution curve for the Ni(II) sarcosyl-L-histidyl-L-lysine complex**.**

3.4.2.1.3 Zn(II)/Sarcosyl-L-histidyl-L-lysine

Z_M-bar for Zn(II) Sar-His-Lys is given in Figure 3.17. The curves resemble those of Zn(II) Sar-His-Lys in the splitting pattern when varying the metal to ligand ratio. The fanning back of the complex formation function at a pA of 6.21 is indicative of mixed hydroxo species.

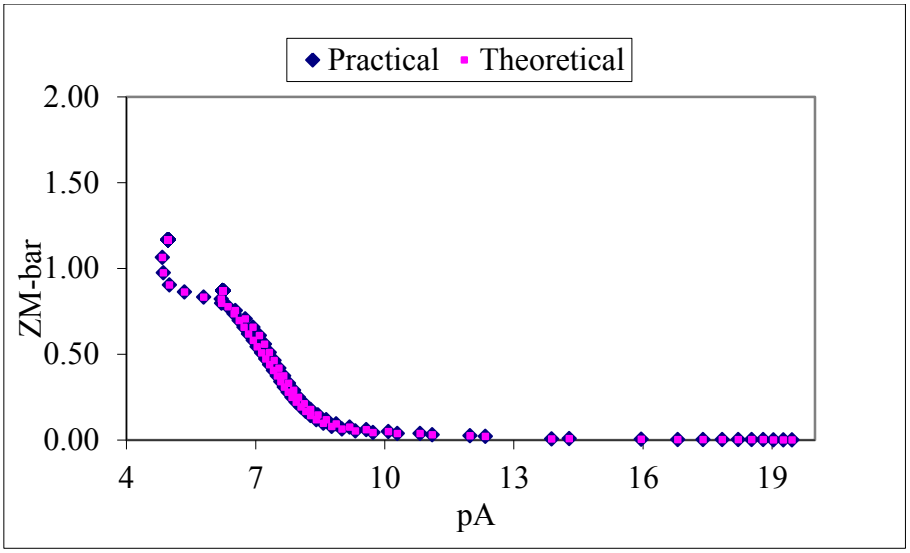

Figure 3.17: Z_M-bar as a function of pA for Zn(II) sarcosyl-L-histidyl-L-lysine complex.

Figure 3.5 shows that the Q-bar function increases in the pH range of 5.29 to 7.37 followed by rising up from pH 9.0, indicating hydroxo species formation. This also means that complexation begins at about pH 5.20.

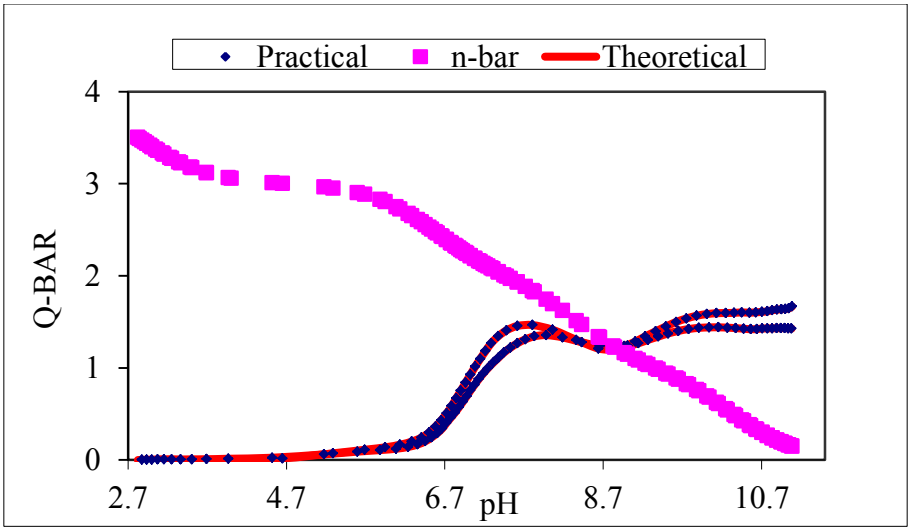

Figure 3.18: Q_M-bar as a function of pH for Zn(II) sarcosyl-L-histidyl-L-lysine complex.

Table 3.8 shows four species obtained in the complexation of Zn(II) with Sar-His-Lys and their stability constants. The standard deviations are reasonably low, and the Hamiltonian R-factor is low thus giving confidence for the model chosen.

Table 3.8: Stability constants (log β_{pqr}) for Zn(II) sarcosyl-L-histidyl-L-lysine complex $\beta_{pqr} = [M_pL_qH_r]/[M]p[L]q[H]r$, I = 0.15 mol.dm^{-3} (NaCl), T = 25 ºC. S. dev denotes standard deviation in logβ_{pqr}; R_f^H is the Hamilton R-factor and R_{lim}^H its limit, n_T is the number of titrations, (n_P) is the number of titration points.

Complexes	p	q	r	log β_{pqr}	S.dev	R_f^H	R_{lim}^H	$n_T(n_p)$
ZnSHK-H	1	1	1	14.39	0.03	0.01	0.004	2(129)
ZnSHK	1	1	0	07.25	0.02			
ZnSHK-H$_{-1}$	1	1	-1	-2.21	0.04			
ZnSHK-H$_{-2}$	1	1	-2	-13.23	0.05			

Speciation for Zn(II) Sar-His-Lys is given in Figure 3.19. The ZnSHK-H distribution curve is for small species and reaches to 36.78 % formation at pH 6.97. From pH 6.18 to 10.73, the predominant species present in solution is ZnSHK and from the pH 7.89 to 10.85 the hydroxo species (ZnSHK-H$_{-1}$ and ZnSHK-H$_{-2}$) have begun to form.

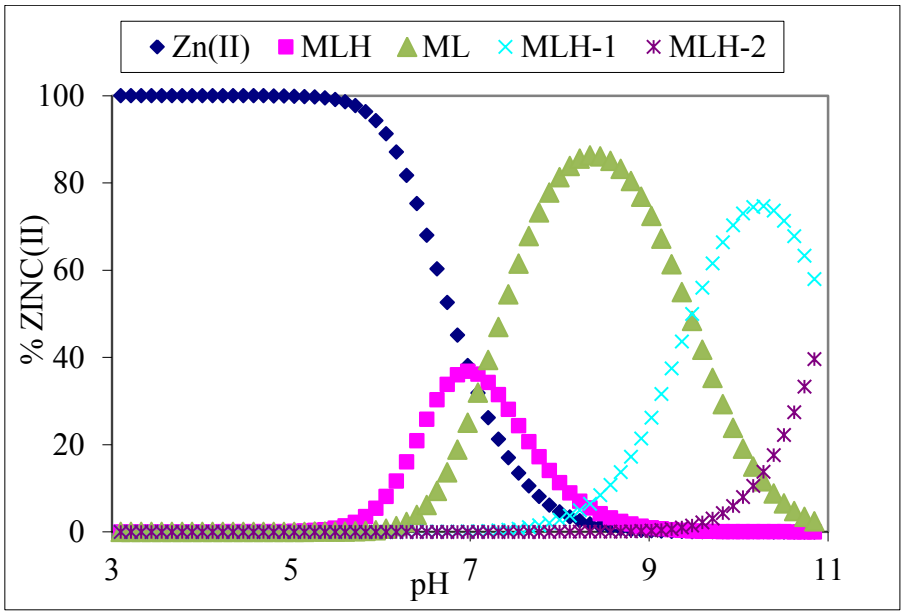

Figure 3.19: The distribution curve for the Zn(II) sarcosyl-L-histidyl-L-lysine complex**.**

3.4.2.2 Sarcosyl-L-lysyl-L-histidine complexes

3.4.2.2.1 Cu(II)/Sarcosyl-L-lysyl-L-histidine

Figure 3.20 shows the formation of function curve, Z_M-bar against pL for Cu(II) sarcosyl-L-lysyl-L-histidine at 25ºC in 0.15 M NaCl. The complexation curves for various metals to ligand ratios starts at pA=14, the formation function rises and the fans back, thus indicating

the formation of hydroxo or mixed-hydroxo complex species in solution. The agreement between the theoretical and practical complex formation curves at different metal to ligand ratios supports the potentiometric model chosen in data analysis.

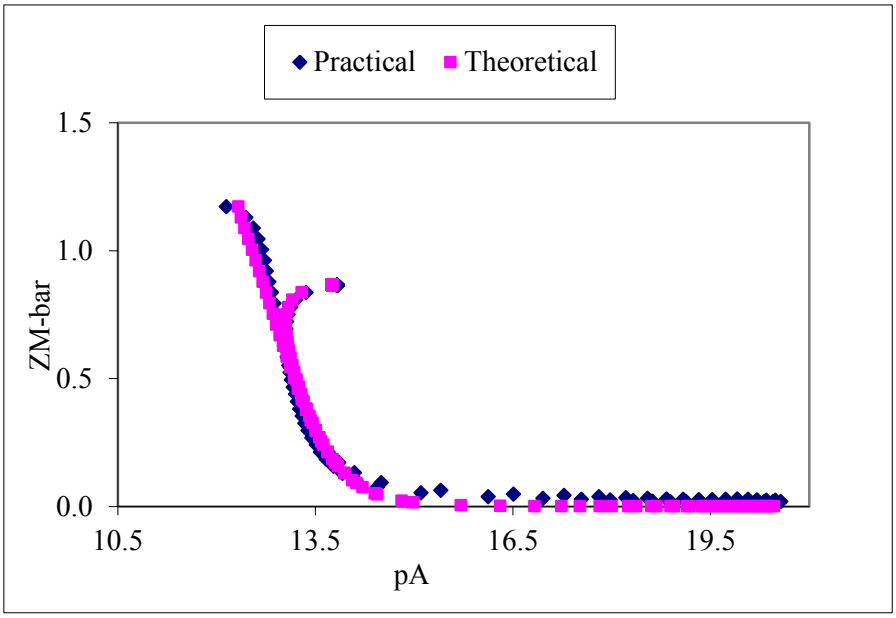

Figure 3.20: Z_M-bar as a function of pA for Cu(II) sarcosyl-L-lysyl-L-histidine complex.

Figure 3.21 shows that at pH values 2.52 the deprotonation function Q-bar of zero indicates that no protons have been displaced due to complexation. The splitting pattern of the curves follows that of the formation curves the protonation function n-bar has a value of 3.53 at this pH confirming that the ligand is still protonated at low pH. For pH values above 4.50 the deprotonation function Q-bar rapidly rises to intersect the protonation curve, n-bar, at a pH of 5.80, reaching a maximum value of about 3.32. The falling of the curves at about pH 6.40 shows that complexation is complete. At about pH 10.09 levelling off at Q-bar = 2 is due to the formation of hydroxo species $CuSKH\text{-}H_{-2}$. This means that two additional protons have been displaced per metal ion from the ligand, resulting in the ligand losing a total of four protons.

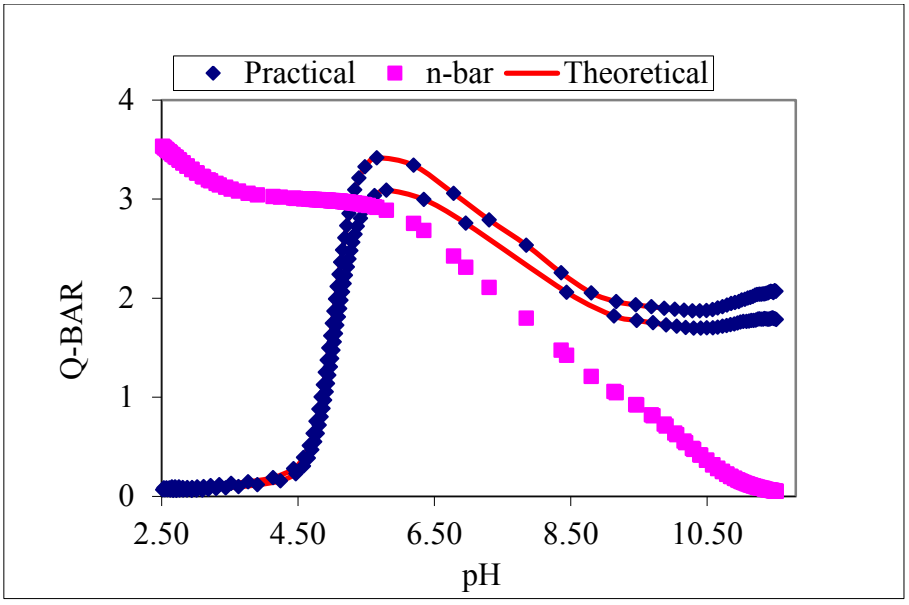

Figure 3.21: Q_M-bar as a function of pH for Cu(II) sarcosyl-L-lysyl-L-histidine complex.

Table 3.9 shows that four species were obtained in the complexation of Cu(II) with Sar-Lys-His (SKH) and their stability constants are also shown. The reported standard deviations of the log β_{pqr} values obtained from potentiometry are reasonably low.

Table 3.9: Stability constants (log β_{pqr}) for Cu(II) sarcosyl-L-lysyl-L-histidine complex $\beta_{pqr} = [M_pL_qH_r]/[M]p[L]q[H]r$, I = 0.15 mol.dm^{-3} (NaCl), T = 25 ºC. S. dev denotes standard deviation in logβ_{pqr}; R_f^H is the Hamilton R-factor and R_{lim}^H its limit, n_T is the number of titrations, (n_P) is the number of titration points.

Complexes	p	q	r	log β_{pqr}	S.dev	R_f^H	R_{lim}^H	$n_T(n_p)$
CuSKH-H	1	1	1	17.2	0.3			
CuSKH	1	1	0	12.96	0.04			
						0.01	0.01	2(178)
CuSKH-H$_{-1}$	1	1	-1	7.55	0.03			
CuSKH-H$_{-2}$	1	1	-2	-2.80	0.05			

The species distribution curve for the complexes of Sar-Lys-His and Cu(II) is shown in Figure 3.22. At pH 4.0, there is 100 % of the free metal ion species. Around pH 4.24, the CuSKH-H species began to form and this is a very small species. The proportion of this species began to fall at pH 5.15, where the formation of CuSKH-H$_{-1}$ commenced; it was formed at the expense of the CuSKH species. The maximum amount of CuSKH-H$_{-2}$ species present in solution at pH 10.85 is 75%.

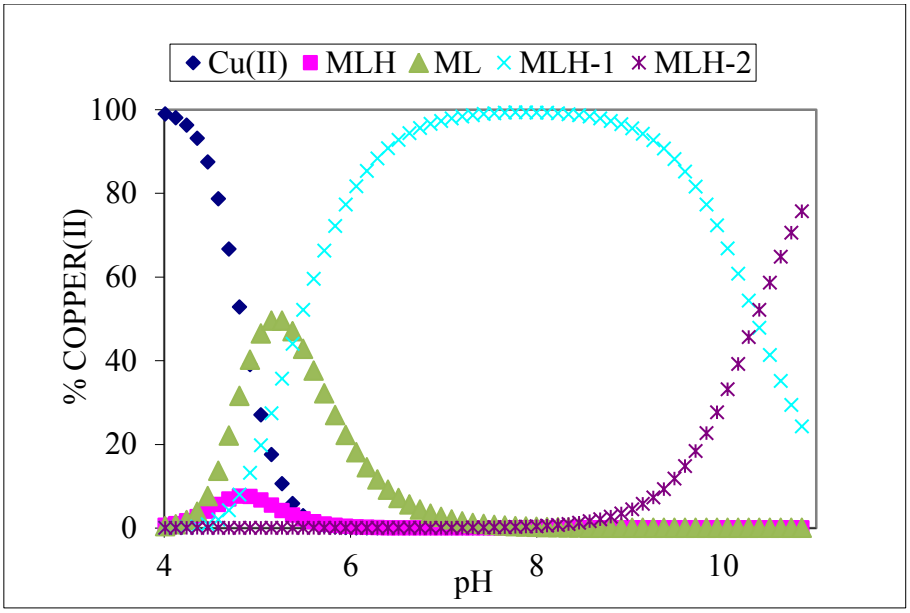

Figure 3.22: The distribution curve for the Cu(II) sarcosyl-L-lysyl-L-histidine complex.

3.4.2.2.2 Ni(II)/Sarcosyl-L-lysyl-L-histidine

The Z_M-bar for the complexes of sarcosyl-L-lysyl-L-histidine and Ni(II) is shown in Figure 3.23. It starts to fan back indicating that the NiSKH species did not predominant in solution due to the formation of hydroxo complex species.

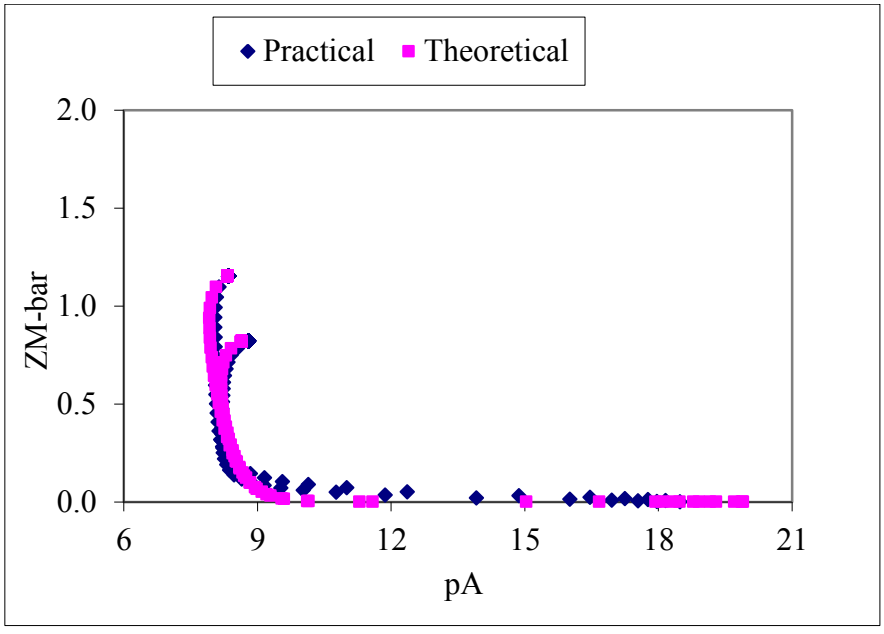

Figure 3.23: Z_M-bar as a function of pA for Ni(II) sarcosyl-L-lysyl-L-histidine complex.

Sar-Lys-His (SKH) has four dissociable protons and it loses two protons upon complexation with Ni(II) (Figure 3.24). The hydroxo species has been formed at pH 9.05. The stability

constants of the complexes of Ni(II) and Sar-Lys-His are presented in Table 3.10. These stability constants were not similar to those of the species from the Cu(II) system.

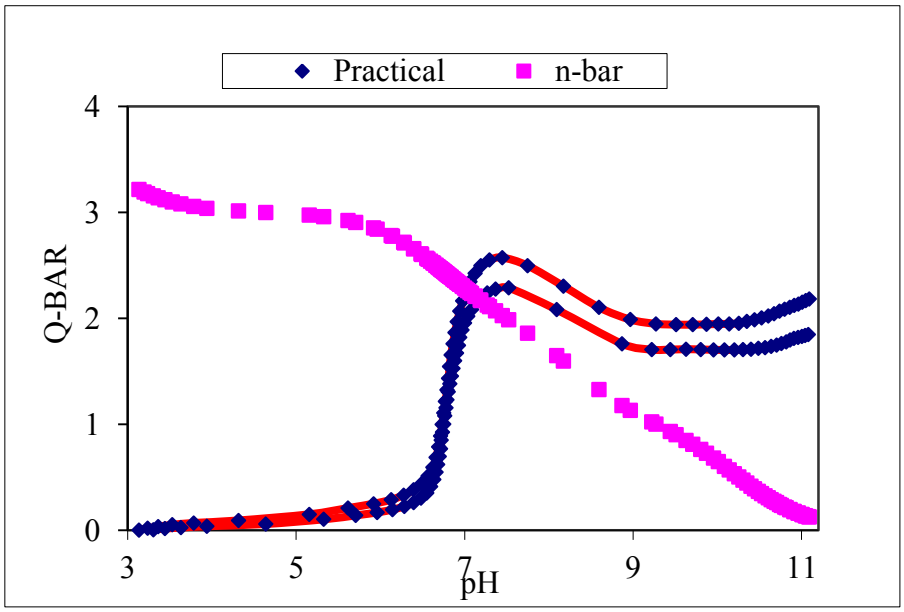

Figure 3.24: Q_M-bar as a function of pH for Ni(II) sarcosyl-L-lysyl-L-histidine complex.

Table 3.10: Stability constants (log β_{pqr}) for Ni(II) sarcosyl-L-lysyl-L-histidine complex $\beta_{pqr} = [M_pL_qH_r]/[M]p[L]q[H]r$, I = 0.15 mol.dm^{-3} (NaCl), T = 25 ºC. S. dev denotes standard deviation in logβ_{pqr}; R_f^H is the Hamilton R-factor and R_{lim}^H its limit, n_T is the number of titrations, (n_P) is the number of titration points.

Complexes	p	q	r	log β_{pqr}	S.dev	R_f^H	R_{lim}^H	$n_T(n_p)$
NiSKH	1	1	0	07.66	0.06			
NiSKH-H$_{-1}$	1	1	-1	0.88	0.03	0.01	0.004	2(139)
NiSKH-H$_{-2}$	1	1	-2	-9.52	0.06			

The distribution graph for Ni(II) Sar-Lys-His is given in Figure 3.25. There was no chemical change from pH 2.00 to pH 5.70. At pH 6.18, the NiSKH species began to form. A maximum of 30.42 % of this species was observed in solution at pH 6.86. The NiSKH-H$_{-1}$ species began to form around the same pH. A maximum of 96.87 % of NiSKH-H$_{-1}$ species was observed at pH 8.57. NiSKH-H$_{-2}$ species began to form at pH 8.57 and there were only two species in solution. The NiSKH-H$_{-1}$ and the NiSKH-H$_{-2}$ species were present at pH 9.48.

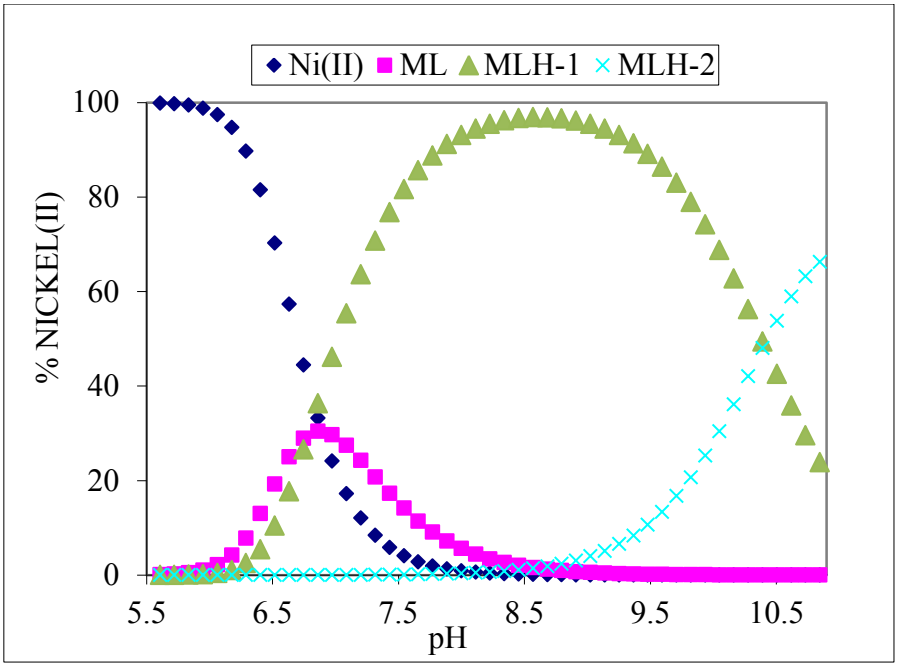

Figure 3.25: The distribution curve for the Ni(II) sarcosyl-L-lysyl-L-histidine complex.

3.4.2.2.3 Zn(II)/Sarcosyl-L-lysyl-L-histidine

Z_M-bar for Zn(II) sarcosyl-L-lysyl-L-histidine is given in Figure 3.26. The curves do not level off and resemble those in the splitting pattern obtained by varying the metal to ligand ratio. The rising and fanning back of the complex formation function at pA of 7.01 is indicative of mixed hydroxo species.

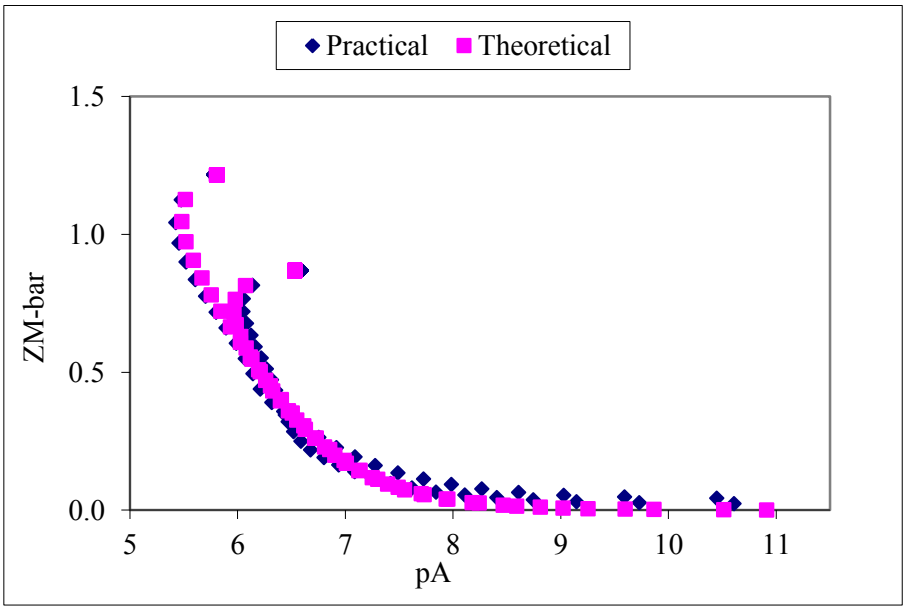

Figure 3.26: Z_M-bar as a function of pA for Zn(II) sarcosyl-L-lysyl-L-histidine complex.

Table 3.11 shows the formation of four species in the complexation of Zn(Il) with Sar-Lys-His and their stability constants. The standard deviations are reasonably low and are not far from those obtained in the Cu(II)- Sar-Lys-His complexation. The Hamiltonian R-factor is low thus giving confidence for the model chosen.

Table 3.11: Stability constants (log β_{pqr}) for Zn(II) sarcosyl-L-lysyl-L-histidine complex $\beta_{pqr} = [M_pL_qH_r]/[M]p[L]q[H]r$, I = 0.15 mol.dm^{-3} (NaCl), T = 25 ºC. S. dev denotes standard deviation in logβ_{pqr}; R_f^H is the Hamilton R-factor and R_{lim}^H its limit, n_T is the number of titrations, (n_P) is the number of titration points.

Complexes	p	q	r	log β_{pqr}	S.dev	R_f^H	R_{lim}^H	$n_T(n_p)$
ZnSKH-H	1	1	1	13.30	0.06	0.01	0.005	2(140)
ZnSKH	1	1	0	6.20	0.02			
ZnSKH-H$_{-1}$	1	1	-1	-2.66	0.06			
ZnSKH-H$_{-2}$	1	1	-2	-13.66	0.10			

However, Sar-Lys-His loses two protons upon complexation with Zn(II). Q_M-bar rises from pH 6.56 and levels off between pH 8.41 and pH 10.96 (Figure 3.27). There is a small depression between pH 10.10 and pH 10.90. This shows that ZnL forms between pH 6.52 and pH 10.28. The depression is due to the formation of hydroxo species.

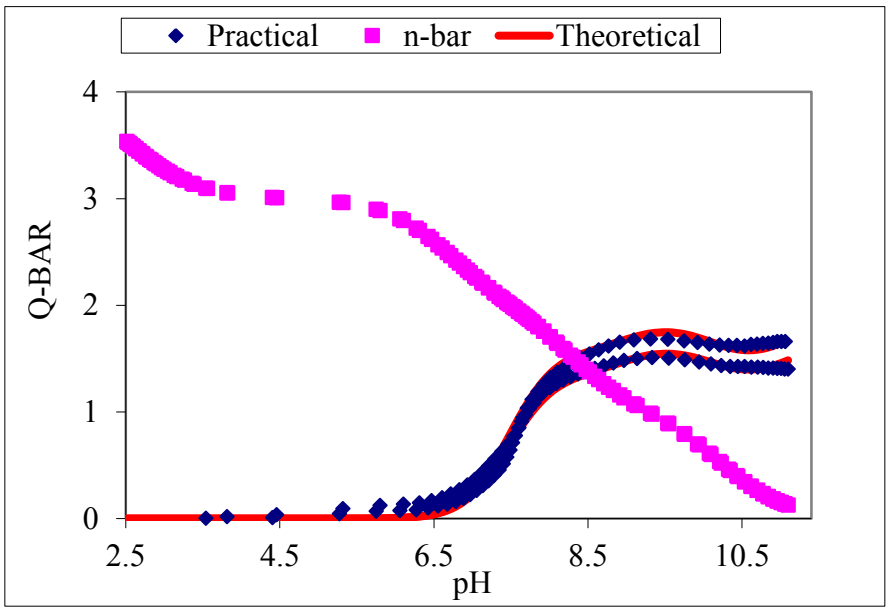

Figure 3.27: Q_M-bar as a function of pH for Zn(II) sarcosyl-L-lysyl-L-histidine complex.

Furthermore, the calculated species distribution curves (Figure 3.28) show that the protonated species (ZnSKH-H) is present at pH 7.32 and a very small amount of Zn(II) also exists. There were ZnSKH, ZnSKH-H_{-1} and ZnSKH-H_{-2} in the whole pH range investigated indicating complexed Zn(II) ions in the solution.

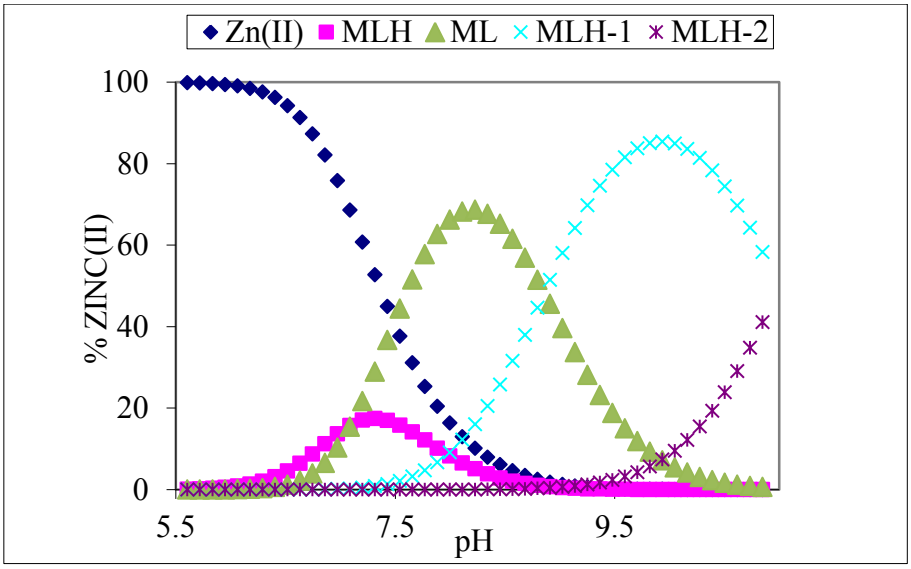

Figure 3.28: The distribution curve for the Zn(II) sarcosyl-L-lysyl-L-histidine complex.

3.4.2.3 Sarcosyl-L-histidyl-L-histidine Complexes

3.4.2.3.1 Cu(II)/Sarcosyl-L-histidyl-L-histidine

Z_M-bar for Cu(II) and sarcosyl-L-histidyl-L-histidine titrations is given in Figure 3.29. At pA of 14.00 the Z_M-bar rising and fanning back of the complex formation function was indicative of mixed hydroxo species.

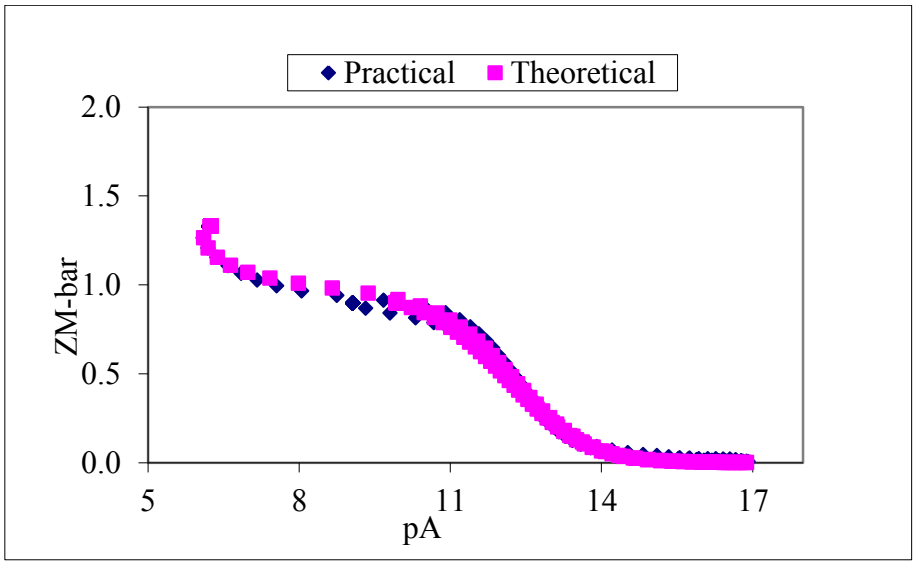

Figure 3.29: Z_M-bar as a function of pA for Cu(II) sarcosyl-L-histidyl-L-histidine complex.

The species and their equilibrium constants are given in Table 3.12. The errors are small; R_f^H is less than R_{lim}^H and the agreement between the theoretical and experimental formation and deprotonation functions as well as the reproducibility of repeat titrations at different metal: ligand ratio also lends confidence to the model.

Table 3.12: Stability constants (log β_{pqr}) for Cu(II) sarcosyl-L-histidyl-L-histidine complex $\beta_{pqr} = [M_pL_qH_r]/[M]p[L]q[H]r$, I = 0.15 mol.dm^{-3} (NaCl), T = 25 ºC. S. dev denotes standard deviation in logβ_{pqr}; R_f^H is the Hamilton R-factor and R_{lim}^H its limit, n_T is the number of titrations, (n_P) is the number of titration points.

Complexes	p	q	r	log β_{pqr}	S.dev	R_f^H	R_{lim}^H	$n_T(n_p)$
CuSHH-H	1	1	1	16.40	0.02	0.01	0.02	2(152)
CuSHH	1	1	0	12.01	0.02			
$CuSHH\text{-}H_{-1}$	1	1	-1	5.27	0.03			
$CuSHH\text{-}H_{-2}$	1	1	-2	-3.780	0.04			

Q_M-bar for Sar-His-His titration is given in Figure 3.30. Sar-His-His loses three protons upon complexation with Cu(II). Q_M-bar rises at pH 2.76, drops at pH 6.14 and levels off between pH 9.13 and pH 10.96 indicating the formation of hydroxo species.

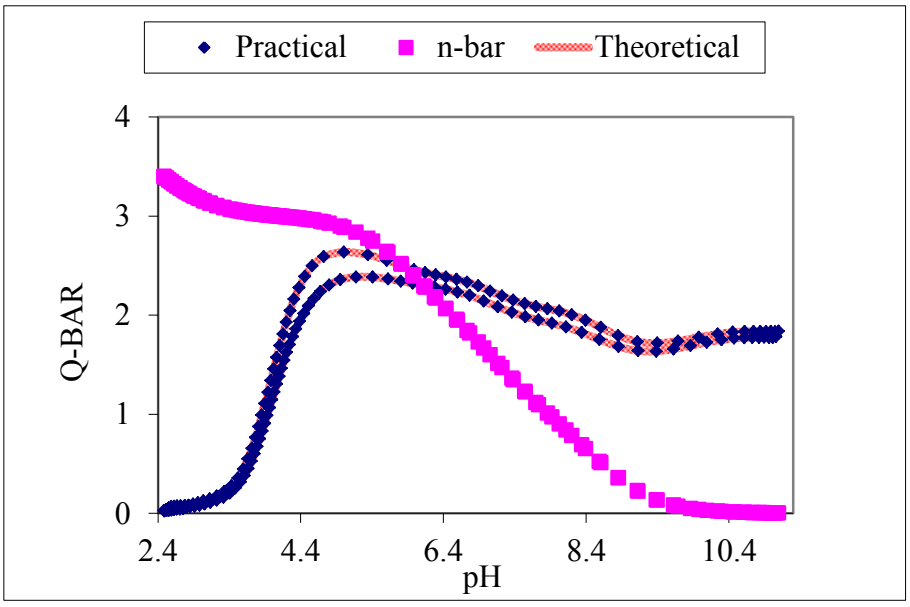

Figure 3.30: Q_M-bar as a function of pH for Cu(II) sarcosyl-L-histidyl-L-histidine complex.

The speciation graph for this titration is given in Figure 3.31. Complexation began at pH 3.10. There are four species formed between Cu(II) and Sar-His-His, CuSHH-H and CuSHH start forming around the same pH.

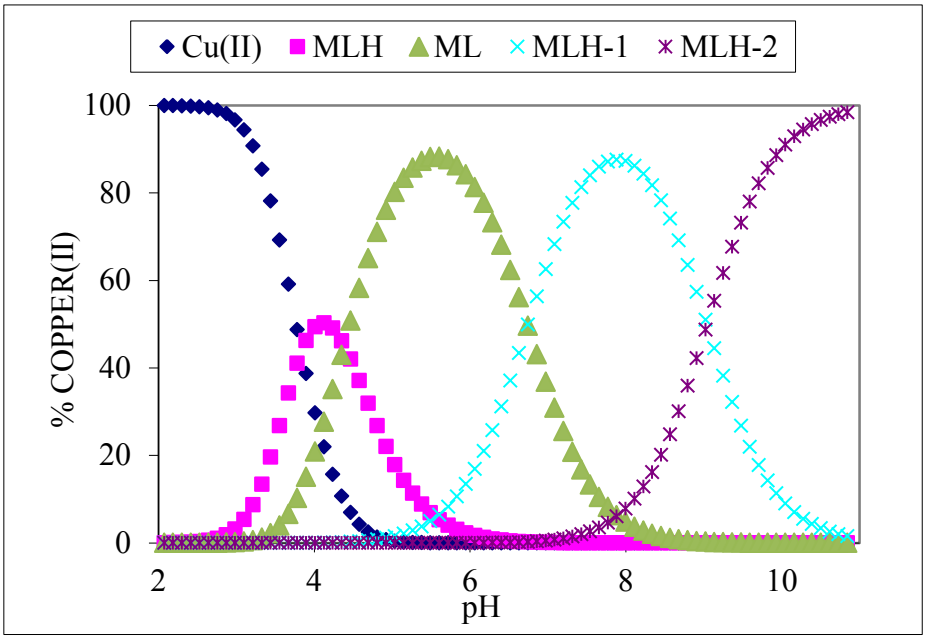

Figure 3.31: The distribution curve for the Cu(II) sarcosyl-L-histidyl-L-histidine complex.

3.4.2.3.2 Ni(II)/Sarcosyl-L-histidyl-L-histidine

Z_M-bar for Ni(II) sarcosyl-L-histidyl-L-histidine titrations is given in Figure 3.32. The Z_M-bar curves start to fan back almost immediately indicating that the NiSHH species did not predominate in solution.

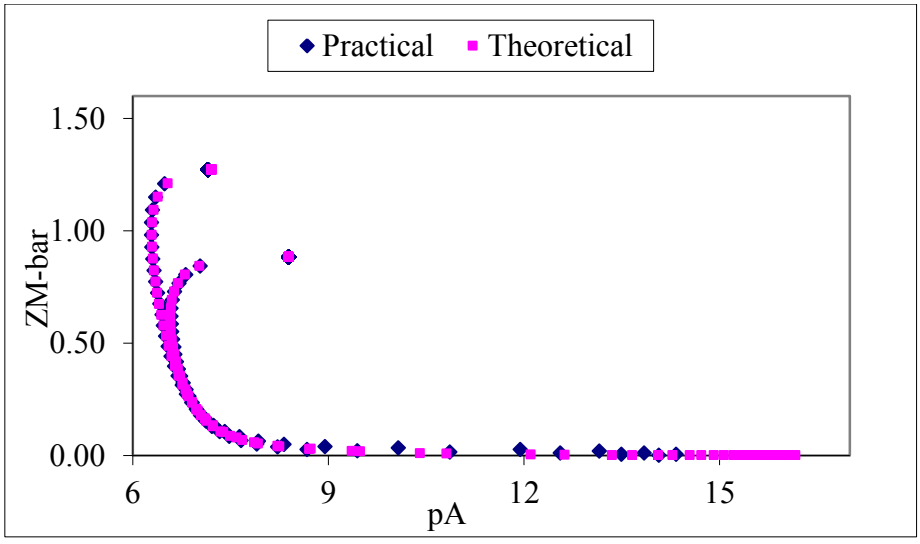

Figure3.32: Z_M-bar as a function of pA for Ni(II) sarcosyl-L-histidyl-L-histidine complex.

Q_M-bar is shown in Figure 3.33. Sar-His-His has four dissociable protons and it loses three protons upon complexation with Ni(II).

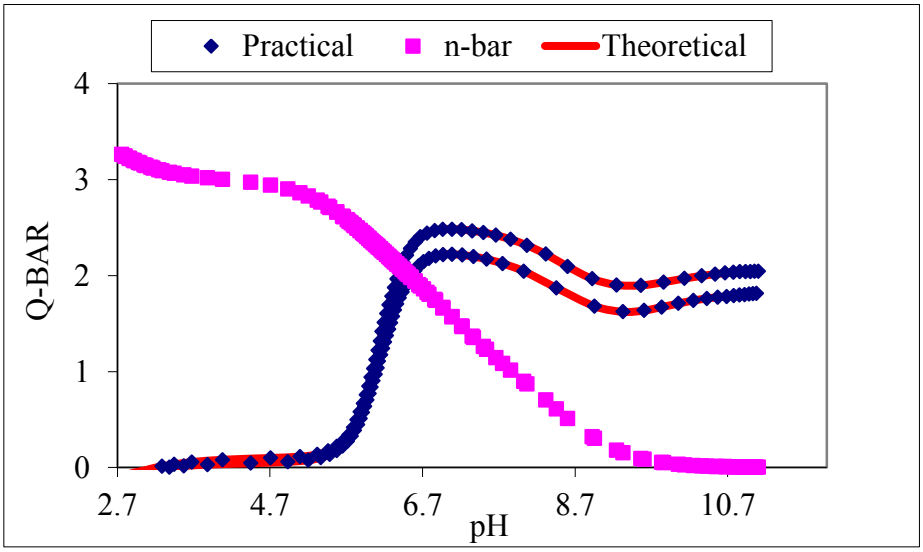

Figure 3.33: Q_M-bar as a function of pH for Ni(II) sarcosyl-L-histidyl-L-histidine complex.

Stability constants for species formed between Ni(II) and Sar-His-His are given in Table 3.13. Four species have been formed in solution. The theoretical and experimental of formation and deprotonation functions are in excellent agreement and reproducibility of repeat titrations at different metal to ligand ratios.

Table 3.13: Stability constants (log β_{pqr}) for Ni(II) sarcosyl-L-histidyl-L-histidine complex $\beta_{pqr} = [M_pL_qH_r]/[M]p[L]q[H]r$, I = 0.15 mol.dm^{-3} (NaCl), T = 25 ºC. S. dev denotes standard deviation in logβ_{pqr}; R_f^H is the Hamilton R-factor and R_{lim}^H its limit, n_T is the number of titrations, (n_P) is the number of titration points.

Complexes	p	q	r	log β_{pqr}	S.dev	R_f^H	R_{lim}^H	$n_T(n_p)$
NiSHH-H_2	1	1	2	18.09	0.13	0.01	0.03	2(141)
NiSHH	1	1	0	06.22	0.04			
NiSHH-H_{-1}	1	1	-1	0.02	0.03			
NiSHH-H_{-2}	1	1	-2	-8.37	0.05			

The distribution for Ni(II)/ Sar-His-His titrations is given in Figure 3.34. NiSHH-H and NiSHH start forming around the same pH. The pH range 5.61–10.05 indicates the presence of NiSHH-H_{-1} mononuclear species as the predominant species, reaching 85.78 % formation.

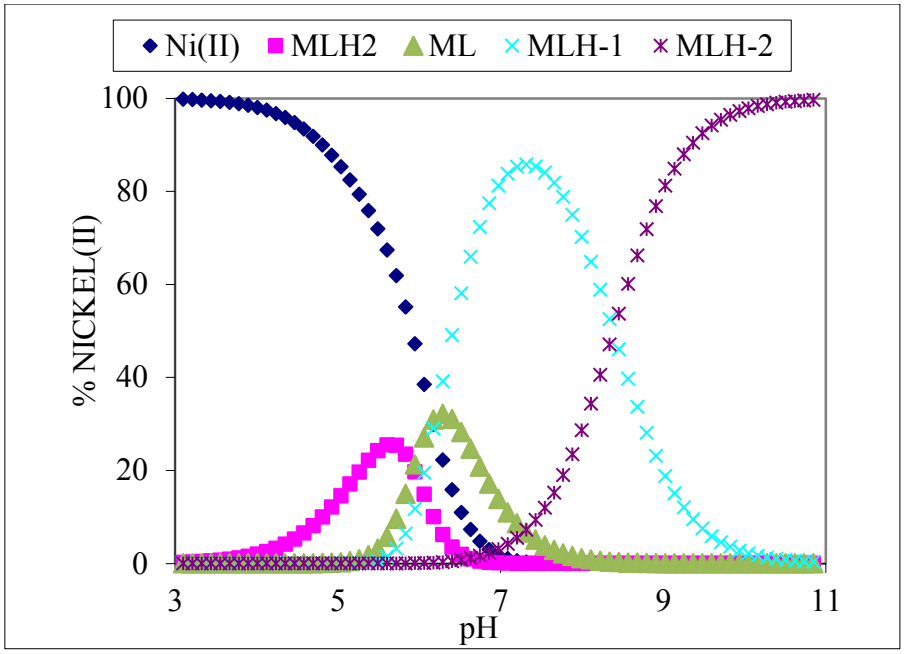

Figure 3.34: The distribution curve for the Ni(II) sarcosyl-L-histidyl-L-histidine complex.

3.4.2.3.3 Zn(II)/Sarcosyl-L-histidyl-L-histidine

ZM-bar was observed for the Zn(II) sarcosyl-L-histidyl-L-histidine titrations as shown in Figure 3.35. As the titration continues, at pA 6.74 the curves rise steeply and fan back indicating the formation of mixed-hydroxo complex species.

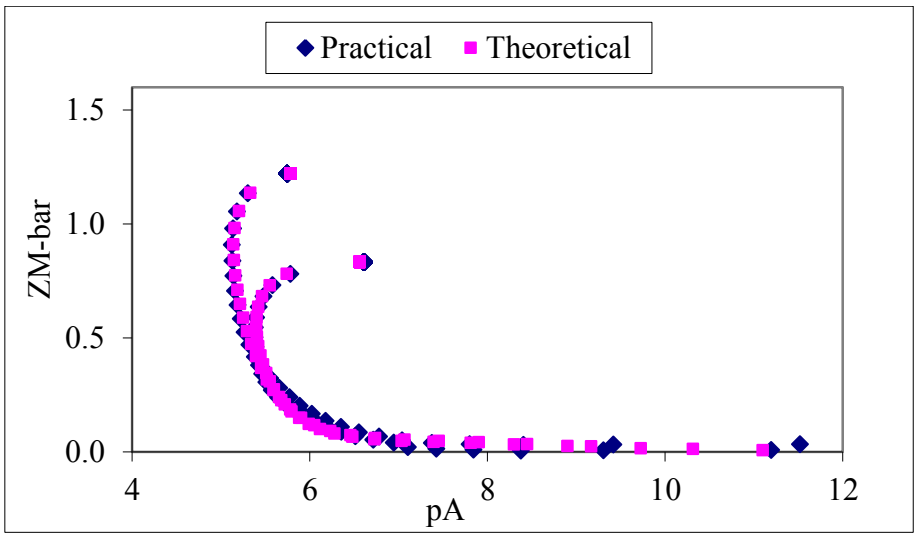

Figure 3.35: Z_M-bar as a function of pA for Zn(II) sarcosyl-L-histidyl-L-histidine complex.

The deprotonation function (Q-bar) in Figure 3.36 shows that at the beginning of the titration, at pH 5.67, Q-bar is greater than zero indicating that complexation has already commenced.

Sar-His-His has four dissociable protons and it losses two protons upon complexation with Zn(II).

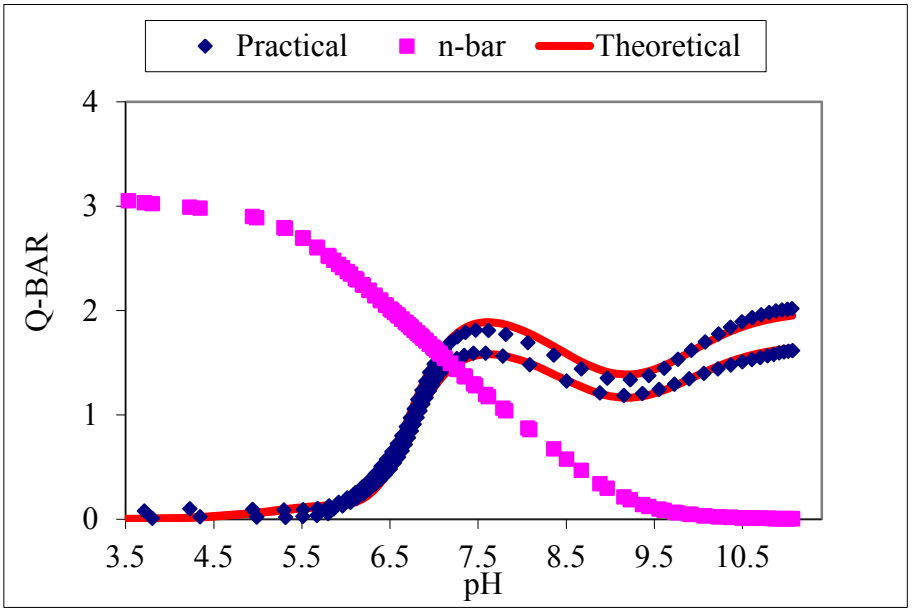

Figure 3.36: Q_M-bar as a function of pH for Zn(II) sarcosyl-L-histidyl-L-histidine complex.

The calculated formation constants in Table 3.14 have reasonably low standard deviations and are comparable to those of copper(II) complexation. The Hamilton R^H-factors indicate that the model is a good description of the equilibria occurring in solution.

Table 3.14: Stability constants (log β_{pqr}) for Zn(II) sarcosyl-L-histidyl-L-histidine complex $\beta_{pqr} = [M_pL_qH_r]/[M]p[L]q[H]r$, I = 0.15 mol.dm^{-3} (NaCl), T = 25 ºC. S. dev denotes standard deviation in logβ_{pqr}; R_f^H is the Hamilton R-factor and R_{lim}^H its limit, n_T is the number of titrations, (n_P) is the number of titration points.

Complexes	p	q	r	log β_{pqr}	S.dev	R_f^H	R_{lim}^H	$n_T(n_p)$
ZnSHH-H_2	1	1	2	18.16	0.06	0.01	0.02	2(116)
ZnSHH	1	1	0	05.20	0.05			
ZnSHH-H_{-1}	1	1	-1	-1.89	0.04			
ZnSHH-H_{-2}	1	1	-2	-11.69	0.05			

The distribution for Zn(II) Sar-His-His titrations is given in Figure 3.37. Four species formed in solution. ZnSHH is less stable than NiSHH and CuSHH of the Sar-His-His.

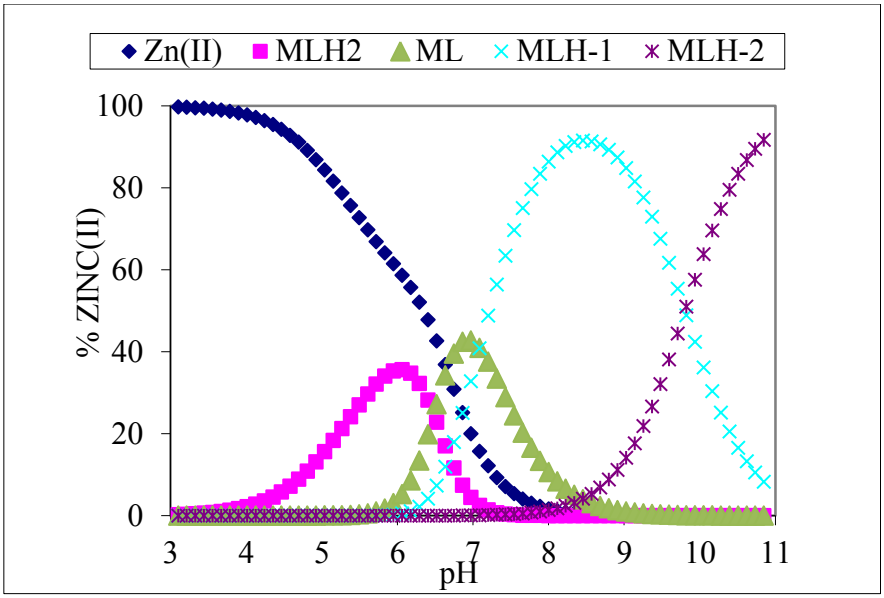

Figure 3.37: The distribution curve for the Zn(II) sarcosyl-L-histidyl-L-histidine complex.

3.4.2.4 Sarcosyl-L-lysyl-L-lysine Complexes

3.4.2.4.1 Cu(II)/Sarcosyl-L-lysyl-L-lysine

Figure 3.38 shows the complex formation curves as a function of pA for the sarcosyl-L-lysyl-L-lysine with Cu(II). The Z_M-bar levels off at ≈ 1.0 indicating that CuSKK is the predominant species in solution. Moreover, the fanning back for higher metal to ligand ratios indicates loss of an amide proton upon metal coordination.

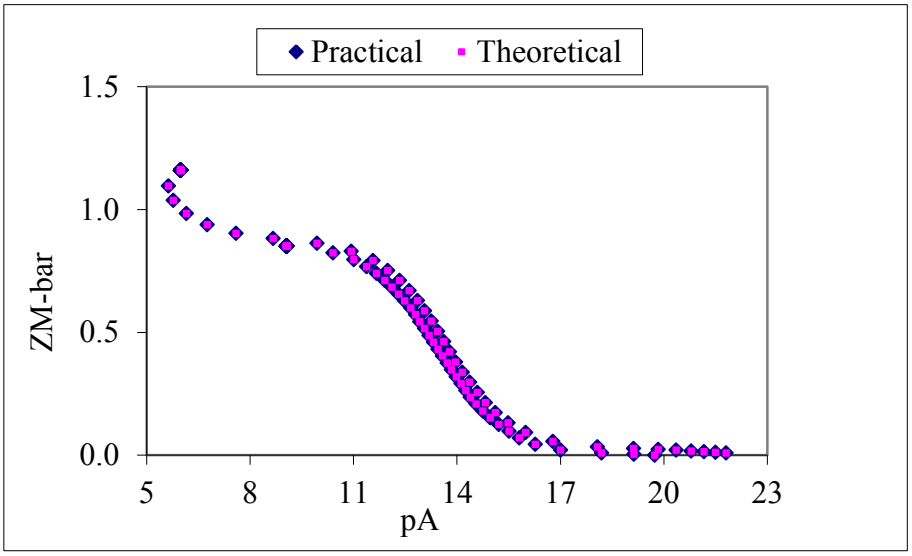

Figure 3.38: Z_M-bar as a function of pA for Cu(II) sarcosyl-L-lysyl-L-lysine complex.

The deprotonation function in Figure 3.39 rises to maximum value of about 2.57 at pH 7.21 indicating that approximately three protons have been released from the Sar-Lys-Lys due to

complexation. In the pH range 9.06-11.00 these curves level off due to the presence of hydroxo and/or mixed hydroxo species or rather formation of the CuSKK-H_{-2} species.

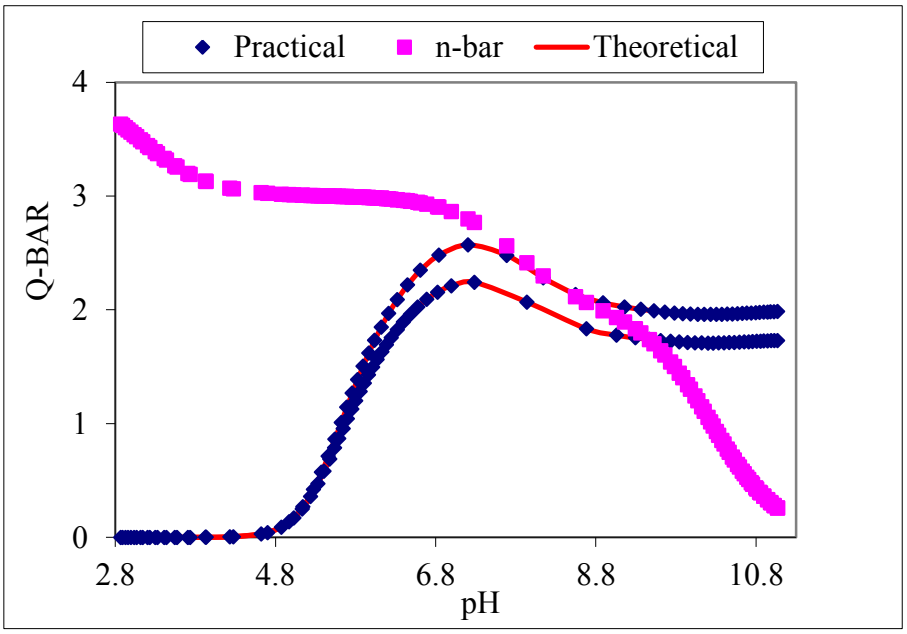

Figure 3.39: Q_M-bar as a function of pH for Cu(II) sarcosyl-L-lysyl-L-lysine complex.

Equilibrium constants for Cu(II) Sar-Lys-Lys titrations are given in Table 3.15. The CuSKK species is more stable than NiSKK and ZnSKK species of this ligand. The good agreement between theoretical and experimental formation and deprotonation functions as well as low standard deviations and Hamilton R-factors confirm the validity of this model.

Table 3.15: Stability constants (log β_{pqr}) for Cu(II) sarcosyl-L-lysyl-L-lysine complex $\beta_{pqr} = [M_pL_qH_r]/[M]p[L]q[H]r$, I = 0.15 mol.dm^{-3} (NaCl), T = 25 ºC. S. dev denotes standard deviation in logβ_{pqr}; R_f^H is the Hamilton R-factor and $R_{lim}{}^H$ its limit, n_T is the number of titrations, (n_P) is the number of titration points.

Complexes	p	q	r	log β_{pqr}	S.dev	R_f^H	$R_{lim}{}^H$	$n_T(n_p)$
CuSKK-H	1	1	1	19.80	0.03	0.01	0.01	2(131)
CuSKK	1	1	0	13.12	0.04			
CuSKK-H_{-1}	1	1	-1	3.18	0.06			
CuSKK-H_{-2}	1	1	-2	-7.45	0.05			

The speciation graphs in Figure 3.40 show species formed by the complexation of Sar-Lys-Lys with Cu(II). CuSKK species predominates over a wide pH range of 5.15-10.85 and,

CuSKK-H_{-1} species reaching 49% formation. It is also observed that complexation commences at about pH 4.13 when the protonated CuSKK-H species was formed.

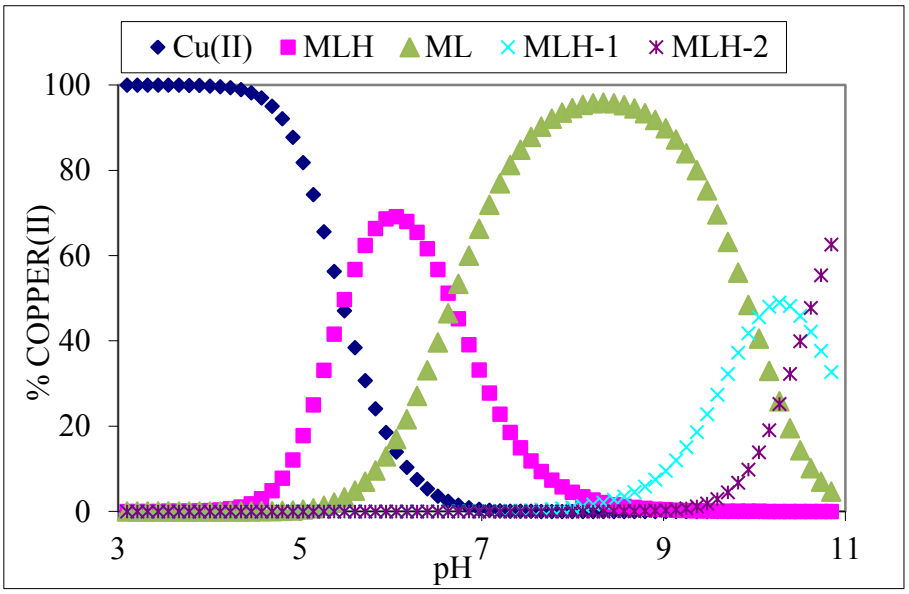

Figure 3.40: The distribution curve for the Cu(II) sarcosyl-L-lysyl-L-lysine complex.

3.4.2.4.2 Ni(II)/Sarcosyl-L-lysyl-L-lysine

The formation function for the Ni(II) Sar-Lys-Lys titrations in Figure 3.41 rises at pA 8.17. The fan back of Z_M-bar is indicative of hydroxo and/or mixed hydroxo species in solution.

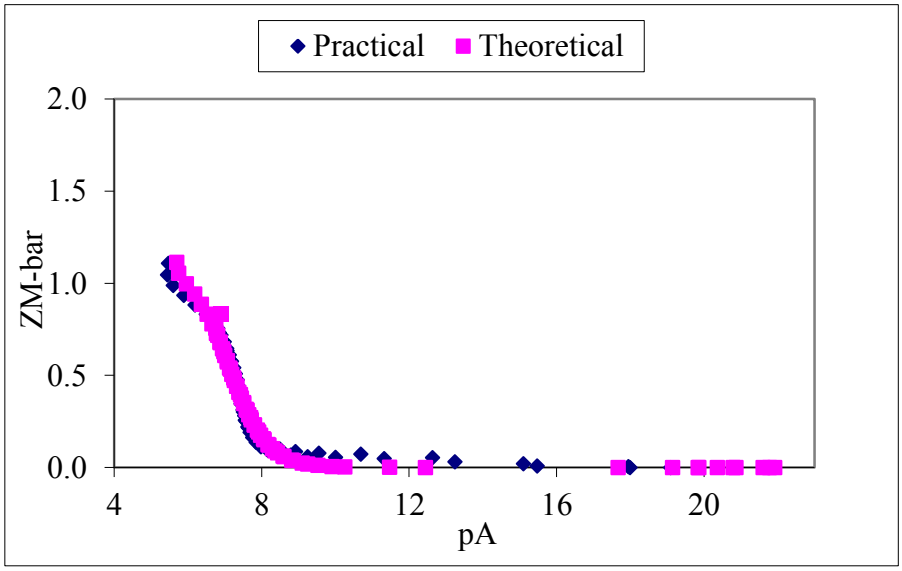

Figure 3.41: Z_M-bar as a function of pA for Ni(II) sarcosyl-L-lysyl-L-lysine complex.

Q_M-bar for Ni(II) Sar-Lys-Lys titrations is given in Figure 3.42. Q_M-bar begins at pH 5.26 and levels off due to the presence of hydroxo species between pH 8.46 and pH 10.86. Sar-Lys-Lys lost two protons upon complexation with Ni(II).

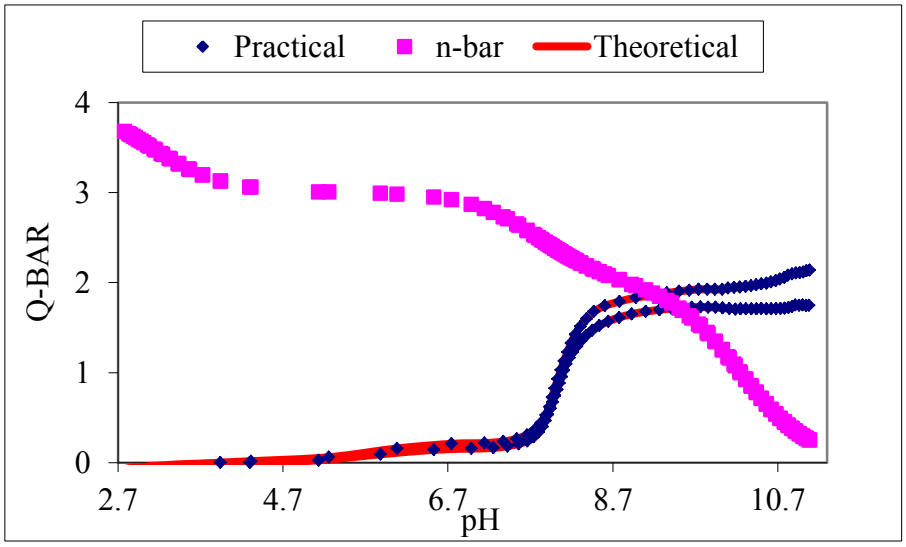

Figure 3.42: Q_M-bar as a function of pH for Ni(II) sarcosyl-L-lysyl-L-lysine complex.

Three species were observed for this titration and the equilibrium constants are given in Table 3.16. The theoretical and experimental formation and deprotonation functions were in good agreement; also there was reproducibility of repeat titrations at various metal: ligand ratios.

Table 3.16: Stability constants (log β_{pqr}) for Ni(II) sarcosyl-L-lysyl-L-lysine complex $\beta_{pqr} = [M_pL_qH_r]/[M]p[L]q[H]r$, I = 0.15 mol.dm^{-3} (NaCl), T = 25 ºC. S. dev denotes standard deviation in logβ_{pqr}; R_f^H is the Hamilton R-factor and R_{lim}^H its limit, n_T is the number of titrations, (n_P) is the number of titration points.

Complexes	p	q	r	log β_{pqr}	S.dev	R_f^H	R_{lim}^H	$n_T(n_p)$
NiSKK	1	1	0	07.25	0.02			
NiSKK-H_{-1}	1	1	-1	-2.78	0.04	0.01	0.002	2(336)
NiSKK-H_{-2}	1	1	-2	-13.44	0.03			

The calculated species distribution graph given in Figure 3.43 indicates the presence of NiSKK species as the predominant species reaching 83.68 % formation in the pH range 7.09-10.85 for the Sar-Lys-Lys titrations. From pH 8.57 to pH 10.85, Ni(II) exists as NiSKK-H_{-1}. NiSKK-H_{-2} was observed at pH 10.85.

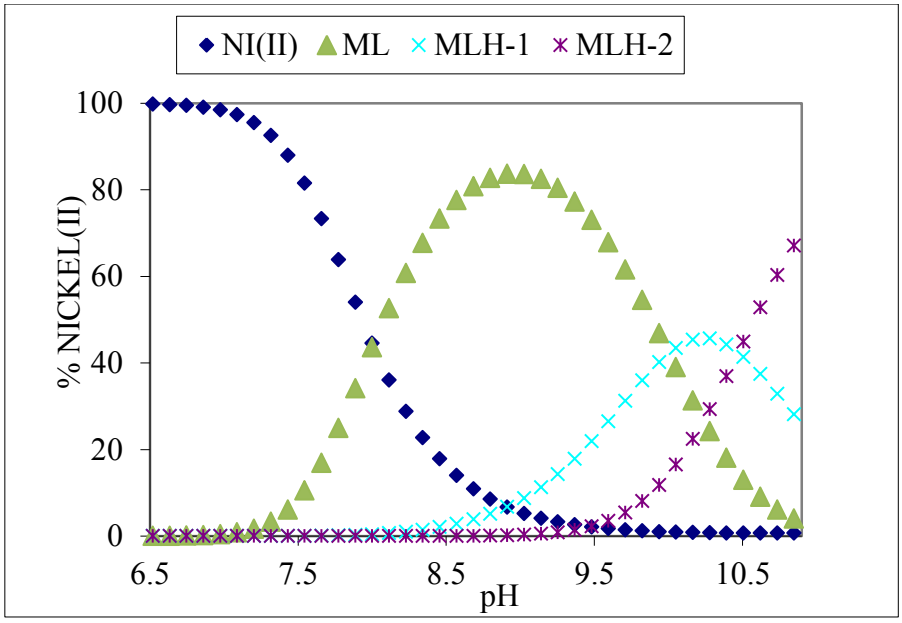

Figure 3.43: The distribution curve for the Ni(II) sarcosyl-L-lysyl-L-lysine complex.

3.4.2.4.3 Zn(II)/Sarcosyl-L-lysyl-L-lysine

The metal ion appears to coordinate to sarcosyl-L-lysyl-L-lysine. This is revealed by the Z_M-bar in Figure 3.44 which rises and fans back at pA 6.79. This is indicative of the formation of mixed hydroxo species.

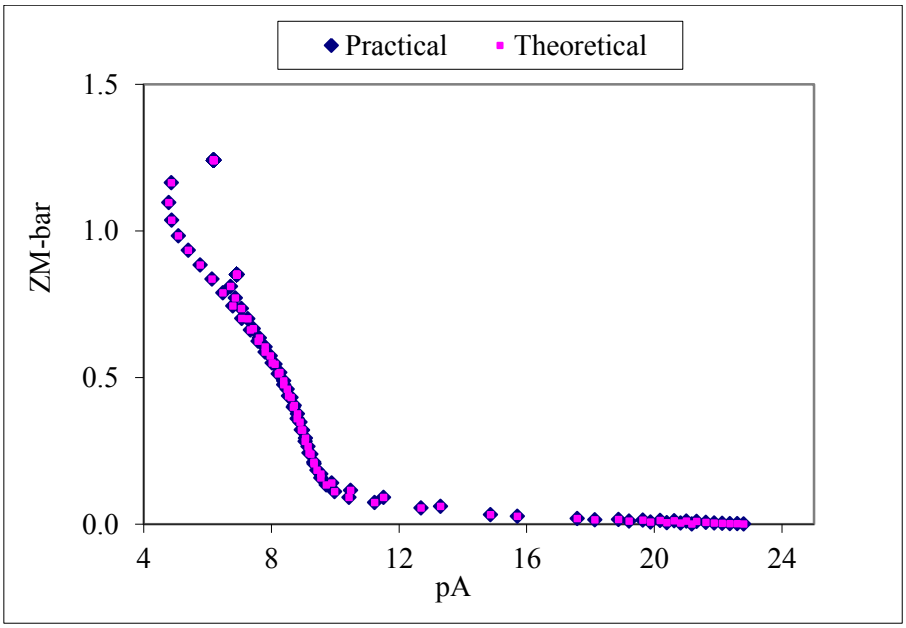

Figure 3.44: Z_M-bar as a function of pA for Zn(II) sarcosyl-L-lysyl-L-lysine complex.

The calculated formation constants for this model presented in Table 3.17 have very low standard deviations and Hamilton R^H-factors. This lends confidence to the model.

Table 3.17: Stability constants (log β_{pqr}) for Zn(II) sarcosyl-L-lysyl-L-lysine complex $\beta_{pqr} = [M_pL_qH_r]/[M]p[L]q[H]r$, I = 0.15 mol.dm^{-3} (NaCl), T = 25 ºC. S. dev denotes standard deviation in logβ_{pqr}; R_f^H is the Hamilton R-factor and $R_{lim}{}^H$ its limit, n_T is the number of titrations, (n_P) is the number of titration points.

Complexes	p	q	r	log β_{pqr}	S.dev	R_f^H	$R_{lim}{}^H$	$n_T(n_p)$
ZnSKK-H	1	1	1	16.39	0.02	0.01	0.003	2(143)
ZnSKK	1	1	0	08.26	0.03			
ZnSKK-H$_{-1}$	1	1	-1	-1.95	0.05			
ZnSKK-H$_{-2}$	1	1	-2	-12.85	0.03			

The Q_M-bar rises at pH 5.34 and levels off at Q_M-bar = 1.88 at pH 9.18 as shown in Figure 3.45. It drops before it rises again. This indicates that Sar-Lys-Lys loses two protons upon complexation with Zn(II).

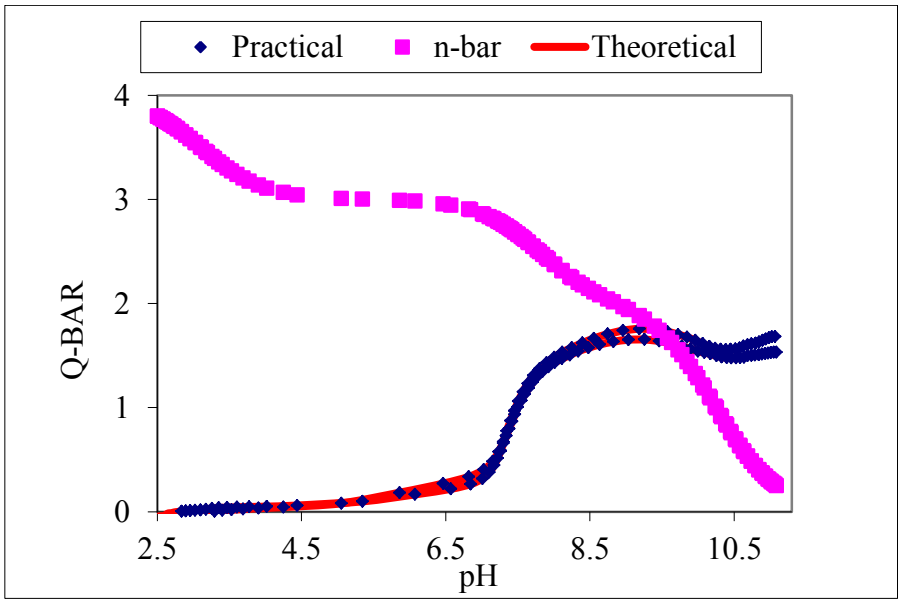

Figure 3.45: Q_M-bar as a function of pH for Zn(II) sarcosyl-L-lysyl-L-lysine complex.

The distribution graph (Figure 3.46) shows that there was free Zn(II) in solution at pH 2.50 to pH 8.80. ZnSKK-H species exist between pH 6.18 and pH 9.59, ZnSKK occurs between pH 6.86 and pH 10.86. ZnSKK-H$_{-1}$ and ZnSKK-H$_{-2}$ occurs from pH 8.88 to pH 10.86 in low concentration.

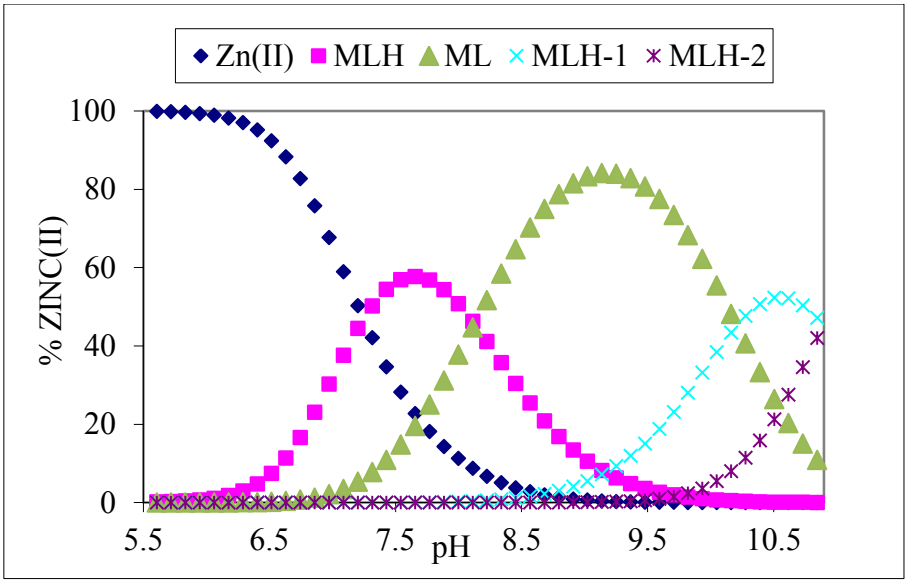

Figure 3.46: The distribution curve for the Zn(II) sarcosyl-L-lysyl-L-lysine complex.

3.4.2.5 Sarcosyl-L-glycyl-L-histidine Complexes

3.4.2.5.1 Cu(II)/Sarcosyl-L-glycyl-L-histidine

Figure 3.47 shows the Z_M-bar curve for Cu(II) sarcosyl-L-glycyl-L-histidine titrations. The deviation of Z_M-bar function from its normal shape indicates that the other, more complex species are forming. Z_M-bar function curves fan back indicating the formation of deprotonated or hydroxide species. The agreement between the theoretical and experimental valves gives confidence in the model.

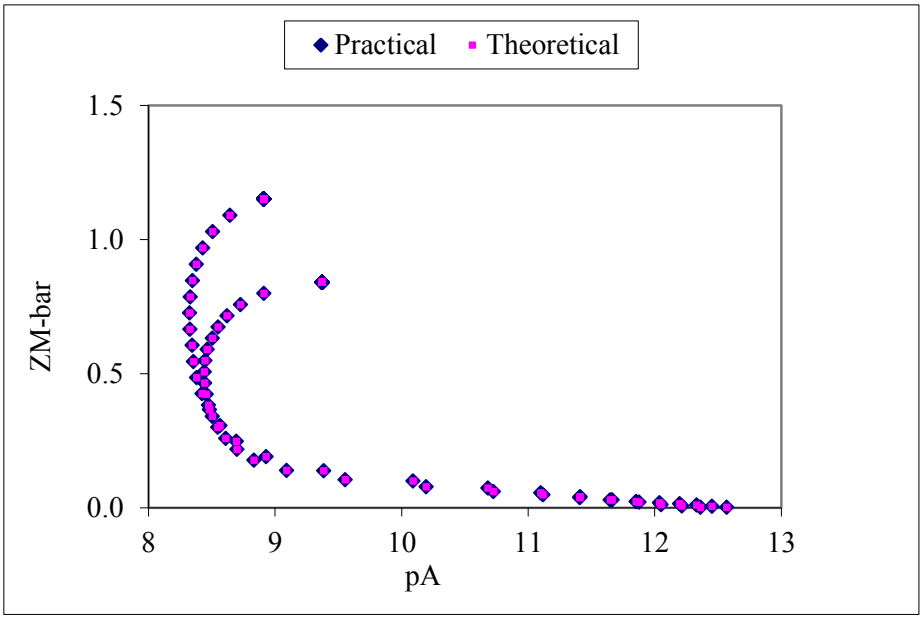

Figure 3.47: Z_M-bar as a function of pA for Cu (II) sarcosyl-L-glycyl-L-histidine complex.

The deprotonation function for the complexes of Cu(II) with Sar-Gly-His is plotted in Figure 3.48. Sar-Gly-His has three dissociable protons and complexation by Cu(II) causes it to lose two protons. At pH 5.81, the Q_M-bar rises to about Q-bar = 2.83. This could happen when one of the amides loses a proton or a coordinated water molecule loses a proton. Thermodynamically these two processes are the same. From pH 5.81 to pH 9.33, the n-bar and Q-bar curves run parallel in this pH range no change in complexation was taking place.

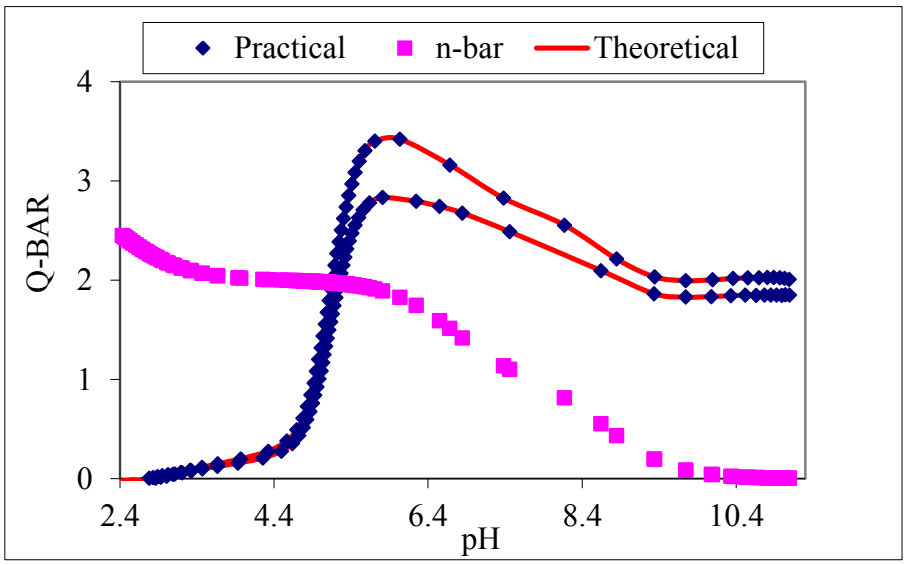

Figure 3.48: Q_M-bar as a function of pH for Cu (II) sarcosyl-L-glycyl-L-histidine complex.

Cu(II) and Sar-Gly-His form three species in solution (CuSGH-H, CuSGH-H_{-1} and CuSGH-H_{-2}). Equilibrium constants for these species are shown in Table 3.18. The standard deviations were small therefore the model was within the maximum allowed experimental error.

Table 3.18: Stability constants (log β_{pqr}) for Cu(II) sarcosyl-L-glycyl-L-histidine complex $\beta_{pqr} = [M_pL_qH_r]/[M]p[L]q[H]r$, I = 0.15 mol.dm^{-3} (NaCl), T = 25 ºC. S. dev denotes standard deviation in logβ_{pqr}; R_f^H is the Hamilton R-factor and $R_{lim}{}^H$ its limit, n_T is the number of titrations, (n_P) is the number of titration points.

Complexes	p	q	r	log β_{pqr}	S.dev	R_f^H	$R_{lim}{}^H$	$n_T(n_p)$
CuSGH-H	1	1	1	12.81	0.07			
CuSGH-H_{-1}	1	1	-1	3.11	0.03	0.01	0.02	2(134)
CuSGH-H_{-2}	1	1	-2	-2.72	0.06			

The species distribution curve for the complexes of Sar-Gly-His and Cu(II) is shown in Figure 3.49. The CuSGH-H species is formed from pH 3.21 to pH 5.61, and a maximum of 61.48% CuSGH-H_{-1} is formed. About 100% of the CuSGH-H_{-2} was reached at pH 7.66 where complexation was completed and there was no change in speciation.

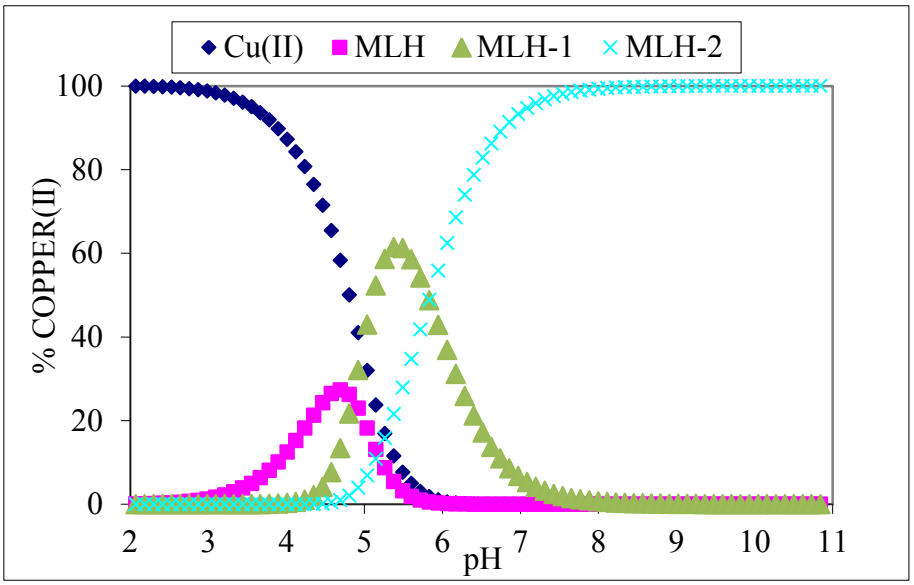

Figure 3.49: The distribution curve for the Cu(II) sarcosyl-L-glycyl-L-histidine complex

3.5 Discussion

The protonation constants of all five tripeptides are presented in Table 3.19. The tripeptides contain four groups, respectively, which are capable of reversible proton binding. These groups are the carboxyl group of Lys and His, the N^3 imidazole nitrogens of His, N-terminal of Sar and the ε-amino group of Lys.

Table 3.19: Protonation constants of all tripeptides in this study.

Tripeptides	pK_{a4}	pK_{a3}	pK_{a2}	pK_{a1}
Sar-His-Lys (SHK)	10.33	08.37	06.57	02.83
Sar-Lys-His (SKH)	10.25	08.30	06.69	02.57
Sar-His-His (SHH)	08.57	07.17	05.90	02.30
Sar-Lys-Lys (SKK)	10.54	9.95	7.80	3.11
Sar-Gly-His (SGH)	-	08.72	6.72	2.35

The N-terminal amino group of Sar is less basic than the ε-amino group of Lys due to the former's proximity to the electron-withdrawing carbonyl group of the first peptidic bond. The corresponding pK_a value is 2.21 log units lower than that of free Sar (10.01). The experimental values of the protonation constants of tripeptides estimated using ESTA1were optimised using ESTA2. These titrations have not been reported before; however, the effect of the N-terminal amino group of sarcosine on the log values is not the same in glycine peptides due to the inductive effect possessed by the methyl substituent. In particular, pK_a of N-terminal amine protonation is high when sarcosine is in the first position of the peptide chain as a result of inductive effects.

The equilibrium constants of the reaction progress of Cu(II) tripeptide species are given in Table 3.20. The measurable interaction between the Sar-His-Lys and Cu(II) starts at pH 3.1 and, as is shown by the concentration distribution curves calculated at 1:1 ratio, CuLH is the first species appearing in measurable concentration formed by deprotonation of the one amide, N-terminal amino and nitrogen N^3-imidazole (it is still protonated below pH 6) and water molecule (pK_a = 4.52). The value of pK_a of $[Cu(Him)]^{2+}$ =4.07, which is consistent with the presence of a Cu(II) ion coordinated by amino, dissociated amide and N^3-imidazole nitrogens [22]. The stoichiometry of the CuLH complex suggests that the His and the Lys residues remain protonated.

Table 3.20: Equilibrium constants of the reaction progress of Cu(II) tripeptide species.

The reaction progress	Sar-His-Lys	Sar-Lys-His	Sar-His-His	Sar-Lys-Lys	Sar-Gly-His
$CuLH \leftrightarrow CuL + H^+$	04.52	04.24	04.39	06.68	-
$CuL \leftrightarrow CuLH_{-1} + H^+$	09.44	05.41	06.74	09.94	-
$CuLH_{-1} \leftrightarrow CuLH_{-2} + H^+$	10.65	10.35	09.05	10.63	05.83

At pH 6.75 CuL is the predominant species in the range 4-10. Further deprotonation of this complex take place with pK_a's of 9.44. On the other hand, the presence of the ε-amino function of the Lys residue in Sar–His–Lys does not affect complexation equilibria. Similar prominence of the $CuLH_{-1}$ complex was also found for Cu(II) complexes of Ala–His [23], Gly–His–Gly [24,25], glycylhistamine [26], and Gly–His–Lys [25,27,28]. The crystal structures of Cu(II) complexes with Gly-His [29], Gly–His–Gly [30] and Gly–His–Lys [31] support the 3N coordination in the $CuLH_{-1}$ complex. The formation of the $CuLH_{-2}$ species

by the deprotonation of lysine side-chain amino group, and the pK_a = 10.65 which is almost the same as of free tripeptide (SHK).

In the pH range 2.5-11 and with the ratio of Cu(II): Sar-Lys-His at 1:1 it was shown that the coordination of Cu(II) starts in acidic solution at a pH of about 4 and the first species formed is CuLH. The stability constant of CuLH (17.20) is higher than that of complexes of the same formula, and only 1N coordination of Cu(II) with the peptides GGH (12.24) [32], GGHist (12.02) [23], DAH (12.85) [24] and of 2N coordination [NH_2, Nim] (CuLH) with HVH (15.41) [33], suggesting the participation of two nitrogen atoms in the coordination sphere of Cu(II). The CuLH species might contain two nitrogen atoms [NH_2, N^-] coordinated in the equatorial plane of the Cu(II). The stoichiometry of the CuLH species suggests that the His and the Lys residues remain protonated and uncoordinated. In more basic solutions, complexes of CuL stoichiometry are formed. The CuLH released a proton with pK_a 4.70, which is comparable to the values for peptides with peptide nitrogen coordination [34,35-37]. The proton is abstracted from the next amide nitrogen, forming a complex with stoichiometry CuL. The formation of the CuL complex suggests the participation of four nitrogen atoms [NH_2, 2N−, N_{im}] in the equatorial plane of the Cu(II) forming a very stable chelate ring. This is typical of analogous Cu(II) complexes with peptides containing the N-terminal sequence Xaa-Yaa-His [33,38,39]. The stoichiometry of the CuL species and the pH range of its formation, which is below the deprotonation range of the His side chain in free tripeptide, indicates that the imidazole ring of His and ε-amino group of Lys residues remain protonated [40]. The next species formed upon pH increase is $CuLH_{-1}$. This species predominates in the pH range 4.0-10.7. This phenomenon is characteristic of the stability caused by the tetradentate chelate ring [NH_2, 2N−, N_{im}] of Cu(II) complexes with peptides containing the N-terminal sequence Xaa-Yaa-His [41,42].

Above pH 9.0 deprotonation of the $CuLH_{-1}$ species takes place with a pK_a value of 10.35, forming the $CuLH_{-2}$ species. In the case of $CuLH_{-2}$, although the ε-amino group of the Lys residue is deprotonated it remains uncoordinated. This is similar to the analogous Cu(II) complexes with tetrapeptide SHHK- and SAHK-, and other peptides containing the Lys residue [35,39]. The pK_a value of 10.35 is very similar to the pK_a corresponding to the protonation of the ε-amino group of the Lys.

For Sar-His-His, in the pH range 2.0-6.3, the refinement of potentiometric data indicates that only mononuclear species are present in solution even in the presence of excess of Cu(II).

The first species in solution, CuLH, is formed by the N^3-imidazole (1), N-terminal amino, carbonyl oxygen and one water molecule. The imidazole group of His in third position will be protonated [22]. Loss of a proton from the MLH species gives rise to the ML complex. The pK_a for this process $\boldsymbol{CuLH \rightleftharpoons CuL + H^+}$ is 4.39 was formed by stepwise deprotonation of the second imidazole ring. This is suggesting that the presence of the Cu(II) ion in the complex has no impact on the proton from the 2nd His supports binding of the N-terminal amino group, imidazole nitrogens, carbonyl oxygen and water molecule to the metal ion.

Two species are present above pH~6.5 in the Cu(II) sarcosyl-L-histidyl-L-histidine complexes. The $CuLH_{-1}$ species (pK_a = 6.74), this can be compared to the same process occurring with glycinamide (pK_a = 6.8), where it is known that coordination swap from the amide oxygen to amide nitrogen. The conversion of $CuLH_{-1}$ to $CuLH_{-2}$ occurs in the reaction $\boldsymbol{CuLH_{-1} \rightleftharpoons CuLH_{-2} + H^+}$ (pK_a = 9.05). At this pK_a value the deprotonation of Sar-His-His with Cu(II) can be interpreted either by the deprotonation of the water molecule or by the deprotonation and coordination of a second amide group to Cu(II). For the binding of Cu(II) with the amide nitrogens of the peptide systems, the deprotonation of the second amide nitrogen seems to be easier for His-His peptides; the pKa of the reaction is 9.00, which is around 1.5 units lower than that for His-Xaa-His peptides. The pK_a value of 9.05 is in the range expected for metal assisted deprotonation of the amide proton [43-45], rather than hydrolysis of the complex. On the other hand, the coordination chemistry of any peptides with the amino acid sequence X–Y–His has already been described by the exclusive formation of the species $CuLH_{-2}$ with [NH_2, 2×N_{amide}, N_{im}] coordination [38,46]. The same finding was obtained in the Cu(II) with Sar-Lys-His and Sar-Gly-His complexes. With Sar-His-His axial N^3 coordination of His at position II cannot be excluded.

The coordination of Cu(II) with Sar-Lys-Lys starts below pH 5, with MLH species formation. The concentration of this species reaches its maximum at pH 6, binding all the Cu(II) ion and remaining the only species in solution up to pH 8. At higher pH values, the CuLH species undergoes three deprotonation steps leading to the species CuL, $CuLH_{-1}$ and $CuLH_{-2}$. The pKa value of $\boldsymbol{CuLH \rightleftharpoons CuL + H^+}$ is compatible with amide deprotonation and the type of coordination (-NH, N^-, $2H_2O$). The next two deprotonation steps $\mathbf{CuL \rightleftharpoons CuLH_{-1} + H^+}$ and $\mathbf{CuLH_{-1} \rightleftharpoons CuLH_{-2} + H^+}$, are very close to the protonation pK_a values of the two side Lys, suggesting that no interaction occurs between the ε-NH_2 groups and the copper ion. The

above hypothesis is true, because the geometry of the CuLH species is not the same of the others species (see Chapter 4).

The concentration of the MLH species for Cu(II) Sar-Gly-His reaches its maximum at pH 5, binding all the Cu(II) ion and remaining the only species in solution. The CuLH species undergoes two deprotonation steps leading to the species $CuLH_{-1}$ and $CuLH_{-2}$. The CuLH is always present in very low concentration. Its binding mode can be interpreted either by the coordination of the N-terminal amino and neighbouring carbonyl oxygen donors with the protonated imidazole side chain or by the monodentate coordination of an imidazole nitrogen with a protonated amino group. Earlier studies led to the conclusions that N^3 of imidazole is the primary binding site of these peptides [38,47,48], but careful consideration of the result obtained for the species formed at higher pH strongly supports the existence of amine binding for all possible stoichiometries. Its presence can be verified in all cases and its signal overlaps well with those of tripeptide with [NH_2, CO, N_{im}] coordination. The second species in solution $CuLH_{-1}$ is formed by binding of the N-terminal amino group, imidazole nitrogens and two peptide groups. However the imidazole group of the histidine is still protonated. As a consequence, the latter coordination mode can be suggested as the cause of the high stability, $CuLH_{-2}$, appears to have the same coordination as $CuLH_{-1}$, but the imidazole group of the histidine was deprotonated [49].

3.6 Conclusions

Investigation of the Cu(II), Ni(II) and Zn(II) complexes of sarcosyl-L-histidyl-L-lysine (SHK), sarcosyl-L-lysyl-L-histidine (SKH), sarcosyl-L-histidyl-L-histidine (SHH), sarcosyl-L-lysyl-L-lysine (SKK) and sarcosyl-L-glycyl-L-histidine (SGH) showed a significantly different coordination behavior of all tripeptides in acidic/neutral and basic pH range. The results presented in this study approved that the metal ion complexation strongly depends on the position of histidine in the amino acid sequence of the tripeptide molecules. The detailed potentiometric analysis of Cu(II) ions with all tripeptides, around pH~7, could be best fitted by the involvement of a species CuL or $CuLH_{-1}$ into the model, these species being proposed to coordinate equatorially with the N-terminal amino group, deprotonated amide, the imidazole nitrogens with N^3 and a water molecule.

The CuLH and CuL species of Sar-His-Lys (SHK) was more stable than those of CuLH with the others tripeptides. The $CuLH_{-1}$ complexes of Sar-Lys-His (SKH) were more stable than those of Cu(II) with the others tripeptides. This CuL species was not observed in the Sar-

Gly-His (SGH) system. The similar stability of $CuLH_{-2}$ species formed for Sar-Lys-His (SKH) and Sar-Gly-His (SGH) system, which were more stable than others tripeptides.

The Cu(II) Gly tripeptides, such as Gly-Gly-His, saturate the copper coordination plane at the most acidic pH of 4.4, compared to other peptide ligands. Consequently, the best ligand for binding copper depends on the particular application [50]. However, the methyl group does have an inductive effect making the Sar tripeptides more basic than Gly tripeptides. A similar effect is seen with the Cu(II) Sar-His-Lys and Sar-Gly-His complexes, the thermodynamic stabilities of these N-terminal amino group of sarcosine are more basic than the analogous tripeptides in slightly basic solution. For the Cu(II) tripeptides with the sarcosine-containing ligand the presence of coordination is supported by spectroscopic methods (see Chapter 4).

Moreover, all tripeptides in the present study are more stable and selective for Cu(II) than Ni(II) and Zn(II). This trend agrees with the Irving-Williams stability series [51,52]. However, the ZnL of the Sar-Lys-Lys species was 1.01 log units more stable than the NiL complex (Table 3.16 and Table 3.17), which runs contrary to the Irving-Williams stability series [53].

Finally, the results presented here confirm that Cu(II) forms stable complexes with all the tripeptides studied. This is the first requirement of the main aim of this study, which is to develop lipophilic copper complexes for dermal absorption.

References

1. G. Meinrath, a. Kufelnicki, and M. Świątek, *Accredit. Qual. Assur.*, 2005, **10**, 494–500.

2. Fujinaga. T and Thomas J. D. R, *Phil.Trans. R. Soc. Lond. A*, 1982, **305**, 631–644.

3. P. M. M. Kevin B. Murray, *ESTA: Equilibrium Simulation for Titration Analysis*, University of Wales Institute of Science and Technology (UWIST) Department of Applied Chemistry, 1984.

4. G. Mohamed and H. Ben Hander, *Res. J. Chem. Sci.*, 2012, **2**, 12–20.

5. L. S. Molochnikov, E. G. Kovalyova, A. a. Zagorodni, M. Muhammed, Y. M. Sultanov, and A. a. Efendiev, *Polymer (Guildf).*, 2003, **44**, 4805–4815.

6. T. Nishio, *Biophys. Chem.*, 1998, **71**, 173–84.

7. G. Sharma and J. P. Tandon, *J. Inorg. Nucl. Chem.*, 1970, **32**, 1273–1278.

8. L. M. Schwartz, *J. Chem. Educ.*, 1987, **64**, 947.

9. Y.-H. Lee and C. Brosset, *Water. Air. Soil Pollut.*, 1978, **10**, 457–469.

10. N. N. Golovnev, O. S. Romanova, and N. V. Busygina, *J. Anal. Chem.*, 2000, **55**, 457–460.

11. M. R. Martell A.E., *Determination and Use of Stability Constants*, VCH, New York., New York., 1988.

12. M. T. Beck and I. Nagypal, *Chemistry of Complex Equilibria*; Ellis Horwood Limited: New York., 1990.

13. G. G. Guilbault, D. N. Kramer, and P. Goldberg, *J. Phys. Chem.*, 1963, **67**, 1747–1749.

14. P. D. Gaikwad, D. J. Shirale, P. A. Savale, K. Datta, P. Ghosh, A. J. Pathan, and G. Rabbani, *Int. J. Electrochem. Sci.*, 2007, **2**, 488–497.

15. N. H. Oxtoby, and G. W. Nachtrieb, *Principles of Modern Chemistry*, Saunders College Publishing, 1985.

16. R. W. M. Wedderburn, *Biometrika*, 1974, **61**, 439–447.

17. P. M. May and K. Murray, *Talanta*, 1988, **35**, 927–932.

18. P. M. May, K. Murray, and D. R. Williams, *Talanta*, 1988, **35**, 825–830.

19. A. Vacca, A. Sabatini, and M. A. Gristina, *Coord. Chem. Rev.*, 1972, **8**, 45–53.

20. S. J. Lau and B. Sarkar, *Biochem. J.*, 1981, **199**, 649–56.

21. G. C. de Witt, P. M. May, J. Webb, and G. Hefter, *Inorganica Chim. Acta*, 1998, **275-276**, 37–42.

22. G. Arena, R. P. Bonomo, G. Impellizzeri, R. M. Izatt, J. D. Lamb, and E. Rizzarelli, *Inorg. Chem.*, 1987, **26**, 795–800.

23. T. Gajda, B. Henry, A. Aubry, and J. Delpuech, *Inorg. Chem.*, 1996, **35**, 586–593.

24. E. Farkas, I. Sóvágó, T. Kiss and A. Gergely, *J. Chem. Soc. Dalt. Trans.*, 1984, **3**, 611.

25. M. J. A. Rainer and B. M. Rode, *Inorganica Chim. Acta*, 1985, **107**, 127–132.

26. T. Gajda, B. Henry, and J. Delpuech, *J. Chem. Soc. Dalt. Trans.*, 1993, 1301.

27. S. J. Lau and B. Sarkar, *Biochem. J.*, 1981, **199**, 649–56.

28. P. M. May, J. Whittaker, and D. R. Williams, *Inorganica Chim. Acta*, 1983, **80**, L5–L7.

29. J. F. Blount, K. A. Fraser, H. C. Freeman, J. T. Szymanski, and C. H. Wang, *Acta Crystallogr.*, 1967, **22**, 396–405.

30. R. Österberg, B. Sjöberg and R. Söderquist, *J. Chem. Soc. Chem. Commun*, 1972, 983.

31. C. M. Perkins, N. J. Rose, B. Weinstein, R. E. Stenkamp, L. H. Jensen, and L. Pickart, *Inorganica Chim. Acta*, 1984, **82**, 93–99.

32. T. Sakurai and A. Nakahara, *Inorg. Chem.*, 1980, **19**, 847–853.

33. A. Myari, G. Malandrinos, Y. Deligiannakis, J. C. Plakatouras, N. Hadjiliadis, Z. Nagy, and I. Sòvágó, *J. Inorg. Biochem.*, 2001, **85**, 253–261.

34. K. Várnagy, J. Szabó, I. Sóvágó, G. Malandrinos, N. Hadjiliadis, D. Sanna, and G. Micera, *J. Chem. Soc. Dalt. Trans.*, 2000, 467–472.

35. M. Mylonas, G. Malandrinos, J. Plakatouras, N. Hadjiliadis, K. S. Kasprzak, A. Krężel, and W. Bal, *Chem. Res. Toxicol.*, 2001, **14**, 1177–1183.

36. M. Mylonas, J. C. Plakatouras, N. Hadjiliadis, A. Krężel, and W. Bal, *Inorganica Chim. Acta*, 2002, **339**, 60–70.

37. T. Kowalik-Jankowska, M. Ruta-Dolejsz, K. Wiśniewska, L. Łankiewicz, and H. Kozłowski, *J. Chem. Soc. Dalt. Trans.*, 2000, **100**, 4511–4519.

38. H. Kozłowski, W. Bal, M. Dyba, and T. Kowalik-Jankowska, *Coord. Chem. Rev.*, 1999, **184**, 319–346.

39. P. Mlynarz, D. Valensin, K. Kociolek, J. Zabrocki, J. Olejnik, and H. Kozlowski, *New J. Chem.*, 2002, **26**, 264–268.

40. M. Mylonas, J. C. Plakatouras, and N. Hadjiliadis, *Dalton Trans.*, 2004, 4152–60.

41. M. Sokolowska, A. Krezel, M. Dyba, Z. Szewczuk, and W. Bal, *Eur. J. Biochem.*, 2002, **269**, 1323–1331.

42. J. Ueda, N. Ikota, A. Hanaki, and K. Koga, *Inorganica Chim. Acta*, 1987, **135**, 43–46.

43. C. Jubert, A. Mohamadou, C. Gérard, S. Brandes, A. Tabard, and J.-P. Barbier, *J. Chem. Soc. Dalt. Trans.*, 2002, 2660.

44. D. Chen, Y. Sun, A. E. Martell, and M. J. Welch, *Inorganica Chim. Acta*, 2002, **335**, 119–124.

45. A. Jancsó, K. Selmeczi, P. Gizzi, N. V Nagy, T. Gajda, and B. Henry, *J. Inorg. Biochem.*, 2011, **105**, 92–101.

46. C. Harford and B. Sarkar, *Acc. Chem. Res.*, 1997, **30**, 123–130.

47. M. Jezowska-Bojczuk, H. Kozlowski, L. D. Pettit, G. Micera, and P. Decock, *J. Inorg. Biochem.*, 1995, **57**, 1–10.

48. L. D. Pettit, S. Pyburn, W. Bal, H. Kozlowski, and M. Bataille, *J. Chem. Soc. Dalt. Trans.*, 1990, 3565.

49. K. Várnagy, J. Szabó, I. Sóvágó, G. Malandrinos, N. Hadjiliadis, D. Sanna, and G. Micera, *J. Chem. Soc. Dalt. Trans.*, 2000, 467–472.

50. R. R. Khoury, G. J. Sutton, D. Ebrahimi, and D. B. Hibbert, *Inorg. Chem.*, 2014, **53**, 1278–87.

51. H. Irving and R. J. P. Williams, *J. Chem. Soc.*, 1953, 3192.

52. H. Irving and R. J. P. Williams, *J. Chem. Soc.*, 1949, 1841.

53. L. R. Solomon, A. M. Bond, J. W. Bixler, D. R. Hallenbeck, and K. M. Logsdon, *Inorg. Chem.*, 1983, **22**, 1644–1648.

CHAPTER FOUR

SPECTROSCOPY IN STRUCTURAL STUDIES

4.1 UV-VISIBLE SPECTROSCOPY

4.1.1 Introduction

Transition metal ions exhibit absorption bands in the visible region of the spectrum as the species are highly coloured [1]. These colours come from electronic transitions between energy levels whose spacings correspond to the wavelengths available in visible light. In complexes, these transitions are frequently referred to as d-d transitions because they involve molecular orbitals that are mainly metal d in character. Since this spacing depends on factors such as geometry of the complex, the nature of the ligands present, and the oxidation state of the central metal atom, electronic spectra of complexes can provide valuable information related to bonding and structure [2,3]. Absorption spectroscopy is an excellent technique for following ligand-binding reactions, enzyme catalysis and conformational transitions in proteins and nucleic acids [4]. It has been used to predict the structures of Cu(II) complexes [5-7]. The spectrophotometry provides an additional method for comparing possible chemical models which are not available with potentiometry.

Because the Uv-Visible spectra of most complexes contain broad overlapping absorption bands, parameter correlation arises and therefore, it is not usually possible to evaluate stability constants as precisely from spectrophotometric data as compared to potentiometric data. The potentiometric data may lead to a more precise analysis of the wrong model, whereas spectrophotometric data will indicate the correct model but give a less precise analysis of it. Therefore, it is necessary to combine both spectrophotometric and potentiometric data for defining the chemical model and for evaluation of the stability constants respectively [8,9]. As a result, UV-visible spectrophotometry is used as a supplementary technique to glass electrode potentiometry when ionic equilibria are investigated.

4.1.2 Theory

The absorption of electronic transitions is observed in bands where the energy of each band corresponds to the difference in energy between the initial and final states. The relative intensities of absorption bands are governed by a series of selection rules. According to the spin selection rule the transitions between states of different spin multiplicity are forbidden,

ie., transitions between $^4A_2$ and $^4T_1$ states are "spin-allowed," but between $^4A_2$ and $^2A_2$ are "spin-forbidden".

The Laporte selection rule, states that the only transitions with a change of parity, *gerade* to *ungerade* (g → u) and *ungerade* to *gerade* (u → g) but not (g → g) or (u → u) are allowed. This would mean that all d-d transitions in octahedral complexes are Laporte forbidden and therefore many complexes will be colourless.

However, most ions do not have perfect symmetry, and are distorted so that the centre of symmetry is destroyed, resulting in mixing (hybridization) of d and p orbitals [2,3,8]. Even complexes that do have perfect symmetry can give rise to d-d transitions, as this symmetry is momentarily distroyed by molecular vibration. Since electronic transitions are much faster than molecular vibration, it is the instantaneous symmetry of the complex that is important (cf Franck Condon principle) [10]. This breaks down the Laporte selection rule resulting in partially allowed transitions. The greater the distortion, the greater the intensity of the transition.

Many inorganic complexes, including copper complexes, absorb in the visible region (400-700 nm). The chemistry of the copper(II) ion differs from that of the copper(I) ion in that while the latter has a closed shell configuration $(Ar)d^{10}$ and forms diamagnetic and colourless complexes, the former has an incomplete d shell configuration $(Ar)d^9$ and its complexes are predominantly paramagnetic and highly coloured [11]. The aqueous chemistry of copper is largely devoted to Cu(II) compounds because Cu(I) compounds are quite unstable in aqueous solution. Cu(II) peptide complexes have been studied as models for Cu(II)-protein interactions. It was observed that strong Cu(II)-N(peptide) bonds are formed when protons are ionized from peptide nitrogen atoms. In the present study biological important donor atoms such as N(amino), N(imidazole), O(carboxylate), O(peptide), H_2O and OH^- were studied [12].

The Beer-Lambert-Bouger law, commonly called Beer's law, is the fundamental law governing the attenuation of radiation by a specific absorbing species in spectrometry.

$$A = \varepsilon bC \qquad (4.1)$$

where A is the absorbance, ε is the molar extinction coefficient, b is the path length of the sample cell and C is the molar concentration of the absorbing species. If the analyte solution

is a mixture of different species, the total absorbance at a specific wavelength (A^{λ}) can be expressed as;

$$A^{\lambda} = b\left(\varepsilon_1{}^{\lambda}C_1 + \varepsilon_2{}^{\lambda}C_2 + \varepsilon_3{}^{\lambda}C_3 + \cdots \varepsilon_n{}^{\lambda}C_n\right) \quad (4.2)$$

where the superscript λ is a parameter at a certain wavelength and subscripts 1, 2, 3…n are absorbing species. Equation 4.2 can be simplified;

$$A^{\lambda} = b\sum \varepsilon_i{}^{\lambda}C_i \quad (4.3)$$

Billo has proposed the most popular methods of structure determination using valves of λ_{max} [12]. Calculated λ_{max} is expressed as;

$$\lambda_{max} = \frac{10^3}{n_i v_i} \quad (4.4)$$

where n_i is the number of equatorial donor groups and v_i is the ligand field of the complex. Ligands used in this study have four main electron donor atoms; N-donor of the amide, N-donor of the imidazole, N-donor of the amine, O-donor of the carboxylate and O-donor of water. According to Billo [12], subsequently Sigel and Martin [13] and E. Prenesti *et al.*[14] the contribution of the different groups to λ_{max} are given in Table 4.0.

Table 4.0: Electron donor groups and corresponding ligand field.

Electron donor group	amino group ν_{NH}	imidazole group ν_{im}	amide group ν_N	carbonyl ν_O	carboxylate ν_O	water ν_O	hydroxide ν_O
Ligand field (ν_i 10^{-3} cm^{-1})	4.53 ± 0.07	4.34 ± 0.04	4.85 ± 0.05	3.43 ± 0.03	3.53 ± 0.03	2.96 ± 0.03	3.90 ± 0.09

4.1.3 Experimental

Aqueous solutions of 1:1 metal: tripeptides ratios were prepared in the pH range 2.0-11.0. The concentration of the tripeptide and metal were 0.005 M. The visible spectra of the Cu(II) and Ni(II) complexes were recorded on a Hewlett Packard 8452A Diode Array Spectrophotometer in the range 200-820 nm. The solutions were kept at a constant temperature of 25 °C. The spectra at different pH values need to be deconvoluted to yield spectra for individual species. This was done using UV_SPECTRA.EXE, an in-house computer program, which requires the concentration of each and every species in each solution and then calculates the molar extinction coefficients of the species at different

wavelengths. The stability constants determined from potentiometry are used to calculate each species concentration at the different valves of pH. Since each wavelength is treated independently, if the data can be deconvoluted and smooth curves are obtained it lends confidence to the potentiometric data [15,16].

4.1.4 Results and Discussion

4.1.4.1 Copper Tripeptide Complexes

4.1.4.1.1 Cu(II)/Sarcosyl-L-histidyl-L-lysine

Uv-Vis results for Cu(II) Sar-His-Lys are given in Figure 4.1. The spectrum of $[Cu(H_2O)_6]^{2+}$ agrees well with literature. The values of λ_{max}= 610 nm and ε_{max} =67.94 $dm^3\ mo1^{-1}cm^{-1}$ for CuLH are in agreement with data from Gergely and co-workers [17] as well as, Morris and Martin [18] for copper(II) complex of glycyl-L-histidine. The value of λ_{max} calculated for the Uv-Vis band, by the equation proposed by Billo [12], if the coordinating groups are amino, N^3-imidazole nitrogens and carbonyl oxygen in addition to a water molecule is 656 nm. This is 46 nm more than the observed maximum wavelength. A difference of 46 nm between the calculated and the experimental value of λ_{max} may be due the fact that coordination to the carboxylate oxygen is axial. Billo's method [12] assumes no axial coordination. At pH 6.75 CuL is the predominating species and the Cu-O amide bond breaks and the Cu-N amide bonds forms. The calculated d–d spectrum for CuL shows a band with λ_{max} at 607 nm (ε_{max} = 61.39 $dm^3\ mo1^{-1}cm^{-1}$).

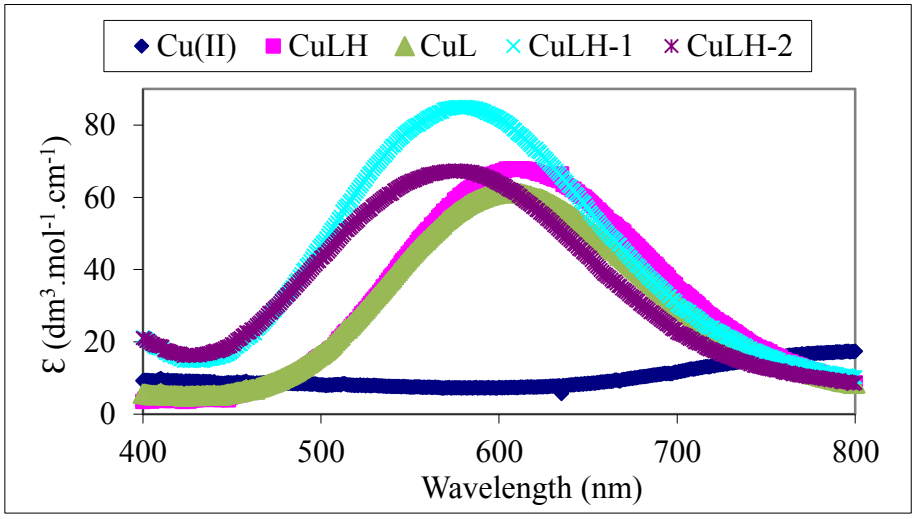

Figure 4.1: Uv-Vis spectra of different species for the Cu(II) Sar-His-Lys system.

Table 4.1 shows observed calculated λ_{max}, when the Billo equation is used and the coordination of an amino-N, deprotonated amide-N, imidazole-N and a water molecule is assumed [12]. The formation of $CuLH_{-1}$ and $CuLH_{-2}$ is followed by a significant blue shift of the d–d absorption maximum, with a decrease of λ_{max} value compared to the preceding species. Such a change is in line with the deprotonation of a coordinated water molecule to form a hydroxo species. Proposed structures are given in Figure 4.2.

Table 4.1: Uv-Vis spectra ε_{max} ($dm^3.mol^{-1}.cm^{-1}$) and λ_{max} (nm) experimental and calculated values are given together with possible donor groups for Cu(II) with sarcosyl-L-histidyl-L-lysine complexes.

Species	Experimental λ_{max} **(nm)**	ε_{max} **($dm^3.mol^{-1}.cm^{-1}$)**	Calculated λ_{max} **(nm)**	Possible donor atoms
CuLH	610	67.94	656	-NH, CO , N_{im}, H_2O
CuL	607	61.39	595	-NH, N^- , N_{im}, H_2O
$CuLH_{-1}$	577	85.05	576	-NH, N^- , N_{im}, OH^-
$CuLH_{-2}$	575	67.47	576	-NH, N^- , N_{im}, OH^-

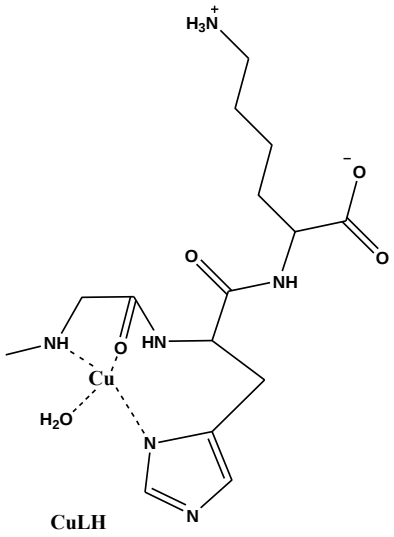

CuLH

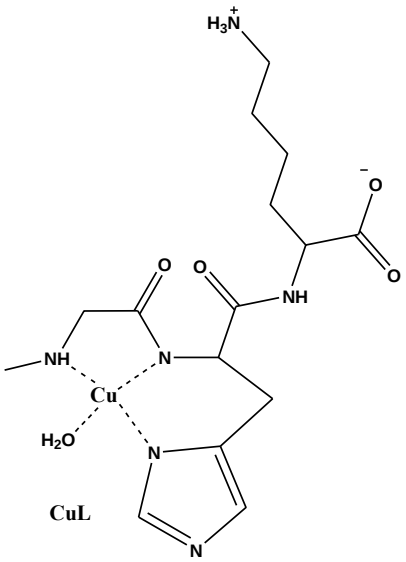

CuL

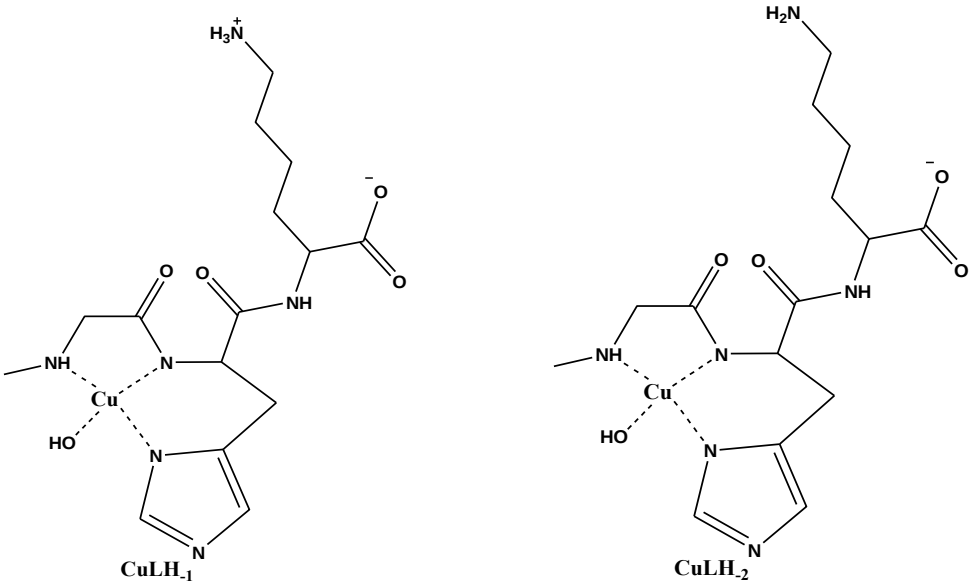

Figure 4.2: Proposed structures of complexes formed between Cu(II) and Sar-His-Lys.

The formation of the $CuLH_{-2}$ species does not have an impact on the spectrum which implies that there is no change in the metal coordination environment. Formation of MLH_{-2} is then assigned to the deprotonation of the lysine side-chain amino group. The pH at which this occurs is 10.65, which is similar to the pK_a of the free tripeptide (SHK).

4.1.4.1.2 Cu(II)/Sarcosyl-L-lysyl-L-histidine

Results for Cu(II) Sar-Lys-His are given in Figure 4.3. The CuLH species could not be detected spectroscopically because to its overlap with CuL in the speciation diagram and its very low concentration.

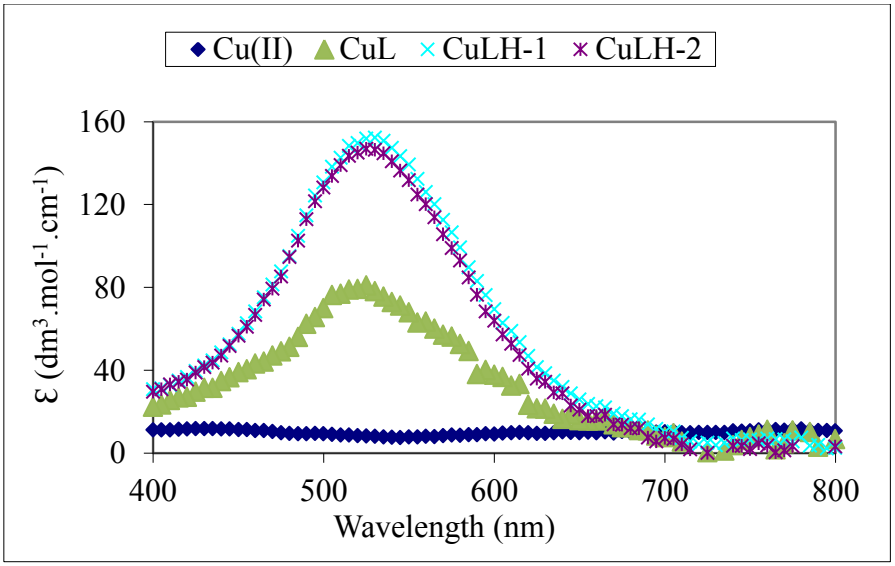

Figure 4.3: Uv-Vis spectra of different species for the Cu(II) Sar-Lys-His system.

Experimental and calculated λ_{max} for the complex species are given in Table 4.2. The spectroscopic parameters of CuL, $CuLH_{-1}$ and $CuLH_{-2}$ species suggest the participation of four nitrogen atoms [NH_2, 2N−, N_{im}] in the equatorial plane of Cu(II) ions forming a very stable chelate ring, typical for analogous Cu(II) complexes with peptides containing the N-terminal sequence Xaa-Yaa-His [19-21]. However, the raw data for Sar-Lys-His was different in that there was no shifting of the single absorption band during the titration. The λ_{max} at 525 nm, is similar to the values for 4N Cu(II) complexes with; λ_{max} = 525 nm, HVH [20]; λ_{max} = 520 nm, DAH [22]; λ_{max} = 520 nm, SSH [22]; λ_{max} =520 nm, DAHK [23]. The $CuLH_{-1}$ species predominates in the pH range 4.0-10.7. This phenomenon is characteristic of the stability caused by the tetradentate chelate ring [NH_2, 2N−, N_{im}] of Cu(II) complexes with peptides containing the N-terminal sequence Xaa-Yaa-His [19,20,21].

Table 4.2: Uv-Vis spectra ε_{max} ($dm^3.mol^{-1}.cm^{-1}$) and λ_{max} (nm) experimental and calculated values are given together with possible donor groups for Cu(II) with sarcosyl-L-lysyl-L-histidine complexes.

Species	Experimental λ_{max} **(nm)**	ε_{max} **($dm^3.mol^{-1}.cm^{-1}$)**	Calculated λ_{max} **(nm)**	Possible donor atoms
CuL	525	80.84	533	-NH, 2 N^-, N_{im}
$CuLH_{-1}$	525	146.84	533	-NH, 2 N^-, N_{im}
$CuLH_{-2}$	525	151.78	533	-NH, 2 N^-, N_{im}

The ε-amino group of the Lys is deprotonated, but remains uncoordinated. This is similar to the analogous Cu(II) complexes with tetrapeptide SHHK- and SAHK-, and other peptides containing the Lys residue [24,25]. Predicted structures are given in Figure 4.4.

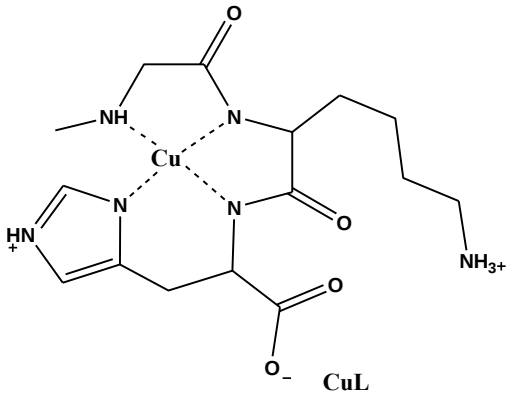

CuL

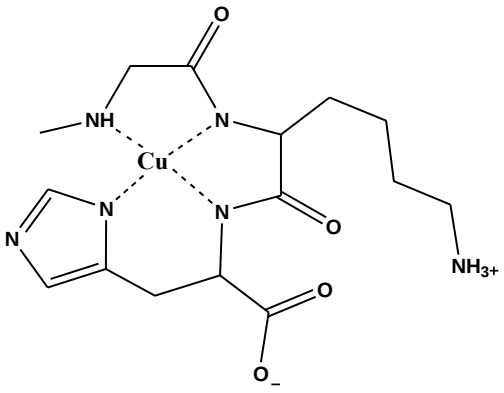

$CuLH_{-1}$

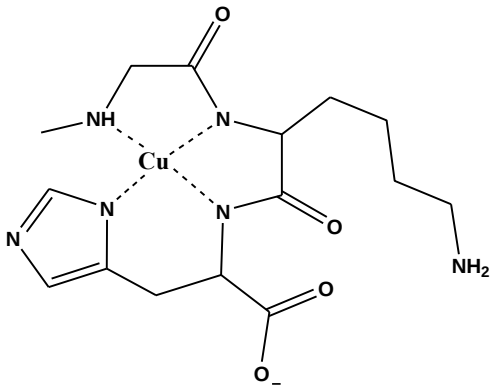

$CuLH_{-2}$

Figure 4.4: Proposed structures of complexes formed between Cu(II) and Sar-Lys-His.

4.1.4.1.3 Cu(II)/Sarcosyl-L-histidyl-L-histidine

Results for Cu(II) Sar-His-His are given in Figure 4.5. λ_{max}= 630 nm for CuLH indicates that Cu(II) coordinates to amino, N^3-imidazole nitrogens, carbonyl oxygen and in addition to a water molecule [20,26]. The λ_{max} of CuL is very similar (610 nm), which indicates that the coordination sphere is the same. The difference between the two species is that the uncoordinated imidazole is protonated in CuLH. A small blue shift is observed for CuL species. This might be a result of H-bonding between the non-coordinated COO^- and the solvent [27,28].

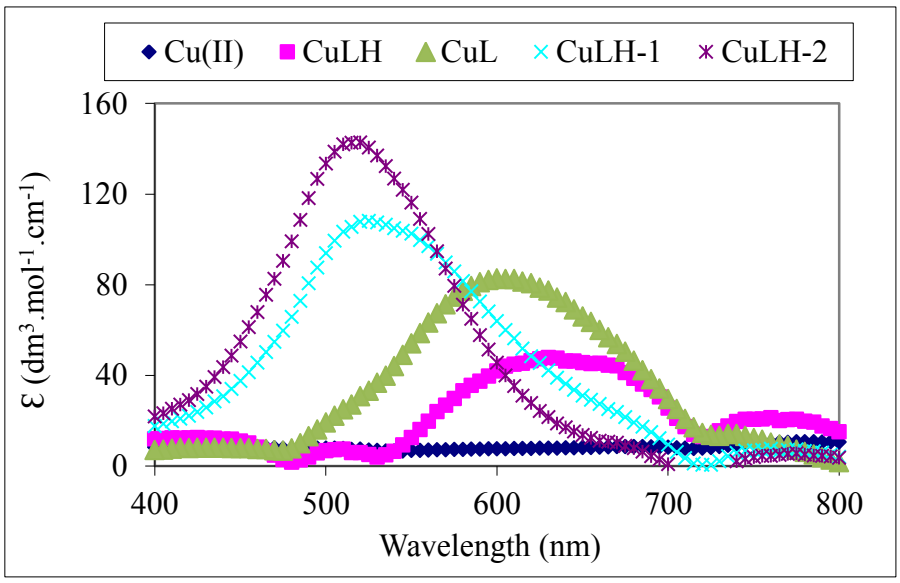

Figure 4.5: Uv-Vis spectra of different species for the Cu(II) Sar-His-His system.

Experimental and calculated values of λ_{max} for the complex species are given in Table 4.3. The band shifts to a much lower maximum wavelength when $CuLH_{-1}$ forms. This can be explained by a bond rearrangements; Cu-O_{amide} bond breaks and Cu(II) coordinates to the N_{amide}. This suggest that Cu(II) coordinates to amino-N, deprotonated amide-N, imidazole-N and a water molecule. There is another band shifts to a lower maximum wavelength of 525 nm, when $CuLH_{-2}$ forms, this is suggest an increase of electron density around the metal ion. The results of the Uv-Vis spectra absorption spectroscopy are consistent with the findings of species distribution that $CuLH_{-2}$ is the major species detected above pH 10.63 and the determined λ_{max} was close to those determined for Cu(II)-oligopeptide complexes with a suggested [-NH, $2N^-$, N_{im}] type environment [29,30]. The proposed structures are given in Figure 4.6.

Table 4.3: Uv-Vis spectra ε_{max} ($dm^3.mol^{-1}.cm^{-1}$) and λ_{max} (nm) experimental and calculated values are given together with possible donor groups for Cu(II) with sarcosyl-L-histidyl-L-histidine complexes.

Species	Experimental λ_{max} **(nm)**	ε_{max} **($dm^3.mol^{-1}.cm^{-1}$)**	Calculated λ_{max} **(nm)**	Possible donor atoms
CuLH	630	47.74	656	-NH, CO, N_{im}, H_2O
CuL	610	82.40	656	-NH, CO, N_{im}, H_2O
$CuLH_{-1}$	545	103.72	595	-NH, N^-, N_{im}, H_2O
$CuLH_{-2}$	520	142.78	533	-NH, 2 N^-, N_{im}

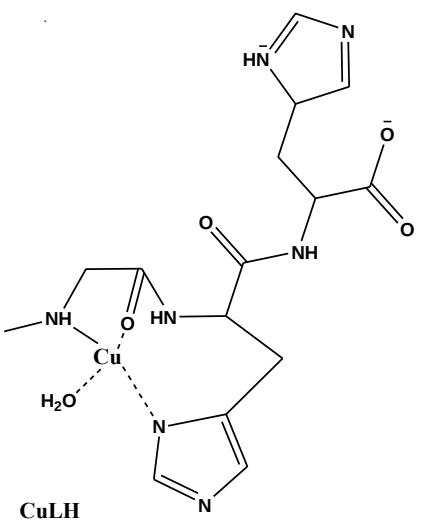

CuLH

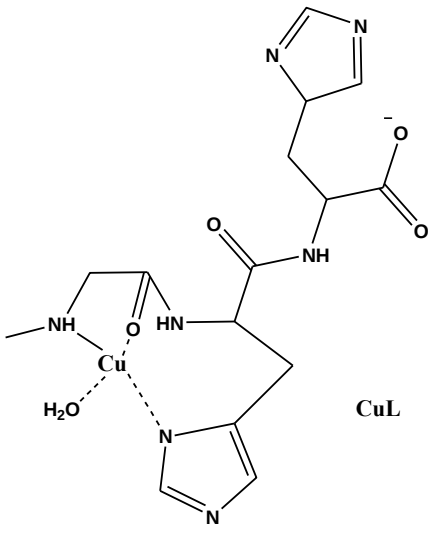

CuL

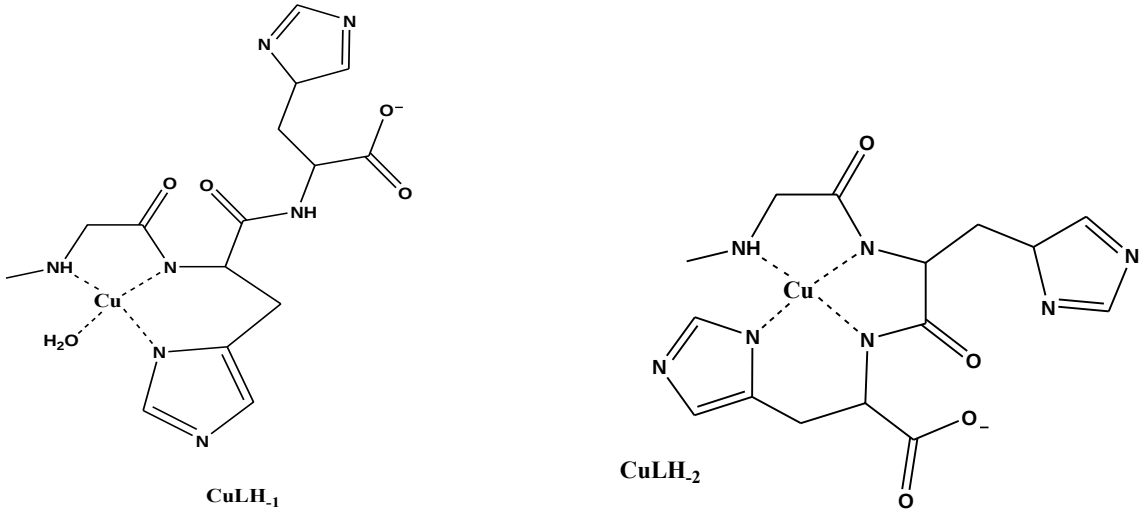

Figure 4.6: Proposed structures of complexes formed between Cu(II) and Sar-His-His.

4.1.4.1.4 Cu(II)/Sarcosyl-L-lysyl-L-lysine

The CuLH species geometry is not the same as that of the anther species (CuL, $CuLH_{-1}$ and $CuLH_{-2}$). This conclusion is fully supported by spectroscopic results, reported in Figure 4.7 and summarised in Table 4.4. The absorption spectra of CuLH as characterised by Uv-Vis spectroscopy, show that the wavelength of maximum absorption is 660 nm, close to the calculated value of 654 nm, which can be computed by means of the empirical formula developed by Sigel and Martin [13] for the coordination of two nitrogen atoms to Cu(II) [-NH, N^-, $2H_2O$].

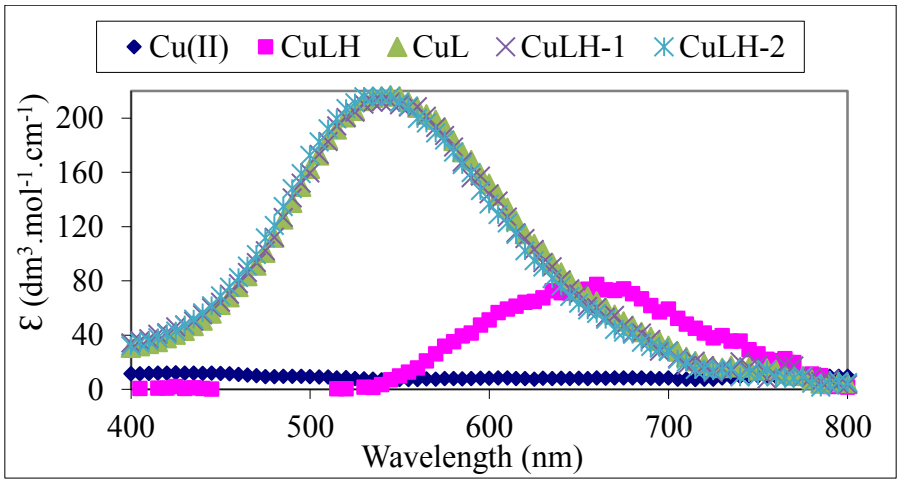

Figure 4.7: Uv-Vis spectra of different species for the Cu(II) Sar-Lys-Lys system.

Table 4.4: Uv-Vis spectra ε_{max} ($dm^3.mol^{-1}.cm^{-1}$) and λ_{max} (nm) experimental and calculated values are given together with possible donor groups for Cu(II) with sarcosyl-L-lysyl-L-lysine complexes.

Species	Experimental λ_{max} **(nm)**	ε_{max} **($dm^3.mol^{-1}.cm^{-1}$)**	Calculated λ_{max} **(nm)**	Possible donor atoms
CuLH	660	77.32	654	-NH, N^-, 2 H_2O
CuL	545	216.98	558	-NH, 2 N^-, COO^-
$CuLH_{-1}$	540	212.90	558	-NH, 2 N^-, COO^-
$CuLH_{-2}$	540	216.10	558	-NH, 2 N^-, COO^-

Predicted structures are given in Figure 4.8. In the CuL, $CuLH_{-1}$ and $CuLH_{-2}$ species the tripeptide binds the copper ion in a tetradentate complex by its N-terminal amino group *via* N, the first two amide nitrogens and the C-terminal carboxylate group via O. This way of coordination is typical of tripeptides, like Gly-Gly-Gly (GGG) in $CuLH_{-2}$ [13]. The values of λ_{max}= 540 nm and ε_{max} = 216.10 dm^3 $mo1^{-1}cm^{-1}$ for $CuLH_{-2}$ are in very good agreement with data for Gly-Gly-Gly, Gly-Leu-Tyr and Ala-Ala-Asp-Ala [31] for the same species.

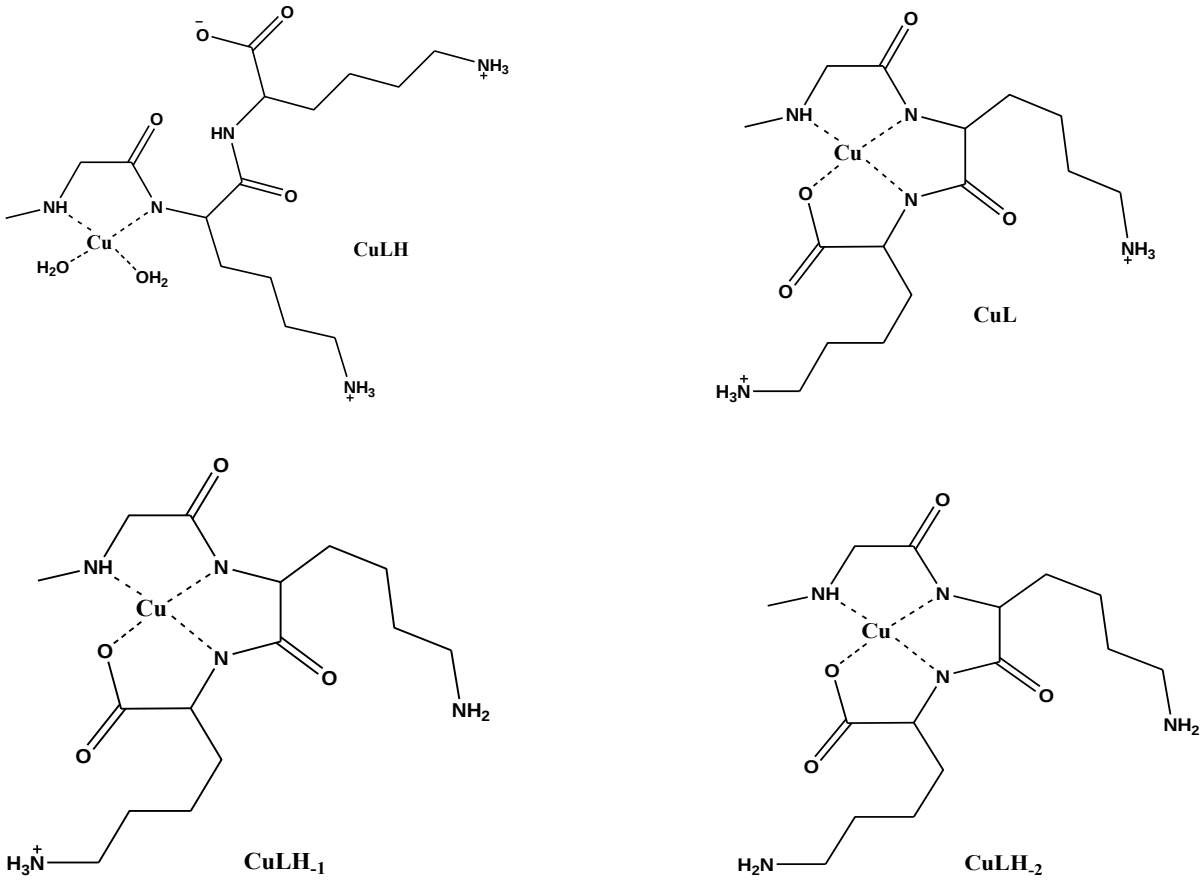

Figure 4.8: Proposed structures of complexes formed between Cu(II) and Sar-Lys-Lys.

4.1.4.1.5 Cu(II)/Sarcosyl-L-glycyl-L-histidine

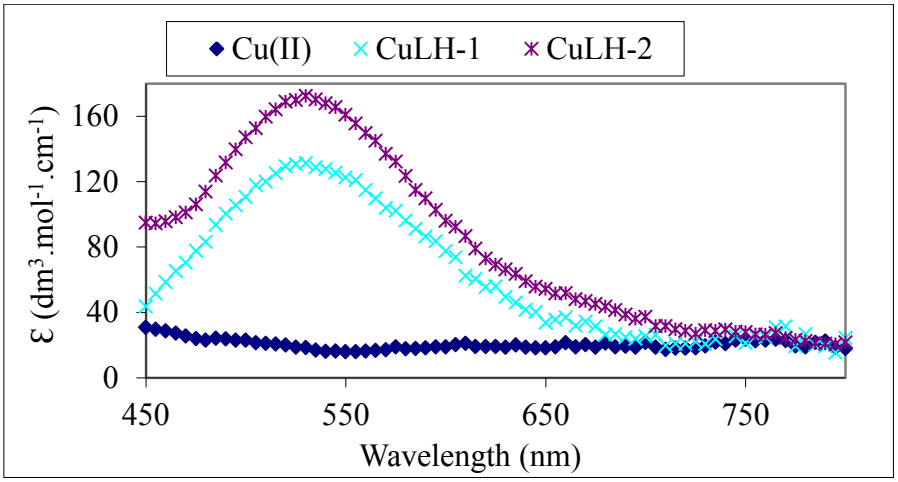

Figure 4.9: Uv-Vis spectra of different species for the Cu(II) Sar-Gly-His system.

Figure 4.9 shows that the Uv-Vis spectroscopic data, obtained for the Cu(II) Sar-Gly-His species formed at high pH, strongly support the existence of amine binding for all possible stoichiometries. Unfortunately, the low concentration of the CuLH species does not make it possible to calculate the spectroscopic data of this species. Table 4.5 shows the absorption spectra of $CuLH_{-1}$ and $CuLH_{-2}$ as characterised by Uv-Vis spectroscopy.

Table 4.5: Uv-Vis spectra ε_{max} ($dm^3.mol^{-1}.cm^{-1}$) and λ_{max} (nm) experimental and calculated values are given together with possible donor groups for Cu(II) with sarcosyl-L-glycyl-L-histidine complexes.

Species	Experimental λ_{max} **(nm)**	ε_{max} **($dm^3.mol^{-1}.cm^{-1}$)**	Calculated λ_{max} **(nm)**	Possible donor atoms
$CuLH_{-1}$	530	131.20	533	-NH, 2 N^-, N_{im}
$CuLH_{-2}$	530	172.45	533	-NH, 2 N^-, N_{im}

The proposed structures are given in Figure 4.10. The λ_{max} is 530 nm, close to the value of 533 nm, which can be computed by means of the empirical formula developed by Sigel and Martin [32] for the coordination of an N-terminal amino group, the two amide nitrogens and the imidazole group via N^3. This way of coordination is typical of tripeptides, like Gly-Gly-His (GGH) in $CuLH_{-2}$ [33]. The values of λ_{max}= 530 nm and ε_{max} =172.45 $dm^3mo1^{-1}cm^{-1}$ for $CuLH_{-2}$ are in agreement with data of Gly-Gly-His [33] for the same species.

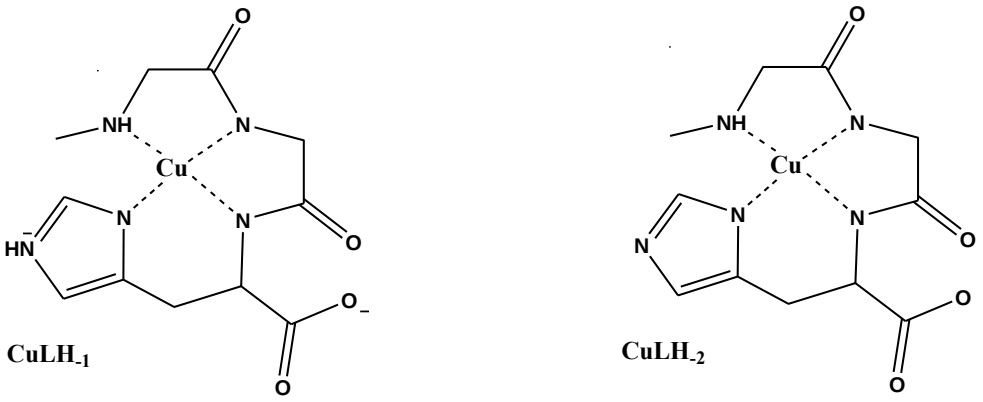

Figure 4.10: Proposed structures of complexes formed between Cu(II) and Sar-Gly-His.

4.1.4.2 Nickel Tripeptide Complexes

4.1.4.2.1 Ni(II)/Sarcosyl-L-histidyl-L-lysine

The absorption spectra and electronic spectra for individual species of the Ni(II) Sar-His-Lys complexes, as a function of pH, are given in Figure 4.11. At pH 5 the solution colour starts to change from light green to yellow. The deprotonation of two or more amide nitrogens in nickel(II) peptide complexes is often followed by fundamental changes of Uv-Vis spectra, representing a geometrical shift of the complexes from octahedral (light green) to square planar (yellow) structures [25,34,35].

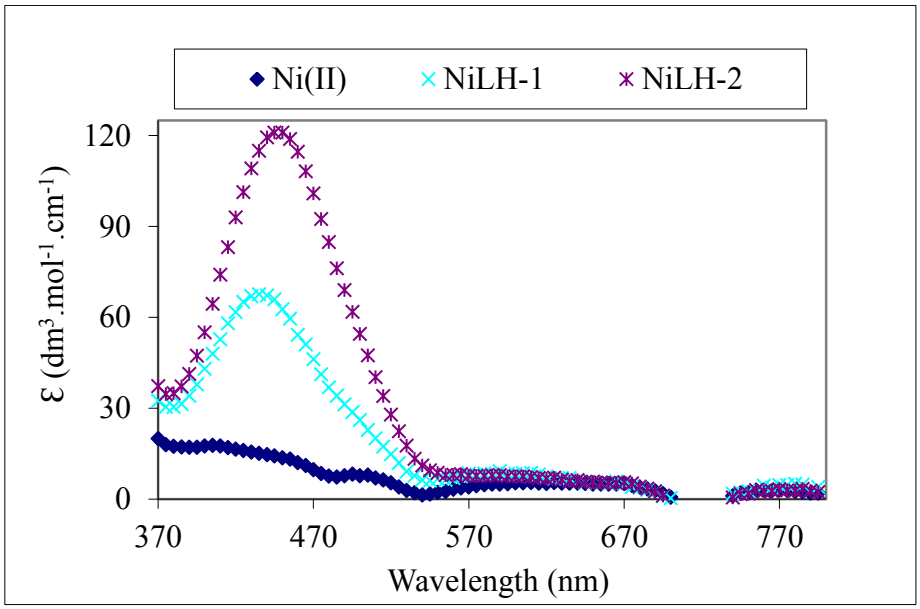

Figure 4.11: Uv-Vis spectra of different species for the Ni(II) Sar-His-Lys system.

Table 4.6 shows the wavelength and molar extinction coefficient values corresponding to maximum absorption of the Ni(II) species formed in solution with possible donor groups for this ligand. On the other hand, the individually calculated λ_{max} band of $NiLH_{-1}$ (λ_{max} = 435 nm, Ɛ = 67.56 M^{-1} cm^{-1}) supports unambiguously amino, peptide, imidazole nitrogens and hydroxide donors in the coordination sphere [36].

Table 4.6: Uv-Vis spectra $Ɛ_{max}$ ($dm^3.mol^{-1}.cm^{-1}$) and λ_{max} (nm) experimental value, with possible donor groups for Ni(II) with sarcosyl-L-histidyl-L-lysine complexes.

Species	Experimental λ_{max} **(nm)**	ε_{max} **($dm^3.mol^{-1}.cm^{-1}$)**	Possible donor atoms
$NiLH_{-1}$	435	67.56	-NH, N^-, N_{im}, OH^-
$NiLH_{-2}$	445	120.95	-NH, N^-, N_{im}, OH^-

4.1.4.2.2 Ni(II)/Sarcosyl-L-lysyl-L-histidine

The results for Ni(II) Sar-Lys-His are given in Figure 4.12. The first species formed is probably NiL at pH value around 6.32. In contrast, the NiL, $NiLH_{-1}$ and $NiLH_{-2}$ species present similar spectroscopic parameters, supporting the idea of the same coordination in all modes of Ni(II) ions.

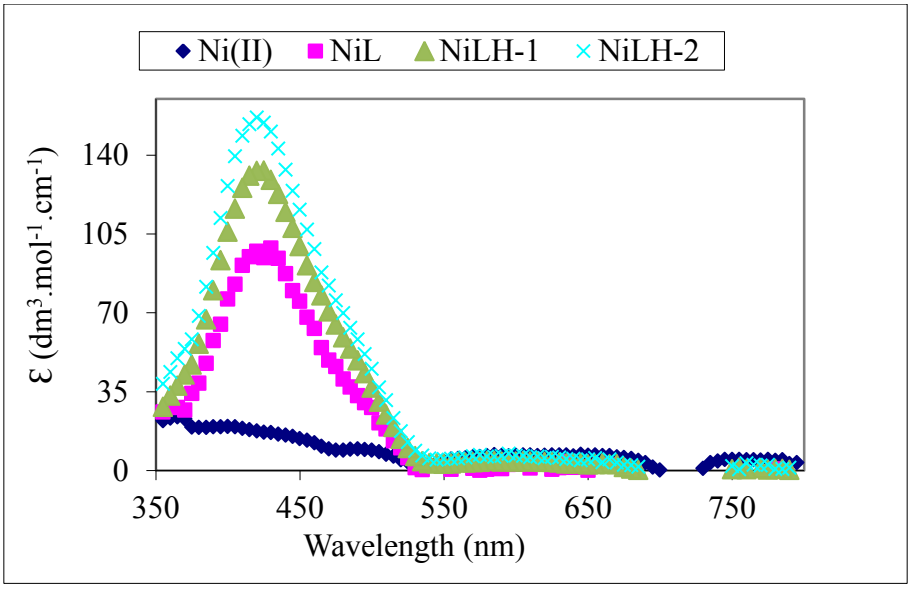

Figure 4.12: Uv-Vis spectra of different species for the Ni(II) Sar-Lys-His system.

The maximum wavelength near 420-430 nm, for these complex species are comparable with the values for analogous 4N [NH_2, $2N^-$, N_{im}] Ni(II) complexes with the Gly-Gly-Histamine GGHist [23] (λ_{max} = 425 nm) and Gly-Gly-His GGH [37] (λ_{max} = 425 nm). Thus, the

simultaneous equatorial coordination of the imidazole ring of His, the N-terminal amino group and the two amide nitrogens, in a square-planar Ni(II) arrangement, is suggested. A very stable tetradentate ring is thus formed, typical for analogous Ni(II) complexes with peptides containing the N-terminal sequence Xaa-Yaa-His [38,39]. Experimental valves of λ_{max} are given in Table 4.7.

Table 4.7: Uv-Vis spectra ε_{max} ($dm^3.mol^{-1}.cm^{-1}$) and λ_{max} (nm) experimental value, with possible donor groups for Ni(II) with sarcosyl-L-lysyl-L-histidine complexes.

Species	Experimental λ_{max} **(nm)**	ε_{max} **($dm^3.mol^{-1}.cm^{-1}$)**	Possible donor atoms
NiL	420	98.72	-NH, 2 N^-, N_{im}
$NiLH_{-1}$	430	133.06	-NH, 2 N^-, N_{im}
$NiLH_{-2}$	425	156.56	-NH, 2 N^-, N_{im}

4.1.4.2.3 Ni(II)/Sarcosyl-L-histidyl-L-histidine

Figure 4.13 shows the Uv-Vis spectroscopic data obtained at pH 4. The first species, which appears in high concentration, is $NiLH_2$. For representative concentration distribution curves see Figure 3.34 (Chapter 3).

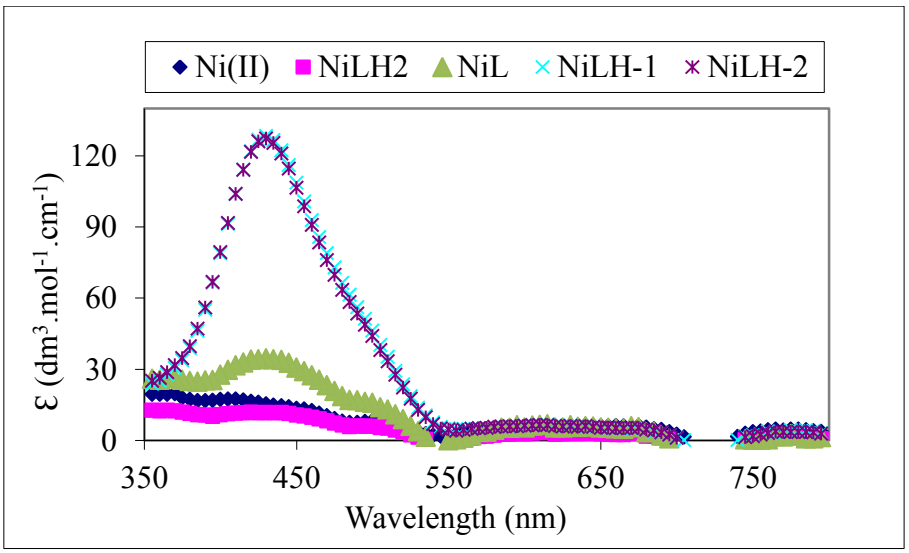

Figure 4.13: Uv-Vis spectra of different species for the Ni(II) Sar-His-His system.

If the logarithmic protonation constants of both the imidazole groups from $\log\beta_{NiLH2}$ are subtracted (18.09–5.90–7.17), the value obtained suggests predominant N-terminal amino and carbonyl-O group coordination (perhaps carbonyl-O group weak coordination of the

peptide). In this species, both imidazole groups are still protonated. Upon increasing the pH, cooperative release of one proton occurs and the NiL species appears in measurable concentration. The analysis of the data suggests that the bonding mode of NiL formed with Sar-His-His is the same as it is in NiL of Gly-His, but the imidazole group of the second histidine is still protonated [40].

Table 4.8 shows experimental valves of λ_{max} and the composition of the species $NiLH_{-1}$ of similar coordination mode which is the most likely. Above pH 6.29 the previously colourless sample turns yellow. This change in the colour, which can be attributed to a single absorption band (λ_{max} = 430 nm), strongly suggests the formation of square-planar complexes. This behaviour is similar to that of the Ni(II)-Gly-His species, which is formed below pH 8. The most stable coordination mode of occurs via the terminal amino-N, peptide-N and imidazole-N donors [41]. As a consequence, the latter coordination mode found in the high stability planar complex of $NiLH_{-2}$, for which the individually calculated spectrum has a λ_{max} at 430 nm and ε = 127.31 M^{-1} cm^{-1}, suggests the coordination of a deprotonated peptide-N [18] at the fourth equatorial site.

Table 4.8: Uv-Vis spectra ε_{max} ($dm^3.mol^{-1}.cm^{-1}$) and λ_{max} (nm) experimental value, with possible donor groups for Ni(II) with sarcosyl-L-histidyl-L-histidine complexes.

Species	Experimental λ_{max} **(nm)**	ε_{max} **($dm^3.mol^{-1}.cm^{-1}$)**	Possible donor atoms
$NiLH_2$	430	11.8	-NH, CO, $2H_2O$
NiL	430	34.64	-NH, CO , N_{im}, H_2O
$NiLH_{-1}$	430	128.46	-NH, N^- , N_{im}, H_2O
$NiLH_{-2}$	430	127.31	-NH, 2 N^- , N_{im},

4.1.4.2.4 Ni(II)/Sarcosyl-L-lysyl-L-lysine

Above pH 7.5 the previously colourless sample turns yellow. The absorption spectra confirmed that above pH 7.5 planar species NiL, $NiLH_{-1}$ and $NiLH_{-2}$ are present with a characteristic λ_{max} at 425 nm. When the pH increases the NiL species appears in measurable concentration. The analysis of the data suggests that the bonding mode of NiL formed with Sar-Lys-Lys is the same as it is in $NiLH_{-2}$ of Gly-Gly-Gly, but the ε-amino group of both lysine residues are still protonated [42]. The spectrum show in Figure 4.14 also confirms amide deprotonation and coordination of the amide nitrogen donor atoms, resulting in the

same species as reported for Cu(II). In the formation of $NiLH_{-1}$ and $NiLH_{-2}$ species, the two protons lost are assigned to deprotonation and de-coordinated of two lysine side-chain ε-amino groups. The pKa valves of 10 and 10.47 respectively, were almost the same as these for free Sar-Lys-Lys.

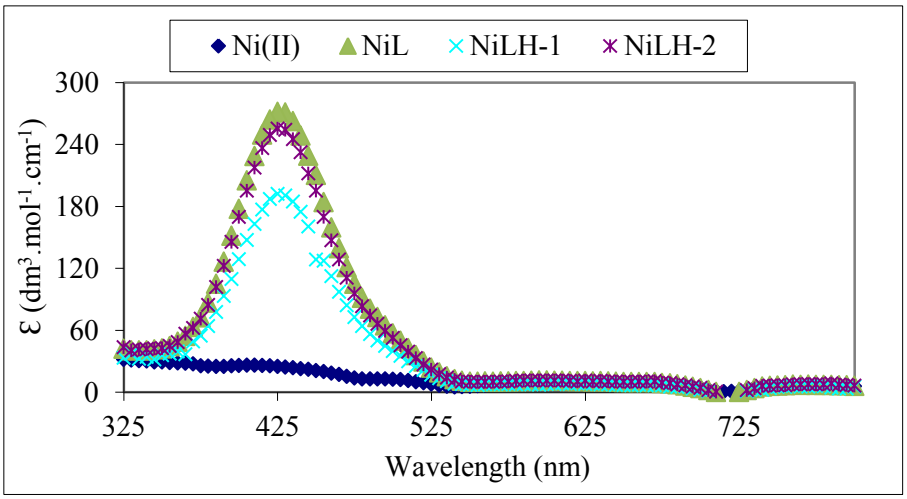

Figure 4.14: Uv-Vis spectra of different species for the Ni(II) Sar-Lys-Lys system.

The experimental valves of λ_{max} with possible donor groups and molar extinction coefficients are given in Table 4.9. The valve of λ_{max} = 425 nm, from literature supports unambiguously the presence of amino, two deprotonated amide nitrogens and a carboxylate group in the coordination sphere [36].

Table 4.9: Uv-Vis spectra ε_{max} ($dm^3.mol^{-1}.cm^{-1}$) and λ_{max} (nm) experimental value, with possible donor groups for Ni(II) with sarcosyl-L-lysyl-L-lysine complexes.

Species	Experimental λ_{max} **(nm)**	ε_{max} **($dm^3.mol^{-1}.cm^{-1}$)**	Possible donor atoms
NiL	425	271.42	-NH, $2N^-$, COO^-
$NiLH_{-1}$	425	192.01	-NH, $2N^-$, COO^-
$NiLH_{-2}$	425	255.07	-NH, $2N^-$, COO^-

4.2 ^{1}H NMR SPECTROSCOPY

4.2.1 Introduction

Proton magnetic resonance spectroscopy (^{1}H NMR) is an analytical chemistry technique used to determine the structure of molecules. It can also be used to assign the site of protonation or the structure of metal complexes. In the case of Cu(II), the protons near the site of coordination generally show characteristic broad signals or shifts in the ^{1}H NMR spectrum of the coordinated species verses its uncoordinated counterparts [43,44]. The structural features of Cu(II) complexes can be studied by ^{1}H NMR despite the broadening of the signal caused by the presence of the metal unpaired electron, provided that exchange conditions are sufficiently fast to observe an average between the free and the bound ligand [45]. The broadening can be a "through bond effect" (Fermi contact interaction) or a "through space effect" which is dependent on the distance between the paramagnetic center and the observed nucleus. The differential effect of the metal ion on the ligand can then be used to determine the structure of the complex.

4.2.2 Experimental

^{1}H-NMR experiments were performed on a Bruker Avance 400MHz spectrometer. The one-dimensional experiments were carried out in 1: 9 D_2O: H_2O mixtures at 25 $^{\circ}$C. The pH of the solutions was adjusted with NaOH/HCl. A CRISONmicro pH meter equipped with a Metrohm glass electrode was used to measure the pH. The spectra were recorded in the pH range 2.00-11.00 with tert-butyl alcohol as an internal reference. NMR spectra were recorded using the zgesgp pulse sequence. This sequence effectively suppresses the solvent signal using excitation sculpting. The common pre-saturation technique could not be used as this also suppresses amide protons through chemical exchange. Spectra were recorded at different pH values and at different copper concentrations [43,46,47]. The data were processed using MestReNova version 9.1 software.

4.2.3 Results

4.2.3.1 Protonation Titrations

In ^{1}H NMR spectroscopy, the diamagnetic contribution to chemical shift dominates over the paramagnetic contribution. This makes non-exchanging, carbon-bound protons a good probe

of local electron density and thus group-specific ionization. The range of influence of a protonating moiety can be studied using a homologous series of monoprotic systems [48].

4.2.3.1.1 Protonation of the sarcosyl-L-histidyl-L-lysine

Figure 4.16 shows the ^{1}H NMR spectra obtained at different pH values. The assignments of the spectra are indicated and follow the numbering in Figure 4.15. In going from low to high pH, the signals **a** and **b** were the first to shift from low to high field. This is ascribed to deprotonation of the imidazole nitrogen group. These signals started shifting at low pH and were still shifting to some extent at pH 7.

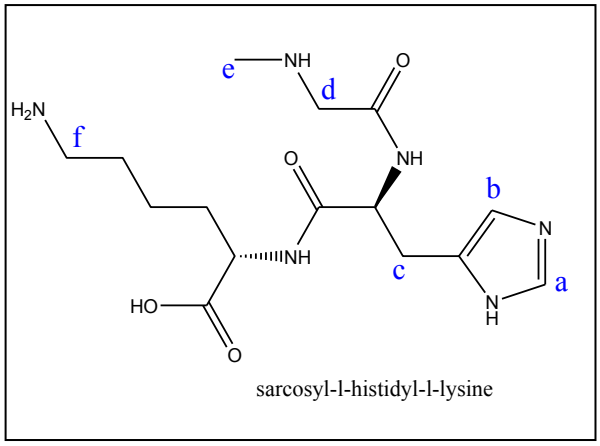

Figure 4.15: The structure of the Sar-Lys-His shows the proton labels in Figure 4.16 & 4.17.

Signal **d** shifts between pH 5.5 and 9.0. This indicates that the terminal amine is being deprotonated in this pH range. From pH 8.5 to pH 11.5 the lysine H_{ε} proton shifts as the lysine side-chain is deprotonated. The change in chemical shifts as a function of pH of protons near e possible coordination sites is shown in Figure 4.17. Based on these results, the sequence of protonation of sarcosyl-L-histidyl-L-lysine is; the pK_a= 8.5. of 2.283 corresponded to the protonation of the carboxylic group, the protonation of the imidazole nitrogens was at pK_a = 6.57, the terminal -NH corresponded to pK_a = 8.37 and the N-terminal of lysine residues NH_2 corresponded to pK_a = 10.33.

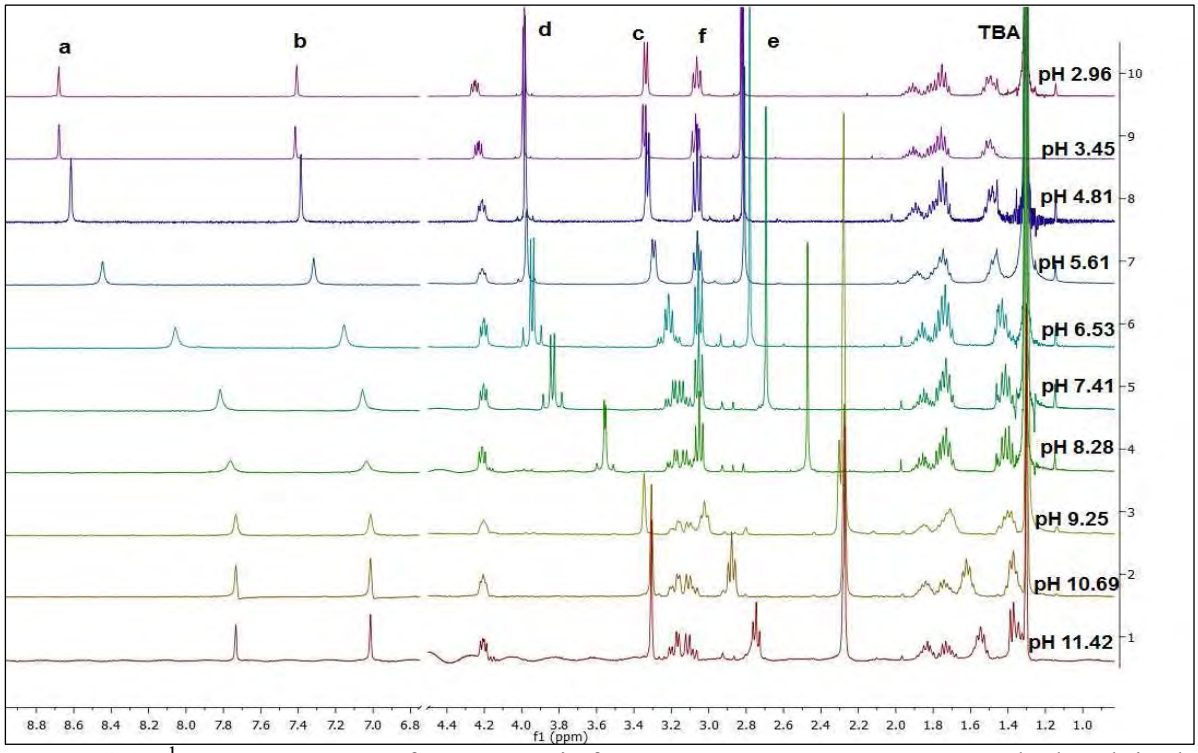

Figure 4.16: ^{1}H NMR spectra of Sar-Lys-His form pH 2.02 to pH 11.01. Note the break in the f1 dimension at 4.4 ppm. The proton assignments are according to Figure 4.15.

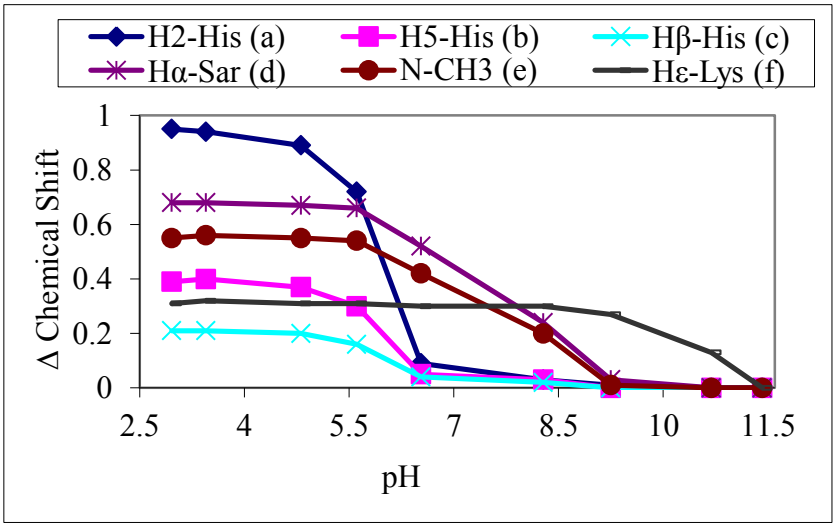

Figure 4.17: Change of chemical shifts of selected protons of Sar-Lys-His as a function of pH. The assignment is given in Figure 4.15.

4.2.3.1.2 Protonation of the sarcosyl-L-histidyl-L-histidine

Figure 4.19 shows the ^{1}H NMR spectra obtained at different pH values. The assignment of the protons is given in Figure 4.18. From the potentiometric results, Sar-His-His has 4 dissociable protons; the carboxylic acid, the two histidine imidazole protons and the terminal

amine proton. The signals **a1**, **a2** and **b1**, **b2** were the first to shift from low to high field. These assignments were complicated by the presence of two His residues in the tripeptide sequence. What is clear is that the two **a** protons and the two **b** protons have a differential shift. That is they shift apart and then back together again indicating that first imidazole **a2** is protonated and then the imidazole **a1** of the C-terminal histidine.

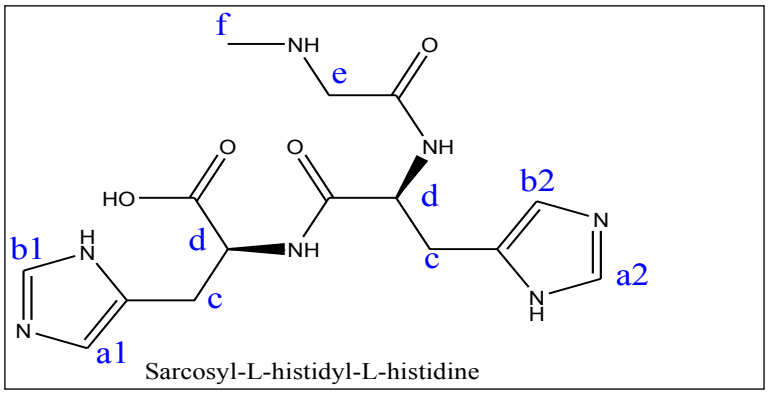

Figure 4.18: The structure of the Sar-His-His shows the proton labels in Figures 4.19 & 4.20.

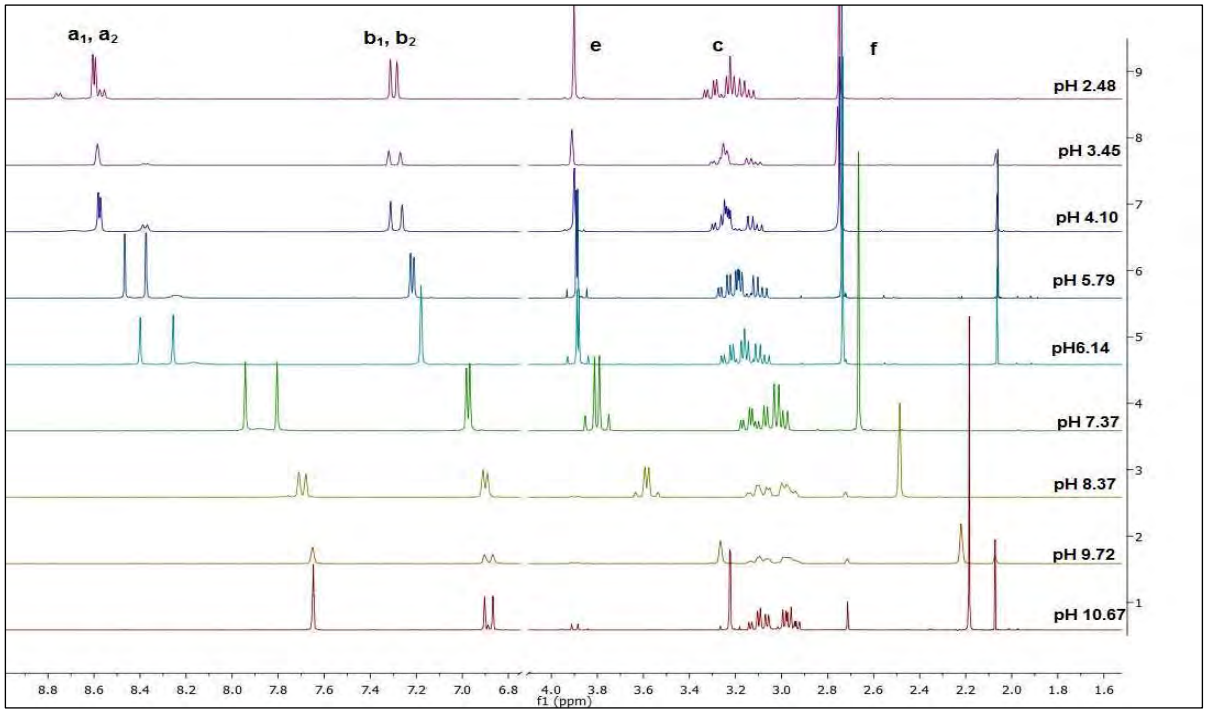

Figure 4.19: ^{1}H NMR spectra of Sar-His-His form pH 2.02 to pH 11.01. Note the break in the f1 dimension at 4.4 ppm. The proton assignments are according to Figure 4.18.

Signal **e** started to shift from pH 7.37. This is due to the deprotonation of the terminal amine nitrogen. Figure 4.20 shows a plot of selected protons of SHH as a function of pH.

Finally, the pK_a value of the carboxyl group of His (pK_a = 2.3) could not be observed, potentiometrically, since it occurred at a very low pH.

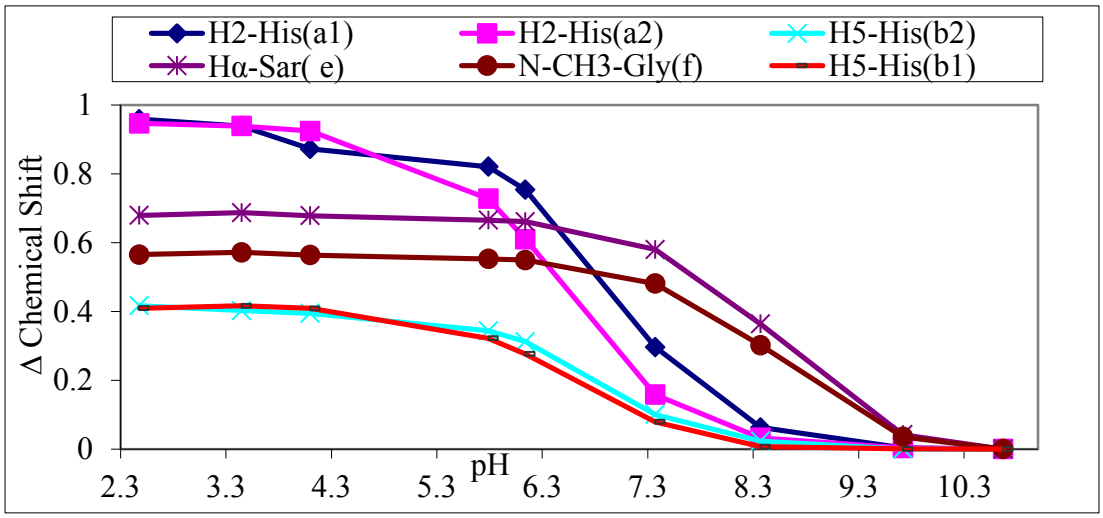

Figure 4.20: Change of chemical shifts of selected protons of Sar-His-His as a function of pH. The assignment is given in Figure 4.18.

4.2.3.1.3 Protonation of sarcosyl-L-lysyl-L-lysine

The proton labels for Sar-Lys-Lys are given in Figures 4.21 and the ^{1}H NMR spectra in Figure 4.22. The changes of chemical shifts of selected protons are given in Figure 4.23. Signal **a** shifted from pH 8.13 to pH 10.91. Since the spectra are recorded in D_2O/H_2O the amide protons are observed at ~ 8.2 ppm. Between pH 2.0 and 3.0 the one amide doublet shift significantly as the terminal lysine carboxylic acid is deprotonated. Above pH 5-6 these protons are in rapid exchange and so are no longer observed.

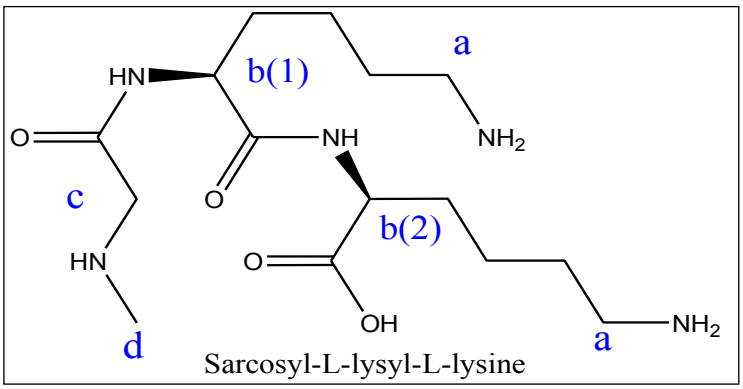

Figure 4.21: The structure of the Sar-Lys-Lys shows the proton labels in Figures 4.22 &4.23.

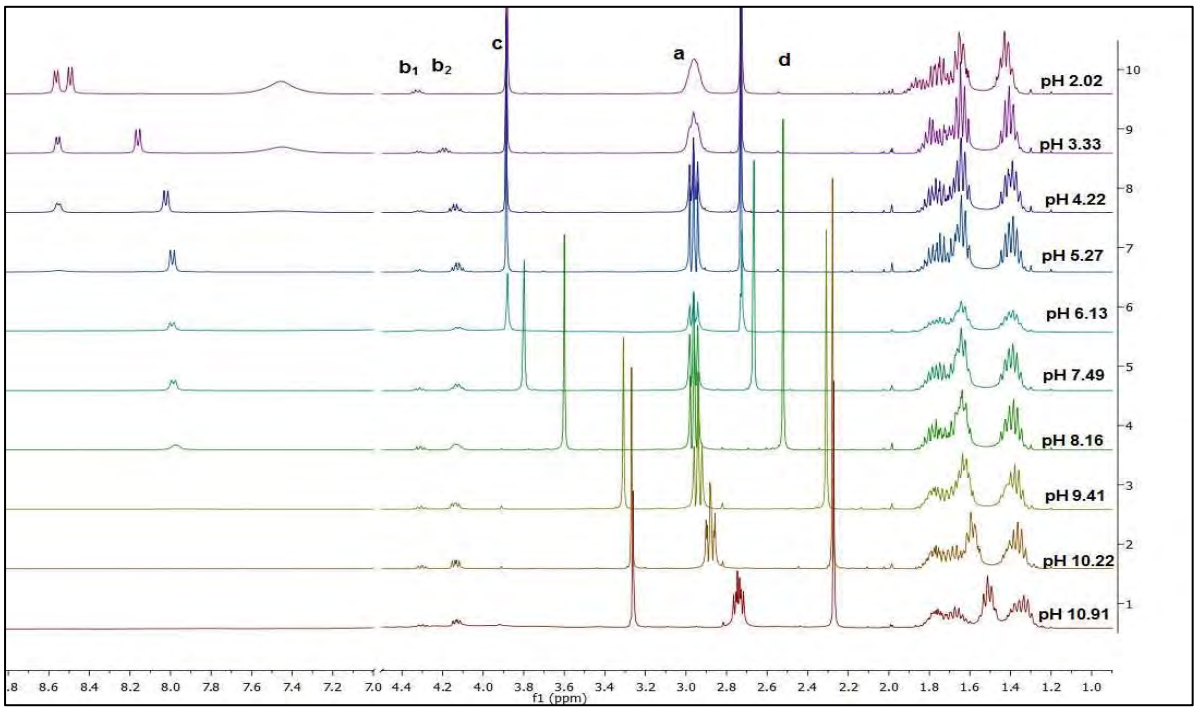

Figure 4.22: ^{1}H NMR spectra of Sar-Lys-Lys form pH 2.02 to pH 11.01. Note the break in the f1 dimension at 4.4 ppm. The proton assignments are according to Figure 4.21.

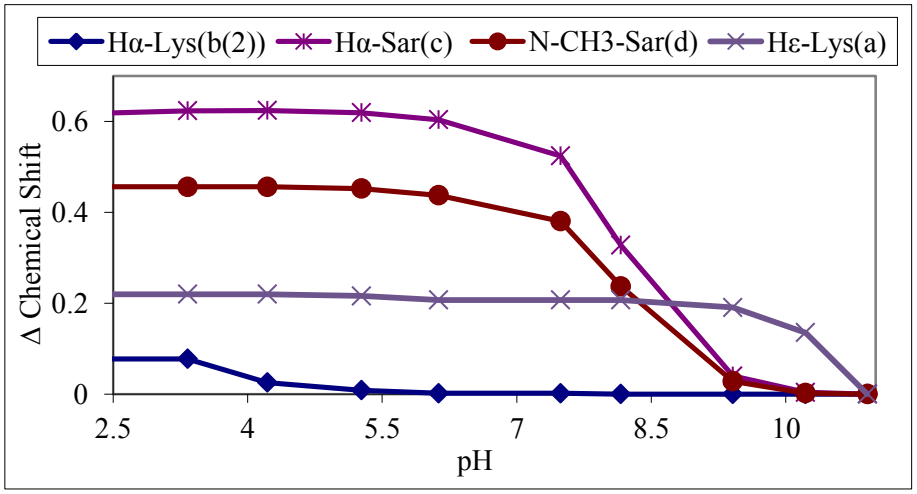

Figure 4.23: Change of chemical shifts of selected protons of Sar-Lys-Lys as a function of pH. The assignment is given in Figure 4.21.

The signals that shift the most are signals **c** and **d** assigned to the protons of the α-carbon of the N-terminal and the protons of the methyl substituent respectively. These signals shift mostly from pH 6.13 to pH 10.91, Log K_{LH3} = 7.80, which indicates the protonation of the amine terminal. Signal **b2** shifted between pH 2.02 and pH 4.22. Log K_{LH4} = 3.11. These data agree with the potentiometric results (see Chapter 3).

4.2.3.1.4 Protonation of Sarcosyl-L-glycyl-L-histidine

The proton labels used in the ^{1}H NMR spectra are given in Figure 4.24.

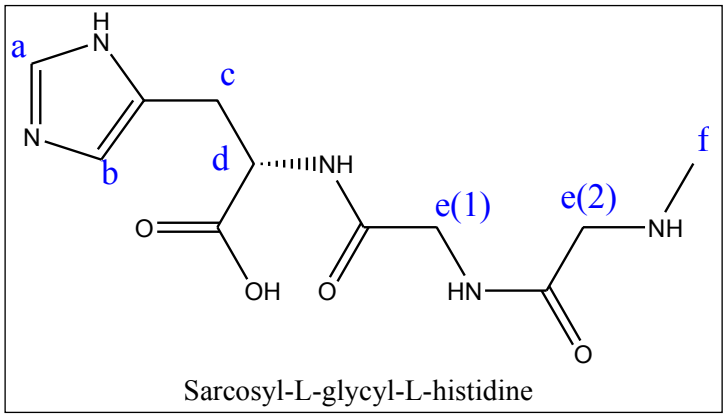

Figure 4.24: The structure of the Sar-Gly-His shows the proton labels in Figures 4.25 &4.26.

Figure 4.25 shows the ^{1}H NMR spectra. Change of chemical shifts of protons near the possible coordination sites of the free Sar-Gly-His as a function of pH is shown in Figure 4.26. Going from low to high pH, the signals **a** and **b** were the first to shift to high field. This is due to the protonation of the imidazole nitrogen group. These signals showed a shift from pH 2.30 to pH 9. Signal **e2** shifted from pH 8.32 to pH 10.37. This is due to the protonation of the N-terminal amino group of the Sar-residue. The amide protons are observed at ~ 8.2 ppm in D_2O/H_2O. In the pH range 2.3- 5.8 the one amide doublet shifts significantly as the C-terminal histidine carboxylic acid is deprotonated (pK_a = 2.3).

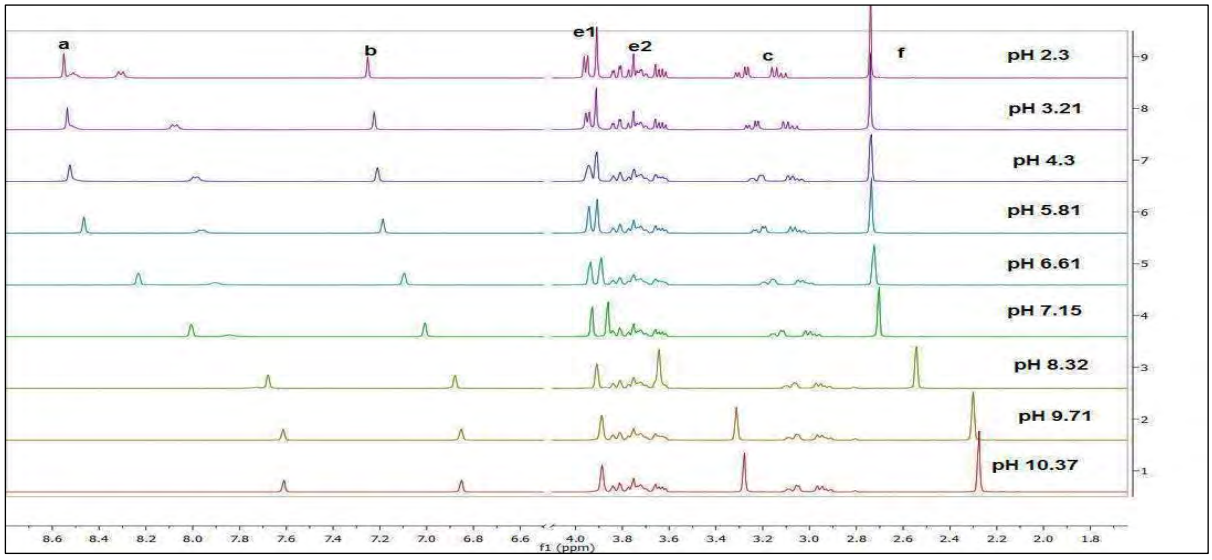

Figure 4.25: ^{1}H NMR spectra of Sar-Gly-His form pH 2.02 to pH 11.01. Note the break in the f1 dimension at 4.4 ppm. The proton assignments are according to Figure 4.24.

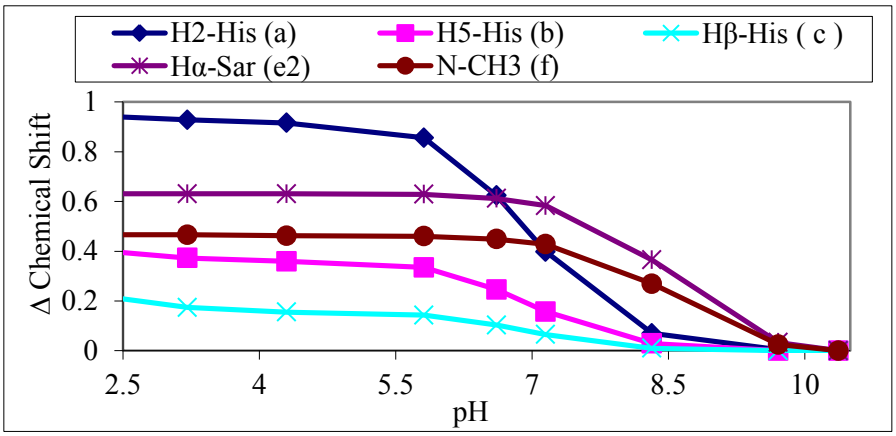

Figure 4.26: Change of chemical shifts of selected protons of Sar-Gly-His as a function of pH. The assignment is given in Figure 4.24.

4.2.3.2 Complex formation titrations

The chemical shifts of protons near the possible coordination sites of the Cu(II) complexes are shown as a function of pH in Figures 4.27 to 4.30.

4.2.3.2.1 Cu(II) sarcosyl-L-histidyl-L-lysine complexes

When the pH was kept constant at 4.5and Cu(II) titrated into the tripeptide solution, some of the signals broadened (Figure 4.27). The C_2H **a** and C_5H **b** resonances of the imidazole are shifted upfield after peptide coordination through the N^3 nitrogen atom of the imidazole to Cu(II). The higher field chemical shifts for the C_2H with respect to the C_5H proton result from the fact that this proton is closer to the N^3 binding center. In particular, the imidazole protons broadened indicates that this group must be coordinating to the Cu(II). At the same time, the lysine amide proton is clearly visible. This means that this amide is not coordinated. Unfortunately, the absence of the histidine amide cannot be used to infer coordination of this group as this amide is also absent in the free ligand spectrum. The H_ε-lysine signal **f** did not broaden indicating that the Cu(II) is not coordinated here. The most predominant species at pH 4.5-5.12 is the CuLH species and so we would postulate that in this species, coordination is to the terminal amino-N, imidazole N^3 and the histidine amide N or amide O. The stoichiometry supports coordination to the amide O for this species. The signals broadened and shifted significantly when the pH was varied and the amount of Cu(II) was kept constant. The shifting is due to the pH change and the broadening is due to changes in the Cu(II) coordination. The spectrum at pH 7.5 shows that the imidazole is coordinated (**a**, **b** and **c** substantially broadened) but that the terminal amine is not

coordinated (very little broadening of **d** and **e**). At this pH CuL predominates. At pH 8.15 $CuLH_{-1}$ starts to form and protons **d** and **e** broaden substantially. This implies that the terminal amine is now coordinating. The same applies to $CuLH_{-2}$ which predominates at pH 10.8.

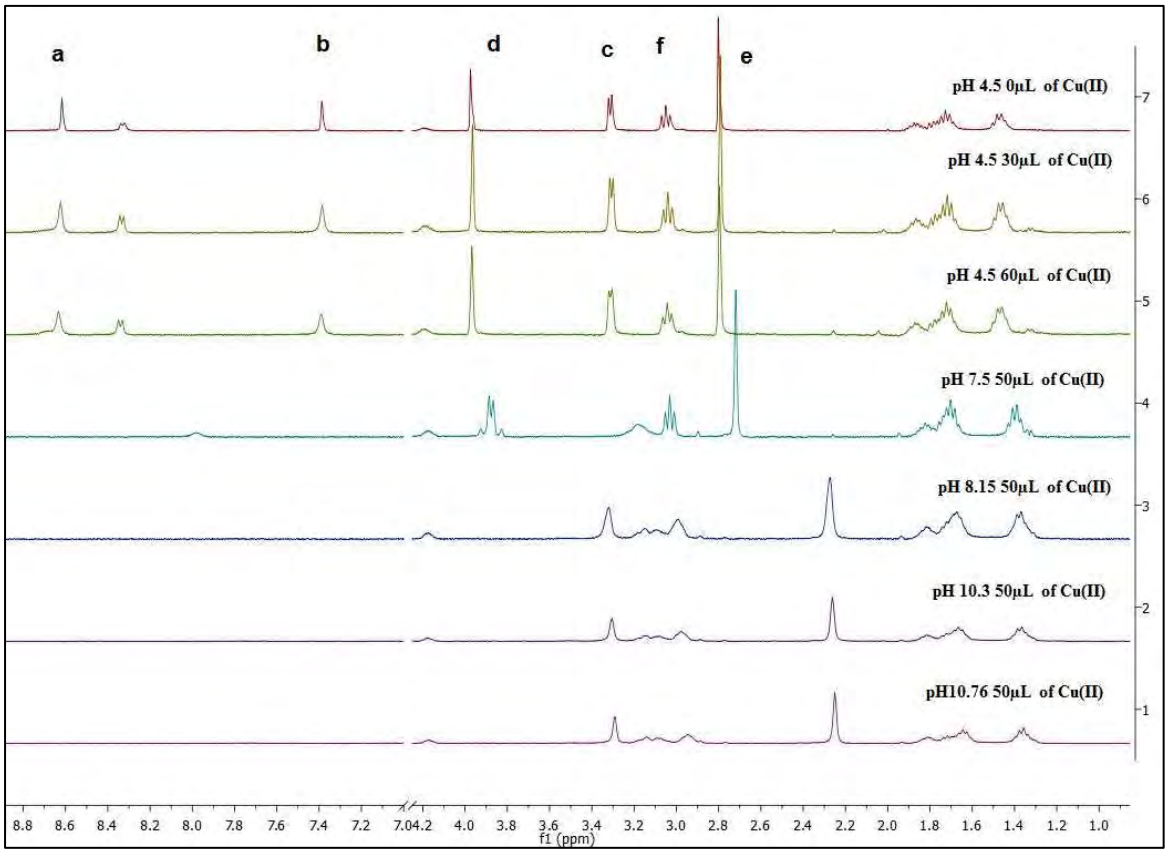

Figure 4.27: ^{1}H NMR titration for the complexation of Sar-His-Lys (0.075M) with Cu(II) (0.0118M) in D_2O:H_2O 1:9 mixture. Note the break in the f1 dimension at 4.4 ppm. The proton assignments are according to Figure 4.15.

4.2.3.2.2 Cu(II) sarcosyl-L-histidyl-L-histidine complexes

^{1}H NMR results for the complexation of SHH with Cu(II) are given on Figure 4.28. The small amounts of Cu(II) used in the ^{1}H NMR study should enable the observation of significant differential broadening of the resonances of protons close to the copper binding. At pH 4.10, CuLH is the predominant species in solution. The overlapping His H-C_2 **a1**, **a2** and H-C_5 **b1**, **b2** resonances were both broadened, suggesting that the His imidazole groups coordinate to the Cu(II) ion. The binding of imidazole group nitrogens is common in histidine-containing Cu(II) complexes [21,24,29]. Only one His amide proton is observed

and this broadens with the addition of Cu(II). This broadening is also attributable to binding of the Cu(II). However, since the amide proton is still observed this amide-N cannot be coordinated. There does not appear to be significant broadening on protons **e** and **f** indicating that the terminal amine may not be coordinated.

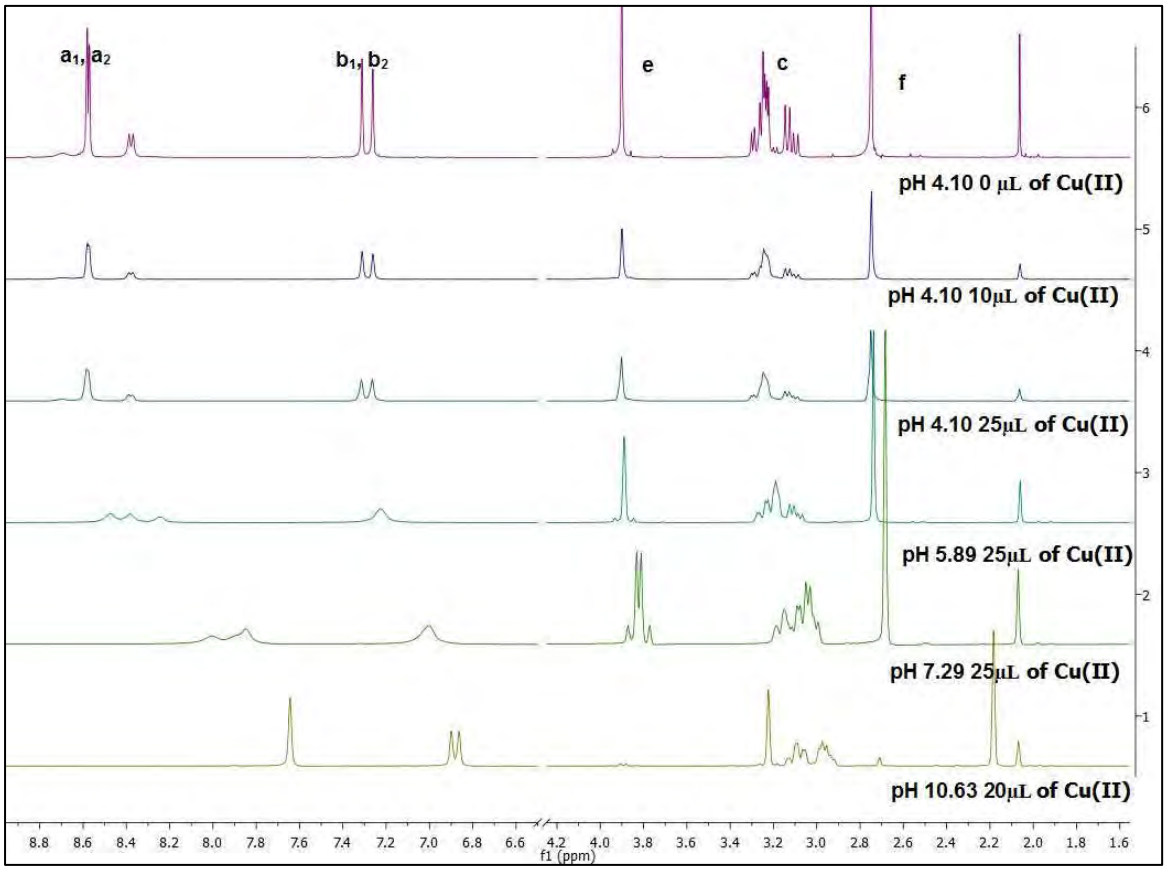

Figure 4.28: ^{1}H NMR titration for the complexation of Sar-His-His (0.11 M) with Cu(II) (0.0118 M) in D_2O:H_2O 1:9 mixture. Note the break in the f1 dimension at 4.4 ppm. The proton assignments are according to Figure 4.18.

When the pH was increased from 4.10 to 7.29, **a1**, **a2** and **b1**, **b2** disappeared almost completely implying that the imidazoles are both coordinated. At pH 7.29, CuL and $CuLH_{-1}$ predominate. At this pH the **e** and **f** protons have the same appearance as in the spectra without Cu(II). This implies that the terminal amine is still not coordinated. At the same time the amide protons have disappeared. However, nothing can be concluded from this as, at this pH, amide resonances are in fast exchange with the solvent and so are generally not be observed in the ^{1}H NMR spectrum. At pH 10.6, $CuLH_{-2}$ predominates but the spectrum sharpens and remains sharp irrespective of the amount of Cu(II) added. This is due to

chemical exchange as will be explained later. Hence at this pH the NMR spectrum gives no information about the structure of the copper complex.

4.2.3.2.3 Cu(II) sarcosyl-L-lysyl-L-lysine complexes

The effects of Cu(II) addition on the ^{1}H NMR spectrum of Sar-Lys-Lys are shown in Figure 4.29. The addition of small amounts of Cu(II) to tripeptides caused differential broadening of resonances, which provided an indication of the location of copper binding. In the case of this peptide we would like to confirm if the C-terminus is coordinated or not. Comparing resonances **b1** and **b2**, **b2** is more affected by the Cu(II) and so we postulate that the carboxyl of the terminal lysine is coordinated.

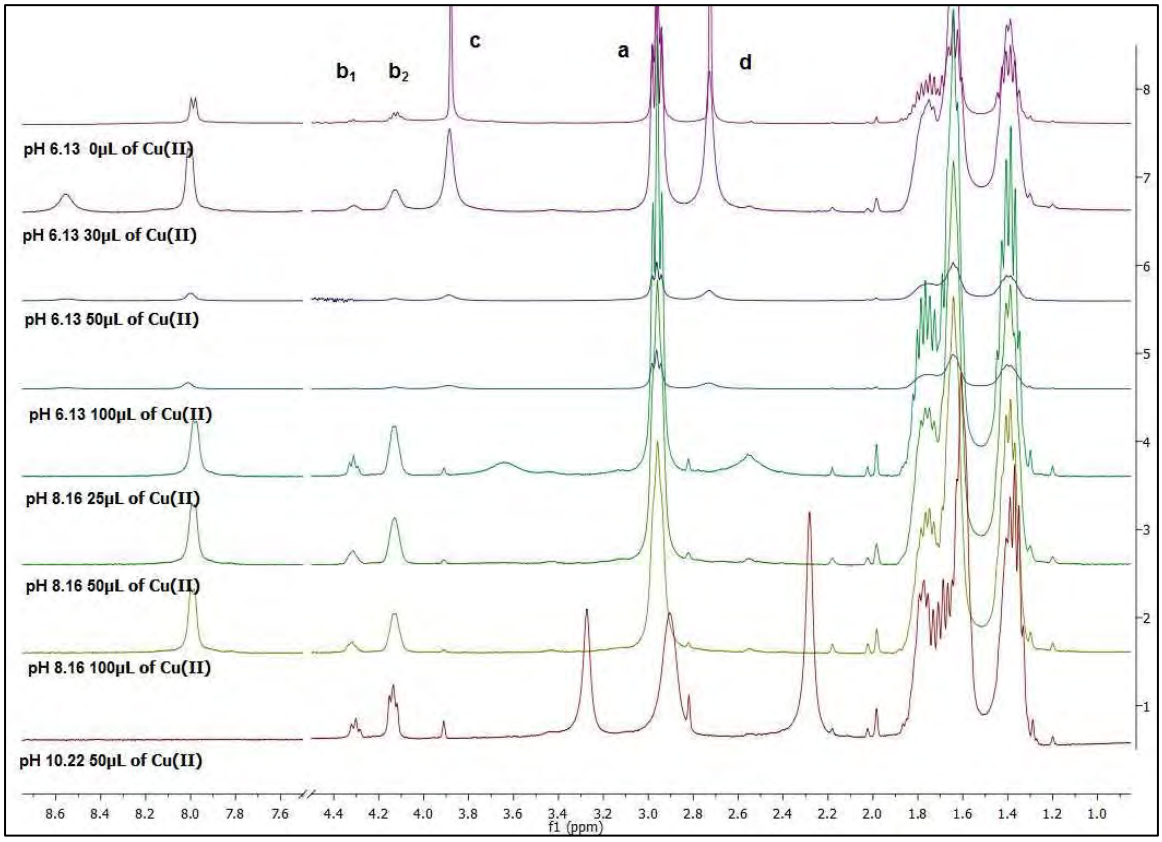

Figure 4.29: ^{1}H NMR titration for the complexation of Sar-Lys-Lys (0.09 M) with Cu(II) (0.0118 M) in D_2O:H_2O 1:9 mixture. Note the break in the f1 dimension at 4.4 ppm. The proton assignments are according to Figure 4.21.

CuLH species is the most predominant species at pH 6.13. At this pH the **c** and **d** protons are broadened implying that the terminal amine is coordinated. Note the difference between

this result and that of the peptides containing a histidine residue. When the pH was increased from 6.13, signal **c** disappeared. The stoichiometry supports coordination to the N-terminal amine, both amide N's and the carboxylate O when $CuLH_{-2}$ forms. There was no significant broadening of the Lys, H_{ε} **a** signals in this tripeptide indicating that neither lysine side chain amine is coordinated. Note again that at high pH the spectra become independent of the Cu(II) concentration.

4.2.3.2.4 Cu(II) sarcosyl-L-glycyl-L-histidine complexes

Figure 4.30 shows the effect of Cu(II) ions at different pH values. The interesting observation is that for each of Sar, Gly and His signals there is a characteristic linewidth depending on the specific pH value.

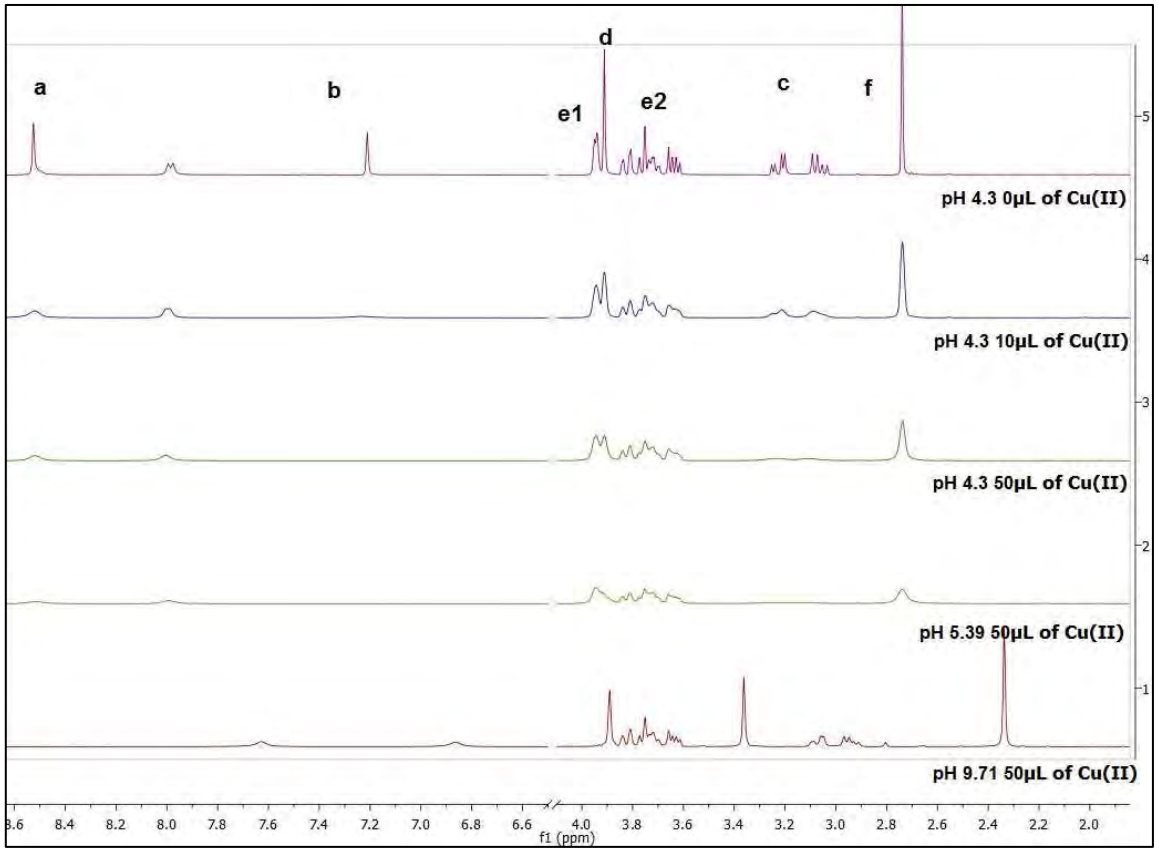

Figure 4.30: ^{1}H NMR titration for the complexation of Sar-Gly-His (0.09 M) with Cu(II) (0.0118 M) in D_2O:H_2O 1:9 mixture. Note the break in the f1 dimension at 4.4 ppm. The proton assignments are according to Figure 4.24.

CuLH is the predominant species at pH 4.3. The broadening of signals **a, b** and **c** indicate coordination to the imidazole N. The resonances **d** and **e1**, are affected by the Cu(II) and so

we postulate that the amide N or amide O is coordinated. The stoichiometry supports coordination to the amide O for this species. At pH 5.39 $CuLH_{-1}$, predominant species and protons **e2** and **f** broaden substantially. This implies that the terminal amine is now coordinating. The same applies to $CuLH_{-2}$ which predominates at pH 9.71. In strongly basic conditions, all the signals appear again and sharpen.

4.2.4 Discussion

The structure of Cu(II) complexes with tripeptide were studied by ^1H NMR. The possible binding sites for these tripeptides are the imidazole nitrogen, the amide nitrogen or amide oxygen, the N-terminal nitrogen (-NH) and C-terminal oxygen (COO^-). The ^1H NMR spectra were recorded at various pH values, where the maximum concentrations of the various species are observed, as deduced from the speciation diagram. From the chemical shifts of Cu(II) complexes with Sar-His-Lys, Sar-His-His and Sar-Gly-His the imidazole ring of the histidine residue, with its two N^3 and N^1 nitrogen atoms, has been shown to be a good metal-binding site in the reaction of histidine-containing peptides with Cu(II) complexes. It is well known that Cu(II) anchored to the N^3 nitrogen atom in the histidine side chain is highly effective in displacing the amide proton and forms very a stable six-membered chelate ring [23-25,49].

The Cu(II) Sar-His-His and Sar-Gly-His complexes where a [-NH, N^-, N^-, N_{im}] donor set was reported in basic pH, the third equatorial position is occupied by the C-terminal imidazole nitrogen. Unfortunately, the ^1H NMR experiments did not give precise information on the conformation adopted by the tripeptides [29]. Resonances assigned to the ε-amino group of lysine were relatively unaffected by copper addition, indicating that lysine does not coordinate to the Cu(II) [50].

Finally, in strongly basic conditions, all the signals appear again and sharpen when the pH rises. Recently, a similar observation has also been made with a cyclic peptide [51] and a linear peptide [52]. Since in solution, the concentration of the ligand is very much greater than that of Cu(II), the effect of Cu(II) coordination is transferred to the bulk free ligand via chemical exchange. The sharpening of the signals with increasing pH is explained by the slowing down of the exchange [52-54].

4.3 ELECTROSPRAY IONISATION MASS SPECTROMETRY

4.3.1 Introduction

Quantitative bonding studies are necessary in order to determine the affinity of the copper compounds to amino acids, tripeptides and proteins. The influence of varied concentrations of the reactants on the observed interactions can provide valuable information regarding the association constants [55]. The complex of copper species with tripeptides and proteins that are now described for the synthetic solutions must be investigated in real biological samples. Electrospray ionization mass spectrometry (ESI-MS) has been widely used for the characterization of a wide variety of inorganic complexes in the gaseous phase [56]. ESI-MS is an extremely important tool for studying molecular weights and structures of metal complexes [57,58]. Moreover, it has been used to provide both qualitative (structure) and quantitative (molecular mass or concentration) information on analyte molecules after their conversion to ions [59]. In this study, ESI-MS was used to obtain information about the molecular mass of the metal complex species so as to confirm the assumed structures from potentiometric and spectroscopic studies. In addition, fragmentation patterns from ESI-MS may provide more structural information. By studying Cu(II) tripeptide species as a function of pH, it was possible to observe the appearance of all species in solution that are dependent on pH. As in potentiometry, Cu(II) and tripeptide concentrations and ratios were used for ESI-MS experiments in order to facilitate the detection of all possible Cu(II) complex species observed in the same pH range.

4.3.2 Experimental

ESI-MS spectra were recorded on Agilent 6120 Quadruple LC/MS system with ESI resource. ESI-MS spectra were acquired in the 1500 amu region using 20 ms dwell time. An ion spray voltage of 4000V was applied in positive ion mode [55]. The orifice potential of 70V was established as offering the best signal intensity causing partial fragmentation of the tripeptide [60]. The Cu(II) complex solutions were prepared by dissolving the tripeptide and Cu(II) in water at 1:1 ratio with the concentration of tripeptide 0.005 M. The solutions were investigated in the pH range 3.04-10.22 where the pH values were adjusted with HCl or NaOH.

4.3.3 Results and Discussion

The mass spectra of the Cu(II) complexes of Sar-His-Lys are shown in Figures 4.31 and 4.32. From this, it is clear that fragmentation of the complex has taken place with the peak at m/z = 355.2 due to the free Sar-His-Lys. Using the isotopic ratio of ^{63}Cu (69%) and ^{65}Cu (31%) it is possible to identify peaks due to the complex. The spectra relative to the ion present shows successive loss of water molecules. Presented in Table 4.10 are ions registered in positive ions mode (PIM) in mass spectra of solutions of the SHK-Cu complexes in the pH range 3.04-10.22 [61].

Table 4.10: Ionized species observed in ESI-MS of Cu-SHK.

pH	*m/z*	Proposed ion
3.04-8.28	417.20	$[^{63}CuSHK]^+$
	452.10	$[^{63}CuSHK.2H_2O]^+$
	474.20	$[^{63}CuSHK.3H_2O]^+$
	488.10	$[^{63}CuSHK.4H_2O]^+$
9.22-10.22	416.25	$[^{63}CuSHK]^+$
	431.00	$[^{63}CuSHK+OH^-]^+$

In the mass spectrometric investigations various interactions of copper with Sar-His-Lys were found. The peak corresponding to the $[CuSHK.(H_2O)_n]$ complex appeared simultaneously with the peak of the free SHK in the ESI-MS spectra. Solvent adducts very often form under ESI-MS conditions, due mainly to coordination with the metal center. The formation of pseudomolecular or adduct ions (Na^+ and Cl^-) during ESI-MS is very common. These adducts almost never exist at equilibrium but they are artefacts of ESI. As before, the stoichiometric recognition of the species in solution is not impaired but may become more difficult [62]. Although ESI does result in fragmentation polymerization is sometimes observed both for free and bound ligand molecules and depending on the extent of this phenomena, the recognition of all peaks may become more difficult or even impossible, thus impairing the analysis [63]. However, the addition or loss of a proton is a very quick process. Therefore, ESI-MS is not able to individuate the ionizable proton content of the species, regardless of the kinetic properties of the metal–ligand displacements. Generally, only one $[CuSHK.(H_2O)_n]$ peak was detected by ESI-MS, while different number of water

molecules were expected in solution. This, of course, must be considered as an intrinsic limitation of ESI, and cannot be overcome. Moreover, it may also represent an advantage because the addition and/or loss of protons allow the detection of neutral species [64].

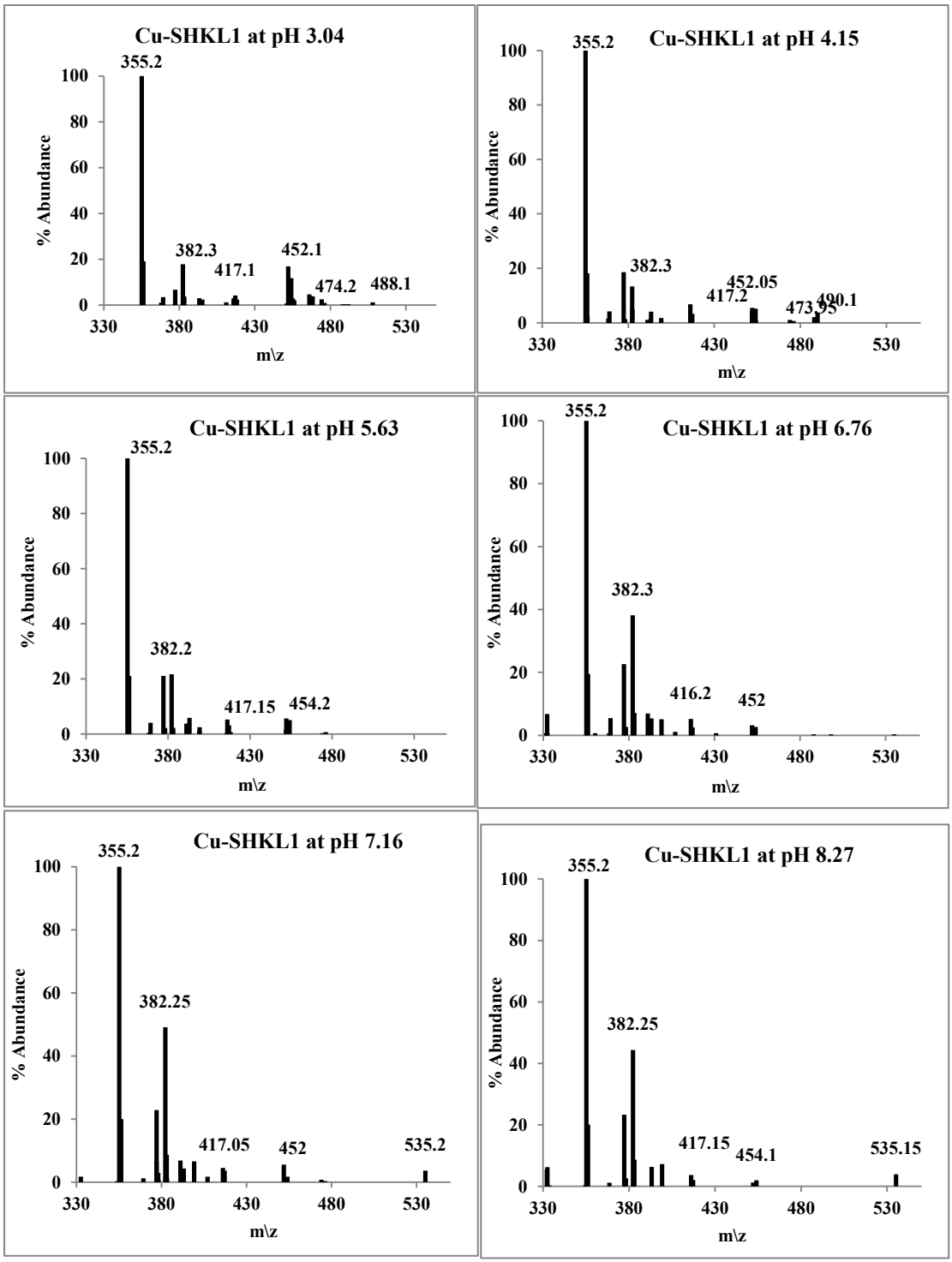

Figure 4.31: Mass spectra of the solutions of Cu-SHK species in the range pH 3.04-8.28.

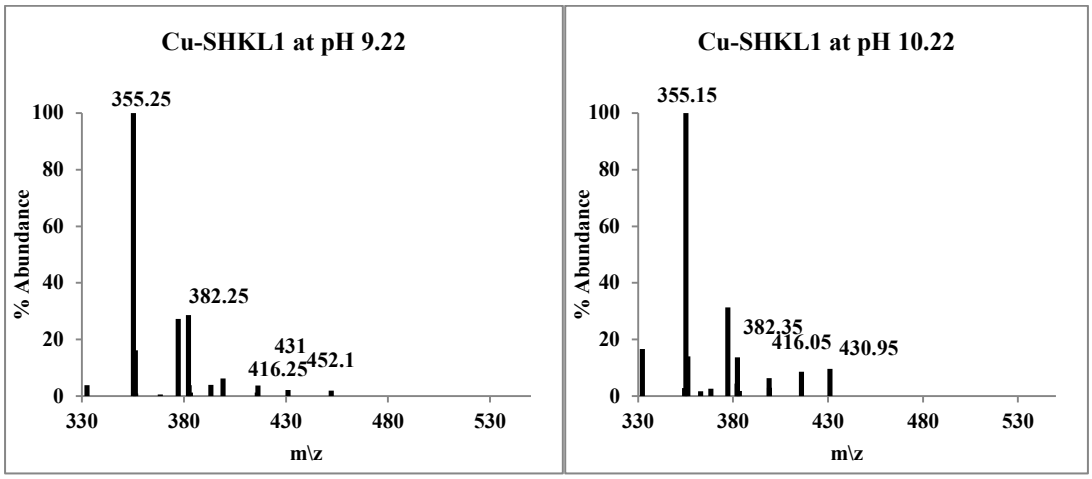

Figure 4.32: Mass spectra of the solutions of Cu-SHK species in the range pH 9.22-10.22.

ESI-MS spectra are from moderate to very sensitive to the instrumental parameters employed, such as spray voltage, capillary temperature, capillary voltage, tube lens offset, and especially cone voltage [65]. In addition, different chemical species usually have different response factors due to the different efficiency of the processes which lead to the production of gas-phase ions from the species in solution [66,67]. Although, the ESI-MS technique showed that complexation of Cu(II) with Sar-His-Lys occurred it was not possible to assign peaks to specific species to show speciation of Cu(II) at different pH values using this technique. Thus, the identity and speciation of the Cu(II) complexes could not be compared with those obtained from the potentiometric and spectroscopic studies.

4.3.4 Conclusion

In this study, we explored the potential application of ESI-MS for probing the interactions of Cu(II) ion with tripeptide. The effect of pH on the formation of Cu(II) tripeptide complex species was not observed. Therefore, the ESI-MS technique did not provided useful information on the structures of the Cu(II) tripeptide complex species. Thus, further work is needed to explore the sensitivity and resolution of the mass spectrometer and also investigate the benefits and limitations of this promising method in more detail.

4.4 MOLECULAR MECHANICS

4.4.1 Introduction

Computer modelling is now widely used as an aid in the interpretation of experimental results and in the design of new materials with desirable properties. Its wide use is primarily due to its computational simplicity and efficiency. Quantum mechanical modelling, however, is far more computationally intensive than other computer modelling programs and until recently has been used only for a few metal complexes [68,69]. Molecular mechanics (MM) is a model that has been developed out of a need to describe molecular structures and properties in a practical manner [70,71]. The strain energy calculations of a molecule are done using force fields, but the choice of which force fields to use in a calculation is entirely dependent on the type of complex or molecule (i.e. organic or inorganic) of interest and the software program used to run the simulation [72]. In addition, there are a limited number of reliable force fields to use for the MM calculation involving metal ions. Therefore, MM calculations involving transition metal ions are not done to the same extent as organic molecules [73,74].

4.4.2 Theory

The structures are built using molecular orbital and valance bond theories. Their conformation is optimised using force fields where the strain energy (E) of these structures is calculated. The basis of the molecular mechanics method is that a good estimate of the geometry of a molecule can be obtained by taking into account all the forces between atoms and calculated using a mechanical approach.

The geometry is optimised such that the total bond deformation strain (E_b), the total steric strain/van der Waals strain (E_s), the angle strain (E_a), and the torsional strain (E_t) are minimised. The total strain energy (E_{tot}) can therefore be expressed as;

$$E_{tot} = E_b + E_s + E_a + E_t \tag{4.5}$$

The individual energy terms are calculated using simple functions with bonds modelled as springs that obey Hooke's law [75];

$$E_b = \sum_{bonds} \frac{1}{2} k_l (l - l_0)^2 \tag{4.6}$$

where k_l is the force constant or spring strength and l is the bond length when the structure is deformed and l_0 is the length of the bond when the structure is at equilibrium. E_b can also be expressed in terms of the Morse function [76,77];

$$E_b = \sum_{bonds} D_b \left(1 - e^{-a(l-l_0)}\right)^2 \quad (4.7)$$

The steric/van der Waals strain is the strain experienced by a molecule that has non-bonded electrons from different substituents that repel each other. Rappé and co-workers [78] have derived an equation for calculating total steric strain as:

$$E_s = \left[D_{IJ}\left(\frac{6}{\zeta-6}\right)e^{\zeta}\right]e^{-\zeta\left(\frac{x}{x_{IJ}}\right)} - \left[D_{IJ}\left(\frac{\zeta}{\zeta-6}\right)x_{IJ}{}^6\right] \quad (4.8)$$

where D_{IJ} is the finite energy for breaking bonds, x_{IJ} is the van der Waals bond length, x is the atomic van der Waals distance, and ζ is the shape factor.

The angle deformations can also be estimated using Hooke's law.

$$E_a = \sum_{angles} \frac{1}{2} k_b (b - b_0)^2 \quad (4.9)$$

where k_b is the force constant for a particular angle, b is the bond angle when the structure is deformed and b_0 is the bond angle when the structure is at equilibrium.

Torsional strain is experienced when a molecule undergoes a complete rotation around one bond. This is expressed as:

$$E_t = \frac{V_1}{2}(1 + \cos(w)) + \frac{V_2}{2}(1 + \cos(2w)) + \frac{V_3}{2}(1 + \cos(3w)) \quad (4.10)$$

where V_1 is a term assigned to van der Waals interactions/residual dipole-dipole interactions, V_2 is a term assigned to conjugation/hyper-conjugation and V_3 is assigned to steric or bonding/anti-bonding interactions. The geometry of the copper complexes was optimized using different force fields. The generic force field, extensible systematic force field (esff) which requires atomic coordinates and the force field parameters, including partial charges, were used as input [76].

The advantage of esff is its capability to model most of the elements of the periodic table. Esff employs semi-empirical rules to translate atomic-based parameters to parameters typically associated with a covalent valence force field. In general, force field terms are

derived empirically with the target of reproducing experimental structures and energy distributions [69,79,80]. However, the goal of molecular mechanics is to find the geometry with minimum strain energy. The force field has been applied to molecular simulations of a wide variety of systems including nucleic acids, peptides, hydrocarbons, porphyrins, transition metal complexes, zeolites and organometallic compounds.

4.4.3 Simulation

The chemical and physical understanding of copper tripeptide species gained through simulation will be directly applicable to combined molecular orbital and empirical energy function calculations planned to examine the detailed interaction of molecular mechanics with electronic structure [81,82]. The esff force field was used in the MM simulations. The different chemical species in solution were constructed using the BUILD module of the Accelrys Biosym/MSI software package and were based on the speciation models obtained from Uv-Vis spectroscopy and potentiometry studies. Geometry optimization and energy calculations were performed using the Discover_3 program which was run as an application in the Insight II package [83].

4.4.4 Results and Discussion

The output data for internal energy (E_{int}), bond (E_b), angle (E_a), torsion (E_t) and out-of-plane (E_{Oop}) deformation energies (kcal mol^{-1}) of different proposed species are given in Table 4.11. The system makes many changes in the atom position through rotation and calculates energy in every position. This process is repeated several times to find the best position with minimum energy [84,85].

Table 4.11: Internal energy (E_{int}), bond (E_b), angle (E_a), torsion (E_t) and out-of-plane (E_{Oop}) deformation energies (kcal mol^{-1}) of different Cu(II) tripeptide complex species present in solution.

	A	**B**	**C**	**D**	**E**	**F**
	-NH, CO, N_{im}, H_2O	-NH, N^-, N_{im}, H_2O	-NH, $2N^-$, N_{im}	-NH, N^-, $2H_2O$	-NH, $2N^-$, COO^-	NH, $2N^-$, N_{im}, (N_{im})
E_{int}	32.93	14.16	22.71	11.60	26.71	105.70
Bond	01.54	00.68	01.54	02.68	03.21	7.14
Angle	25.33	09.14	13.26	06.53	16.77	50.66
Torsion	05.85	04.24	07.24	02.24	06.26	44.67
Oop	00.22	0.10	00.67	00.15	00.48	3.24

The energy minimised Cu(II) complexes of different proposed species present in solution are shown in Figure 4.33. Molecular mechanics (MM) has been considered here as a method for calculation of molecular structures, conformational energy minimised and support of the solution structures postulated from potentiometric and spectroscopic data. In this regard, some structures of species postulated from both potentiometry and spectroscopy have been considered for each Cu(II) tripeptide species.

Figure 4.33: Energy minimised Cu(II) complexes of different proposed species present in solution. **A:** Energy minimised Cu(II) complexes showing the coordination by an amino nitrogen, a carbonyl oxygen and an imidazole nitrogen donor atoms, giving a 5,8 chelate ring sequence (32.93 kcal mol^{-1}) for the CuSHK-H, CuSHH-H and CuSHH species.

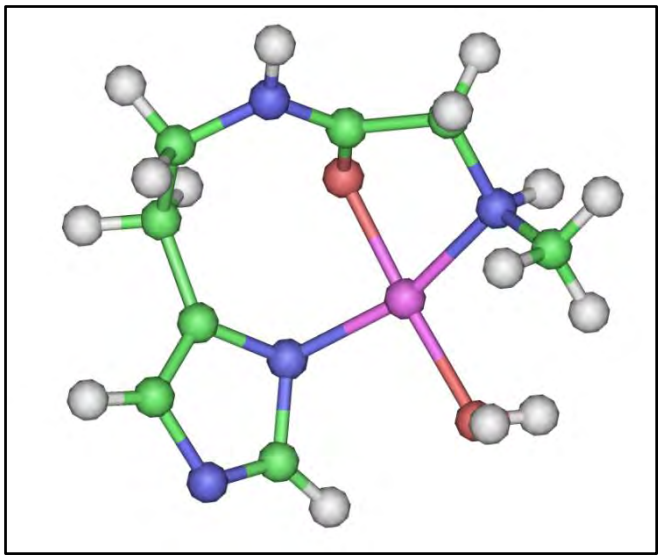

B: Energy minimised Cu(II) complexes showing the coordination by an amino, an amide and an imidazole nitrogens donor, giving a 5,6 chelate ring sequence (14.6 kcal mol^{-1}) for the CuSHK, CuSHK-H_{-1}, CuSHK-H_{-2} and CuSHH-H_{-1} species.

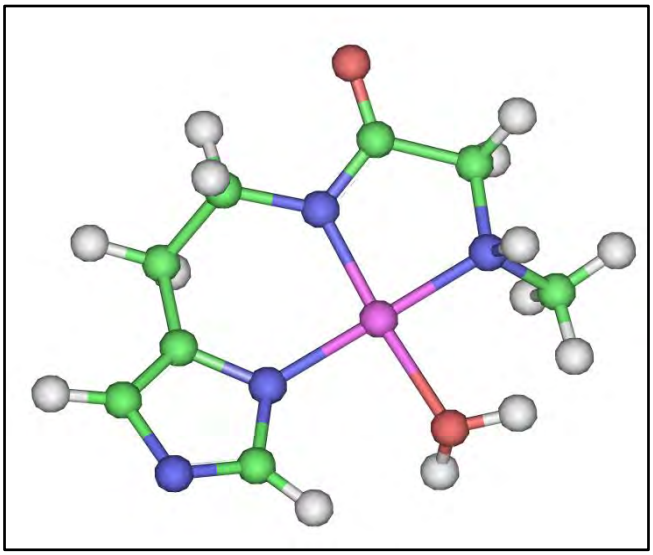

C: Energy minimised Cu(II) complexes showing the coordination by an amino, two amides and an imidazole nitrogens donor, giving a 5,5,6 chelate ring sequence (22.71 kcal mol^{-1}) for the CuSKH, CuSKH-H_{-1}, CuSKH-H_{-2}, CuHH-H_{-2}, CuSGH-H_{-1} and CuSGH-H_{-2} species.

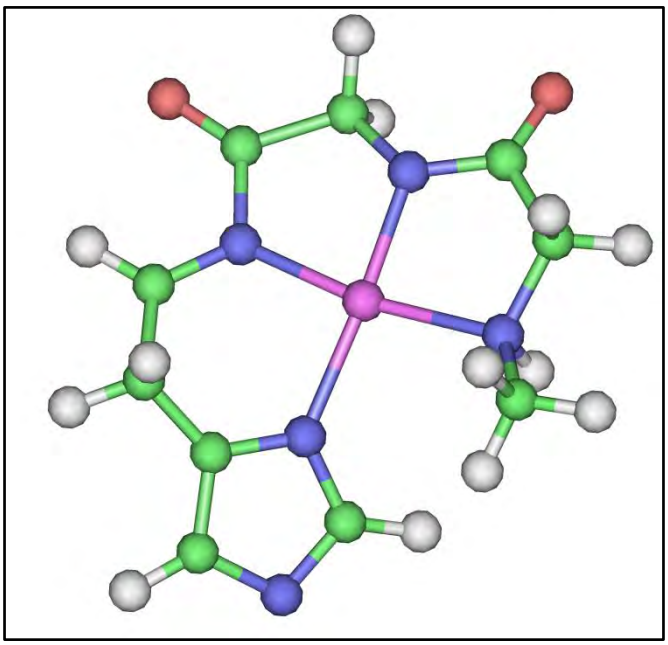

D: Energy minimised Cu(II) complexes showing the coordination by an amino and an amide nitrogens donor, giving a 5 chelate ring sequence (11.60 kcal mol^{-1}) for the CuSKK-H species.

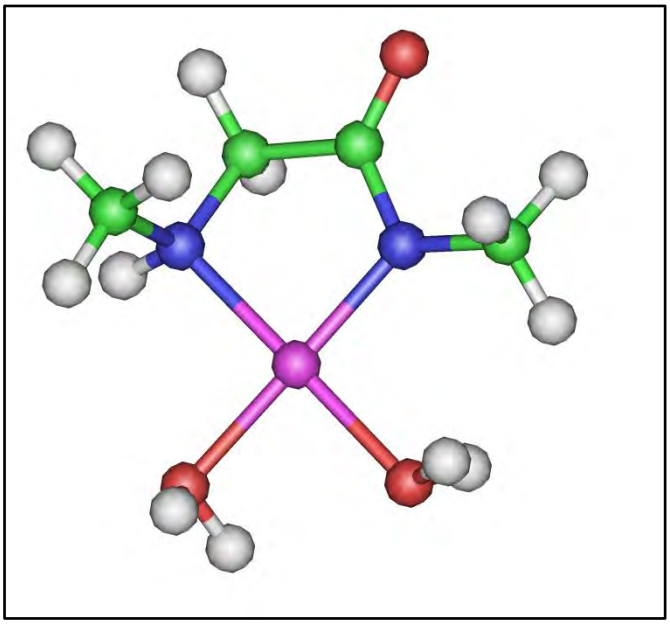

E: Energy minimised Cu(II) complexes showing the coordination by an amino, two amide nitrogens and carboxylate oxygen donor, giving a 5,5,5 chelate ring sequence (26.71 kcal mol^{-1}) for the CuSKK, CuSKK-H_{-1} and CuSKK-H_{-2} species.

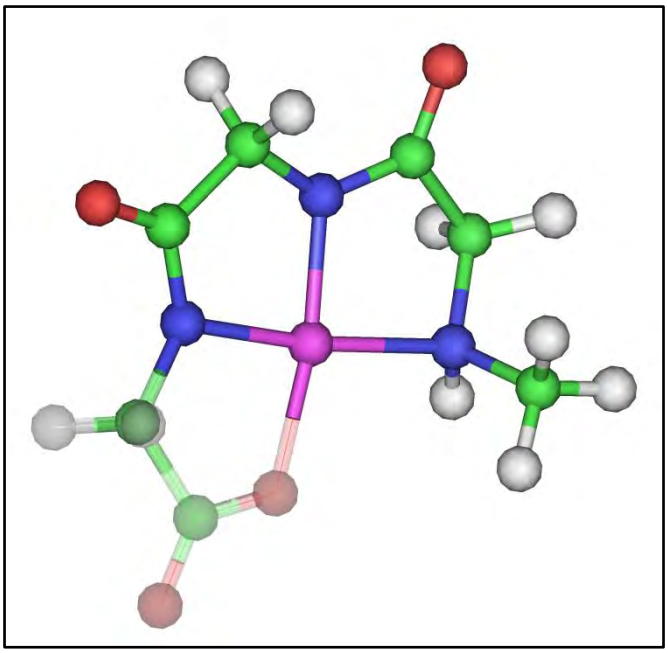

F: Energy minimised Cu(II) complexes showing the coordination by an amino, two amides and an imidazole nitrogens in equatorial and axial of imidazole nitrogen donor in position II, giving a highly strained (105.76 kcal mol^{-1}) for the CuSHH-H_{-1} and CuSHH-H_{-2} species.

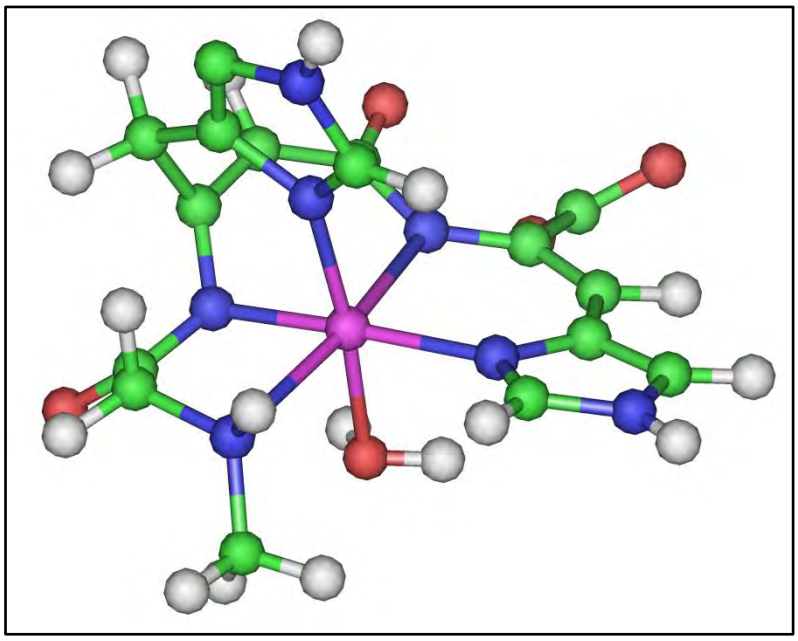

The results from stability constant determination indicated that the complexes are quite stable under biological conditions. The obtained binding energies for the Cu(II) species

coordinated to each of these tripeptides were very similar and not very far from those determined for the N-terminal metal binding site of the protein, attesting to the high stability of copper when inserted into this kind of environment [86]. The presence of six-membered chelates in internal or C-terminal positions of fused chelate rings generally enhances the thermodynamic stability of peptide complexes, while if they are in N-terminal position, the metal binding affinity is significantly reduced [33]. Angular distortions in the square plane are also caused by the different bite angles in the five- and six- membered chelate rings. The distortion of the structures from square planar to tetrahedral can be evaluated through the parameter Δ introduced by Galy *et al.* [87] and applied by Ribas and Kahn [88].

The other source of strain contribution to the differences in stability is the energy associated with torsion of bonds as the different donor atoms are oriented for coordination to the metal ion. Bond stretching seems to have less significant contribution to the differences in strain energies of these structures. Most differences in internal energy contribution arises from twisting of bonds and bending of angles as coordinating atoms are accommodated around the central metal ion.

In all calculations, electronic contributions, ie Jahn-Teller distortion are not taken into account. Nor are entropy effects, both in terms of chelate effect of the ligand and solvent [89,90]. In addition, the bond formation energies were not taken into account, but only the contribution of their distortion from ideality was considered.

The proposed structure for the CuSHK-H, CuSHH-H and CuSHH species is given in Figure 4.33(A). The ^{1}H NMR study showed that the imidazole nitrogen is coordinated at the beginning of complexation. It was also shown that the structures involving carbonyl oxygen donor atoms which coordinated to the metal ion are relatively more strained. The rigidity of the imidazole moiety seems to contribute to the strain energy when the carbonyl oxygen donor atom is coordinated to the metal ion. Therefore, the strain energy of these structures arises from both the sequence and the size of the rings formed around the metal ion upon different donor atom coordination. However, the 5,8 structure (A) had a high angle bending energy (25.33 kcal mol^{-1}) and torsion energy (5.85 kcal mol^{-1}). This came about because the planarity of the amide group has been compromised. It was expected that as the pH increased, Cu(II) would induce ionization of the amide proton and there would also be a transition from Cu-O to Cu-N coordination [91,92]. In structure (B), the amide coordination

was likely due to the close proximity of the metal ion enhanced by the coordination of an amino, an amide and an imidazole nitrogens donor for the CuSHK, CuSHK-H_{-1}, CuSHK-H_{-2} and CuSHH-H_{-1} species. The result of energy minimized structures showed that the 5,6 chelate structure (B) has a slightly lower internal energy. The main contribution to the internal energy is from the angle strain which is generated when forming the 6 membered rings.

An alternative structure (C), is where an amino, two amides and an imidazole nitrogen donor are coordinated to the Cu(II) ion forming a 5,5,6 chelate rings sequence (22.71 kcal mol^{-1}). Based on the MM calculations, it can be seen that the tripeptide is not a tetradentate ligand, but behaves as a tridentate ligand. In terms of the internal energies of the structure (C), a 5,5,6 chelate structure had a considerably low strain energy (22.71 kcal mol^{-1}) and there was a slightly high angle bending energy. The coordination of the imidazole nitrogen donor atom is likely to occur once the amino and two amidic groups are coordinated. Moreover, the coordination of the two deprotonated amide groups ensures planarity of these groups, resulting in restriction on the chelate geometry [93]. From the potentiometric and Uv-Vis spectroscopy data a similar solution structure was postulated as predicted by the MM calculations with a λ_{max} value of 530 nm. This value clearly suggests a square planar geometry for the $CuLH_{-1}$ and $CuLH_{-2}$ species of the Cu(II) Sar-Lys-His, Cu(II) Sar-His-His and Cu(II) Sar-Gly-His complexes. These MM calculations give extra experimental evidence in support of this geometry. Structure (D) was chosen as the most likely representative structure for the coordination by an amino and an amide nitrogens donor, giving a 5 chelate ring sequence (11.60 kcal mol^{-1}) for the CuSKK-H species. This is consistent with the structure proposed from the Uv-Vis spectroscopy study. Despite a high torsion energy in the 5,5,5 chelate structure (E), formation of the 5,5,5 chelate ring is more probable because of the close proximity of the second coordinating amide nitrogen donor in the coordination sphere. The 5,5,5 chelate structure supported by MM calculations has also been postulated from potentiometric data and this therefore, lends confidence to the presence of this species in solution for the CuSKK, CuSKK-H_{-1} and CuSKK-H_{-2} species.

Structure (F) has a weakly bound axial coordination of imidazole ring in position II. However, the major contribution to the internal strain energy comes from the bend angle (50.66 kcal mol^{-1}) and torsion angle (44.67 kcal mol^{-1}) energies, as well as the effect of the bonds on the axial ligands which distorts the octahedral geometry of Cu(II) complexes.

In general, the distances to the axial ligands are longer than to the equatorial, but also shortening of the axial bonds has been observed. In addition, the structure (F) of the $CuLH_{-2}$ species in Sar-His-His is likely to be overall octahedral with a weak axial imidazole nitrogen donor, which are not observed in the Uv-vis spectroscopic.

The λ_{max} was observed at 520 nm for $CuLH_{-2}$ of the Sar-His-His. This value corresponds to a square planar geometry with one amine, two amides and an imidazole nitrogen donor in equatorial positions. Similar λ_{max} values of $CuLH_{-2}$ with Sar-Lys-His and Sar-Gly-His were observed, when the axial imidazole in position II did not exist. Moreover, the coordination of the two deprotonated amide groups ensures planarity of these groups, resulting in restriction on the chelate geometry. The MM calculation gives extra experimental evidence in support of a square planar geometry. Such a result clearly demonstrates the limitations of MM calculations as a computational tool for Cu(II) complex species since it does not account for electronic contributions of the metal or entropy effects, both in terms of the chelate effect of the ligand and the solvent.

4.5 GENERAL CONCLUSIONS

The structural variety of the Cu(II) complex formation processes of tripeptides comes from a large number and many different arrangements of donor atoms both in the backbone and the side chains of the molecules. In the present study, by using potentiometry, spectroscopy and molecular mechanics different binding sites for Cu(II) tripeptide species were observed. The geometrical structure of species gave the square planar shape for tripeptides having His at position II (Sar-His-Lys) in the formation of 3N [-NH, N^-, N_{im}]. The square planar shape was also observed for tripeptides having His at position III (Sar-Lys-His & Sar-Gly-His) in the formation of 4N [-NH, N^-, N^-, N_{im}] and tripeptide that does not have His (Sar-Lys-Lys) in the formation of 3N [-NH, N^-, N^-, COO^-]. In addition, with the exception of Sar-His-His, Uv-vis spectroscopic and MM calculations suggest a weak axial coordination of imidazole ring. In contrast, the same ring remained uncoordinated in the case of the $NiLH_{-2}$ species with Sar-His-His. A possible participation of the ε-amino group of the Lys residue in the coordination sphere of metal ions was not observed, although its deprotonation of MLH_{-1} led to MLH_{-2} species which are the same protonation of the ε-amino group of the Lys residue in free tripeptides.

References

1. M. H. Brooker, *Synth. React. Inorg. Met. Chem.*, 1981, **11**, 181–182.
2. S. L. Upstone, *Ultraviolet/Visible Light Absorption Spectrophotometry in Clinical Chemistry*, John Wiley & Sons Ltd, Chichester, Beaconsfieldr, UK, 2000.
3. K. A. L. Huheey J.E., Keiter E.A., *Inorganic Chemistry, Principles of Strucrure and Reactivity*, Harper Collins College Publishers, New York, 4th ed., 1993.
4. Franz-Xaver Schmid, *Biological Macromolecules: UV-visible Spectrophotometry*, John Wiley & Sons, Ltd, Chichester, UK, 2001.
5. P. L. Holland and W. B. Tolman, *J. Am. Chem. Soc.*, 1999, **121**, 7270–7271.
6. A. Lakatos, B. Gyurcsik, N. V Nagy, Z. Csendes, E. Wéber, L. Fülöp, and T. Kiss, *Dalton Trans.*, 2012, **41**, 1713–26.
7. J. N. Zvimba and G. E. Jackson, *Polyhedron*, 2007, **26**, 2395–2404.
8. A. R. Hartley F.R, Burgess C., *Solution Equilibria*, Ellis Horwood, Chichester, 1980.
9. S. Timári, C. Kállay, K. Osz, I. Sóvágó, and K. Várnagy, *Dalton Trans.*, 2009, 1962–71.
10. U. Fantz and D. Wünderlich, *At. Data Nucl. Data Tables*, 2006, **92**, 853–973.
11. M. J. A. Wilkinson G., Gillard R.D., *Comprehensive Coordination Chemistry.*, Pergamon Press, Oxford, Oxford, 3rd edn., 1987.
12. E. J. Billo, *Inorg. Nucl. Chem. Lett.*, 1974, **10**, 613–617.
13. H. Sigel and R. B. Martin, *Chem. Rev.*, 1982, **82**, 385–426.
14. E. Prenesti, P. Daniele, M. Prencipe, and G. Ostacoli, *Polyhedron*, 1999, **18**, 3233–3241.
15. S. Odisitse, *MSc Thesis*. University of Cape Town, 2003.
16. K. Mokalane, *MSc Thesis*. University of Cape Town, 2011.
17. E. Farkas, I. Sóvágó, T. Kiss and A. Gergely, *J. Chem. Soc. Dalt. Trans.*, 1984, **3**, 611.
18. P. J. Morris and R. Bruce Martin, *J. Inorg. Nucl. Chem.*, 1971, **33**, 2913–2918.
19. H. Kozłowski, W. Bal, M. Dyba, and T. Kowalik-Jankowska, *Coord. Chem. Rev.*, 1999, **184**, 319–346.

20. A. Myari, G. Malandrinos, Y. Deligiannakis, J. C. Plakatouras, N. Hadjiliadis, Z. Nagy, and I. Sòvágó, *J. Inorg. Biochem.*, 2001, **85**, 253–261.

21. T. Kowalik-Jankowska, M. Ruta-Dolejsz, K. Wiśniewska, L. Łankiewicz, and H. Kozłowski, *J. Chem. Soc. Dalt. Trans.*, 2000, **100**, 4511–4519.

22. P. Mlynarz, D. Valensin, K. Kociolek, J. Zabrocki, J. Olejnik, and H. Kozlowski, *New J. Chem.*, 2002, **26**, 264–268.

23. T. Gajda, B. Henry, A. Aubry, and J. Delpuech, *Inorg. Chem.*, 1996, **35**, 586–593.

24. M. Mylonas, G. Malandrinos, J. Plakatouras, N. Hadjiliadis, K. S. Kasprzak, A. Krężel, and W. Bal, *Chem. Res. Toxicol.*, 2001, **14**, 1177–1183.

25. M. Mylonas, J. C. Plakatouras, N. Hadjiliadis, A. Krężel, and W. Bal, *Inorganica Chim. Acta*, 2002, **339**, 60–70.

26. P. G. Daniele, O. Zerbinati, R. Aruga, and G. Ostacoli, *J. Chem. Soc. Dalt. Trans.*, 1988, **3**, 1115.

27. M. Gustiananda, P. I. Haris, P. J. Milburn, and J. E. Gready, *FEBS Lett.*, 2002, **512**, 38–42.

28. G. E. Jackson and B. S. Nakani, *J. Chem. Soc. Dalt. Trans.*, 1996, 1373–1377.

29. K. Várnagy, J. Szabó, I. Sóvágó, G. Malandrinos, N. Hadjiliadis, D. Sanna, and G. Micera, *J. Chem. Soc. Dalt. Trans.*, 2000, 467–472.

30. T. Kowalik-Jankowska, M. Ruta-Dolejsz, K. Wiśniewska, and L. Łankiewicz, *J. Inorg. Biochem.*, 2002, **92**, 1–10.

31. B. D.-L. Reverend, L. Andrianarijaona, C. Livera, L. D. Pettit, I. Steel, and H. Kozlowski, *J. Chem. Soc. Dalt. Trans.*, 1986, 2221.

32. J. R. J. Sorenson, In Metal Ions in Biological Systems, Marcel Dekker, New York, Vol.14 edn., 1982.

33. I. Sóvágó and K. Osz, *Dalton Trans.*, 2006, 3841–54.

34. W. Bal, H. Kozlowski, R. Robbins, and L. D. Pettit, *Inorganica Chim. Acta*, 1995, **231**, 7–12.

35. W. Bal, M. Dyba, and H. Kozłowski, *Acta Biochim. Pol.*, 1997, **44**, 467–76.

36. E. Farkas, É. A. Enyedy, G. Micera, and E. Garribba, *Polyhedron*, 2000, **19**, 1727–1736.

37. A. Wattenberg, H. D. Barth, and B. Brutschy, *J. Mass Spectrom.*, 1997, **32**, 1350–1355.

38. M. Mylonas, J. C. Plakatouras, and N. Hadjiliadis, *Dalton Trans.*, 2004, 4152–60.

39. M. Sokolowska, A. Krezel, M. Dyba, Z. Szewczuk, and W. Bal, *Eur. J. Biochem.*, 2002, **269**, 1323–31.

40. A. Fago, A. J. Mathews, S. Dewilde, L. Moens, and T. Brittain, *J. Inorg. Biochem.*, 2006, **100**, 1339–43.

41. E. Farkas, I. Sóvágó, and A. Gergely, *J. Chem. Soc. Dalt. Trans.*, 1983, 1545.

42. R. H. R. and F. R. Walter L. Koltun and N. Gurd, *J. Biol. Chem.*, 1963, **238**, 124–31.

43. L. W. Jelinski, *Anal. Chem.*, 1990, **62**, 212R–223R.

44. H.-J. van Manen, K. Nakashima, S. Shinkai, H. Kooijman, A. L. Spek, F. C. J. M. van Veggel, and D. N. Reinhoudt, *Eur. J. Inorg. Chem.*, 2000, **2000**, 2533–2540.

45. M. Findeisen and S. Berger, *Magn. Reson. Chem.*, 2003, **41**, 431–434.

46. C. Conato, W. Kamysz, H. Kozłowski, M. Łuczkowski, Z. Mackiewicz, P. Młynarz, M. Remelli, D. Valensin, and G. Valensin, *J. Chem. Soc. Dalt. Trans.*, 2002, 3939.

47. C. Conato, W. Kamysz, H. Kozłowski, M. Łuczkowski, Z. Mackiewicz, F. Mancini, P. Młynarz, M. Remelli, D. Valensin, and G. Valensin, *Eur. J. Inorg. Chem.*, 2003, **2003**, 1694–1702.

48. H. Sterk and H. Holzer, *Org. Magn. Reson.*, 1974, **6**, 133–143.

49. M. Mylonas, A. Krezel, J. C. Plakatouras, N. Hadjiliadis, and W. Bal, *Bioinorg. Chem. Appl.*, 2004, 125–40.

50. J. H. Viles, F. E. Cohen, S. B. Prusiner, D. B. Goodin, P. E. Wright, and H. J. Dyson, *Proc. Natl. Acad. Sci. U. S. A.*, 1999, **96**, 2042–7.

51. J. P. Laussac, A. Robert, R. Haran, and B. Sarkar, *Inorg. Chem.*, 1986, **25**, 2760–2765.

52. S. J. Lau, J. P. Laussac, and B. Sarkar, *Biochem. J.*, 1989, **257**, 745–50.

53. J. P. Laussac, R. Haran, and B. Sarkar, *Biochem. J.*, 1983, **209**, 533–9.

54. Z. Szabó, *Coord. Chem. Rev.*, 2008, **252**, 2362–2380.

55. E. Farkas, E. Csapó, P. Buglyó, C. Damante, and G. Di Natale, *Inorganica Chim. Acta*, 2009, **362**, 753–762.

56. F. Turecek, *Mass Spectrom. Rev.*, 2007, **26**, 563–82.

57. S. Kumar Kailasa, N. Hasan, and H.-F. Wu, *Talanta*, 2012, **97**, 539–49.

58. R. Sekar, S. K. Kailasa, Y.-C. Chen, and H.-F. Wu, *Chinese Chem. Lett.*, 2014, **25**, 39–45.

59. C. S. Ho, C. W. K. Lam, M. H. M. Chan, R. C. K. Cheung, L. K. Law, L. C. W. Lit, K. F. Ng, M. W. M. Suen, and H. L. Tai, *Clin. Biochem. Rev.*, 2003, **24**, 3–12.

60. J. J. Hostynek, F. Dreher, and H. I. Maibach, *Inflamm. Res.*, 2011, **60**, 79–86.

61. A. Sun, B. Gao, X. Ding, C. Huang, and P. P. But, *J. Anal. Methods Chem.*, 2012, **2012**, 936131.

62. I. A. Kaltashov, C. E. Bobst, and R. R. Abzalimov, *Protein Sci.*, 2013, **22**, 530–44.

63. S. Banerjee and S. Mazumdar, *Int. J. Anal. Chem.*, 2012, **2012**, 1–40.

64. S. Daydé, V. Brumas, D. Champmartin, P. Rubini, and G. Berthon, *J. Inorg. Biochem.*, 2003, **97**, 104–117.

65. V. B. Di Marco and G. G. Bombi, *Mass Spectrom. Rev.*, 2006, **25**, 347–79.

66. P. Kebarle, *J. Mass Spectrom.*, 2000, **35**, 804–17.

67. W. J. Jackson, A. Moen, B. K. Nicholson, D. G. Nicholson, and K. a. Porter, *J. Chem. Soc. Dalt. Trans.*, 2000, 491–498.

68. P. Comba, T. W. Hambley, M. Gerloch, and E. C. Constable, *Molecular Modeling*, Wiley-VCH Verlag GmbH, Weinheim, Germany, 1995.

69. Peter Comba; Trevor W Hambley; Bodo Martin, *Molecular modeling of inorganic compounds*, Weinheim : Wiley-VCH, ©2009., 2009.

70. B. P. Hay and J. R. Rustad, *J. Am. Chem. Soc.*, 1994, **116**, 6316–6326.

71. W. D. Cornell, P. Cieplak, C. I. Bayly, I. R. Gould, K. M. Merz, D. M. Ferguson, D. C. Spellmeyer, T. Fox, J. W. Caldwell, and P. A. Kollman, *J. Am. Chem. Soc.*, 1995, **117**, 5179–5197.

72. P. V Bernhardt and P. Comba, *Inorg. Chem.*, 1992, **31**, 2638–2644.

73. E. T. Nomkoko, G. E. Jackson, B. S. Nakani, and S. A. Bourne, *Dalton Trans.*, 2004, 1789–96.

74. T. E. Nomkoko, G. E. Jackson, B. S. Nakani, and R. Hunter, *Dalton Trans.*, 2006, 4029–38.

75. A. Hinchliffe, *Molecular Modelling for Beginners*, by John Wiley & Sons Ltd, Chichester, 2003.

76. S. Shi, L. Yan, Y. Yang, J. Fisher-Shaulsky, and T. Thacher, *J. Comput. Chem.*, 2003, **24**, 1059–76.

77. J. Huang, M. Devereux, F. Hofmann, and M. Meuwly, *Computational Organometallic Chemistry*, Springer Berlin Heidelberg, Berlin, Heidelberg, 2012.

78. A. K. Rappe, C. J. Casewit, K. S. Colwell, W. A. Goddard, and W. M. Skiff, *J. Am. Chem. Soc.*, 1992, **114**, 10024–10035.

79. I. M. Neelov, D. B. Adolf, T. C. B. McLeish, and E. Paci, *Biophys. J.*, 2006, **91**, 3579–88.

80. P. Daisy, P. Vijayalakshmi, C. Selvaraj, S. K. Singh, and K. Saipriya, *Indian J. Pharm. Sci.*, 2012, **74**, 217–22.

81. B. R. Brooks, C. L. Brooks, A. D. Mackerell, L. Nilsson, R. J. Petrella, B. Roux, Y. Won, G. Archontis, C. Bartels, S. Boresch, A. Caflisch, L. Caves, Q. Cui, A. R. Dinner, M. Feig, S. Fischer, J. Gao, M. Hodoscek, W. Im, K. Kuczera, T. Lazaridis, J. Ma, V. Ovchinnikov, E. Paci, R. W. Pastor, C. B. Post, J. Z. Pu, M. Schaefer, B. Tidor, R. M. Venable, H. L. Woodcock, X. Wu, W. Yang, D. M. York, and M. Karplus, *J. Comput. Chem.*, 2009, **30**, 1545–614.

82. B. R. Brooks, R. E. Bruccoleri, B. D. Olafson, D. J. States, S. Swaminathan, and M. Karplus, *J. Comput. Chem.*, 1983, **4**, 187–217.

83. Insight II. System Guide. July 2005.

84. F. Bano, S. Naeem, N. Akhtar, and M. A. Haleem, *Pak. J. Pharm. Sci.*, 2005, **18**, 66–70.

85. C. J. Cramer and D. G. Truhlar, *J. Comput. Aided. Mol. Des.*, 1992, **6**, 629–66.

86. M. A. A. Azzellini, M. P. Abbott, A. Machado, M. T. M. Miranda, L. C. Garcia, G. F. Caramori, M. B. Gonçalves, H. M. Petrilli, and A. M. C. Ferreira, *J. Braz. Chem. Soc.*, 2010, **21**, 1303–1317.

87. J. Galy, J.-J. Bonnet, S. Andersson, A. F. Andresen, E. Hoyer, V. P. Spiridonov, and T. G. Strand, *Acta Chem. Scand.*, 1979, **33a**, 383–389.

88. J. Ribas, C. Diaz, R. Costa, Y. Journaux, C. Mathoniere, O. Kahn, and A. Gleizes, *Inorg. Chem.*, 1990, **29**, 2042–2047.

89. J. N. Zvimba, *PhD Thesis.*University of Cape Town, 2005.

90. S. Odisitse, *PhD Thesis*. University of Cape Town, 2006.

91. K. S. Bai and A. E. Martell, *J. Am. Chem. Soc.*, 1969, **91**, 4412–4420.

92. C. Jubert, A. Mohamadou, C. Gérard, S. Brandes, A. Tabard, and J.-P. Barbier, *J. Chem. Soc. Dalt. Trans.*, 2002, 2660.

93. P. M. Kroneck, V. Vortisch, and P. Hemmerich, *Eur. J. Biochem.*, 1980, **109**, 603–12.

CHAPTER FIVE

IN VIVO MODELLING AND TISSUE PERMEABILITY STUDIES OF COPPER COMPLEXES

5.1 BLOOD PLASMA MODEL

5.1.1 Introduction

The nutritional and pharmacological activity of trace metals has been reported extensively in the literature [1]. It has also been well demonstrated that Cu(II) complexes are effective in treating inflammation associated with rheumatoid arthritis. This pharmacological effect was first associated with the concentration of the free labile copper (II) in the body. Sorenson reported that the active forms of anti-inflammatory drugs may well be the Cu(II) complexes of such drugs *in vivo* [2].

The chemical analysis of all the metal species present in a complex solution like blood plasma is not really possible. However, assuming that the system is at equilibrium, a computer model can be used to calculate this speciation [3]. The Evaluation of Constituent Concentrations in Large Equilibrium Systems (ECCLES) program [4] and its associated database is able to do this. Therefore, the focus of this study was to investigate the efficiency of tripeptides (drug) in mobilising copper *in vivo* using the plasma modelling program ECCLES [4].

In this context, mobilization is defined as the ability of the ligand/drug to increase the concentration of low molecular weight (l.m.w) species in plasma. Numerically this is given by the plasma mobilizing index (p.m.i), which the ratio of the l.m.w. Cu(II) concentration in the absence of the ligand/drug to the concentration in the presence of the drug/ligand. In calculating p.m.i., Cu(II) complexation with endogenous ligands as well as complexation of the ligand by endogenous metal ions is taken into account. In other words, the specificity and strength of Cu(II) chelation is taken into account. A strong specific Cu(II) chelator would a have high p.m.i value at low drug concentrations, indicating a potentially useful therapeutic agent.

5.1.2 Data Analysis

The ECCLES database consists of 7 metal ions, 40 ligands, 250 published mononuclear binary constants measured under physiological conditions, with another 400 measured under non-physiological condition and 100 ternary complex constants [5,6]. The stability constants of H^+, Cu(II), Ni(II) and Zn(II) complexes of the tripeptides (drugs) measured in this study were added to the ECCLES database so as to calculate their plasma mobilizing indices. The total ligand concentration was varied over the range 10^{-1}- 10^{-10} M at constant pH of 7.40.

In the blood plasma model, Ca(II) is in high concentration and even though its metal complexes are likely to be much weaker than Cu(II), because it is in such high concentration it may interfere with the Cu(II) binding. For this reason it is important to include the Ca(II) tetrapeptide stability constants in the model. Unfortunately these were not measured in this study but their values can be estimated from linear free energy relationships [7,8]. Figure 5.0 shows the linear free energy relationship between Ca(II) and Cu(II). A regression coefficient of 0.9 was obtained and from this the stability of the Ca(II) complexes of the tripeptides were estimated (Table 5.0).

Table 5.0: Database of the linear free energy relationship between Ca(II) and Cu(II).

Ligand	**Species**	**Ca(II)**	**Cu(II)**
GLY-GLY Glycylglycine	ML	2.04	5.62
HIS Histidine	ML_2H	15.4	21.82
	MLH	9.35	12.88
	ML	0.95	9.56
ASP Aspartic acid	ML	1.6	8.83
ALA Alanine	ML	1.24	8.14
B-ALA Beta-alanine	ML	1.639	6.99
3-Phos-ALA 3-phos-alanine	ML	1.82	9.6
D-GLA D- Glutamic acid	MLH_{-1}	-10.15	-2.6
2-OxOsuccinic acid	ML	2.6	4.22
bis(imidzol-2-yl)methane	ML	1.8	9.64
	ML	10.7	21.43
H_6L^1 1,4,7-triazaheptane-4-methylphosphonic acid-1,1,7,7-tetraacetic acid	MLH	18.27	28.29
	MLH_2	23.83	31.95
	M_2L	13.23	28.15
	ML	9.38	19.47
H_5L^2 1,4,7-triazaheptane-4-methyl(phenyl)phosphinic acid-1,1,7,7-tetraacetic acid	MLH	15.48	23.3
	MLH_2	21.03	25.9
	M_2L	11.62	24.1
H_{5dtpa} 1,4,7-triazaheptane-1,1,4,7,7-pentaacetic acid	ML	10.75	21.2
	MLH	16.86	26

The stability of Ca(II) MLH_{-1} and MLH_{-2} species were not calculated as Ca(II) only coordinates to the oxygen donors of the peptide [9,10]. There is exception to this, where the metal coordinates to the imidazole nitrogen, but this only happens at pH 7.0 [11,12].

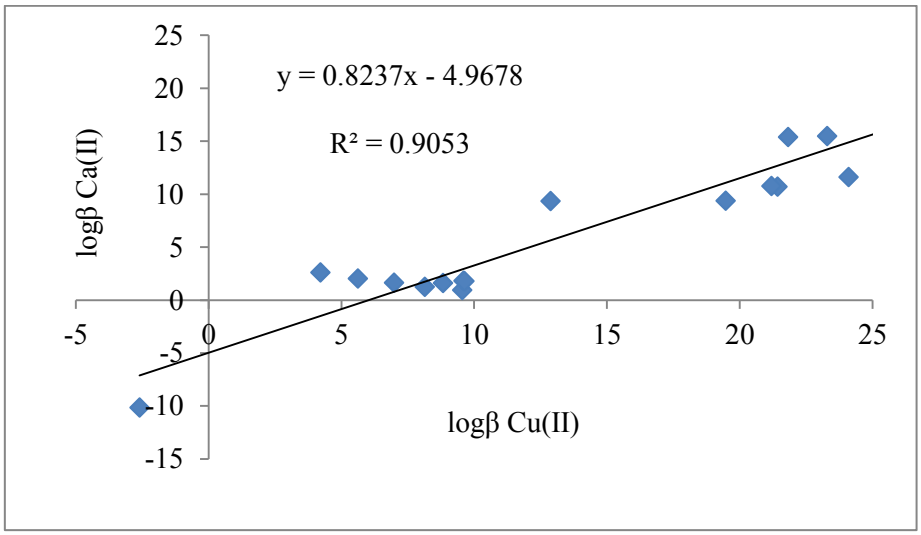

Figure 5.0: Linear free energy relationships between log*β* Cu(II) and log*β* Ca(II) of amino acid and peptides complex species at the same ionic strength and temperature. Data were taken from ref [9,13,14].

5.1.3 Results

5.1.3.1 Sar-His-Lys

The p.m.i, as a function of the ligand concentration is given in Figure 5.1. A log p.m.i. of 1 means a 10 fold increase in the l.m.w.

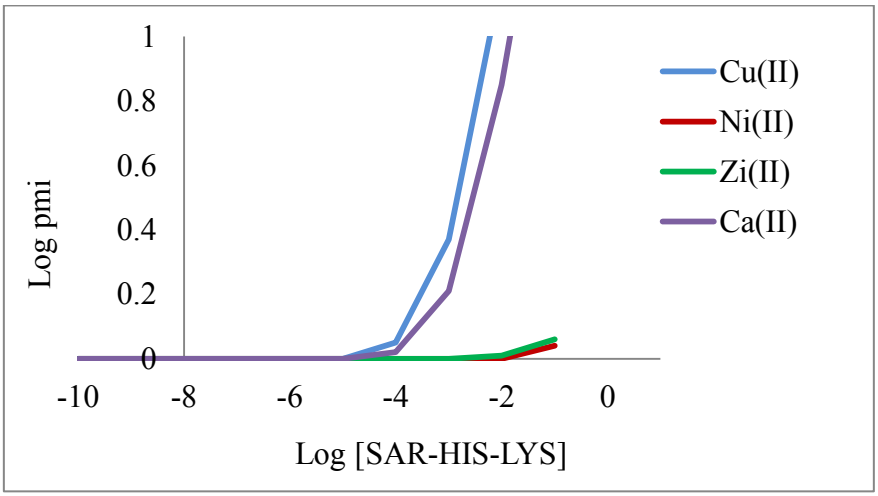

Figure 5.1: log p.m.i as a function of log [Sar-His-Lys] for Cu(II), Ni(II), Zn(II) & Ca(II) complexes.

At low ligand concentrations, between 10^{-6} and 10^{-5} M, Sar-His-Lys was able to mobilise Cu(II) and Ca(II). Meanwhile at ligand concentrations > 10^{-3} it started to mobilise Ni(II) and Zn(II).

5.1.3.2 Sar-Lys-His

Log p.m.i curves for Sar-Lys-His are given in Figure 5.2. At ligand concentrations above 10^{-5} M, Sar-Lys-His mobilised Cu(II) more than Ni(II), Zn(II) and Ca(II).

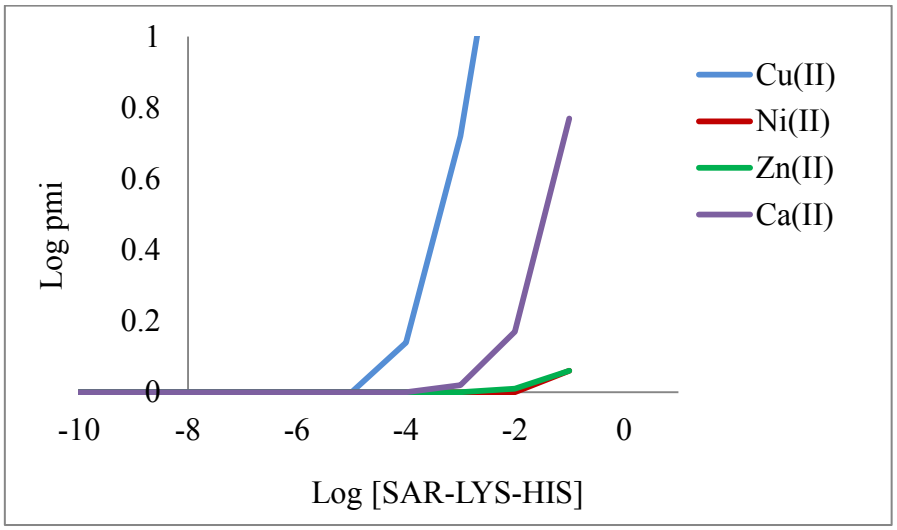

Figure 5.2: log p.m.i as a function of log [Sar-Lys-His] for Cu(II), Ni(II), Zn(II) & Ca(II) complexes.

5.1.3.3 Sar-His-His

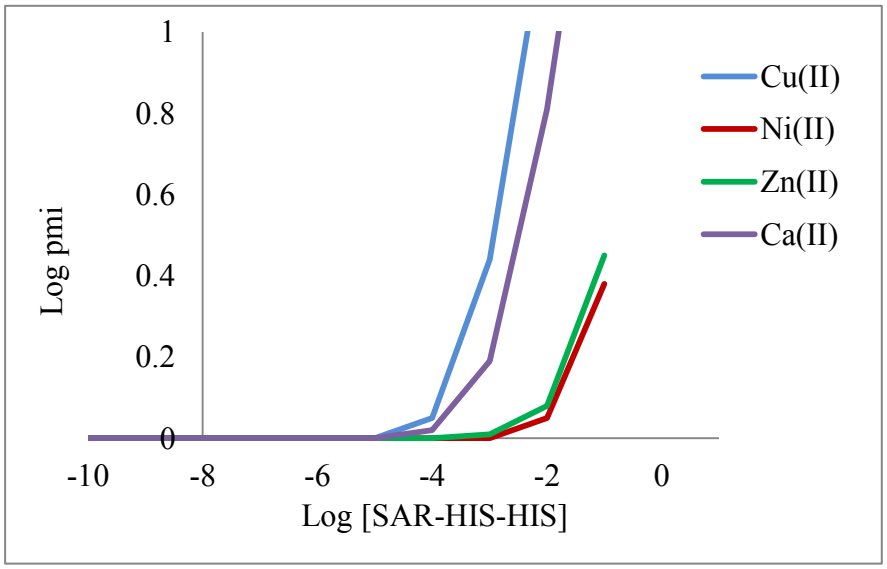

Figure 5.3: log p.m.i as a function of log [Sar-His-His] for Cu(II), Ni(II), Zn(II) & Ca(II) complexes.

Log p.m.i for complexes of Sar-His-His with Cu(II), Ni(II), Zn(II) and Ca(II) are shown in Figure 5.3. Sar-His-His mobilised Cu(II) more than Ca(II), Zn(II) and Ni(II) in blood plasma at concentrations of ligand above 10^{-4} M.

5.1.3.4 Sar-Lys-Lys

The log p.m.i curves for Sar-Lys-Lys with Cu(II), Ni(II), Zn(II) and Ca(II) complexes are shown in Figure 5.4. This ligand mobilised Zn(II) over Cu(II) and Ca(II) at concentrations of 0.1 M. Therefore, this ligand was not able to mobilise copper *in vivo*.

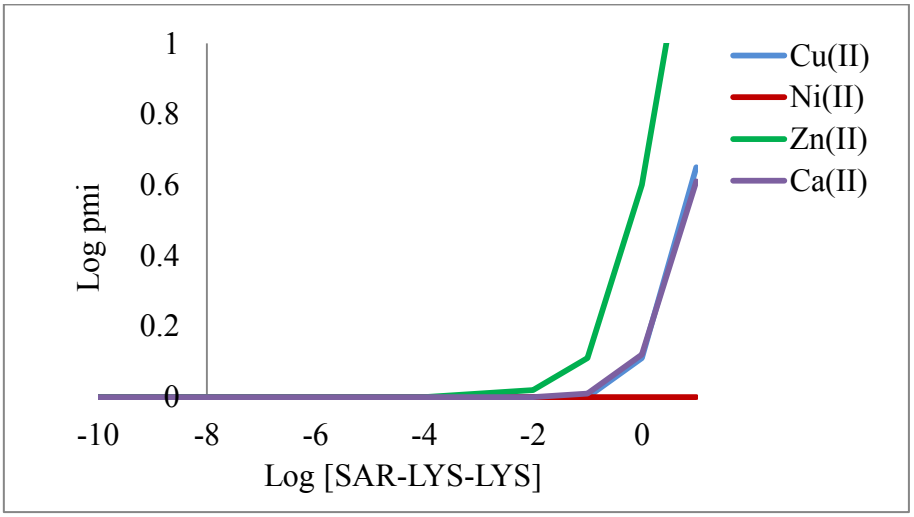

Figure 5.4: log p.m.i as a function of log [Sar-Lys-Lys] for Cu(II), Ni(II), Zn(II) & Ca(II) complexes.

5.1.3.5 Sar-Gly-His

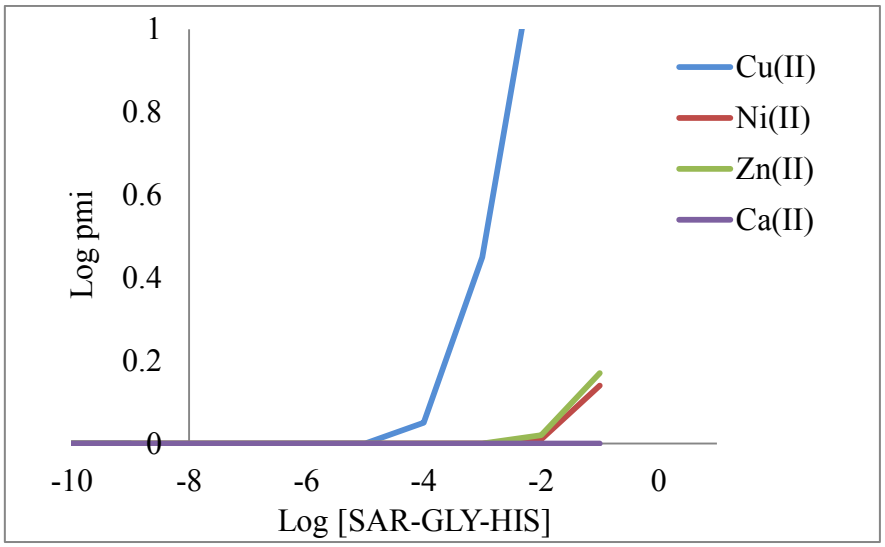

Figure 5.5: log p.m.i as a function of log [Sar-Gly-His] for Cu(II), Ni(II), Zn(II) & Ca(II) complexes.

Figure 5.5 shows log p.m.i curves for Cu(II), Ni(II), Zn(II) and Ca(II) plotted against the concentration of Sar-Gly-His. It was able to cause a more than 10 fold increase in l.m.w Cu(II) concentration at a total ligand concentration of 10^{-4} M.

5.1.4 Discussions

For any ligand metal system, a high log pmi value at low ligand concentration indicates that the ligand is a good competitor against other potential ligands present in the blood plasma [15]. Figure 5.6 shows log p.m.i of different tripeptides in this study complexed with copper as a function of tripeptide concentration. The Cu(II) mobilising ability was in the order of Sar-Lys-His > Sar-Gly-His ≈ Sar-His-His ≈ Sar-His-Lys > Sar-Lys-Lys.

Sar-Lys-Lys was not able to mobilise copper *in vivo.* The reason for this is the relatively high affinity of Sar-Lys-Lys for Zn(II). The lack of an imidazole group this ligand means that it is not as selective for copper. With the high *in vivo* concentration of Zn(II), Cu(II) is not able to compete effectively. Although it has been reported that tripeptides containing an imidazole residue are not particularly good at mobilising Cu(II) *in vivo* [16], it seems the better mobilisation arising from Sar-Lys-His, Sar-Gly-His, Sar-His-His, Sar-His-Lys as opposed to Sar-Lys-Lys are as a result of the high basicity of the imine nitrogen of the imidazole ring with a reported pK_a value of 6.95 [17,18]. However better mobilisation of Cu(II) as compared to Ni(II), Ca(II) and Zn(II) could be due to the preferential binding of ligands to Cu(II) compared to Ni(II), Ca(II) and Zn(II).

Poor mobilisation of Ni(II) was observed in this study even though Ni(II) formed more stable complexes compared to Zn(II) and Ca(II). *In vivo*, the free concentrations of Ca(II) and Zn(II) are 10^{15} and 10^{9} times greater than the free concentration of Ni(II) and this higher concentration means that they are able to displace Ni(II) from its complexes [19].

The p.m.i curves of different tripeptides and triethylenetetramine TRIEN [20,21] are shown in Figure 5.6. In comparison, TRIEN is six to three orders of magnitude better at mobilizing Cu(II) *in vivo* than Sar-Lys-His, Sar-Gly-His, Sar-His-His and Sar-His-Lys. The improved mobilizing ability of TRIEN compared to these tripeptides is related to the stable Cu(II) complexes of TRIEN and weak Ca(II) binding. This is also shown by EDTA, which is a poor mobiliser of Cu(II) even though it form very stable complexes. For EDTA the Ca(II) complex is also very stable.

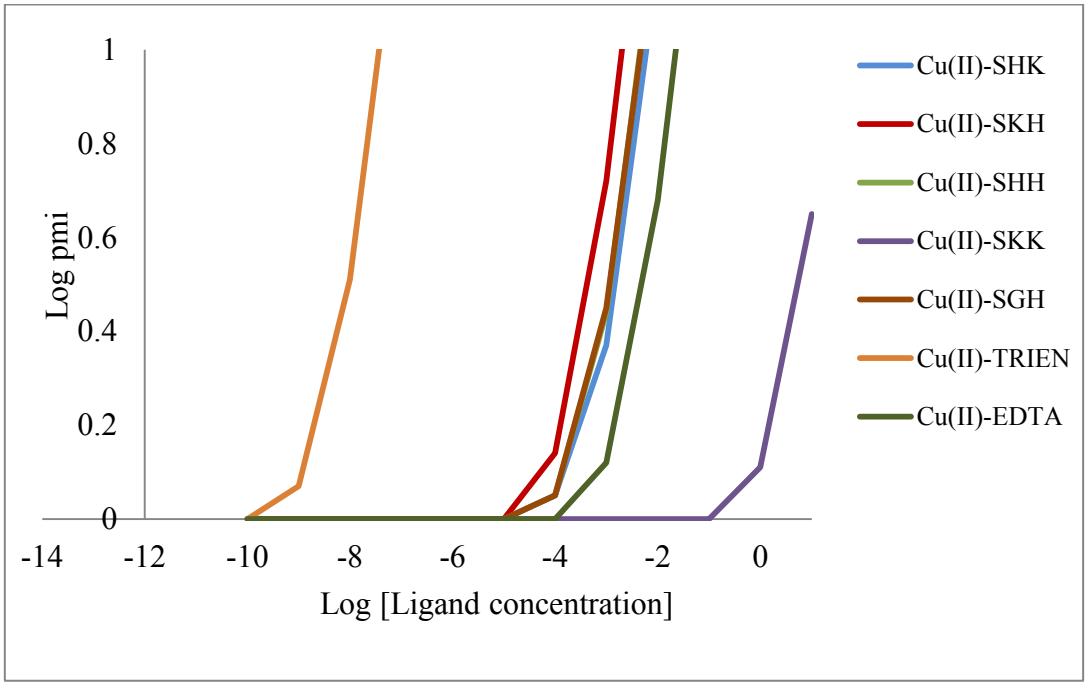

Figure 5.6: Plasma mobilising index for Cu(II) with tripeptide and TRIEN complexes.

In summary, the results show that, with the exception of Sar-Lys-Lys, all the tripeptides are predicted to mobilise Cu(II). At the same time, however, the speciation of Ca(II) is also effected. This is an unwanted side effect and is a result of the higher than anticipated stability of the Ca(II) complexes. As these stability constants were only estimated it is important that their values be measured. This will be the focus of future work.

5.2 OCTANOL / WATER PARTITION COEFFICIENTS

5.2.1 Introduction

Cu(II) complexes can be administered orally or by injection either intravenously or intraperitoneally. Although these two methods allow easy drug administration to increase the available Cu(II), it is difficult to move the coordinated metal across body compartments without protein binding [22]. The usefulness of a procedure in drug administration depends on the lipophilicity and molecular weight of the drug [23,24]. Partition coefficient measurements can be used as a reference parameter for hydrophobicity in biochemical and pharmacological systems. This is a powerful tool in estimating the tissue permeability of drugs. The partition coefficient between octanol and water is defined as:

$$\log P_{\mathrm{oct\backslash aq}} = \log\left(\frac{[\mathrm{Cu(II)}]_{\mathrm{oct}}}{[\mathrm{Cu(II)}]_{\mathrm{aq})}}\right) \tag{5.1}$$

where $[Cu(II)]_{oct}$ is the amount of Cu(II) extracted into octanol and $[Cu(II)]_{aq}$ is the amount of Cu(II) left in the water phase. The amount of Cu(II) transferred from aqueous solution to organic layer changes with pH because speciation changes with pH and the different species have different partition coefficients. This study seeks a viable transdermal alternative of copper with tripeptide as a therapy for inflammatory disorders and therefore the degree of lipophilicity is important.

5.2.2 Experimental

The Shake Flask method was used to measure partition coefficients where the organic phase was 1-octanol pre-saturated with water [25]. Standard solutions of Cu(II) were prepared as described [15,26,27]. Copper to tripeptide solutions, at a ratio of 1:1, were prepared in distilled/deionised water (0.005 M). 5 ml aliquots of 1:1 Cu(II): tripeptide solutions, in the pH range 2.00 – 11.00, into 10 glass vials were dispersed. 6 ml of 1-octanol (99 %) was added into each solution. The mixture was then shaken for two minutes and left for five minutes so that the two phases could separate at a constant temperature of 25 °C. To determine Cu(II) in the organic phase, 5 ml aliquots were withdrawn and extracted back into an aqueous phase with 6 ml of 5 % HNO_3. 4 ml aliquots were then withdrawn from the new aqueous phase (5 % HNO_3). The concentration of copper in each phase was measured using Microwave Plasma-Atomic Emission Spectrometry (MP-AES). The measure of hydrophobicity can be expressed as the logarithm of the partition coefficient between

l-octanol and an aqueous phase. The partition coefficients of Cu(II)-complex as a drug were calculated using Equation 5.1.

5.2.3 Results

5.2.3.1 Cu(II) Sar-His-Lys

The results for Cu(II) Sar-His-Lys are shown in Figure 5.7, which shows the log $P_{oct\backslash aq}$ results and the speciation graph for Cu(II) Sar-His-Lys as a function of pH. The Cu(II) complexes of Sar-His-Lys were more soluble in water than in 1-octanol, as is shown by the negative values of log $P_{oct\backslash aq}$. The partition coefficients changed as the pH increased due to the formation of various species. Comparison of the speciation diagram and the log $P_{oct\backslash aq}$ curve is interesting as it clearly shows how the partition coefficient changes as the CuL species is formed and transformed into $CuLH_{-1}$. In fact the Log $P_{oct\backslash aq}$ of -3.02 at pH 7.15 can be ascribed to this species.

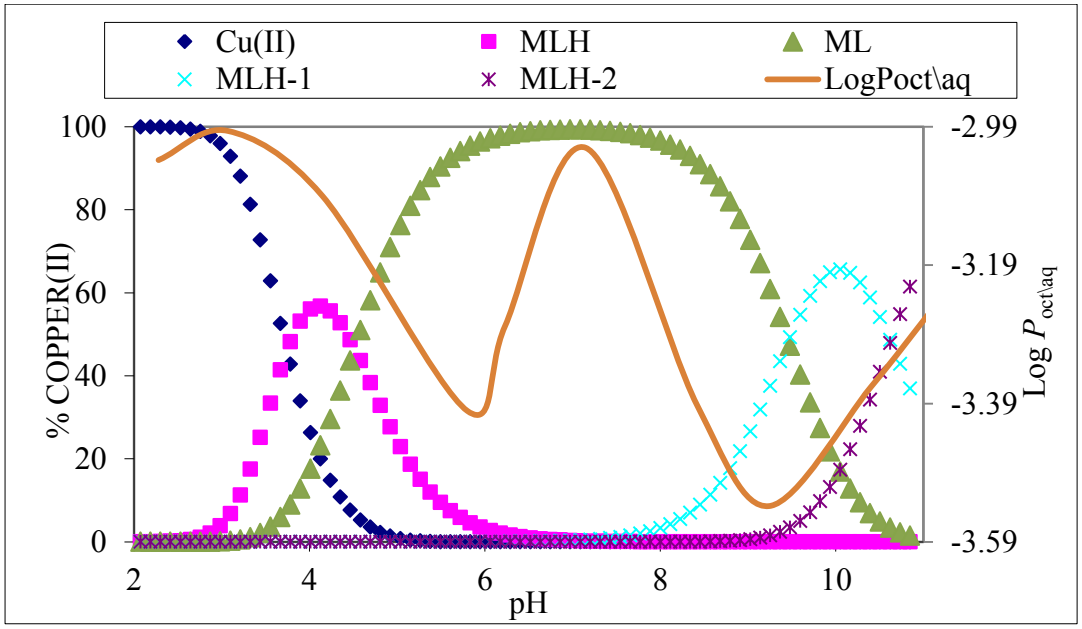

Figure 5.7: Log $P_{oct\backslash aq}$ and speciation graph as a function of pH for 1:1 Cu(II):SHK system.

5.2.3.2 Cu(II) Sar-Lys-His

Results for Cu(II) Sar-Lys-His are presented in Figure 5.8. The solubility in 1-octanol increased from low pH to pH 7.07. At physiological pH, $CuLH_{-1}$ was the predominant Cu(II) species at 97 %. At this pH, only 0.88 % of the Cu(II) was extracted into the organic phase of the octanol-water mixture. This complex is relatively hydrophilic by virtue of

having a negative log $P_{oct\backslash aq}$ value. At pH 10.4, $CuLH_{-2}$ was the most predominant species with a log $P_{oct\backslash aq}$ value of ~-2.79.

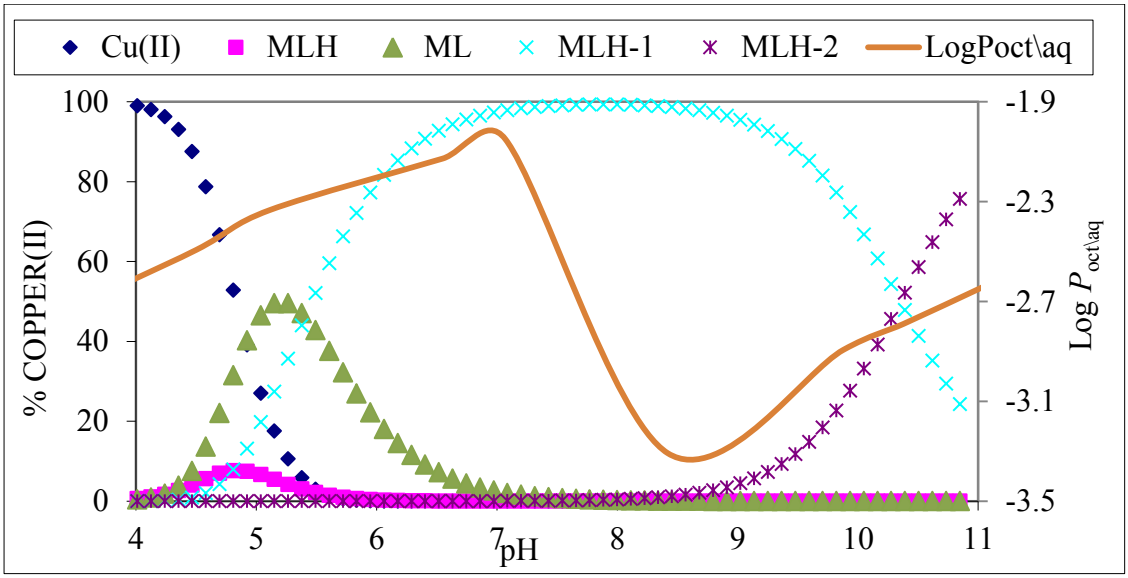

Figure 5.8: Log $P_{oct\backslash aq}$ and speciation graph as a function of pH for 1:1 Cu(II):SKH system.

5.2.3.3 Cu(II) Sar-His-His

The negative values of log $P_{oct\backslash aq}$ for Cu(II) Sar-His-His show that this complex is largely hydrophilic (Figure 5.9). The partition coefficient profile is quite complex in that it increases, decreases and then increases again. This profile, however, is easily rationalised by reference to the speciation diagram. At pH 4.13, the most predominant species was CuLH, with a log $P_{oct\backslash aq}$ = -2.43; at pH 7.43 the most predominant species was $CuLH_{-1}$, with a log $P_{oct\backslash aq}$ = -2.9 and at pH 10.05 the most predominant species was $CuLH_{-2}$, with a log $P_{oct\backslash aq}$ = -2.74.

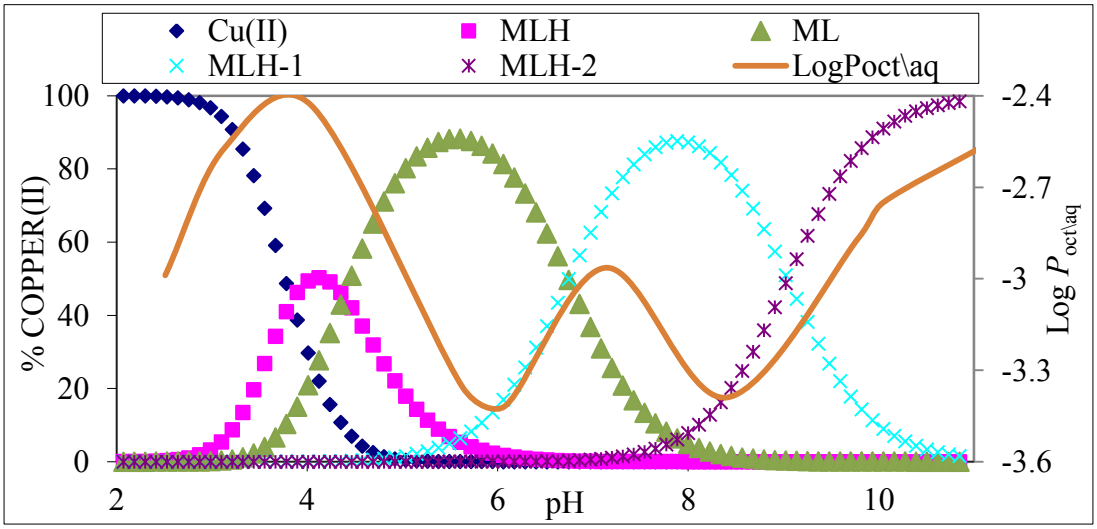

Figure 5.9: Log $P_{oct\backslash aq}$ and speciation graph as a function of pH for 1:1 Cu(II):SHH system.

5.2.3.4 Cu(II) Sar-Lys-Lys

Results for Cu(II) Sar-Lys-Lys are given in Figure 5.10. The solubility in 1-octanol increased from low to high pH. There was a rapid increase in log $P_{oct\backslash aq}$ values as the pH increased from 6.15-11.10 due to the formation of CuL (95.67 %) with maximum log $P_{oct\backslash aq}$ values of -2.6. The relatively hydrophilicity of this species in addition to the charge distributions, explains the preference of the complexes for the aqueous layer resulting in negative values of log $P_{oct\backslash aq}$.

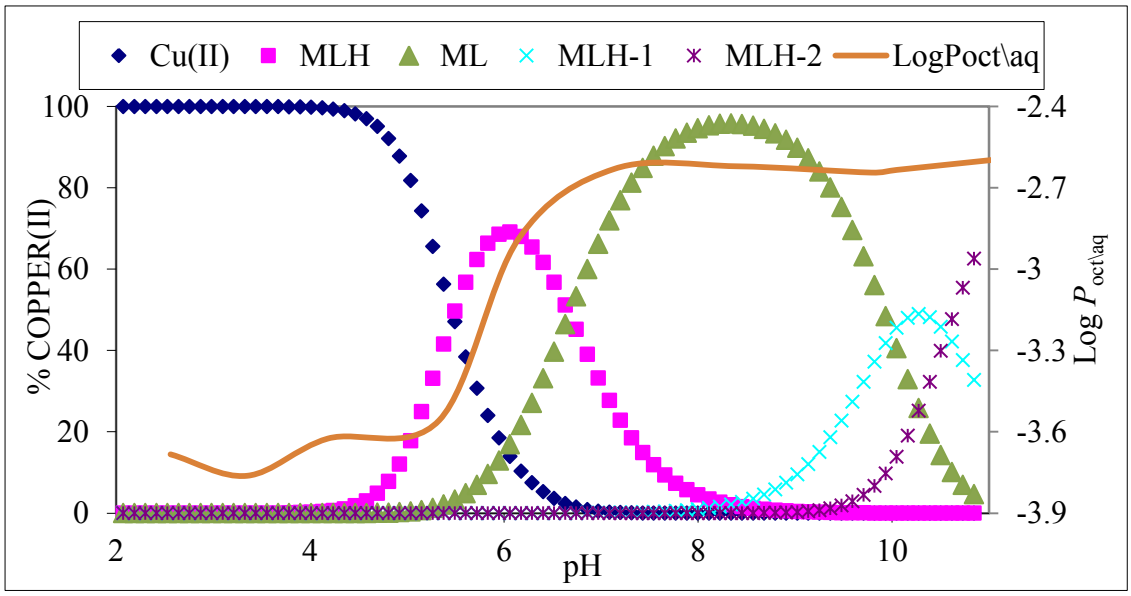

Figure 5.10: Log $P_{oct\backslash aq}$ and speciation graph as a function of pH for1:1 Cu(II):SKK system.

5.2.3.5 Cu(II) Sar-Gly-His

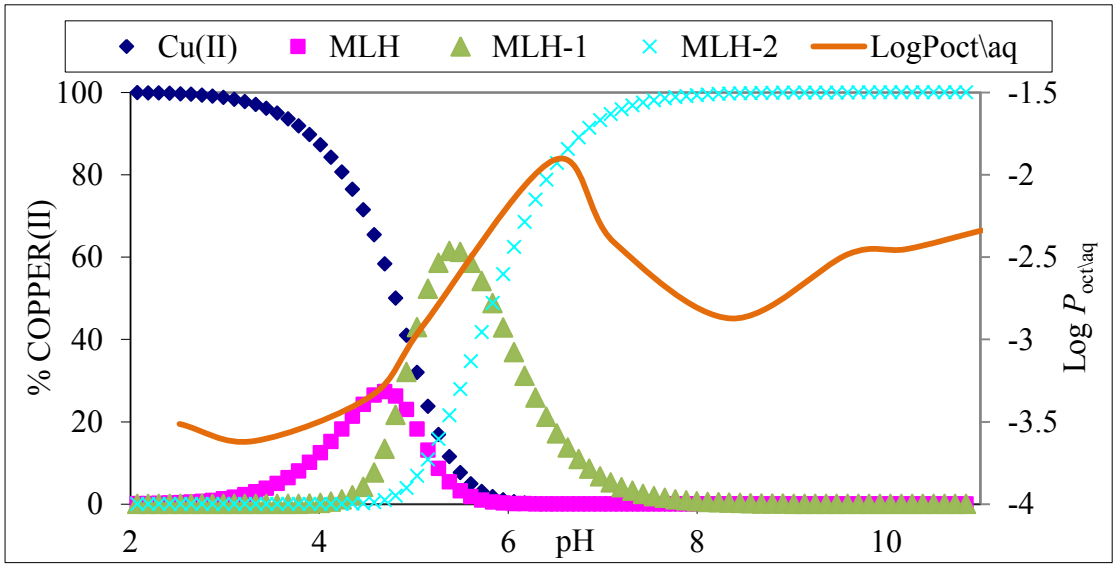

Figure 5.11: Log $P_{oct\backslash aq}$ and speciation graph as a function of pH for1:1 Cu(II):SGH system.

The results for Cu(II) Sar-Gly-His are given in Figure 5.11. The CuLH species was the predominant species at pH 4.56, where the log $P_{oct\backslash aq}$ was -3.34. At pH 6.48, the log $P_{oct\backslash aq}$ values of Cu(II) Sar-Gly-His was -1.91 and the $CuLH_{-2}$ species was predominant at this pH. There was an increase in log $P_{oct\backslash aq}$ values from pH 2.52 to 6.48, where upon it decreased. This partition coefficient profile does not exactly match the species distribution curves. The explanation for these observations is that the MLH_{-2} species has a higher partition coefficient than MLH_{-1} although the curve decreased above pH 7 as the concentration of MLH_{-2} increased.

5.2.4 Discussion

The log $P_{oct\backslash aq}$ values for complexes of Cu(II) with different tripeptides at pH 7.4 is given in Table 5.1. With the exception of the Sar-Lys-Lys and Sar-Gly-His systems, where there is some discrepancy, the partition coefficient curves mirror the change in speciation with pH. This is satisfactory since the two parameters were measured independently. Novel Cu(II)-based anti-inflammatory drugs with log $P_{oct\backslash aq}$ above zero at a physiological pH of 7.4 have been reported [3]. All four tripeptides increased the lipophilicity of the Cu(II) but all the complexes were hydrophobic, with a negative log $P_{oct\backslash aq}$. Deprotonation of the ligand does improve the lipophilicity as does N-methyl substituent on the terminal amine.

Table 5.1: Log $P_{oct\backslash aq}$'s for Cu(II) complexes with different tripeptides at pH 7.4.

	Sar-His-Lys	Sar-Lys-His	Sar-His-His	Sar-Lys-Lys	Sar-Gly-His
Species	CuL (99 %)	$CuLH_{-1}$ (98 %)	CuL (25 %) $CuLH_{-1}$ (73%)	CuL (77 %) $CuLH_{-1}$ (21%)	$CuLH_{-2}$ (96 %)
-Log $P_{oct\backslash aq}$	3.02± 0.01	2.05± 0.01	2.96± 0.01	2.63± 0.01	2.40± 0.01

Previous studies showed that complexes with log $P_{oct\backslash aq} < 2.5$ are considered to have low lipophilicity whereas, those with log $P_{oct\backslash aq} > 5$ are believed to have high lipophilicity. Furthermore, complexes with log $P_{oct\backslash aq}$ between 2.5 and 5 are considered to have intermediate lipophilicity [28]. The lipophilicity of complex species improves with an increase in pH, except in systems where Cu(II) precipitates out when excess amounts of NaOH are added. Zvimba and Jackson, however, suggest that the log $P_{oct\backslash aq}$ of 0.60 is sufficient enough to allow trans-dermal transportation of drugs [29]. In fact compounds that

are too lipophilic are poorly absorbed through the skin as they become trapped in the dermal layer. Jackson and coworkers [30] reported log $P_{oct/aq}$ values for the related Cu(II) complexes of dioxo N5-donor ligands to be in the range -3.70 to -6.63 for the CuLH, CuL, $CuLH_{-1}$ and $CuLH_{-2}$ species. Nomkoko and coworkers [31] also reported log $P_{oct/aq}$ value of -1.25 at physiological pH 7.4 for the related dioxo N5-donor ligand.

The partition coefficient GHK-Cu at pH 7.4 has been reported as -4.5 [32,33] and used to explain skin penetration typical for highly hydrophilic solutes [34,35]. Our Sar analogue. Sar-His-Lys is more lipophilic (a log $P_{oct\backslash aq}$ = -3.02). In order to increase their lipophilic properties, these small peptides could be transformed as palmitoyl derivatives, which exhibit a better delivery across skin [36].

The results for all the Cu(II) complex species studied showed log $P_{oct\backslash aq}$ values below zero, because the Cu(II) complexes of tripeptides are relatively hydrophilic. The factors that contribute to the hydrophilicity of these complexes are the presence of coordinated water molecules, hydrogen bonding between charged groups in these species and the solvent molecules, the overall charge of the complex and hydrogen bonding interactions between the carbonyl oxygen and bulk water molecules. However, the present study indicates that topical administration of copper in the form of tripeptide may offer an effective alternative to injection.

5.3 MEMBRANE PERMEABILITY STUDIES (*in vitro*)

5.3.1 Introduction

Dermal absorption of chemicals has been tested in split-thickness skin and/or in epidermal sheets of various species including human, rat, rabbit, pig and mouse [37]. The potency of percutaneous absorption of chemical substances and drugs is characterised by the total dermally penetrated amount, the percentage of absorption of applied dose, the flux (J) and the permeability coefficient (K_p cm/h). The relation between permeability coefficient and steady-state flux is given by the equation:

$$K_p = \frac{J}{Ci} \tag{5.2}$$

where, J is the amount of permeant crossing the membrane at a constant rate (mg/cm^2. h); this occurs after a lag phase when the amount continues to increase [38,39], and Ci is the concentration of a metal such as Cu(II) in the donor phase at that point. The amount of permeant crossing the membrane J can be expressed as:

$$J = \frac{Q}{A.t} \tag{5.3}$$

where Q (mg) is the quantity of Cu(II) transported through the membrane in time t (hrs), and A is the area of exposed membrane in cm^2.

The Franz diffusion cell technique is a common method used in permeation studies [39,40]. It is based on vertical diffusion between donor and acceptor phase. In the Franz diffusion cell, a biological membrane is normally used to determine the diffusion of the metal ion. However, the use of an industrial Franz diffusion cell with a biological membrane in permeation studies is impractical and difficult for several reasons. Firstly, the setting up of the Franz cell is difficult because of its vertical design and it also requires large sample volumes. Secondly, the efficiency of a biological membrane is dependent on the time they were obtained and on the conditions of conservation and treatment. Lastly, the age, sex and weight of the membrane have to be taken into account during the studies. However, these considerations for the biological membranes are unnecessary when using artificial membranes.

In the present study, a horizontal Franz cell fitted with an artificial membrane, (Cerasome 9005), was used. This membrane is a lipid solution which mimics human stratum corneum. Cerasome 9005 was purchased from Germany (Lipoid GmbH, Frigenstr.4, D-67065 Ludwigshafen, 2008) and possessed the following characteristics: consistency (aqueous, transparent to opaque dispersion), colour (off-white), solid matter (10%), phosphorus (0.11%), pH (7.1) and mean particle size (200 nm) [40,41].

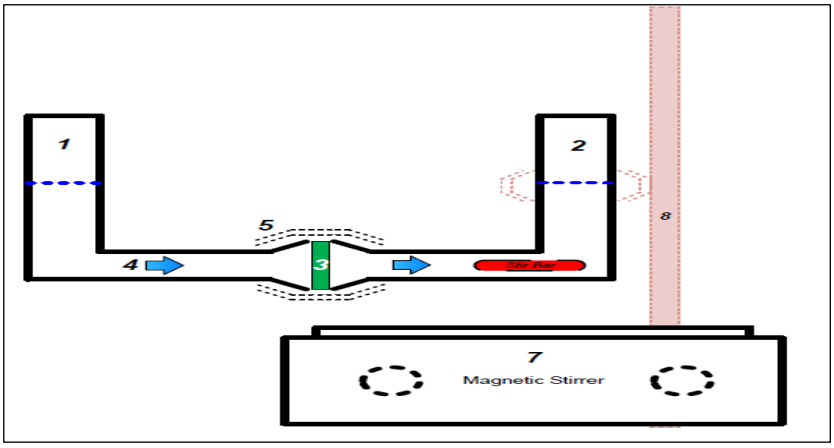

Figure 5.12: Modified Franz cell apparatus using in this study.

Where;

1. Donor phase filled with 20ml of Cu(II) tripeptide complex.
2. Receiver phase filled with blank solution (distilled/deionised water).
3. The artificial membrane (0.085 g).
4. Passive diffusion direction.
5. Clamp.
6. Stirrer bar.
7. Magnetic stirrer.
8. Burette stands with clamp.

5.3.2 Experimental

Figure 5.12 shows the details of a modified Franz diffusion cell used in this study for the permeability experiments. The receiver cell was filled with 20 ml of distilled/deionised water. Copper tripeptide solutions (0.005 M) were prepared in distilled/deionised water and 20 ml samples at pH 7.0 were placed in the donor phase compartment. The artificial membrane was prepared using a filter paper (Whatman, of 2.54 cm^2 discs and thickness

0.002cm) which was submerged in Cerasome 9005, dried for a few minutes at room temperature and then weighed. The amount of lipid absorbed determined by mass difference, was 0.085 g. The available diffusion area between cells was 0.709 cm^2. The contents of the cells were stirred by a magnetic stirrer. The experiments were conducted over a period of 72 hours at room temperature. During this period, both cells were covered so that the water could not evaporate and the experiments were conducted at room temperature. Copper concentration (ppm) was determined using an Agilent 4100 Microwave Plasma-Atomic Emission Spectrometer (MP-AES). The instrumental detection limit for copper at a wavelength of 324.75 nm was 0.2 ppb. For analysis, samples were appropriately diluted using 5% HNO_3 immediately prior to analysis. Standard solutions of Cu(II) were prepared from certified standards (ULTRASPEC) as described before [15,26,27]. Measurements were done in triplicate, using the points from 24 to 72 hours. Results are expressed as mean ± SE.

5.3.3 Results and Discussion

5.3.3.1 Franz cell

The concentrations of Cu(II) tripeptide complexes at pH 7.0 as a function of time (h) are plotted in Figure 5.13 and shown in Table 5.1.

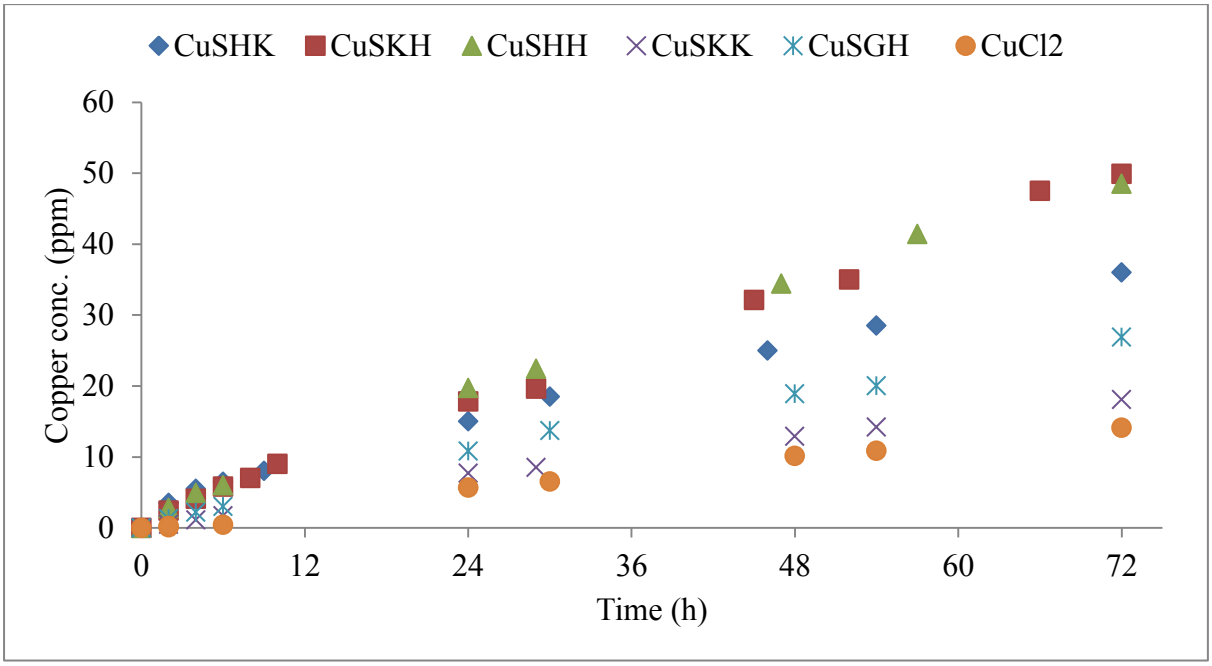

Figure 5.13: Variation of Cu(II) conc. vs. time through Cerasome 9005 membrane at pH 7.0.

It can be seen that the diffusion of the copper complexes is slow for the first 6 hours of the experiment. This is followed by a further phase of rapid diffusion, called the steady state, from 6 to 72 hours.

The reason for the observed induction period was attributed to the development of equilibrium between the donor phase and the membrane as a result of the complex diffusing through it [42,43]. Thereafter, there was a steady state flux of copper into the receiver phase. This is shown by the straight line from 24 to 72 hours as shown in Figure 5.13. From the slope of the curve the steady state flux permeability coefficient can be calculated (Table 5.3).

Table 5.2: Cu(II) concentration (ppm) in receiver phase of Franz cell at pH 7.0 as a function of time (h).

Time (h)	SHK	SKH	SHH	SKK	SGH	Cl^-
0	0	0	0	0	0	0
2	3.5 ± 0.1	2.4 ± 0.1	2.8 ± 0.1	0.5 ± 0.1	1.3 ± 0.1	0.08 ± 0.1
4	5.5 ± 0.1	4.1 ± 0.1	4.9 ± 0.1	1.1 ± 0.1	2.2 ± 0.1	0.24 ± 0.1
6	6.5 ± 0.1	5.8 ± 0.1	6.0 ± 0.1	1.7 ± 0.1	3.0 ± 0.1	0.44 ± 0.1
24	15.0 ± 0.1	17.8 ± 0.1	19.7 ± 0.1	7.7 ± 0.1	10.8 ± 0.1	5.68 ± 0.1
30	18.5 ± 0.1	19.6 ± 0.1	22.4 ± 0.1	8.5 ± 0.1	13.7 ± 0.1	6.52 ± 0.1
48	25.0 ± 0.1	32.1 ± 0.1	34.4 ± 0.1	12.9 ± 0.1	18.9 ± 0.1	10.12 ± 0.1
54	28.5 ± 0.1	35.0 ± 0.1	41.4 ± 0.1	14.2 ± 0.1	20.0 ± 0.1	10.88 ± 0.1
72	36.0 ± 0.1	49.9 ± 0.1	48.5 ± 0.1	18.1 ± 0.1	26.9 ± 0.1	14.12± 0.1

Table 5.3: Flux of diffusion *J* and permeability coefficient K_p of copper tripeptide complexes through Cerasome 9005 membrane at pH 7.0.

Complexes	*J* mg\cm^{2}h	K_p cm\h
Cu-SHK	0.009 ± 0.01	0.049 ± 0.01
Cu-SKH	0.013 ± 0.01	0.047 ± 0.01
Cu-SHH	0.012 ± 0.01	0.041 ± 0.01
Cu-SKK	0.005 ± 0.01	0.038 ± 0.01
Cu-SGH	0.007 ± 0.01	0.061 ± 0.01
$CuCl_2.2H_2O$ *pH 4.20	0.004 ± 0.05	0.028 ± 0.07

5.3.3.2 Flux (*J*) and permeability coefficient (K_p) calculations

The flux was calculated from the slope of the linear portion of the plot of cumulative amount of Cu(II) penetrated per square centimetre through Cerasome 9005 membrane as a function of time (Figure 5.13). The permeability coefficient K_p was calculated using Equation 5.2. The flux values and permeability coefficients are presented in Table 5.3 and are shown graphically in Figures 5.14 and 5.15, respectively.

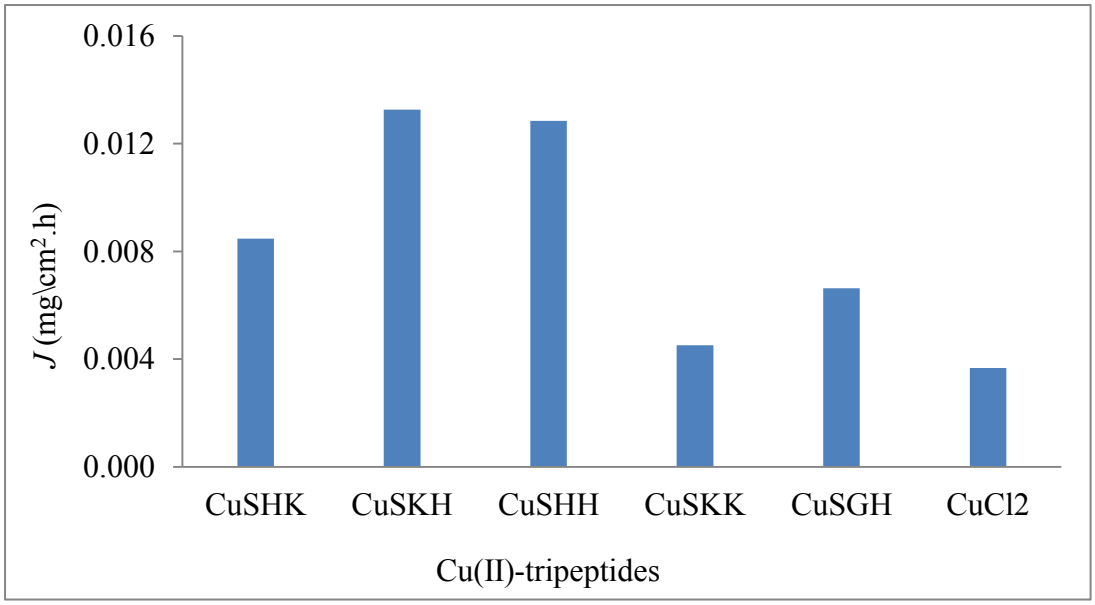

Figure 5.14: Effect of different tripeptides on the flux of copper through Cerasome 9005 membrane in modified Franz cell from 24-72 h at pH 7.0.

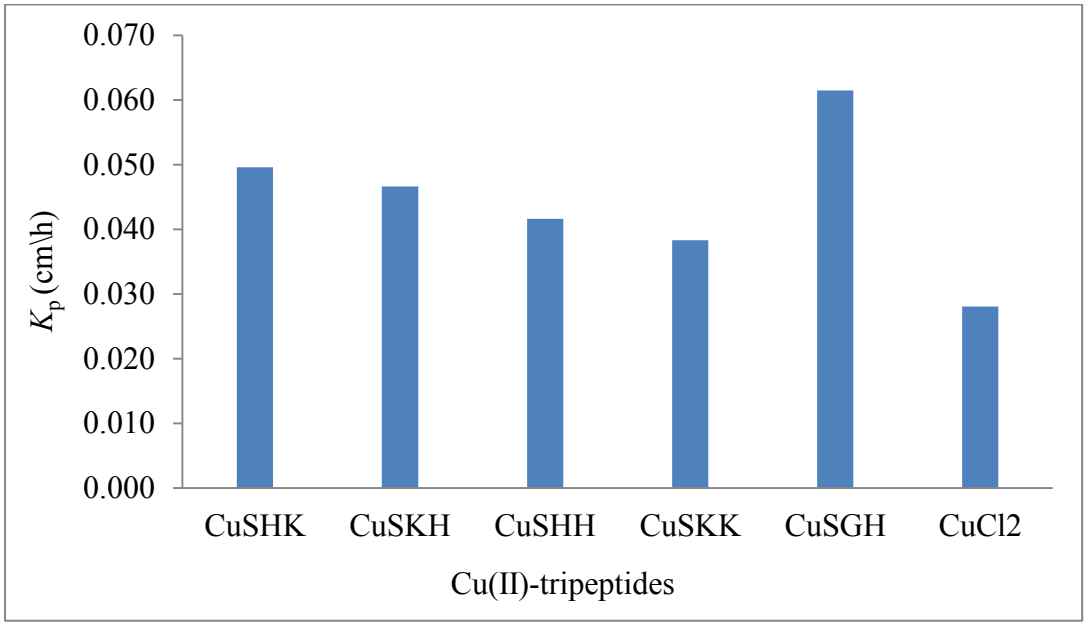

Figure 5.15: Influence of tripeptides on the permeability of copper complexes through Cerasome 9005 membrane at pH 7.0.

The results show the influence of different tripeptide systems on the flux and the permeability coefficients of copper ions through the Cerasome 9005 as a membrane. These results suggest that the complexation of Cu(II) ions with tripeptides greatly increases the permeation rate of copper ions, as K_p values for complexed species are significantly higher than the one for $CuCl_2$. The following order of permeability coefficient Cu-Sar-Gly-His > Cu-Sar-His-Lys > Cu-Sar-Lys-His > Cu-Sar-His-His > Cu-Sar-Lys-Lys > $Cu\text{-}Cl^-$ was obtained.

In previous studies, the permeabilities of the Cu(II) complexes with amino acids were closely related to their stabilities, as described by log *K* [44]. The permeability coefficients (K_p) and stability constants (log *K*) for copper complexes with alanine, glycine, valine, and lysine were similar. However, both the K_p and the log *K* values for the copper histidine complex were higher than those evaluated for the other amino acid complexes due to its higher molecular weight [[45]]. This effect of MW on the flux of copper complexes was observed by Potts *et al* [[42]].

Jurij *et al.* [46] determined the skin permeability coefficient K_p for Gly-L-His-L-Lys cuprate diacetate *in vitro* and found it to be $2.43 \pm 0.51 \times 10^{-4}$ cm/h using an isolated stratum corneum (model membrane). He predicted, therefore, that copper as a tripeptide complex will be delivered in potentially therapeutically effective amounts for inflammatory disease. The copper peptide complexes might be a good source not only for copper ions but also for peptides. The

investigations of the influence of complexing agents on the skin migration rate of copper ions have yielded evidence for their hampering role in this process [47].

5.3.3.3 Relationship between logarithm of permeability coefficient (Log K_p) and molecular weight (MW) of copper complexes

Table 5.4 is a summary of Cu(II) speciation at pH 7.4, MW and the permeation coefficient of the copper (II) tripeptide complexes.

Table 5.4: The permeability coefficients values of Cu(II) speciation in the presence of different tripeptides at pH 7.4.

	Sar-His-Lys	Sar-Lys-His	Sar-His-His	Sar-Lys-Lys	Sar-Gly-His
Species	CuL (99 %)	$CuLH_{-1}$ (98 %)	CuL (25 %) $CuLH_{-1}$ (73%)	CuL (77 %) $CuLH_{-1}$ (21%)	$CuLH_{-2}$ (96 %)
MW	434.96	415.96	425.93	407.97	343.48
-Log K_p	1.35± 0.01	1.38± 0.01	1.43± 0.01	1.46± 0.01	1.26± 0.01

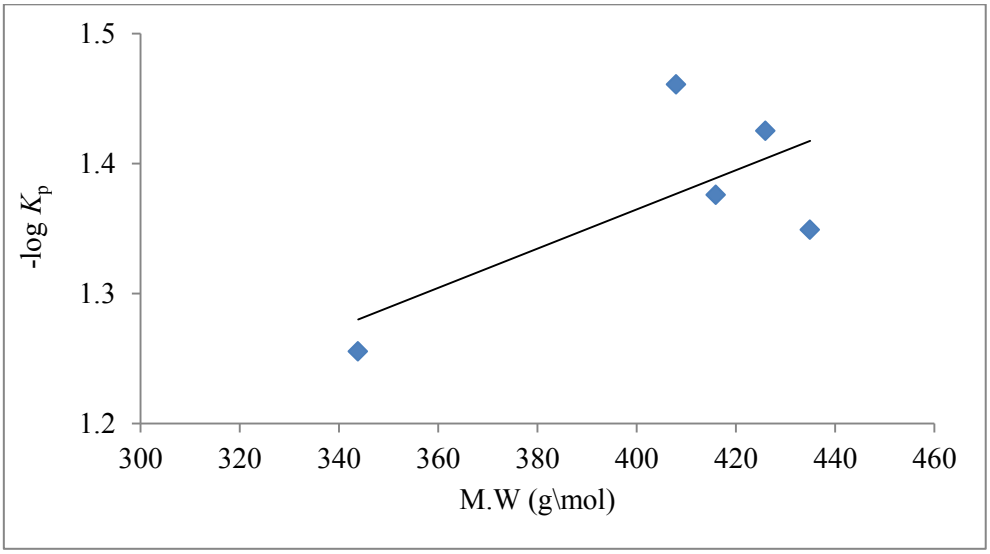

Figure 5.16: Logarithm of permeability coefficient plotted against molecular weight of Cu(II) tripeptide complexes.

In calculating the molecular weight, it is assumed that the metal is square planar with free coordination sites occupied by water. This is necessary because the water of coordination is generally not specified in the stoichiometry but needs to be inferred from the structure. The coefficient of correlation obtained from Figure 5.16 was $R^2 = 0.7306 \pm 0.005$, which is the correlation between the -log K_p and MW of His tripeptide complexes. This concludes the 73%

of the variability can be explained by MW of the Cu(II) complexes. If Cu-Sar-Lys-Lys include in the regression analysis a correlation coefficient of $R^2 = 0.477 \pm 0.01$ was obtained. This means that the His residue has a big effect on the permeability of the complex.

5.3.3.4 Relationship between permeability coefficient (Log K_p), octanol/water partition coefficient (Log $P_{oct\backslash aq}$) and molecular weight (MW) of copper complexes

The effect of molecular weight (MW) of a complex on its flux was also observed and reported by Potts *et al* [42]. This effect can be obtained quantitatively from their equation based on two physicochemical properties of octanol-water partition coefficient log $P_{oct\backslash aq}$ and molecular weight MW of complex and is given by the linear relationship [48]. The following equation was used to predict skin permeability [49] :

$$\text{Log } K_p = \text{Log } (D^0/h) + f \text{ Log } P_{oct\backslash aq} - \beta' \text{ MW} \qquad (5.4)$$

where, K_p= the permeability coefficient; D^0= the diffusivity of hypothetical molecule having zero molecular weight; h = the membrane thickness; f = constant which accounts for the difference between the partitioning domain presented by octanol and that presented by the membrane lipids; $P_{oct\backslash aq}$ = the octanol/water partition coefficient; MW = molecular weight, β' = a constant which includes a conversion factor for the substitution of molecular weight for molecular volume. The Cerasome 9005 membrane thickness was (h=0.002cm).

In this study, was used this model to examine the permeability data through a Cerasome 9005 membrane, although the model was initially used to describe skin permeabilities of non-ionic drugs dissolved in water. Multiple linear regression analysis of log K_p upon log $P_{oct\backslash aq}$ and MW was used to obtain values for β', log (D^0/h) and f.

Table 5.5: The permeability coefficients and the partition coefficient values of Cu(II) speciation in the presence of different tripeptides at pH 7.4.

	Sar-His-Lys	Sar-Lys-His	Sar-His-His	Sar-Lys-Lys	Sar-Gly-His
Species	CuL (99 %)	$CuLH_{-1}$ (98 %)	CuL (25 %) $CuLH_{-1}$ (73%)	CuL (77 %) $CuLH_{-1}$ (21%)	$CuLH_{-2}$ (96 %)
MW	434.96	415.96	425.93	407.97	343.48
-Log K_p	1.35± 0.01	1.38± 0.01	1.43± 0.01	1.46± 0.01	1.26± 0.01
-Log $P_{oct\backslash aq}$	3.02± 0.01	2.05± 0.01	2.96± 0.01	2.63± 0.01	2.40± 0.01

The coefficient of correlation obtained from relationship between octanol/water partition coefficients (log $P_{oct\backslash aq}$) and molecular weights of the bases (MW) were found not to correlate with permeability coefficients (log K_p) is $R^2 = 0.44 \pm 0.01$, which is far from 1, demonstrating that there is no correlation between permeability coefficient, partition coefficient and molecular weights of all complexes.

5.3.4 Conclusion

The presented results suggest that the complexation of Cu(II) ions by the different tripeptides greatly influences the diffusion of copper ions across the membrane because different flux and permeability coefficients values were obtained for the different copper (II) tripeptide complex species studied. The K_p value for the Cu-Sar-Lys-Lys was lower than the other copper tripeptide complexes, because histidine is not present in this ligand. When comparing the permeation coefficient of copper tripeptide complexes of Cu-Sar-Gly-His and Cu-Sar-His-His, there was a decrease in K_p and this was attributed to the higher molecular weight of Cu-Sar-His-His. The obtained results show that the permeability rate of tripeptide Cu(II) complexes through Cerasome 9005 membrane depend on which species predominate in solution at pH 7.0.

In addition, copper complexes with tripeptides penetrate through the model membrane as copper complexes. In this study, however, the transport of copper through a model membrane with tripeptides greatly increased the permeation rate of copper ions since K_p values for complex species were significantly higher than those for simple Cu(II) ions. Furthermore, it can be concluded from the obtained results that no correlation was found between molecular weight, logarithm of partition coefficient and permeability coefficient.

References

1. D. R.William, *The Metals of Life*, Van Norstrand Reinhold, London, 1971, London, 1971.

2. J. R. Sorenson, *J. Med. Chem.*, 1976, **19**, 135–48.

3. J. N. Zvimba and G. E. Jackson, *J. Inorg. Biochem.*, 2007, **101**, 1120–8.

4. P. M. May, P. W. Linder, and D. R. Williams, *J. Chem. Soc. Dalt. Trans.*, 1977, **2**, 588.

5. J. R. Zeevaart, N. V Jarvis, W. K. . Louw, G. E. Jackson, I. Cukrowski, and C. J. Mouton, *J. Inorg. Biochem.*, 1999, **73**, 265–272.

6. J. N. Zvimba and G. E. Jackson, *J. Inorg. Biochem.*, 2007, **101**, 148–58.

7. D. Vlassopoulos, S. A. Wood, and A. Mucci, *Geochim. Cosmochim. Acta*, 1990, **54**, 1575–1586.

8. T. D. Matthews and D. R. Williams, *Anal. Chim. Acta*, 2003, **480**, 119–122.

9. R. Huber, M. Schneider, I. Mayr, J. Römisch, and E.-P. Paques, *FEBS Lett.*, 1990, **275**, 15–21.

10. N. C. Strynadka, M. Cherney, A. R. Sielecki, M. X. Li, L. B. Smillie, and M. N. James, *J. Mol. Biol.*, 1997, **273**, 238–55.

11. E. Gaggelli and G. Valensin, *J. Chem. Soc. Perkin Trans. 2*, 1990, 401.

12. E. J. Baran, *Biochem. Biokhimiia*, 2000, **65**, 789–97.

13. J. Kotek, F. K. Kálmán, P. Hermann, E. Brücher, K. Binnemans, and I. Lukeš, *Eur. J. Inorg. Chem.*, 2006, **2006**, 1976–1986.

14. M. Vavrusova and L. H. Skibsted, *J. Agric. Food Chem.*, 2013, **61**, 5380–4.

15. S. Odisitse, G. E. Jackson, T. Govender, H. G. Kruger, and A. Singh, *Dalton Trans.*, 2007, 1140–9.

16. G. E. Jackson and M. J. Kelly, *Inorganica Chim. Acta*, 1988, **152**, 215–217.

17. J. Ueda, M. Miyazaki, Y. Matsushima, and a Hanaki, *J. Inorg. Biochem.*, 1996, **63**, 29–39.

18. J. Alí-Torres, L. Rodríguez-Santiago, and M. Sodupe, *Phys. Chem. Chem. Phys.*, 2011, **13**, 7852–61.

19. S. Odisitse and G. E. Jackson, *Bioinorg. Chem. Appl.*, 2014, **2014**, 863612.

20. G. E. Jackson and M. J. Kelly, *J. Chem. Soc. Dalt. Trans.*, 1989, 2429.

21. J. Aaseth, *Erud. J. Drugs Pharmacol. Res*, 2012, **1**, 1–3.

22. G. E. Jackson, P. M. May, and D. R. Williams, *J. Inorg. Nucl. Chem.*, 1978, **40**, 1227–1234.

23. A. Leo, C. Hansch, and D. Elkins, *Chem. Rev.*, 1971, **71**, 525–616.

24. T. X. Xiang and B. D. Anderson, *J. Membr. Biol.*, 1994, **140**, 111–22.

25. I. N. T. U. Ction, *Test No. 107: Partition Coefficient (n-octanol/water): Shake Flask Method*, OECD Publishing, 1995.

26. M. Mohajane, *PhD Thesis*.University of Cape Town, 2013.

27. J. N. Zvimba, *PhD Thesis*.University of Cape Town, 2005.

28. M. Gertz, P. J. Kilford, J. B. Houston, and A. Galetin, *Drug Metab. Dispos.*, 2008, **36**, 535–42.

29. J. N. Zvimba and G. E. Jackson, *Polyhedron*, 2007, **26**, 2395–2404.

30. G. E. Jackson, L. Mkhonta-Gama, A. Voyé, and M. Kelly, *J. Inorg. Biochem.*, 2000, **79**, 147–152.

31. E. T. Nomkoko, G. E. Jackson, and B. S. Nakani, *Inorg. Chem. Commun.*, 2003, **6**, 335–338.

32. S. J. Lau and B. Sarkar, *Biochem. J.*, 1981, **199**, 649–56.

33. J. J. Hostynek, F. Dreher, and H. I. Maibach, *Inflamm. Res.*, 2011, **60**, 79–86.

34. J. L. Wallace and M. N. Muscará, *Dig. Liver Dis.*, 2001, **33 Suppl 2**, S21–8.

35. R. W. Gorter, M. Butorac, and E. P. Cobian, *Am. J. Ther.*, 2004, **11**, 453–8.

36. L. R. Robinson, N. C. Fitzgerald, D. G. Doughty, N. C. Dawes, C. A. Berge, and D. L. Bissett, *Int. J. Cosmet. Sci.*, 2005, **27**, 155–60.

37. A. M. Barbero and H. F. Frasch, *Toxicol. In Vitro*, 2009, **23**, 1–13.

38. T. Lundh, A. Boman, and B. Åkesson, *Int. Arch. Occup. Environ. Health*, 1997, **70**, 309–313.

39. G. Korinth, K. H. Schaller, and H. Drexler, *Arch. Toxicol.*, 2005, **79**, 155–9.

40. E. U. Tsumbu, *MSc Thesis.* University of Cape Town, 2010.

41. K. Mokalane, *MSc Thesis.* University of Cape Town, 2011.

42. J. A. Zeitler, P. F. Taday, D. a Newnham, M. Pepper, K. C. Gordon, and T. Rades, *J. Pharm. Pharmacol.*, 2007, **59**, 209–23.

43. S. Odisitse and G. E. Jackson, *Inorganica Chim. Acta*, 2009, **362**, 125–135.

44. R. M. Smith and A. E. Martell, *Critical Stability Constants*, Springer US, Boston, MA, 1989.

45. L. Mazurowska, K. Nowak-Buciak, and M. Mojski, *Anal. Bioanal. Chem.*, 2007, **388**, 1157–63.

46. J. J. Hostýnek, F. Dreher, and H. I. Maibach, *Food Chem. Toxicol.*, 2006, **44**, 1539–43.

47. L. Mazurowska and M. Mojski, *Int. J. Cosmet. Sci.*, 2009, **31**, 72–73.

48. S.-F. Ng, J. Rouse, D. Sanderson, and G. Eccleston, *Pharmaceutics*, 2010, **2**, 209–223.

49. I. Bosman, *Int. J. Pharm.*, 1998, **169**, 65–73.

CHAPTER SIX

CONCLUDING *REMARKS*

Copper complexes have been found to exhibit lower toxicity and higher anti-inflammatory activity as compared to their parent compounds or ligands [1]. The present study focuses on the design of new drugs that will alleviate the inflammation associated with rheumatoid arthritis. There are two ways of increasing the available pool of low molecular weight Cu(II) species *in vivo*, endogenously or exogenously. Endogenous increase means that the drug releases Cu(II) from natural stores ie serum albumin. Exogenous means that Cu(II) is administered orally, dermally or by injection. Of these three methods we prefer dermal absorption as offering one obvious advantage of being less painful and hence tolerable to the patient [2]. For this reason the drugs were designed so that they could be administered dermally and be selective for Cu(II) so that they do not affect the speciation of other metal ions in blood plasma.

The first step in this investigating was to design new ligands. In normal blood plasma, Cu(II) is transported complexed to the N-terminus of serum albumin. The binding site is Asp-Ala-His. For this reason, histidine containing tripeptides were chosen for evaluation. In addition N-methyl glycine was used as this is commercially available, is less susceptible to metabolism *in vivo,* and it may increase the lipophilicity of the complex, without compromising its Cu(II) binding. The ligands chosen were sarcosyl-L-histidyl-L-lysine (SHK), sarcosyl-L-lysyl-L-histidine (SKH), sarcosyl-L-histidyl-L-histidine (SHH), sarcosyl-L-lysyl-L-lysine (SKK) and sarcosyl-L-glycyl-L-histidine (SGH). Having decided on the ligands, the next step was to measure their Cu(II) binding and selectivity using glass electrode potentiometry. The equilibrium constants of H^+, Cu(II), Ni(II), and Zn(II) at 25°C and in 0.15 M $Na^+(Cl^-)$ were measured. The Cu(II) tripeptide species showed a significantly different coordination behaviour at physiological pH. At this pH, the Cu(II) tripeptide complexes showed formation of CuL 99% (SHK); $CuLH_{-1}$ 98%(SKH); CuL 25%, $CuLH_{-1}$ 73% (SHH); CuL 77%, $CuLH_{-1}$ 21% (SKK) and $CuLH_{-2}$ 73% (SGH). Moreover, the tripeptides with histidine produced the strongest ligand field and the most stable CuL species was with Sar-His-Lys (SHK). The results presented in this study showed that the metal ion complexation strongly depends on the position of histidine in the amino acid sequence of the tripeptide molecules. The methyl group also had an inductive effect, making the Sar tripeptides more basic than Gly tripeptides. Similarly the Cu(II) complexes of Sar-His-Lys and Sar-Gly-His were more stable than their Gly analogues.

The formation equilibria for Ca(II), Ni(II) and Zn(II) show that these metal ions also form relatively stable complexes with the tripeptides, although their stability is lower than that of Cu(II). The selectivity of the ligands for Cu(II) at physiological pH was Cu(II)/Ca(II) > Cu(II)/Zn(II) > Cu(II)/Ni(II). This then suggests that the tripeptide species are likely to complex Cu(II) *in vivo*, despite competition from Ca(II), Ni(II) and Zn(II). However, high concentrations of Ca(II) and Zn(II) *in vivo* could upset the favourable selectivity for Cu(II).

In order to evaluate the Cu(II) mobilising ability of the ligands an *in vivo* speciation model of the blood plasma, ECCLES, was used. The simulations showed that, because the concentration of Ca(II) and Zn(II) in blood plasma is much higher than Cu(II), even though the Cu(II) complexes are more stable, these metal ions do affect the Cu(II) mobilisation. It was shown that the Cu(II) mobilising ability of the ligands was in the order Sar-Lys-His > Sar-Gly-His ≈ Sar-His-His ≈ Sar-His-Lys > Sar-Lys-Lys. At a concentration of 10^{-5} to 10^{-4} mol dm^{-3} the ligands were able to cause a 10 fold increase in the concentration of low molecular weight Cu(II) complexes. However, Sar-His-Lys and Sar-His-His also affected the speciation of Ca(II).

Having established that these ligands are able to complex Cu(II) *in vivo* and in order to understand the difference in stability of the different Cu(II) complexes their chemical structures were determined. This was done using Uv-Vis, ^{1}H NMR, ESI-MS spectroscopy as well as molecular mechanics calculations. It was also important to know their structure as this would determine their physical properties and hence bioavailability. The colours of Cu(II) tripeptide species at different pHs are shown in Figure 6.1. A visual check can distinguish between species as colours vary from light blue to purple. This change in colour indicates a change in coordination as different species are formed e.g. the formation of the 4N species, $CuLH_{-2}$ from the 3N species, $CuLH_{-1}$. The potentiometric and spectroscopic results obtained for the tripeptide containing His at position II reported the formation of $CuLH_{-1}$ as a 3N complex and a light blue colour. The copper was ligated to Sar-His-Lys via three bonds in the equatorial plane. The fourth equatorial position could be a water molecule. When the His was at position III a λ_{max} of 520 nm (purple colour) was obtained indicating the formation of 4N [-NH, $2N^{-}$, N_{im}] species for $CuLH_{-2}$. The Uv-Vis spectra of copper binding with the tripeptide containing His simultaneously at the second and third positions Sar-His-His showed patterns similar to those of the complexes with Sar-His-Lys and Sar-Lys-His.

Sar-Lys-Lys does not have His and therefore, both amide groups can be in the equatorial plane and deprotonated to give the $CuLH_{-2}$ species. This is the same as Gly-Gly-Gly with 3N [-NH,2N^{-},O(COO^{-})] [3,4].

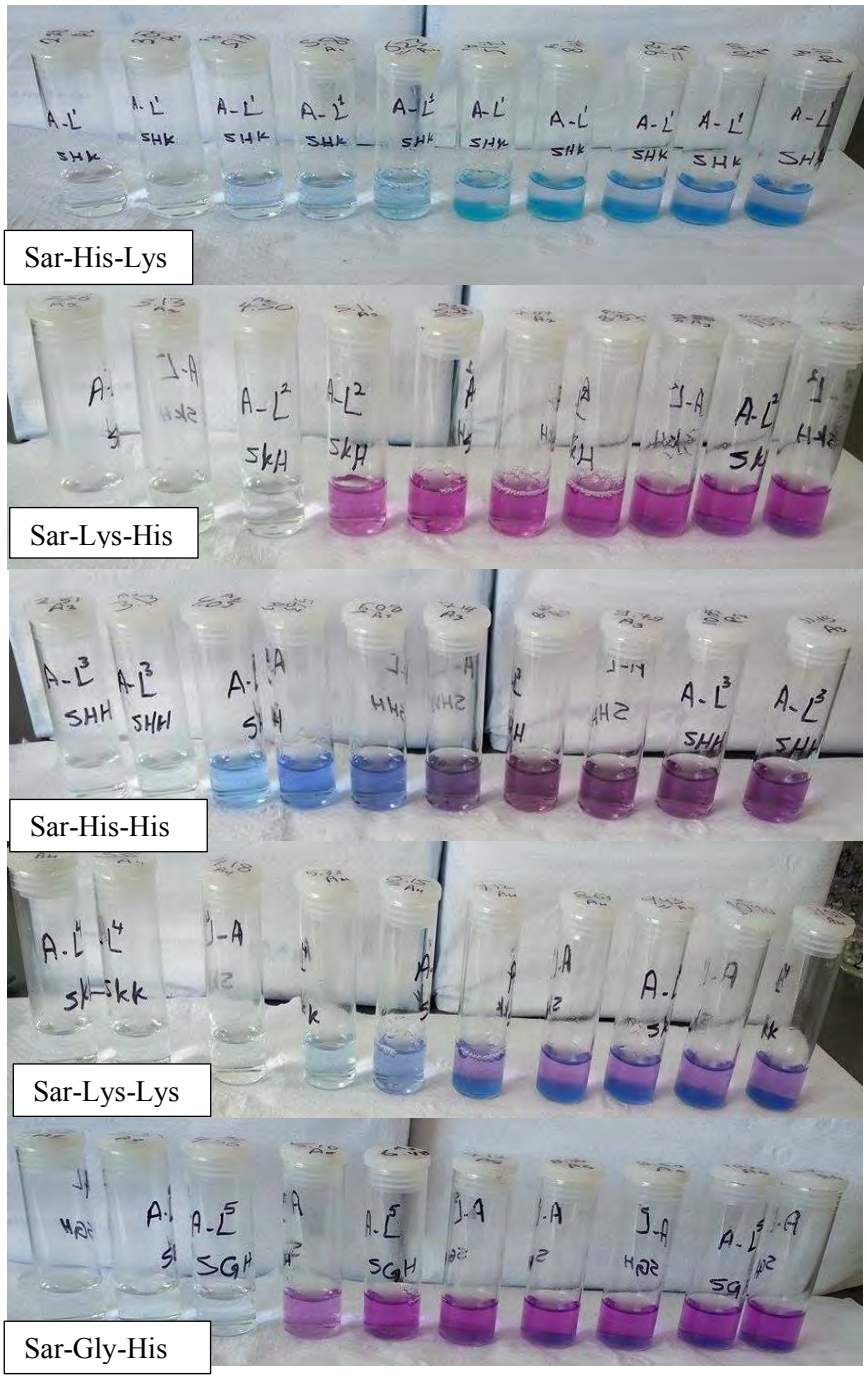

Figure 6.1: Cu(II) tripeptide showing the colour of the $CuLH_{-1}$ 3N and $CuLH_{-2}$ 4N species.

The ^{1}H NMR studies showed that the active binding sites for tripeptide are the imidazole nitrogen, the amide nitrogen and the terminal -NH groups. The imidazole nitrogen was involved in coordination first, followed by the amide and terminal amine groups. From the

chemical shifts of Cu(II) complexes of Sar-His-Lys, Sar-His-His and Sar-Gly-His, the imidazole ring of the histidine residue, with its two N^3 and N^1 nitrogen atoms, were shown to be a good metal-binding site in the reaction of histidine-containing peptides with Cu(II). The ε-amino group of lysine were relatively unaffected by copper addition, indicating that the lysine side chain does not coordinate to the Cu(II) [5].

Attempts to confirm the speciation of the Cu(II) complexes using ESI-MS were not that successful. The different species differ by one or two protons. The addition or the loss of a proton are very quick processes, which occurred during the electro-spray ionization. For this reason, while it was possible to see the Cu(II) complexation, it was not possible to get the accurate stoichiometry.

While it is possible to suggest the structure of different species from potentiometry and spectroscopy, it is not clear that these structures are physically feasible. For this reason, molecular mechanics (MM) modelling was used to calculate the strain energies (internal energy) of different possible copper complex geometries under biological conditions. This can guide the choice of peptides for the sequestration of copper such as sensing the presence of copper with the highest sensitivity, forming the most stable copper complex or removing the greatest amount of copper. At physiological pH, all the ligands formed square planar complexes with low stain energy. These results were in agreement with the potentiometric and spectroscopy studies.

One of the objectives of the study was to develop Cu(II) complexes that could be administered trans-dermally. Traditionally, octanol/water partition coefficients are used as an indication of transdermal absorption. Different species can have different partition coefficients and so we measured these as a function of pH. The results showed that all the Cu(II) complex species studied had log $P_{oct\backslash aq}$ valves below zero indicating that the complexes were relatively hydrophilic. Deprotonation of the ligand as well as N-methyl substituent on the terminal amine improved the lipophilicity. One of the reasons for using N-methyl substitution was to improve lipophilicity and these results confirm that this was achieved.

Although partition coefficients are traditionally used as a proxy for dermal absorption, these studies have used organic drugs not metal complexes. In order to confirm that partition coefficients can be used in this way, skin permeability was measured using an artificial

membrane. The permeability coefficient K_p for the Cu(II) tripeptide complexes was in the order : Cu-Sar-Gly-His > Cu-Sar-His-Lys > Cu-Sar-Lys-His > Cu-Sar-His-His > Cu-Sar-Lys-Lys > Cu-Cl^-. Sar-Gly-His increased the permeability of Cu(II) 2 fold. However, from the results obtained, there was no correlation between partition coefficient and permeability coefficient. Other researchers have proposed that multiple linear regressions should be used where molecular weight is included in the regression. From our results a correlation was only found between K_p and molecular weight. This indicates that care must be exercised when using partition coefficients as a proxy for tissue permeability.

Sar-Lys-His and Sar-Gly-His have a higher mobilising capacity than all the other tripeptides. The results obtained from this study were compared with the terminal amino acid sequence of serum albumin, which is the endogenous copper transport protein. Our study demonstrated that the Cu(II)-binding affinity of these ligands are comparable with those of glycyl-glycyl-L-histidine (Gly-Gly-His) and L-aspartyl-L-alanyl- L-histidine N-methyl amide (Asp-Ala-His-NHMe). The present study has contributed to the understanding of some aspects and problems involved in the development of copper complexes agents for the alleviation of inflammation associated with rheumatoid arthritis (RA).

In the present study, the design of these ligands was based on the structure of human serum albumin (HSA). At the same time the tripeptides with histidine demonstrated that the metal ion complexation strongly depends on the position of histidine in the tripeptide molecules. Besides introducing new ideas that can be successfully applied in solution chemistry, the study has clearly outlined the approach that could be followed in future studies for investigating new anti-inflammatory drugs for RA. Lysine was used in this study, but our results show that its side chain does not coordinate to the Cu(II). Thus it would be better to use a more lipophilic amino acid in future. Furthermore, it would be interesting to investigate the copper bio-distribution in animal experiments using ^{64}Cu(II) as a radiotracer. In addition, *in vivo* experiments using an animal model of inflammation, like Carrageenan foot edema, using the most promising complexes could be investigated as well.

References

1. D. H. Brown, W. E. Smith, J. W. Teape, and A. J. Lewis, *J. Med. Chem.*, 1980, **23**, 729–34.

2. E. T. Nomkoko, G. E. Jackson, and B. S. Nakani, *Dalton Trans.*, 2004, 1432–40.

3. L. D. Pettit, I. Steel, G. Formicka-Kozlowska, T. Tatarowski, and M. Bataille, *J. Chem. Soc. Dalt. Trans.*, 1985, 535.

4. H. Strasdeit, *Angew. Chemie Int. Ed. English*, 1993, **32**, 301–301.

5. J. H. Viles, F. E. Cohen, S. B. Prusiner, D. B. Goodin, P. E. Wright, and H. J. Dyson, *Proc. Natl. Acad. Sci. U. S. A.*, 1999, **96**, 2042–7.